CHARACTERISING THE ROLE OF AMIGO3 IN OLIGODENDROCYTES AND DEMYELINATING DISEASES

By

Simon Foale

A thesis submitted to the University of Birmingham for the degree of

DOCTOR OF PHILOSOPHY

Neuroscience and Ophthalmology

Institute of Inflammation and Ageing (IIA)

College of Medical and Dental Sciences

University of Birmingham

August 2018

Abstract

Demyelination disrupts neuronal signalling and can have profound effects on neurological control. No therapies currently exist to encourage remyelination and treatment options are based on preventing further demyelination highlighting the need to develop effective therapies for demyelinating diseases. Recent trials aimed at the leucine rich repeat (LRR) protein, LINGO1 to encourage remyelination have shown promising preclinical data however phase II clinical trials have been unsuccessful. The analogous LRR protein, AMIGO3 is predicted to overcome LINGO1 inhibition and therefore needs to be investigated for its role in oligodendroglia. We have investigated the expression profile of AMIGO3 in myelination and demyelinating disease. AMIGO3 is upregulated rapidly in oligodendrocyte precursor cells (OPCs) following trauma and in experimental autoimmune encephalomyelitis (EAE). Downregulation of AMIGO3 also corresponds with development myelination however AMIGO3 mRNA levels do not change following induction of OPC maturation *in vitro*. As AMIGO3 is raised following trauma, AMIGO3 could provide a pathological inhibition of OPC maturation in demyelinating diseases. We have also identified the NgR1 receptor complex on OPCs highlighting a potential biding partner that AMIGO3 could function through in disease. These data suggest that therapies aimed at inhibiting AMIGO3 will be promising in encouraging remyelination and treating demyelinating diseases.

Acknowledgements

Contents

List of figures

List of tables

List of abbreviations

ABC	avidin-biotin complex
ADB	antibody diluting buffer
ADHD	attention-deficit/hyperactivity disorder
AMIGO3	amphoterin-induced gene and open reading frame 3
AMPA	α-amino-3-hydroxy-5-methyl-4-isoxazolepropionic acid
AP	action potential
APC	antigen presenting cell
APS	ammonium persulphate
ATP	adenosine triphosphate
BBB	blood brain barrier
BMSU	Biomedical Services Unit
BSA	bovine serum albumin
CAII	carbonic anhydrase 2
CC	corpus callosum
CC1	adenomatous polyposis coli
cDNA	complementary DNA
CIS	clinically isolated syndrome
CNP	2'3'-cyclic-nucleotide 3'-phosphodiesterase
CNPase	2', 3'-cyclic-nucleotide 3'-phosphodiesterase
CNS	central nervous system
CSF	cerebrospinal fluid

CSPG	chondroitin sulphate proteoglycan
CTZ	cyclothiazide
DAB	diaminobenzidine
DAPI	4', 6-diamidino-2-phenylindole
DMEM	Dulbecco's modified Eagle's medium
dpf	day post-fertilisation
dsDNA	double stranded DNA
EAE	experimental autoimmune encephalomyelitis
ECL	electrochemiluminescence
EM	electron microscopy
ErbB2	human epidermal growth factor receptor
ESC	embryonic stem cells
FACS	fluorescence-activated cell sorting
FBS	foetal bovine serum
GalC	galactocerebroside
GDNF	glial cell line-derived neurotrophic factor
GSN	gelsolin
HRP	horse radish peroxidase
ICC	immunocytochemistry
IFN	interferon
IGF1	insulin-like growth factor 1
IHC	immunohistochemistry
IL	interleukin

LINGO1	leucine rich repeat and Ig domain containing 1
LPC	lysolethicin
LRR	leucine rich repeats
MAG	myelin-associated glycoprotein
MAG	myelin associated glycoprotein
MBP	myelin basic protein
MHC	major histocompatibility complex
MOG	myelin oligodendrocyte protein
MRI	magnetic resonance imaging
MS	multiple sclerosis
MSWM	MS white matter lesions
NAWM	normal appearing white matter
NgR1	neurite outgrowth inhibitor-66 receptor 1
Nogo-A	neurite outgrowth inhibitor A
NPC	neural precursor cell
NSC	neural stem cell
OCT	optimal cutting temperature media
OL	oligodendrocyte
OLG	oligodendroglia
OMGP	oligodendrocyte myelin glycoprotein
OPC	oligodendrocyte precursor cell
p75NTR	p75 neurotrophin receptor
PBS	phosphate buffered saline

PBS-T	PBS Triton
PCR	polymerase chain reaction
PDGFαR	platelet-derived growth factor α receptor
PFA	paraformaldehyde
PLB	protein lysis buffer
PLL	poly-L-lysine
PLP	proteolipid protein
PNS	peripheral nervous system
PPMS	primary progressive multiple sclerosis
PRMS	progressive relapsing multiple sclerosis
PVDF	polyvinylidene difluoride
RGC	retinal ganglion cell
RhoA	Ras homolog gene family, member A
RhoGDI	Rho guanosine diphosphate-dissociation inhibitor
RIS	radiologically isolated syndrome
ROCK	Rho-associated protein kinase
ROI	region of interest
RRMS	relapsing remitting multiple sclerosis
SC	Schwann cell
SCI	spinal cord injury
SDS	sodium dodecyl sulphate
SEM	standard error of the mean
SPMS	secondary progressive multiple sclerosis

tcMMEP	transcranial magnetic motor-evoked potential
TEMED	tetramethylethylenediamine
Th	T helper
TMEV	Theiler's murine encephalitis virus
Trk	tyrosine kinase
TROY	tumor necrosis factor receptor superfamily, member 19

Chapter 1

Introduction

1.1 Myelin and the mammalian nervous system

1.1.1 The role of myelin in saltatory conduction and the metabolic and trophic support of axons

Myelin is an insulating substance found in segments along axons, predominantly but not exclusively in white matter. Each myelin segment tends to be roughly 150µm in length (Aggarwal et al., 2011). Arguably, the primary role of myelin is to maintain proper saltatory conduction. This is achieved by increasing the electrical resistance across the axonal membrane inhibiting the passage of ions, preventing the loss of depolarisation, therefore allowing the charge to flow along the axon (Arancibia-Carcamo and Attwell, 2014). Despite the insulation, as the action potential (AP) travels down the axon, there will always be some loss of charge across the membrane and myelin ensheathment. Small gaps between myelinated segments, known as nodes of Ranvier, and the surrounding paranodal regions, contain the voltage gated Na^+ and K^+ channels respectively that are necessary to replenish the AP. This process of insulation and recharging is known as saltatory conduction, and can upregulate the conduction speed of the APs up to twenty times (Waxman, 1982; Bear et al., 2007; Neishabouri and Faisal, 2014; Carroll, 2017) (fig 1.1). Additionally, because the charge is only replenished at the nodes of Ranvier, regenerative channels are required to regenerate the AP and maintain the depolarisation (Bear et al., 2007).
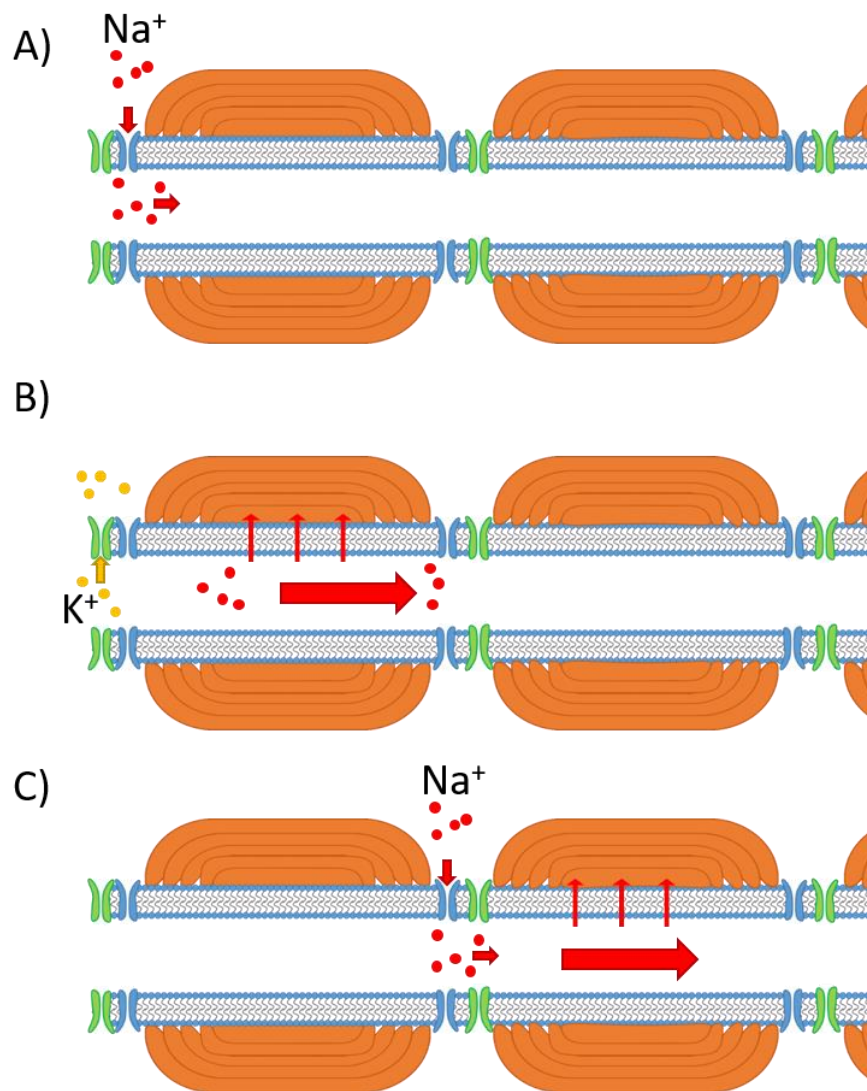
Figure 1.1: Saltatory conduction. (A) An AP is generated at the cell body or at a node of Ranvier through the influx of Na$^+$. This in turn starts to flow down the axon. (B) With an unmyelinated axon, a large amount of the Na$^+$ and therefore charge would flow out of the axon back in to the extracellular space. Myelin however increases the resistance to flow across the membrane, therefore more of the charge flows down the axon, increasing the rate of propagation of the charge down said axon. K$^+$ will flow out through K$^+$ voltage gated channels, allowing for the repolarisation and hyperpolarisation, preventing backflow of the AP. Although the rate of propagation has increased, some of the charge will leak across the membrane through the myelin sheath. (C) To overcome the inevitable loss of charge the AP is topped up at the subsequent node of Ranvier and the AP can continue to fire along the axon at the increased propagation rate.

Myelin may be important in plasticity, providing a method of speeding up and slowing conduction speeds to allow for proper coordination between neurons (Liu et al., 2012; Seidl, 2014; Saab and Nave, 2017). For example, it has been suggested that oligodendrocytes (OLs) may alter internode length and node of Ranvier sizes to alter the rate of propagation (Waxman et al., 1972; Waxman, 1997; Bakiri et al., 2011; Fields, 2014; Hill et al., 2018). Myelin is also known to play an important role in axonal survival, providing both trophic and metabolic support (Yin et al., 2006; Bercury and Macklin, 2015; Purger et al., 2016; Hill et al., 2018). Pyruvate and lactate generated during OL glycolysis can migrate to the ensheathed axon and aid in axonal metabolism supporting these cells in anaerobic conditions (Funfschilling et al., 2012; Morrison et al., 2013; Saab and Nave, 2017). Additionally, OLs produce MMP9, an angiogenic factor, thereby helping to provide vascularisation to the axon (Pham et al., 2012). It should also be noted that myelination helps to reduce axonal metabolic demand as well by reducing the area of the membrane requiring adenosine triphosphate (ATP) dependent Na^+/K^+ transporters to maintain the ion gradients required for the action potential. Denuded axons have to distribute voltage gated sodium and potassium channels across the entire membrane, rather than just at the nodes of Ranvier, to maintain an action potential. This requires a greater number of channels, and therefore a greater amount of ATP to maintain the same function (Nave, 2010; Frühbeis et al., 2013; Freeman et al., 2016). Trophic support is provided through the production of neurotrophic factors and cytokines, such as glial cell line-derived neurotrophic factor (GDNF) and insulin-like growth factor 1 (IGF1) (Wilkins et al., 2003; Miyamoto et al., 2014).

1.1.2 Structure of myelin

Myelin forms in concentric rings around an axon, to make multi-layered and densely packed ensheathing segments around an axon. Two distinct layers have been identified through electron microscopy (EM), a dense cytoplasmic layer known as the major dense line, and a less dense intercellular layer, known as the interperiodic line (fig 1.2). Lipids make up to 81% of the dry weight of myelin's final structure, accounting for 50% of the total lipids in the white matter (Aggarwal et al., 2011; Chrast et al., 2011; Michalski and Kothary, 2015; Saab and Nave, 2017). The high hydrophobicity of myelin causes the proteins and lipids to densely pack together and repel the aqueous cytoplasm and extracellular fluids (O'Brien, 1965; Aggarwal et al., 2011). A high proportion of these lipids have long hydrocarbon chains, increasing the Van der Waal's interactions between local lipids and proteins and therefore increasing the density of the structure (Aggarwal et al., 2011). Myelin also contains a high proportion of hydrophobic proteins/proteolipids. This results in a highly insulative ensheathing material, which makes myelin especially well suited for its role in saltatory conduction.

A number of proteins are included in the structure of myelin, with the predominant proteins being myelin basic protein (MBP) and proteolipid protein (PLP). The cytoplasmic layers of the lipids are held together with MBP, whilst PLP plays a role in zipping the extracellular surfaces together, although it is not integral for this role (Aggarwal et al., 2011; Podbielska et al., 2013) (fig 1.2). Myelin oligodendrocyte

5
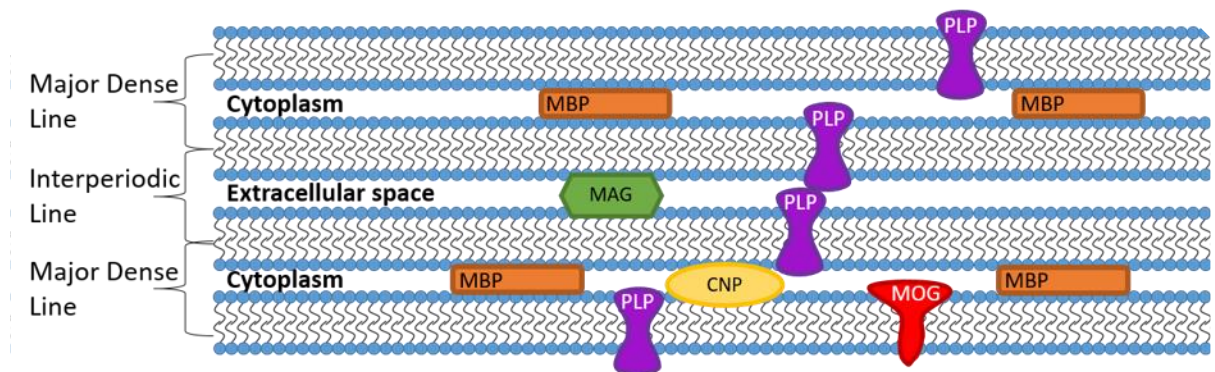
Figure 1.2: Diagram demonstrating the structure of myelin. Dense layers of membranes are held together. Two major layers are observed, the major dense line (cytoplasmic) and interperiodic line (extracellular). MBP and PLP are the two predominant proteins.

protein (MOG), myelin-associated glycoprotein (MAG) and 2'3'-cyclic-nucleotide 3'-phosphodiesterase (CNP) are also integral components of myelin although they are present at much lower levels than MBP and PLP.

1.1.3 Myelin production in mammals

1.1.3.1 Myelin in the central nervous system

In the central nervous system (CNS), myelin is created by OLs (Seidl, 2014). As oligodendrocyte precursor cells (OPCs) mature, they create multiple processes which search for and bind to local axons. This is done in a similar manner as the axon's growth cone, in that lamellipodia and filopodia explore the environment and extend towards their targets (Shao et al., 2017) (fig 1.3).

Once in contact with an axon, the processes extend radially inwards around the axon creating multiple concentric layers which are held together by gap junctions and other myelin proteins (Michailidou et al., 2014; Saab and Nave, 2017). The leading end of the process, known as the inner tongue, pushes underneath the previous layer to produce this effect (Michalski and Kothary, 2015). Once the concentric layers are produced, the cytoplasm of the process is compacted, largely through the action of MBP which binds to and draws the cytoplasmic membranes together (Aggarwal et al., 2011; Michalski and Kothary, 2015). Longitudinal expansion also occurs during this process to produce the full length myelin internode (Michalski and Kothary, 2015). Each OL can produce multiple processes which adhere and ensheath a number of axons (fig 1.3).

7
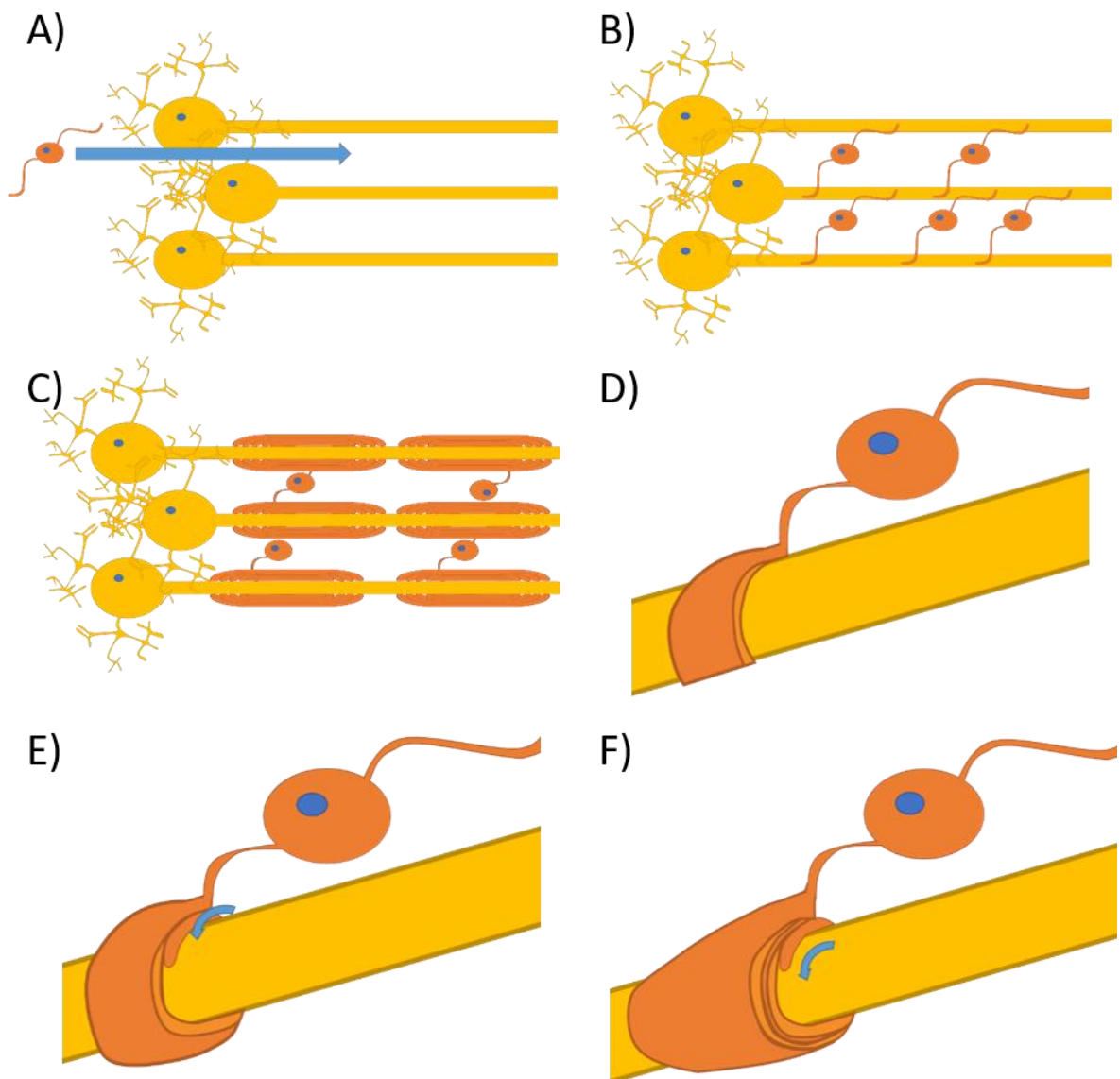
Figure 1.3: (A) OPCs migrate into a nerve in multiple waves during development. (B) Once OPCs are present, they proliferate and adhere to neighbouring axons. (C) After adhering to axons, some OPCs will differentiate, create myelin and ensheath the axons. Multiple axons can be myelinated by a single OL. Not all OPC will mature and a population of OPC will reside to provide a source for further myelination throughout life. (D) When the OL adheres, the process will begin to ensheath the axon. (E) Once the myelinated process has performed one full revolution, the leading end of the process, the inner tongue, will advance underneath the previous layer. (F) Concentric rings of myelinated processes wrap around the axon as the inner tongue continues to push underneath the previous layers. These layers will then become compacted together to create dense ensheathing layers.

1.1.3.1.1 Origins and development of OLs

OPCs the multipotent stem cell line which differentiate to mature OLs, are found throughout the CNS of adults. These OPCs have a consistent turnover in the adult CNS, with local OPCs being able to propagate and differentiate as required (Hill et al., 2018). OPCs are also referred to as NG2+ cells due to the presence of NG2 on the cell membrane which is downregulated as the cells mature. It should also be noted that there is evidence that NG2+ cells also have the ability to differentiate into certain neurons and astrocytes (Nishiyama et al., 2009; Michalski and Kothary, 2015).

As well as NG2, a number of markers have been identified that are useful for determining the stage of differentiation of oligodendroglia (OLG). Markers that have been identified for immature OPCs include platelet-derived growth factor α receptor (PDGFαR) and A2B5, as well as NG2 itself (Polito and Reynolds, 2005; Miron et al., 2011). O4 and O1 are markers of developing OPC. O4 appears to be a sign of OLs which have begun to differentiate, reaching a pro-OL stage, whereas O1 is expressed in the later stages of OPC differentiation, prior to full maturation (Sypecka et al., 1995; Polito and Reynolds, 2005; Abbaszadeh et al., 2014). Galactocerebroside (GalC) has also been identified as a marker of differentiating OPCs (Kuhlmann et al., 2008). Finally, a number of marker proteins have been identified in the CNS that are useful for identifying mature OLs. Firstly as myelin is present in high levels only in mature OLs, proteins such as MBP, MOG and PLP are predominantly in mature OL. Other commonly used markers of mature OLs include adenomatous polyposis coli (with the main antibody against the protein also known

as CC1), carbonic anhydrase 2 (CAII) and 2', 3'-cyclic-nucleotide 3'-phosphodiesterase (CNPase) (Kida et al., 2006; Crawford et al., 2016). These markers, although they have their various weaknesses, all are useful for monitoring the changing phenotypes. Additionally, morphology provides a useful criteria *in vitro* for assessing maturation in OLG cell lines and in primary cultures. Primary OPCs present as small cells with two processes, which transition into more complex stellate forms as differentiation proceeds. It is not until the latter stages of differentiation that myelin is produced, which in culture appears as a membranous layer, known as the myelin sheath, that surrounds the processes (fig 1.4) (O'Meara et al., 2011).

OPCs in both the developing spinal cord and cerebrum, originate from neural precursor cells (NPCs) in the ventral ventricular zone of the medial ganglionic eminence (MGE) (Mitew et al., 2014; Bergles and Richardson, 2015; Takebayashi and Ikenaka, 2015). This appears to be a Sonic Hedgehog derived reaction that induces this differentiation and migration (Nishiyama et al., 2009; Takebayashi and Ikenaka, 2015). A second wave then appears from the lateral ganglionic eminence. These OPC in turn migrate across the developing CNS of the embryonic mouse, although it should be noted that myelination is not achieved during this time (Mi et al., 2004; Bergles and Richardson, 2015). After birth, new OPCs are derived from the cortical ventricular zone. Over time these cortical derived OPCs become the majority OPC, with the first wave of MGE derived cells being entirely removed.
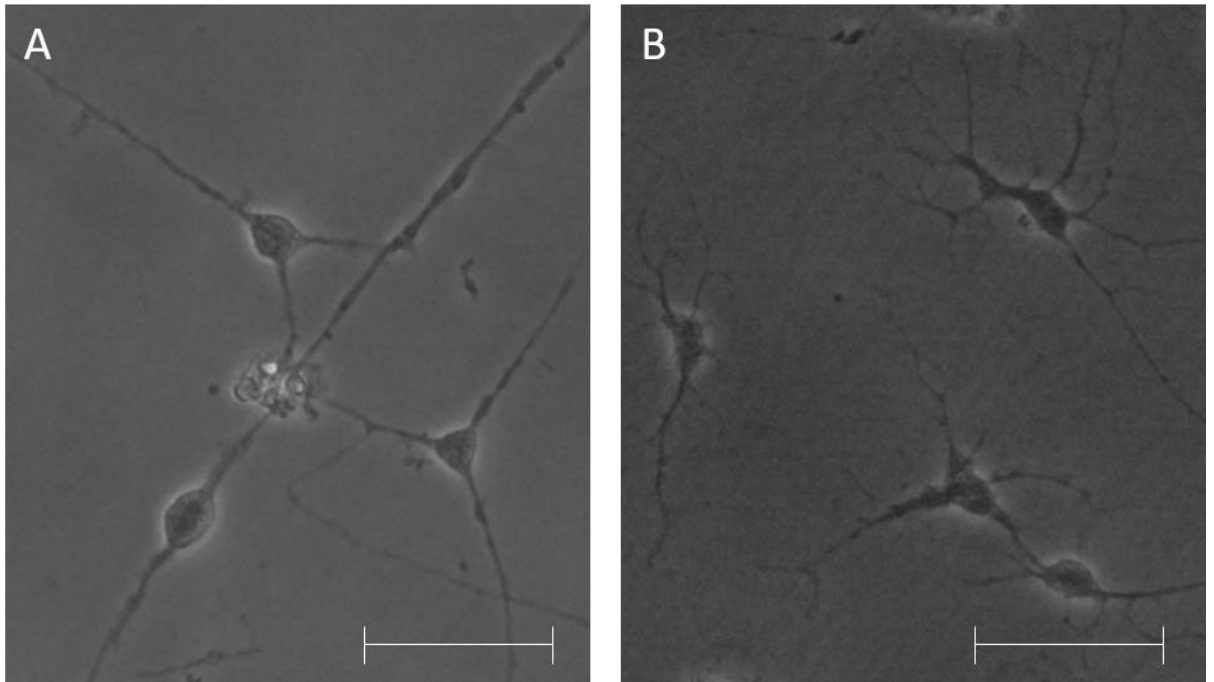
Figure 1.4: Representative images of OLG in culture. (A) OPC cultures before differentiation. OPCs can be seen to have large bright nucleus and are bipolar or multipolar with few processes. (B) OLG further along the differentiation process can be seen to have a more stellate appearance as process expand and diverge to searching for axons to myelinate. Scale bars represent 50µm.

1.1.3.2 Peripheral nervous system

Myelin is also created in the peripheral nervous system (PNS) to insulate and protect peripheral axons. A separate cell line is used to generate myelin in the PNS, known as Schwann cells (SCs). There are two forms of Schwann cells, myelinating and non-myelinating (Monk et al., 2015). Unlike OLs, myelinating Schwann cells are only able to interact with a single axon, although the ensheathing process is very similar in that they adhere to and then wrap multiple layers around the axon to ensheath the axon. Similarly, the cytoplasm of the ensheathing layers contains the myelin to insulate the axon (Belin et al., 2017). Both cells types demonstrate metabolic and trophic support however only the myelinating SCs provide the insulation required for saltatory conduction (Monk et al., 2015; Salzer, 2015). The non-myelinating SCs pack in more densely along the axons, presumably as nodes of Ranvier and saltatory conduction is irrelevant. These cells also are able, like OLs, to bind with multiple axons (Monk et al., 2015). Unlike OPCs, SC precursors derive from the trunk neural crest and can only partially mature to immature SCs until postnatal stages of development. The precursor forms are migratory and disperse throughout the PNS following the developing axons (Dong et al., 1995). These precursors settle with PNS axons and differentiate to the immature form before continuing development postnatally into the myelinating or non-myelinating form, depending on which type of axons they contact. For example, the non-myelinated C-fiber nociceptor neurons signal for non-myelinating SCs (Bhatheja and Field, 2006; Monk et al., 2015). Interestingly, unlike OLG, when both myelinating and non-myelinating SCs lose contact with axons, they are able to de-differentiate back to the immature

form allowing them to be recycled when axonal contact is re-established (Bhatheja and Field, 2006).

1.2 Demyelination and demyelinating diseases

Demyelination is the loss of the myelin sheath that surrounds the axon (Kutzelnigg and Lassmann, 2014). A number of demyelinating diseases exist, which are varied and can be associated with the CNS as well as the PNS, or in rare cases, can affect both (Love, 2006; Zephir et al., 2008). The effects of demyelination can be severe, through the loss of proper signalling, which has been reported produce up to a 20 fold reduction in propagation rate, if not ablating the signal entirely (Waxman, 1982). Additionally, focal damage can result in a lack of synchronicity between neurons, preventing appropriately timed summation or inhibition between neuronal signalling (Cover et al., 2006; Pan et al., 2017).

Demyelination can occur in acute forms through damage to myelin producing cells or through specific diseases. These diseases are varied, and cases exist of CNS, PNS or both simultaneously being affected (Love, 2006; Menon et al., 2014). On top of demyelinating diseases, dysmyelinating diseases are also prevalent, where the myelin is still produced, but it is not produced correctly (Love, 2006; Vanderver et al., 2015). Examples of these include Krabbe's disease, Canavan's disease and Pelizaeus Merzbacher's disease (Torii et al., 2014; Graziano and Cardile, 2015). This could happen through the improper production of the myelin such that it does not produce the dense ensheathing layer, resulting in similar inefficiencies for the

affected axons (Sarbu et al., 2016; Gregath and Lu, 2018). The most prevailing myelin disorder is multiple sclerosis (MS) (Goldenberg, 2012).

1.2.1   Remyelination

Remyelination is the process whereby myelin is restored to neurons following pathological demyelination. This is separate from the act of myelination which is simply the original addition and maintenance of myelin in healthy nervous systems. OLs that survive the demyelination are not able to develop new processes and engage in remyelination. This is clear from labelled endogenous OLs and transplanted OLs that fail to induce any degree of remyelination in models of demyelination (Targett et al., 1996; Crawford et al., 2016). Furthermore, when demyelination occurs however mature OLs survive, the areas of demyelination develop greater number of OLs than before the focal demyelination (Blakemore and Keirstead, 1999; Anastasiadis et al., 2000). Furthermore, labelled mature OLs have been demonstrated to fail to migrate in to focal demyelinated sites in murine spinal cord or even to produce processes from the periphery of the lesion. Instead all novel remyelination was produced by OLs that had been derived from OPCs (Crawford et al., 2016). This demonstrates that there is a drive to create new OLs for novel remyelination rather than activating the surviving OLs to engage in remyelination. OPC are considered to be the principal source of remyelinating OL in the CNS. In acute forms of demyelination, when the axons remain relatively healthy, remyelination will occur as local OPCs mature and adhere to the surviving axons (Franklin and Ffrench-Constant, 2008). OPCs are also able to migrate to the site of demyelination to produce the new OLs and myelin. These OPC create processes

which start to develop expression of myelin. Subsequently, they adhere to and ensheath the surviving axons with a new coat of myelin (Boyd et al., 2013; Bercury and Macklin, 2015).

1.2.2 Multiple sclerosis

MS is primarily considered an immunopathologic disease which is associated with break-down of the blood brain barrier and invasion of immune cells which attack and destroy the myelinating OLs (Goldenberg, 2012). Destruction and phagocytosis of the myelin as well as the denuding of local axons occurs as a result of the autoimmune attack. Inefficient propagation of action potentials and axonal damage/death follows, eventually leading to the development of localised plaques. These plaques and lesion sites are predominantly located at white matter tracts, and are sites of axonal loss and reactive glial scars (Lassmann et al., 2007; Goldenberg, 2012; Kutzelnigg and Lassmann, 2014; Lopes Pinheiro et al., 2016). The exact distribution is somewhat random and does not show an obvious progression pattern, however the regions affected predominantly are the optic nerve, cervical spinal cord, cerebellar white matter and the pons and medulla (Kutzelnigg and Lassmann, 2014). As a result, the disease is characterised by progressive CNS demyelination (Satoh et al., 2005; Patrikios et al., 2006; Patani et al., 2007). In rare cases, and in early stages of MS, minimal disability may be observed, but the majority of patients experience progressive CNS disability and loss of motor control. MS can also result in a number of direct or indirect symptoms including acute/chronic pain, ataxia vertigo, bladder dysfunction, depression, paralysis, visual defects as well as numerous others (Goldenberg, 2012; Jadasz et al., 2012; Boeschoten et al., 2017).

Owing to the limited understanding of MS aetiology, there are a number of clinical classifications of the disease. The earliest form of MS is clinically isolated syndrome (CIS). CIS is defined as the first clinical and symptomatic presentation of MS. This can be further categorised as active or inactive depending on the presentation of lesions identified through magnetic resonance imaging (MRI) (Lublin et al., 2014). Three further forms exist of the 'active' form of the disease, with the most common form of MS being relapsing remitting MS (RRMS). Patients exhibit acute relapses with rapid onset of symptoms, before periods of remission where the symptoms lessen and can ablate entirely in early stages of the disease. The remission rarely returns to symptomatic levels before the relapse, however some degree of recovery is observed until the next relapse (fig 1.5A). This form tends to progress on to secondary progressive (SPMS) where the symptoms continually develop without periods of relapse or remission anymore. Remissions can appear however patients always exert a progressive degree of disability (fig 1.5B). Primary Progressive (PPMS) is similar to SPMS, however patients do not exhibit any form of relapses or remission and show a constant degradation, therefore it does not progress from a relapse and remission stage (fig 1.5C). A further subcategory, known as 'PPMS with activity', or previously as progressive relapsing (PRMS), is similar to PPMS, except that patients also exhibit relapse periods with severe worsening of symptoms but do not observe any degree of recovery (Goldenberg, 2012; Jadasz et al., 2012; Lublin, 2014; Nelson et al., 2016). The final form, radiologically isolated syndrome (RIS) exists, where lesions are observed though MRI, however there are no clinical signs of the disease (Lublin, 2014; Lublin et al., 2014).
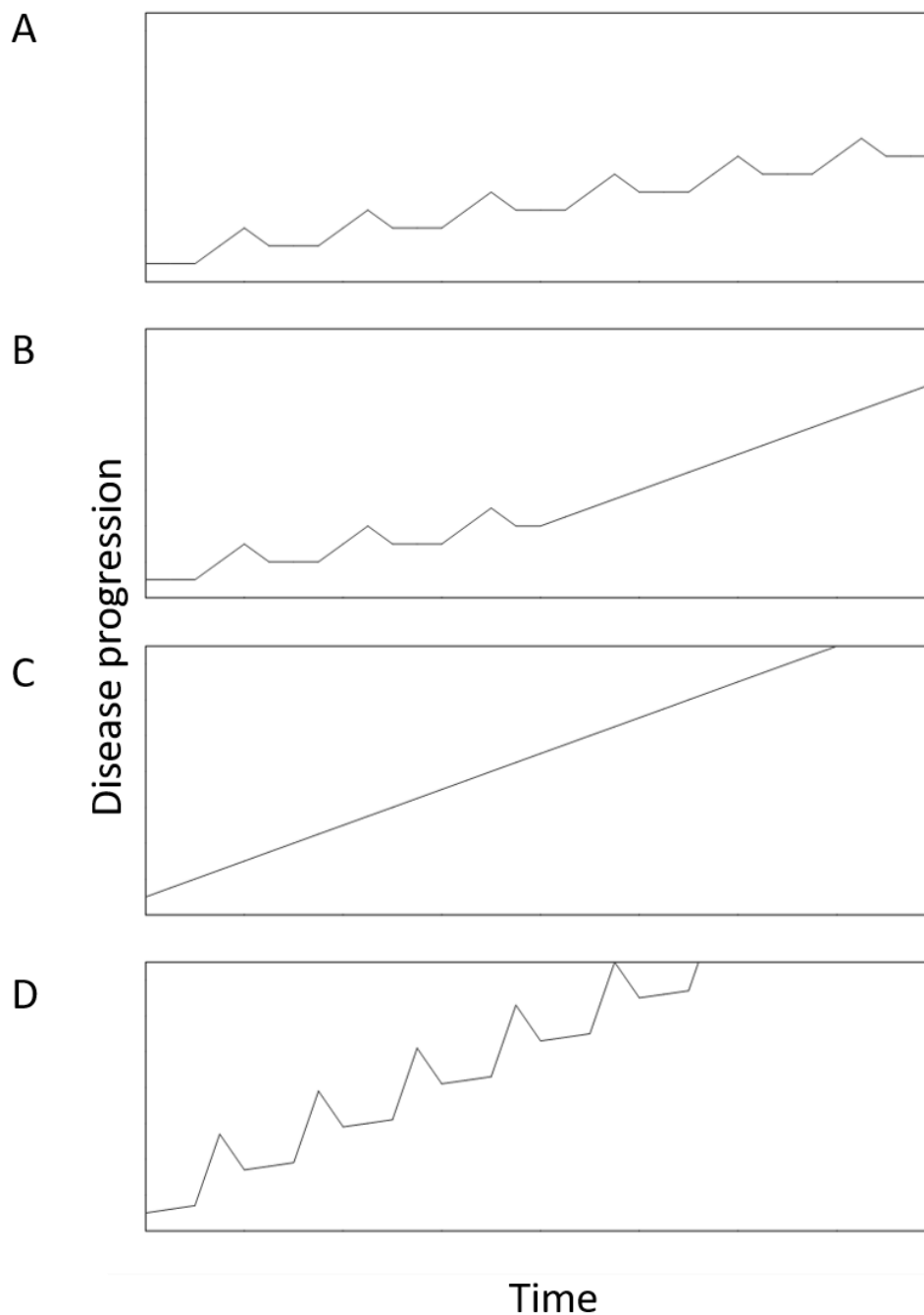
Figure 1.5: Representation of the progression of the different forms of MS. (A) RRMS, where relapses lead to a progression in disease state. Some degree of recover occurs but not returning to the baseline before the relapse. (B) SPMS, where relapses progress on to a constant progressive dehabilitation. (C) PPMS, where constant disease progression occurs independent of a previous relapsing-remission stage of the disease. (D) PPMS with activity, which is similar to RRMS, however disease progression occurs both in the form of remissions and relapses, as well as constantly during the remission stage of disease.

17

As previously stated, MS is the most prevalent CNS demyelinating disease. Modern estimates are difficult to find due to a lack of studies (Marrie et al., 2015), however MS affected 0.54 million people in Europe in 2010 and over 2.5 million worldwide in 2017, as well as up to 100,000-200,000 people in the UK (Multiple Sclerosis International Federation, 2013; Tullman, 2013; DiLuca and Olesen, 2014; Mackenzie et al., 2014; Ponzio et al., 2015). MS has a peak onset of 20-25 years (Lindsay et al., 1997) and is much more prevalent in women than men, with an approximate prevalence ratio of 3:1 for women to men (Wallin et al., 2012; Harbo et al., 2013). Interestingly, there appears to be a geographical distribution, with far more cases observed in Europe and Northern America 100/100,000, compared to 5/100,000 in South America, Africa and Asia (Simpson et al., 2011). Although a genetic factor has been associated, linking Caucasians to a higher risk, latitude also presents an environmental risk factor with family members at a higher risk in northern latitudes (Love, 2006; O'Gorman et al., 2012; Khan et al., 2015). A number of other risk factors have been identified for MS including viruses, specifically the Epstein-Barr virus, vitamin D levels and genetics, through major histocompatibility complex (MHC) modifications as well as proteins involved with the action of vitamin D (Lucas et al., 2011; O'Gorman et al., 2012; Alharbi, 2015).

The prevalence and symptoms of MS alone, without taking account of demyelinating and dysmyelinating diseases, demand further investigation both for the social and economic impacts. Treatment in Europe alone for MS accounted for £12.5 billion in 2010 (Ponzio et al., 2015). Additionally, it should be highlighted that both loss of productivity and employment following MS diagnosis also has a major

socioeconomic impact, estimated to result in production losses almost costing as much as treating the disease itself (van der Hiele et al., 2015). Finally, a number of studies note an increasing incidence of MS, highlighting the need for an effective treatment to be developed (Pugliatti et al., 2006; Jennum et al., 2012; Olesen et al., 2012; Ponzio et al., 2015). These factors validate the need to develop novel treatments to effectively treat patients and prevent the loss of function associated with disease progression.

1.2.2.1   Aetiology of MS

MS is predominantly considered an immunopathologic autoimmune disease, whereby patient's immune system attacks OLs, leading to chronic demyelination (Patani et al., 2007; Goldenberg, 2012; Matveeva et al., 2018). Although remyelination does occur acutely, the remyelination is inadequate and eventually fails resulting in the chronic demyelination observed in developed plaques (Patani et al., 2007). MS is believed to be driven by the activation of T helper (Th) cells, also known as CD4^{+} cells, by antigen presenting cells which have incorrectly taken up epitopes from myelin proteins (Ghasemi et al., 2017). CD4^{+} T cells differentiate in to Th1 or Th17 cells which produce interferon-gamma (IFN-γ) and interleukin-17 (IL-17) respectively. These cells have then been shown to mediate the autoreactivity in experimental autoimmune encephalomyelitis (EAE), the leading rodent model for inflammatory demyelination (see section 2.1.2 for more details) and have been found within lesions and plaques of MS patients in post-mortem tissue (Grigoriadis et al., 2015). Furthermore, preventing the development of these cells in EAE induced mice reduces disease incidence and clinical score, demonstrating the role of these cells in

disease development in EAE (Komiyama et al., 2006; Beurel et al., 2013). Originally believed to be a predominantly Th1 driven disease, studies have shown raised IL-17 transcripts in MS plaques as well as an increased ability of transplanted, activated Th17 cells to induce EAE, compared to Th1 cells (Lock et al., 2002; Langrish et al., 2005; Aranami and Yamamura, 2008). Additionally, mice deficient in components of the Th1 differentiation pathway still maintain the ability to develop EAE (Korn et al., 2009), whereas mice deficient in components of the Th17 pathway differentiation are protected from the disease (Veldhoen et al., 2006). This demonstrates that Th17 cells may be the predominant immune cell type in immune pathogenesis in the EAE model of MS. Th17 cells produce a number of pro-inflammatory cytokines, which draw inflammatory cells to the CNS and exacerbate symptoms. B cells and cytotoxic T cells (CD8^{+}) have also been implemented in the development of EAE and MS (Ghasemi et al., 2017).

One theory is that autoreactive T-cells are generated through a failure of the immune system to prevent their production or potentially due to antigen presenting cells (APCs) taking up and presenting foreign proteins which share similar epitopes to myelin proteins following an infectious agent, such as the Epstein-Barr virus (Baker and Amor, 2014). The autoreactive APCs activate the T cells in secondary lymph tissue, priming the T cells to recognise myelin derived proteins (Podbielska et al., 2013). The now autoreactive T cells manage to breach the blood brain barrier (BBB), reaching perivascular spaces where they re-encounter autoreactive APCs (Podbielska et al., 2013; Baker and Amor, 2014; Lopes Pinheiro et al., 2016). Once activated by these APCs, they induce a pro-inflammatory cascade which disrupts the

BBB and draws further immune cells to the CNS leading to direct damage, as well as indirect damage through inflammatory conditions, to myelin sheaths and the mature oligodendrocytes. Axons may be directly damaged directly by the inflammation, or indirectly due to loss of the myelin and the metabolic and trophic support it provides (Trapp and Nave, 2008). Chronic effects of the repeated inflammation results in reactive gliosis which develops plaques, causing further damage and obstruction of local axons (Podbielska et al., 2013).

It should be noted however that there is evidence, at least in some cases, that oligodendrocyte degradation and apoptosis precedes the immune response (Barnett and Prineas, 2004; Bhat and Steinman, 2009). It is argued that the onset of disease is due to an original neurodegenerative event, presumably due to oligodendrocyte death. The death and abundance of myelin derived proteins then induces the auto-immune response, leading to further degradation (Stys et al., 2012). If this is the case, it is not clear whether the original neurodegeneration is brought about by an intrinsic abnormality or an extrinsic input, again such as a virus or traumatic event.

For the majority of patients, some degree of remyelination will originally occur, leading to a degree of recovery, although the remyelinated sheaths are not as thick as the original layers (Hanafy and Sloane, 2011; Podbielska et al., 2013). Over time however, the remyelination process fails, with only partial myelination observed after 450 days in a murine model of spinal cord induced demyelination (Totoiu and Keirstead, 2005). It is clear that despite the loss of myelin and the development of plaques within the CNS, OPCs survive. Even in the most developed plaques OPCs are still observed (Chang et al., 2002; Harlow et al., 2015). In fact there appears to

be a greater number of OPCs in acute plaques suggesting that OPCs are able to proliferate (Guest et al., 2005; Nakahara et al., 2009). These observations have led to the hypothesis that the failure to remyelinate results from a deficit in OPC differentiation. As remyelination is observed in early stages of disease, progression of MS may be correlated with a progressive impairment of OPC maturation rather than in their migration or proliferation (Compston and Coles, 2008; Hanafy and Sloane, 2011).

It has not been determined exactly why OPC fail to mature and remyelinate. Acute inflammation appears to be an integral promoter of remyelination in acute neuroinflammation, due to the release of neurotrophic factors and the removal of inhibitory factors (Foote and Blakemore, 2005). Preventing the action of local cytokines results in impaired remyelination during murine EAE and toxin induced demyelination (Hanafy and Sloane, 2011; Stone et al., 2017). Despite this, it is likely that the extent of neuroinflammation and subsequent plaque formation create an inhibitory environment for OPC maturation and myelin production following repeated bouts of demyelination (Fitch and Silver, 2008). Additionally, a build up of myelin debris, as a result of repeated attacks combined with incomplete removal by macrophages could also drive the environment towards one that is more inhibitory to OPC maturation and remyelination (Fancy et al., 2010). As such either modifying the environment or modifying the responses of OPC to said environment would be an invaluable method to encourage proper remyelination and relieve the symptoms of MS.

1.2.2.2   Current treatments

1.2.2.2.1   Immunomodulation

Although the aetiology of MS is not fully understood, the disease is predominantly considered an immunopathologic disease (Hemmer et al., 2002; Wu and Alvarez, 2011). As such, all of the available treatments are aimed towards immunomodulation. This is to reduce the number of autoimmune attacks (and subsequent relapses), thus slowing the progression of the disease (Goldenberg, 2012). There are a number of examples of this approach. IFN-β has been a commonly used molecule as a therapy for MS. IFN-β appears to directly lead to anti-inflammation actions by decreasing MHCII expression, altering interleukin transcripts on in APCs and decreasing Th1 and Th17 production, which together leads to a general anti-inflammatory effect (Castro-Borrero et al., 2012; Waschbisch et al., 2014). Glatiramer acetate is another commonly used drug which appears to interact with APCs and change their interactions with T cells, such that they preferentially stimulate the anti-inflammatory Th2 cells (Castro-Borrero et al., 2012). More modern and more effective immunomodulatory therapies include Cladribine; a selective lymphocyte suppressor, Alemtuzumab; a depletory of CD52 expressing lymphocytes, and Ocrelizumab; a recombinant anti CD-20 antibody which was designed to effectively deplete B cells (Olek, 2018). Other medications targeting the immune system include Mitoxantrone, Natalizumab and to a lesser extent Fingolimod (Goldenberg, 2012).

Despite the success of immunomodulatory therapies in modulating and slowing the progression of MS, disease progression still occurs and eventually leads to the

characteristic plaque formation and disability. Additionally, although treatments are effective in the early stages, the immunomodulation is of limited benefit during later, progressive stages of the disease (Lassmann et al., 2007). Presumably, immunodulation therapies do not encourage remyelination or repair of the damaged CNS, therefore once the damage has occurred, these therapies lose their value. There is also the risk of increased opportunistic infections, although this is more of an issue in broad immunosuppressants than direct immunomodulation therapies (Castro-Borrero et al., 2012; Olek, 2018). Furthermore, if MS does follow a neurodegenerative disease profile, then immunomodulation would only be treating the subsequent symptoms rather than helping to prevent the degeneration.

1.2.2.2.2 Neuroprotection

A new therapeutic approach being tested involves the use of neuroprotective agents (Brück, 2005; Wu and Alvarez, 2011; Goldenberg, 2012). Although this treatment won't cure the disease or remove the acute symptoms of demyelination, they could in theory prevent or reduce the damage to axons. However in any nerve when demyelination prevents all signalling then this approach will be unproductive on its own. It is likely that this type of treatment will be useful in combination with other therapeutics, such as targeting the immune system to limit the chronic damage to the CNS. A number of therapeutic drugs are under development following this approach targeting different protective measures. These include direct delivery of neurotrophic factors, oxidative stress protection, mitochondrial maintenance and efficiency, as well as a number of others (Villoslada, 2016).

1.2.2.2.3   Stem cell transplantation

It has been shown that implanted OPCs produce neurotrophic factors however whether they actively engage in remyelination is not clear (Priest et al., 2015). As such, this approach may simply promote neuronal survival. This in turn could indirectly promote endogenous remyelination from local OPCs rather than directly inducing remyelination. Neural stem cells (NSCs), have also shown to have a local immunomodulation effect, providing local protection to their delivery site, which has recently been attributed to regulation of cerebrospinal fluid (CSF) succinate. Succinate has been shown to be an effective biomarker of CNS metabolic stress and inflammation (Mills and O'Neill, 2014; Littlewood-Evans et al., 2016; Peruzzotti-Jametti et al., 2018). Despite a lack of tumour development observed in rats injected with human induced OPCs (Priest et al., 2015), there is always a concern with this approach that unanticipated tumorigenesis could develop. Although this approach may be beneficial, specific sites of demyelination are required to be identified and the transplantation would be invasive, especially if autologous OPCs are required.

Although the neuroprotective and immunomodulation approaches can control progression of the disease, there is currently no procedure that can aid the restoration of damaged neurons or oligodendrocytes *in vivo* (Goldenberg, 2012). As such, it is clear that there is a need to develop alternative therapies which can repair CNS damage before the development of chronic, function-impairing damage.

1.2.2.2.4 Remyelinating therapies involving endogenous OPCs

A recent area of investigation is looking at the ability to encourage remyelination directly by stimulating local OPCs to differentiate. Despite a number of successful pre-clinical studies demonstrating improved remyelination, a viable drug capable of promoting OPC remyelination has not become available (Goldenberg, 2012; Harlow et al., 2015). Two clinically approved drugs for unrelated conditions; miconazole, a topical antifungal and clobetasol, a topical corticosteroid, are capable of promoting remyelination in mouse EAE studies (Najm et al., 2015). Both drugs were capable of increasing the number of CC1 positive, mature OLG in mouse EAE, as well as increasing the extent of MBP positive staining in lesions. Furthermore, similar results were observed with human OPCs derived from embryonic stem cells (ESCs). These data were also correlated to improved clinical observations in the mouse EAE model (Najm et al., 2015). These results show that stimulating endogenous remyelination can aid in restoring the myelin sheath and that this can be beneficial in a preclinical context. Despite this promising data, only two remyelination agents have made it to phase 2 clinical trials. Clemastine, a medication originally produced as an antihistamine, has been shown to encourage OPC differentiation and clinical trials have demonstrated reduced visual-evoked potentials (Green et al., 2017). A further trial will be discussed later (see section 1.4.2.2).

Just as with neuroprotection and immunomodulation, remyelination has been investigated through the direct transplantation of OPCs into focal lesions. Rodent models of traumatic demyelination have produced a degree of success, where animals showed reduced clinical symptoms, higher levels of myelin and reduced

latencies in electrophysiological recordings (Cao et al., 2010; Wu et al., 2011).

Despite this success, transplantation is unlikely to be clinically useful due to the

difficulty locating focal lesions, the invasiveness required to implant the cells and the

risk of tumorigenesis. Additionally demyelination occurs prior to plaque or lesion

development, therefore by the time the focal site has been identified for treatment,

there is likely to already to be significant damage (Wu and Alvarez, 2011)

1.3   Leucine rich repeat molecules in the mammalian CNS

Leucine rich repeat (LRR) containing proteins are a family of proteins containing a

region of multiple LRR motifs. Each motif is made up of a consistent pattern of amino

acids which create a horseshoe structure. The amino acid pattern consists of a

section containing LxxLxLxx$^N/_C$xL, where L represents leucine but can be substituted

for a valine, isoleucine or a phenylalanine, x can be any amino acid, N is an

asparagine and C is a cysteine. Each motif consists of 20-30 amino acids including

this pattern. It has been hypothesised that by creating a horseshoe structure, the

LRR segment leads to a larger surface area for greater protein interaction, with

multiple examples of interactions on both the convex and concave surface of the

structure (Kobe and Kajava, 2001; Matsushima et al., 2005; Bella et al., 2008; de Wit

et al., 2011).

1.3.1   LRR Molecules in Central Nervous System Disorders

A number of LRR proteins have been identified to play a role within the healthy

CNS, and correspondingly have been linked with a number of neuronal disorders

(Chen et al., 2006; Söllner and Wright, 2009; de Wit et al., 2011; Ledda and

Paratcha, 2016). Netrin-G-ligand and Slit are both involved with axon guidance and synaptic development through interactions between Netrin-G1/2 and receptor protein tyrosine phosphatase respectively in cultured neurons (Chen et al., 2006; Takahashi et al., 2012; Yim et al., 2013; de Wit and Ghosh, 2014). Neurite outgrowth inhibitor-66 receptor 1 (NgR1) and its receptor complex inhibit axon extension through interactions with myelin derived proteins (Mi et al., 2004; Ahmed et al., 2013). Tyrosine kinase (Trk) receptors have been identified to bind with neurotrophic factors and regulate axon growth and synaptic development (Chen et al., 2006; Ahmed et al., 2013; de Wit and Ghosh, 2014; Ledda and Paratcha, 2016). From these interactions, LRRs have been associated with CNS plasticity as well as a number of neuronal disorders, including schizophrenia, bipolar disorder, Alzheimer's disease, autism, Rett syndrome and attention-deficit/hyperactivity disorder (ADHD) (de Wit and Ghosh, 2014).

1.4 LINGO1 and AMIGO3

More recently there has been interest in two proteins of the LRR protein family, leucine rich repeat and Ig domain containing 1 (LINGO1) and amphoterin-induced gene and open reading frame 3 (AMIGO3). Both proteins were originally found to be an important component of the NgR1 receptor complex and have since been observed to be important proteins within the CNS (Mi et al., 2004; Ahmed et al., 2013; Mi et al., 2013). LINGO1 and AMIGO3 are structurally analogous proteins of the LRR protein family. The proteins are type 1 transmembrane proteins consisting of a short cytosolic tail, a transmembrane domain, an Ig-like domain and an

extracellular LRR, horseshoe shaped domain, with a signal peptide on the extracellular tail (Kuja-Panula et al., 2003; Chen et al., 2006; Zhang et al., 2009; Zhou et al., 2012; Foale et al., 2015). The only major difference between the structures of the two proteins is the variation in the number of LRR that they possess, with LINGO1 having 12 LRR domains and AMIGO3 having 6 (fig 1.6) (Kuja-Panula et al., 2003; Jepson et al., 2012; Foale et al., 2015).

1.4.1 Endogenous expression

LINGO1 is specifically expressed within the CNS, however levels of mRNA for LINGO1 stay low during embryonic development in murine models (Mi et al., 2004; Haines and Rigby, 2008). It is not until the end of prenatal development, that mRNA for LINGO1 is substantially upregulated, before dropping again after postnatal day (P)1 in mice and rats (Mi et al., 2004; Mi et al., 2005). Similarly, in zebrafish, LINGO1 expression is maintained at low levels during embryogenesis but rises 5 days after fertilisation in early larval stages (Yin and Hu, 2014). There is a debate regarding the peak expression of LINGO1 mRNA during murine postnatal development. While it is agreed that there is an increase postnatally, the peak of expression has been reported variously at P1, P4 and P21. A substantial decrease in expression is observed before stabilisation during adulthood (Mi et al., 2004; Llorens et al., 2008; Shao et al., 2017). A similar pattern is observed with protein levels, which increase to a peak at P21 in mice (Llorens et al., 2008). CNS LINGO1 protein is observed at its highest levels within the axons of neurons, however LINGO1 is also expressed at significant levels in oligodendrocytes, albeit at lower levels (Mi et al., 2005; Satoh et al., 2007; Ahmed et al., 2013; Meabon et al., 2015).
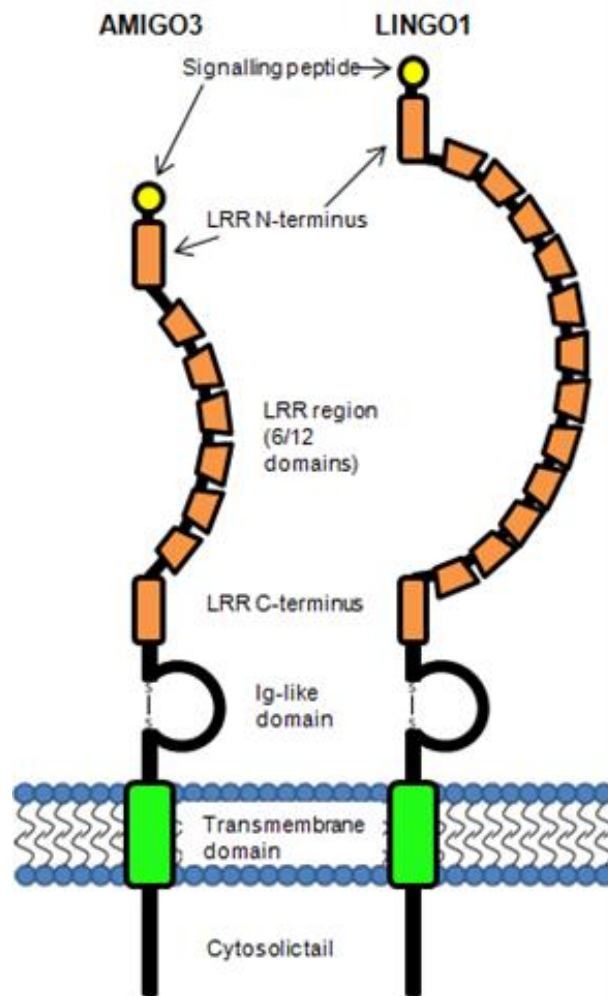
Figure 1.6: Representation of the structures of AMIGO3 and LINGO1. Both structures contain the characteristic components of LRR proteins, a small cytosolic tail, a transmembrane domain and an extracellular structure. The extracellular structure contains an Ig-like domain, the LRR region as well as a signal peptide. The main structural difference between the proteins is that AMIGO3 has 6 LRR compared to 12 for LINGO1 in the LRR domain.

1.4.2   LINGO1: CNS disease

1.4.2.1   CNS Trauma

The first role attributed to LINGO1 in the CNS was the inhibition of axonal regeneration. Mi *et al* (2004) showed that inhibiting LINGO1 through knockdown or treatment with anti-LINGO Fc fusion proteins resulted in an increase in neurite outgrowth of cultured cerebellar granule cells. The reverse was observed when LINGO1 expression was increased. This demonstrates that LINGO1 acts an inhibitor of neurite growth *in vitro* (Mi et al., 2004).

LINGO1 is able to bind to the NgR1 receptor complex and is required for the complex to transduce its signal. The NgR1 receptor complex is able to bind to myelin derived proteins including neurite outgrowth inhibitor A (Nogo-A), oligodendrocyte myelin glycoprotein (OMGP) and myelin associated glycoprotein (MAG), as well chondroitin sulphate proteoglycans (CSPGs) produced by reactive astrocytes (Ahmed et al., 2005; Yiu and He, 2006; Dickendesher et al., 2012; Ahmed et al., 2013; Saha et al., 2014b; Iobbi et al., 2017). Interactions between these proteins and the NgR1 receptor complex leads to downstream signalling through activation of Ras homolog gene family, member A (RhoA)/Rho-associated protein kinase (ROCK) by Rho guanosine diphosphate-dissociation inhibitor (RhoGDI) anchored to the intracellular components of the NgR1 receptor complex. In axons, this leads to activation of cofilin, actin filament reorganisation and ultimately collapse of growth cone and inhibition of axonal extension (Ahmed et al., 2013). Furthermore, Nogo-A knockout mice show greater inactivation of cofilin, as well as greater levels of actin polymerisation in the growth of neurites. This was also correlated with longer

neurites, highlighting the importance of the NgR1 receptor complex for axon regeneration (Sandvig et al., 2004; Montani et al., 2009).

The NgR1-neurotrophin receptor complex consists of NgR1, p75 neurotrophin receptor (p75[NTR])/tumor necrosis factor receptor superfamily, member 19 (TROY) and a third integral protein which was first found to be LINGO1. COS7 cells transfected with the components of the NgR1 complex were only able to cause RhoA activation when also transfected with LINGO1 (Mi et al., 2004; Ahmed et al., 2013; Kwon et al., 2014). Antagonising LINGO1 with LINGO1-Fc leads to decreased activated RhoA in spinal cords and correlates with greater axon regeneration (Mi et al., 2013) *in vivo* after spinal cord injury. As such, it was found that LINGO1 expression must allow for the activation of the NgR1 receptor complex by myelin derived proteins, resulting in the inhibition of axon extension (Mi et al., 2004; Inoue et al., 2007; Jepson et al., 2012) (fig 1.7). Interestingly, LINGO1 mRNA and protein levels do not appear to rise until D10 following spinal cord injury (SCI) in murine models, therefore it appears unlikely that LINGO1 is performing a major function during the acute stages in the injury response (Ahmed et al., 2013).

1.4.2.2   Demyelinating diseases

LINGO1 has also been reported to have an impact on OLG, preventing the full differentiation of OPC and myelination of OL (Mi et al., 2013). LINGO1 knockout mice exhibit early onset myelination during developmental stages (Mi et al., 2005).
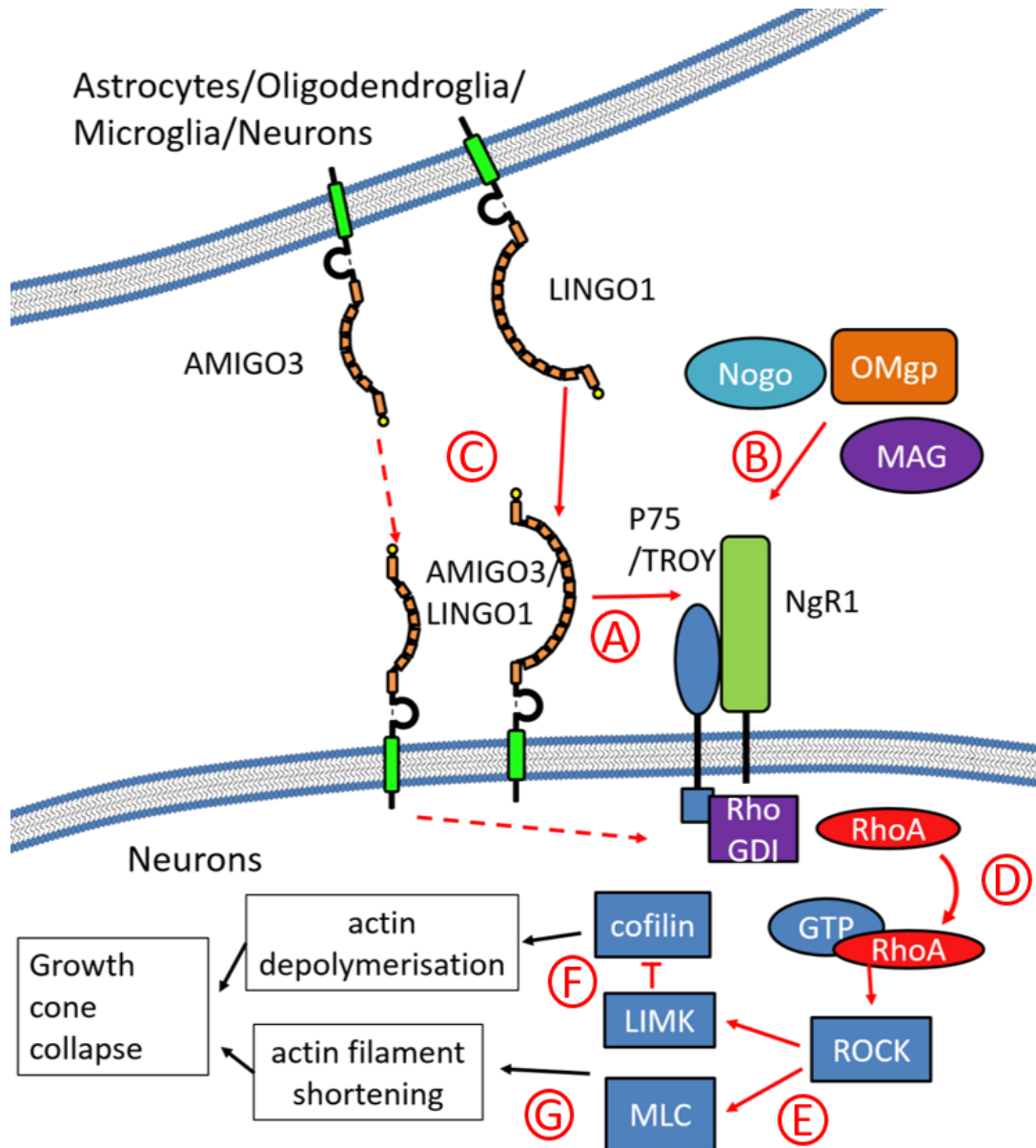
Figure 1.7: The method of action for LINGO1 and AMIGO3 in Neurons. (A) Both AMIGO3 and LINGO1 are able to form a complex with NgR1 and P75/TROY, known as the NgR1 receptor complex. (B) When bound, the tripartite receptor can respond and activate to myelin derived proteins, Nogo, OMgp and MAG. (C) It has also been hypothesised that AMIGO3 and LINGO1 could interact with neighbouring molecules intercellularly. (D) Activation of the NgR1 receptor complex leads to the intracellular activation of RhoA by local RhoGDI, leading to (E) ROCK signalling and further activation of LIMK and myosin light chain (MLC) on actin filaments. (F) LIMK inhibits cofilin resulting in actin depolymerisation (Fujita and Yamashita, 2014). (G) Activation of MLC also leads to shortening of actin filaments. These effects lead to growth cone collapse. Due to similar observations of RhoA activation following LINGO1 upregulation in OPC, it is possible that this method of action could also be present in OLG, affecting process extension and neuron adhesion (Foale et al., 2017).

Furthermore, a number of studies have linked LINGO1 directly to OLs both *in vitro* and *in vivo*. Overexpression of LINGO1 in cultured OLG and treating cultured OLG with soluble LINGO1, leads to a decrease in the production of MBP, with similar observations observed in rodents (Lee et al., 2007; Jepson et al., 2012). Correspondingly, inhibiting LINGO1 appears to have pro-myelinating effects. Inhibition, and genetic knock out, of LINGO1 leads to a greater production of MBP, promotes branching, promotes the production of myelin containing sheets, and correlates with greater OL/OPC ratios in *in vitro* rodent OPC cultures (Mi et al., 2005; Lee et al., 2007; Mi et al., 2008; Bourikas et al., 2010; Mi et al., 2013; Lee et al., 2014).

Furthermore, the inhibitory effects of LINGO1 on remyelination can be observed in disease states as well. In EAE, LINGO1 knock-out mice and mice treated with LINGO1 inhibitors demonstrated improved signs of remyelination compared to untreated and sham controls. This has been shown through greater levels of MBP as well as a larger count of axons ensheathed with myelin and reduced signs of axonal damage in CNS lesions (Mi et al., 2007; Mi et al., 2009; Bourikas et al., 2010; Li et al., 2017). EAE mice also have reduced clinical scores in the disease model and demonstrate greater spatial learning when treated with LINGO1 inhibitors (Bourikas et al., 2010; Mi et al., 2013; Sun et al., 2015). Finally, treating lysolethicin induced demyelinated C57BL/6 mice with anti-LINGO1, led to shorter latencies in the signal from transcranial magnetic motor-evoked potentials (tcMMEPs) 4 weeks after demyelination, indicating an improvement in signal propagation in descending axons of the spinal cord. This demonstrates the functional restoration induced by inhibiting

LINGO1 in the acute demyelinating model (Zhang et al., 2015a). These data provide a strong link between LINGO1 and an inhibitory effect of this protein on remyelination in demyelinating conditions.

1.4.2.2.1 Mechanism of action in oligodendroglia

Various mechanisms of action have been proposed for how LINGO1 is able to produce an inhibitory effect on OPC differentiation and OL myelin production (fig 1.7 & 1.8). Firstly it was proposed that LINGO1 functions in OLG just as in neurons, through activation of the NgR1 complex and subsequent activation of RhoA (fig 1.7). This would theoretically interfere with actin filaments involved with both differentiation of OPC and the creation of processes for myelin production and axon ensheathment. This hypothesis is supported by the fact that myelin debris inhibits OPC maturation and myelin production, a likely response to prevent too much myelin being produced in one area (Plemel et al., 2013). Additionally, higher levels of LINGO1 have been correlated with higher levels of activated RhoA in OPC (Mi et al., 2005; Jepson et al., 2012; Kwon et al., 2014) and LINGO1 has also been found to regulate actin filament formation in cultured rat OPC through the phosphorylation of cofilin (Fujita and Yamashita, 2014; Brown and Verden, 2017; Shao et al., 2017). Despite this data, there is evidence that NgR1 is not expressed on OLG, raising questions to the validity of this hypothesis. The evidence behind this claim is not concrete however, and is from low power images of tissue samples or from hybrid human cancer cell lines generated from skeletal muscle, therefore unlikely to truly represent OLG
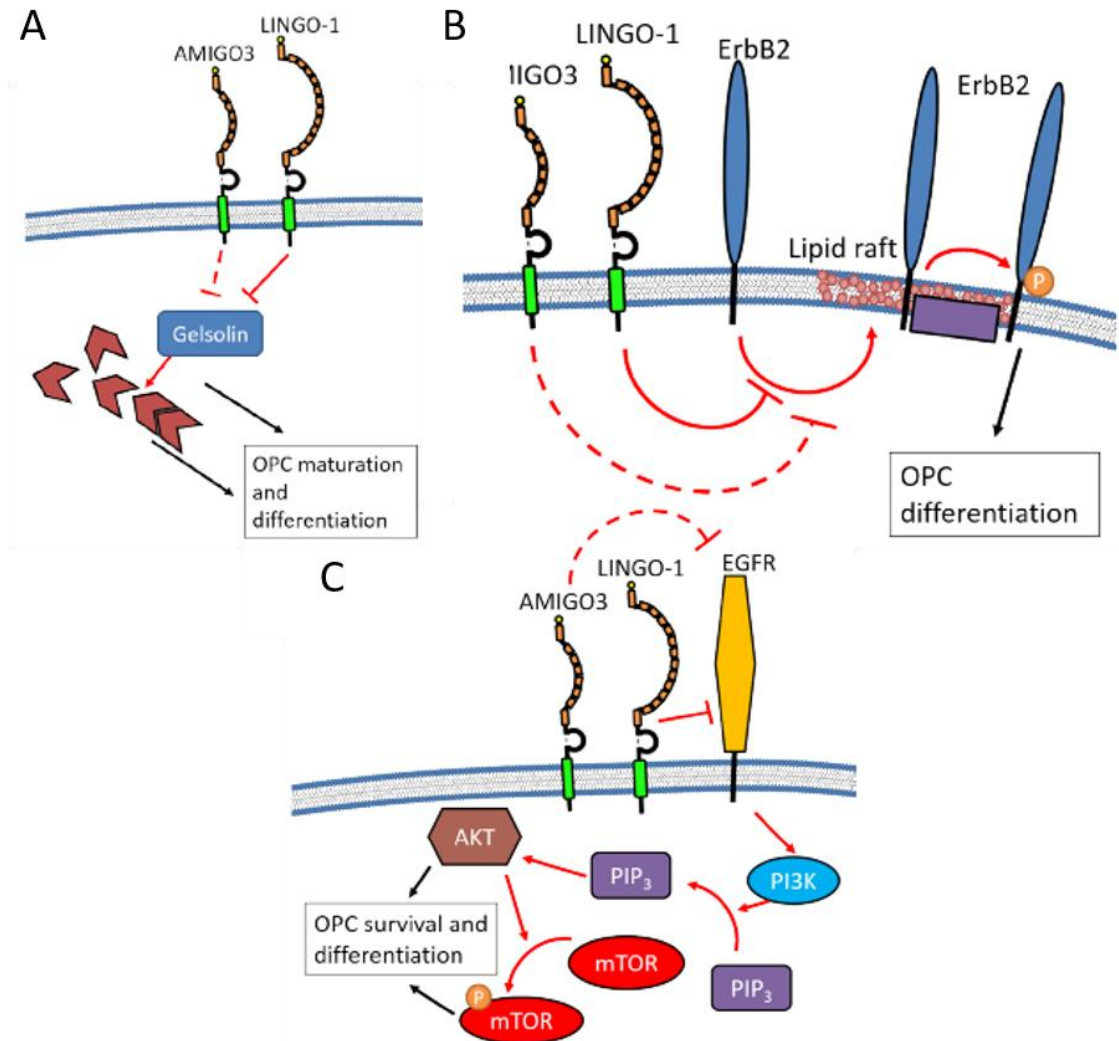
Figure 1.8: Potential methods of action for LINGO1 and AMIGO3 in OLG. (A) LINGO1 binds to ErbB2 and prevent its translocation to the lipid rafts on OLG membranes. ErbB2 is phosphorylated by local kinases and phosphatases at lipid rafts. Phosphorylated ErbB2 induces OPC differentiation by an unknown pathway (Mi et al., 2013; Lee et al., 2014). By inhibiting the translocation of ErbB2, LINGO1 indirectly blocks OPC differentiation. (B) Activated gelsolin is correlated with increased OPC differentiation, presumably through interactions with actin filaments. LINGO1 binds to and inhibits gelsolin, inhibiting its action (Shao et al., 2017). (C) LINGO1 signals through the PI3K/AKT/m-TOR pathway in dopaminergic neurons and OLG. LINGO1 directly inhibits EGFR signalling, preventing EGFR from activating PI3K (Inoue et al., 2007). This in turn prevents phosphorylation and activation of PIP2, consequently preventing the activation of AKT and m-TOR. Both activated AKT and m-TOR are implicated in OPC survival and differentiation, therefore the LINGO1 induced inhibition of EGFR will also lead to inhibition of OPC maturation and could lead to apoptosis (Dienstmann et al., 2014). The homologous structures and roles in neurons suggest that AMIGO3 has the potential to function through the same pathways as LINGO1. Dashed arrows indicate speculative interactions (Foale et al., 2017).

(Satoh et al., 2005; Bourikas et al., 2010; Jepson et al., 2012; Mei et al., 2013). As such, the NgR1 signalling pathway could still be a valid mechanism for LINGO1 actions in OLG.

A number of other signalling pathways have also been identified for LINGO1 in OLG. Gelsolin (GSN), another protein related to the actin cytoskeleton has been linked with LINGO1. LINGO1 decreases the levels of gelsolin (GSN), an actin severing protein. GSN has been associated with myelin production, as demonstrated in both rat OPC cultures and Sprague Dawley rats following lysolethicin induced demyelination. Inhibiting LINGO1 in rat OPCs when simultaneously encouraged to differentiate leads to higher levels of GSN protein and mRNA suggesting a role for GSN in LINGO1's inhibition (Shao et al., 2017) (fig 1.8A).

LINGO1 has been demonstrated to be able to interact homophically with neighbouring LINGO1 molecules. It has been proposed that due to this homophilic interaction between LINGO1 molecules, that LINGO1 may be able to interact intercellularly between neighbouring glia/axons. Rat OLs demonstrate an increased myelin production when cultured with soluble LINGO1 as well as with astrocytes/neurons that were induced to overexpress LINGO1 (Jepson et al., 2012). Conversely, COS7 cells transfected with solely LINGO1 do not show a rise in activated RhoA levels, suggesting that LINGO1 self-interactions do not produce the necessary downstream effects (Mi et al., 2004). Of course, this could simply be a result of COS7 cells lacking the required machinery that OLG possess to transduce the signal.

Lee *et al* (2014) suggested a convincing pathway, through interactions with the tyrosine kinase, human epidermal growth factor receptor 2 (ErbB2). Phosphorylated ErbB2 has been correlated with OPC maturation as well as MBP expression (Mi et al., 2013; Lee et al., 2014). LINGO1 appears to bind to the unphosphorylated ErbB2 and prevent its translocation to lipid rafts on the membrane. As ErbB2 is phosphorylated at the lipid rafts, LINGO1 indirectly prevents the phosphorylation and subsequent MBP production and OPC maturation (Lee et al., 2014) (fig 1.8B).

The AKT/m-TOR, WNK1 and BDNF/TrkB pathways have all also been implicated with LINGO1 signalling in OLG (Sun et al., 2015; Zhang et al., 2015b; Meabon et al., 2016) (fig 1.8C). PIP3 leads to the phosphorylation and activation of the AKT/m-TOR pathway, which appears to be integral in promoting the ensheathing of the axon through regulating the wrapping via the inner surface of the ensheathing process. (Snaidero et al., 2014; Purger et al., 2016). Furthermore, phosphorylated mTOR and constitutively activated AKT have both been correlated with enhanced myelination and OPC differentiation *in vivo* (Flores et al., 2008; Narayanan et al., 2009; Sun et al., 2015). LINGO1 prevents the phosphorylation of both AKT and mTOR, thereby blocking the pro-myelinatory effects of PIP3 (Sun et al., 2015).

WNK1 is an inhibitory protein for both OPC maturation and OL myelin production and incorporating siRNA against WNK1 leads to greater MBP production and a greater number of NG2+ processes visible in cultured rat OPCs. Similarly, WNK1 is able to form precipitates with LINGO1 *in vitro*, and inhibiting the action of WNK1 leads to greater levels of RhoA, admittedly in neurons. Exactly how the interaction between WNK1 and LINGO1 would lead to changes in levels of RhoA is unclear but

this interaction remains another potential method of action for LINGO1 to function within oligodendrocytes.

Finally TrkB has been demonstrated to be integral in OLG, with knockout mice showing a reduced ability to create mature OLs, resulting in unviable pups, as well as conditional knockout mice demonstrating a decrease in myelinated axons (Klein et al., 1993; Wong et al., 2013). LINGO1 has been shown to be able to interact with TrkB, which in turn appears to lead to a reduction in TrkB. It is suggested that LINGO1 aids the translocation of TrkB to lysosomes, resulting in the degradation of TrkB (Meabon et al., 2016). Although this has not been demonstrated to lead to demyelination, it does present another potential pathway for the action of LINGO1 in OL.

1.4.2.2.2   Clinical trials

LINGO1 based therapies have advanced to clinical trials to treat demyelination, with phase 2 trials showing moderate signs of success. Antagonising LINGO1 with an anti-LINGO1 antibody, opicinumab, in patients suffering from optic neuritis led to a greater propagation rate along the retinal nerves following treatment for 24 weeks. However retinal thinning still occurred and there was no significant improvement in disease symptoms (Ledford, 2015; MS-Society, 2016; Cadavid et al., 2017).

1.5 AMIGO3

Another LRR protein of relevance to myelination/demyelination, and one which has recently become of interest to our group is the LINGO1 analogue protein,

AMIGO3. All three proteins of the AMIGO family have been identified in the CNS. Interestingly, AMIGO1 and 2 both appear to have neuroprotective properties, whereas AMIGO3 has recently been shown to inhibit repairing mechanisms of the damaged CNS (Ahmed et al., 2013).

1.5.1 Endogenous expression

Unlike LINGO1, in the adult mouse, AMIGO3 is observed outside of the CNS. Significant levels are found within the adult murine liver, intestines and lungs, although much higher levels are observed in the adult CNS (Kuja-Panula et al., 2003; Hossain et al., 2011; Ahmed et al., 2013). Interestingly, AMIGO1, another protein of the AMIGO family of proteins is purely expressed in the CNS, indicating a possible family specificity for CNS functions (Kuja-Panula et al., 2003). AMIGO3 mRNA has not been detected in embryonic mice (Homma et al., 2009), however unpublished data from our laboratory (Ahmed et al, unpublished), shows the presence of the AMIGO3 protein in the white matter of post-natal rodents indicating that AMIGO3 is present, and likely active, in the murine CNS during the critical stages of developmental myelination. Furthermore, in zebrafish, the transcripts for AMIGO3 are upregulated from day 4 post-fertilisation (dpf4), appearing to stabilise by dpf8 in the zebrafish brain (Zhao et al., 2014). This shows that AMIGO3 expression appears to be upregulated during the same stages of myelination which begins at dpf2 with the majority completed by dpf10 in zebrafish (Brosamle and Halpern, 2002; Strachan et al., 2017). AMIGO3 has been identified most significantly in neurons, but is also present in astrocytes and OLG (Ahmed et al., personal communication). There is currently no evidence to support its expression in inflammatory cells (Tickle, 2013).

1.5.2 Expression profile in disease

Just as with LINGO1, AMIGO3 is upregulated in rodents following CNS injury. A significant increase (four-fold) in AMIGO3 mRNA levels is observed 1 day following SCI, which rises to eight-fold by 10 days. LINGO1 levels however remain unaltered until 10 days following SCI (Ahmed et al., 2013). Similarly, EAE models demonstrate a lag between responses when LINGO1 levels are altered. LINGO1 KO rats and anti-LINGO1 treated rats do not show variation from control rats until the disease is developed, indicating that LINGO1 is unlikely to be playing a role in the acute stages of inflammatory demyelinating disease (Mi et al., 2007).

As well as being upregulated in murine SCI, our group has previously identified AMIGO3 expression in cultured murine OPCs, cultured OPC cell lines, as well as in both chronic progressive and secondary progressive MS samples. Notably, AMIGO3 mRNA expression appears to be increased in both forms of the disease compared to healthy controls, and levels of AMIGO3 mRNA appear to be greater than LINGO1 levels in all forms of the disease (fig 1.9) (Ahmed et al., personal communication; Foale et al,. 2014). This suggests that AMIGO3 is playing a more important role than LINGO1 even in developed forms of MS. On top of this, AMIGO3 has been
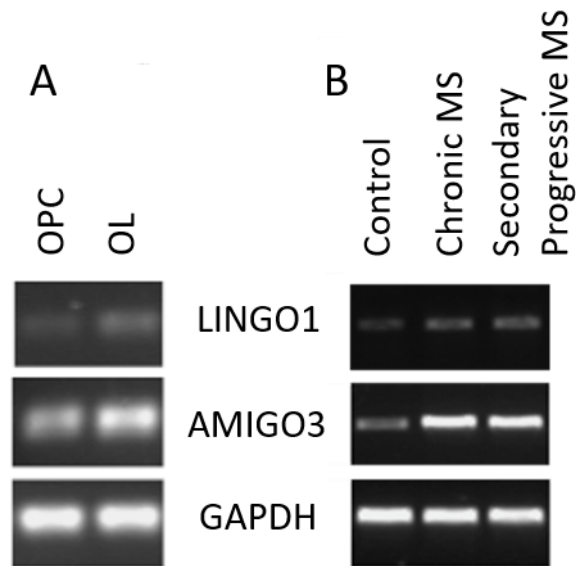
Figure 1.9: AMIGO3 and LINGO1 expression in (A) cultured murine OPC and (B) human MS post-mortem brain samples as measured by RT-PCR after 26 cycles. (A) AMIGO3 expression is found at higher levels in mature OL but also in relatively high levels in OPC. AMIGO3 expression is also observed at higher levels in chronic RRMS and secondary progressive MS than in healthy controls. LINGO1 levels also increase but are not as noticeable compared to AMIGO3 increases. GAPDH used as a housekeeper. Images produced by Ahmed et al (unpublished).

co-localised through immunohistochemistry (IHC) to markers of astrocytes and OLs, in murine EAE and optic neuritis models, demonstrating that AMIGO3 is not purely associated with neurons in demyelinating disease models (fig 1.10) (Ahmed et al., personal communication). These data support the hypothesis that AMIGO3 is playing a more active role than LINGO1 during inflammatory CNS disease states, and that its inhibitory actions in OLs may be relevant to strategies aiming to promote remyelination.

It is believed that the expression of AMIGO3 in astrocytes and, arguably more interestingly, in OLG, indicates that AMIGO3 must have a more diverse role in the injured CNS. Furthermore, as AMIGO3 interacts with the NgR1 receptor complex and functions without LINGO1 in neurons, it is possible that AMIGO3 replicates this function in OLG as similarly hypothesised with LINGO1 (Ahmed et al., 2013; Saha et al., 2014a; Foale et al., 2015). However, due to the conflicting reports of NgR1 expression on OLG, the exact mechanism that AMIGO3 would function through in OLG is unclear. Just as with LINGO1, AMIGO3 is able to form homodimers (Kuja-Panula et al., 2003; Chen et al., 2006; Kajander et al., 2011). It is therefore possible that it is able to bind to and activate itself, whether intercellularly or intracellularly. As OLGs have not been tested with raised AMIGO3 levels, it is unknown whether AMIGO3 self-interactions could modify OPC development. It is also possible that AMIGO3 could signal through any of the pathways that have been hypothesised for LINGO1 (fig 1.7 & 1.8) or even through any of the other pathways that are involved with OPC maturation and OL myelin production.
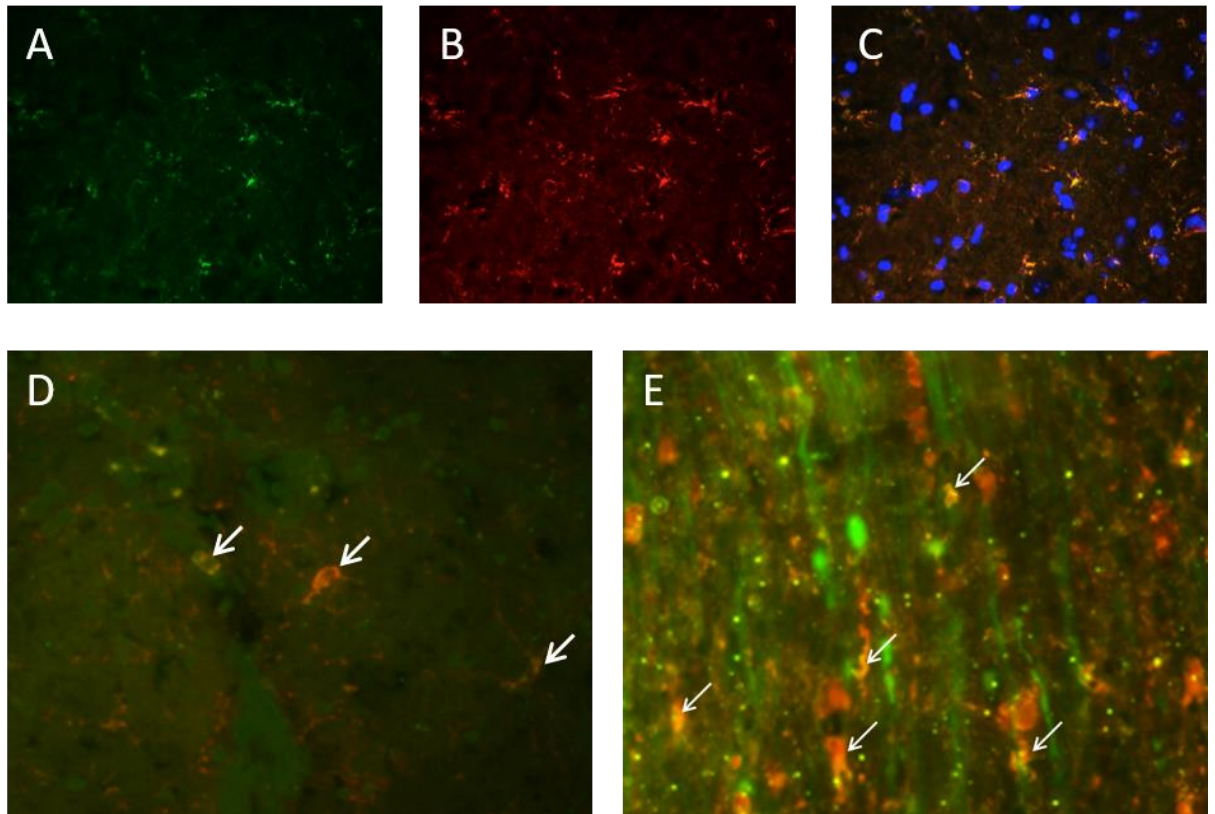
Figure 1.10: AMIGO3 colocalisation staining. (A-C) AMIGO3 (A) and Glial fibrillary acidic protein (B) as well as merged with DAPI (C), shows colocalisation of AMIGO3 with markers of astrocytes in murine samples. (D) AMIGO3 (green) and carbonic anhydrase II (CAII), a marker of mature OL, in EAE samples. (E) AMIGO3 and CAII in murine optic neuritis samples. AMIGO3 can be seen colocalised with markers of OL in animal models of demyelination (arrowheads). Images produced by Ahmed et al (unpublished).

1.6   Study rationale

As AMIGO3 is raised during CNS disease and shares a number of similarities to the inhibitory protein LINGO1, AMIGO3 is likely to be performing similar roles within the murine CNS. This has already been shown to be the case with the axonal NgR1 receptor therefore it is likely that AMIGO3 could perform similar co-interactions in other cell types as well. Along with the preliminary evidence that AMIGO3 is expressed by OLG, it is very likely that AMIGO3 has a function within OLG. Considering that AMIGO3 induces similar actions as LINGO1 in CNS neurons, it is likely that AMIGO3 will have an inhibitory role in OLG, inhibiting their maturation and myelin production.

Despite the promising signs for LINGO1 therapies, there have been a number of recent setbacks. Firstly, a lag of 14 days has been observed between anti-LINGO1 treatment and subsequent effects on clinical score EAE (Mi et al., 2007). This as well as the lag time between CNS injury and increases in LINGO RNA suggest that although LINGO therapies are able to alter OLG generation both *in vitro* and *in vivo*, they do not appear to make any change in the acute stages of demyelination (Ahmed et al., 2013). Secondly, although anti-LINGO1 therapies have also resulted in statistically significant increases in myelin thickens when compared to both IgG controls and untreated animals, as measured by the G-ratio, the changes were minuscule and not clearly beneficial to treated animals (Zhang et al., 2015a). Furthermore, despite anti-LINGO1 antibodies being utilised in clinical trials for treating demyelinating disorders, specifically in optic neuritis, the results have not

been as promising as predicted by the pre-clinical studies in rodents. Anti-LINGO1 antibodies enabled an increase in the propagation rate down the optic nerve, however this did not correlate with any symptomatic relief (Ledford, 2015; MS-Society, 2016; Cadavid et al., 2017). Unfortunately the study was not able to examine direct signs of myelin and OLG health and therefore it is difficult to confirm whether the moderate success was related to remyelination.

It is likely that due to the observed lag time between injury and LINGO1 expression changes, that LINGO1 based therapies will not act in sufficient time to encourage remyelination after the original demyelination. As such, LINGO1 is unlikely to be involved in inhibiting remyelination in acute stages following demyelination and therefore therapies aimed at inhibiting LINGO1 will not be sufficient to encourage rapid and efficient remyelination. Although LINGO1 based therapies may be able to eventually induce remyelination, this delay to remyelination will leave the axons vulnerable, limiting the effectiveness of these therapies.

Due to the much more rapid rise in AMIGO3 expression in the injured CNS, the preliminary evidence that AMIGO3 is expressed in OLG and the preliminary signs of AMIGO3 in MS, it is very possible that AMIGO3 is able to compensate for the function of LINGO1 in the acute stages of OLG disease. As such, examining the role that AMIGO3 plays in acute stages of demyelination could be a promising approach to develop novel therapies for remyelination and address a severe deficit in the treatment for MS and other demyelinating and dysmyelinating disorders.

1.7 Hypothesis and aims

We hypothesise that AMIGO3 is able to exert an inhibitory effect on OLG, preventing their differentiation into mature OLG, and creating the myelin sheath around axons. Additionally we hypothesise that AMIGO3 levels will be high in undifferentiated OPC and that trauma, such as that observed during inflammatory attacks in MS, will lead to an increase in the expression of AMIGO3 *in vivo* and *in vitro*. This in turn will lead to inhibition of remyelination during acute stages following demyelination. Furthermore, we hypothesise that the NgR1 receptor complex will be present on murine OLG and will provide a mechanism of action for AMIGO3 in these cells.

In this study, we aim to:

- Examine AMIGO3 expression during myelination, demyelination and remyelination.
- Examine AMIGO3 expression in OLG trauma and demyelinating disease.
- Determine what role, if any, the NgR1 receptor complex has in AMIGO3 OLG signalling

Chapter 2

Materials and Methods

2.1 *In vivo* procedures

2.1.1   Animals

All animals used in this study, unless stated otherwise, were cared for at the Biomedical Services Unit (BMSU) at the University of Birmingham. Animals were kept in a 12-hour light-dark cycle with food *ad libitum*. All animal procedures used were approved by the University of Birmingham's Ethical Review Committee. All procedures were also in accordance with the UK Home Office Animals (Scientific Procedures) Act (ASPA) 1986 under Home Office Project Licence provided by Dr Zubair Ahmed. Various strains of mice were used in the study, as specified throughout.

2.1.2 Experimental autoimmune encephalomyelitis

2.1.2.1   Principles of EAE

To examine *in vivo* remyelination, demyelination has to be induced. The model used in this study is EAE. EAE evokes autoimmunity to CNS proteins to induce neuroinflammation. It has been used with varying degrees of efficiency to investigate CNS auto-immunity. The primary use of EAE is to investigate MS as it shares a number of clinical and histological features with the human disease (Baker et al., 2011; Robinson et al., 2014b). Similarly to MS, EAE is an autoimmune disease where myelin derived proteins are targeted by the host's immune system, leading to neuroinflammation, oligodendrocyte degradation, and plaque formation within the CNS (Constantinescu et al., 2011).

EAE is induced through the priming of the animal's immune system to target myelin proteins. This can be done by injecting various myelin components, including PLP, MBP and MOG, as well as entire spinal cord homogenates. This is usually done with an adjuvant to activate the immune system (Robinson et al., 2014b). Depending on the exact model, the disease course can be chronic or acute as well as progressive or with relapses (Baker et al., 2011). Models have also been developed to focus on acute stages and only induce optic neuritis so that both early and late stages of the disease can be investigated (Furlan et al., 2009; Constantinescu et al., 2011).

Although rats were the predominate model traditionally used, recent advancements have led to mice being used more commonly, with the C57BL/6 strain the model of choice for most MS researchers (Constantinescu et al., 2011; Croxford et al., 2011; van der Star et al., 2012; Bittner et al., 2014). EAE models have also been described in marmosets and rhesus macaques, where disease course more closely follows MS progression and thus can more directly mimic the human disease (Slierendregt et al., 1995; Kap et al., 2010; Constantinescu et al., 2011; Baker and Amor, 2014). Additionally, a number of variations of the model have been described, inducing varying disease timeframes and courses (Baker and Amor, 2014).

In the early stages of disease, both EAE and MS are T cell mediated (Langrish et al., 2005; Aranami and Yamamura, 2008; Baker and Amor, 2014). CD4^{+} T cells interact with MHC class II molecules and become primed to react to myelin derived proteins. Additionally Th1 and Th17 cells have been shown to mediate EAE progression in a similar manner to MS (Korn et al., 2009). Furthermore, both EAE

and MS produce the characteristic CNS plaques with loss of myelin, a depletion of OLs/OPCs, axonal loss and infiltration of T cells, macrophages and in later stages, B cells (McCarthy et al., 2012).

Despite the similarities, it should be noted that the aetiology of MS is not clear. EAE however is an artificial disease, through induced immunity to CNS derived proteins and their antigens. As such, the model cannot truly compare the onset of disease. This difference in disease onset is also likely to result in discrepancies in disease progression. One of the major differences is that despite the complexity of the immune response in MS, the majority of immune cells found in MS lesions are CD8^{+} T cell derived whereas in EAE, lesions demonstrate a higher concentration of CD4^{+} T cells. Further criticism for EAE comes from the number of successful treatments for EAE that have not translated to MS (Constantinescu et al., 2011; Baker and Amor, 2014). There is a debate as to whether this is due to improper scientific activity by researchers, such as a lack of reproducibility or from making inflated claims from data (Baker and Amor, 2014), however it could also be that the disease course differs due to their variations (Sriram and Steiner, 2005) and may simply be due to the incompatibilities between murine and human immune systems (Baker and Amor, 2014).

Despite these differences, EAE has been instrumental in understanding the pathology of T-cell induced neuroinflammation and demyelination and has had a number of successes in producing therapies for MS demonstrating its value for further research. If used correctly, EAE parameters can be set to appropriately investigate certain features of MS. In this study, we are investigating OPC and OL

responses, rather than the immune response itself. As such, the exact mechanisms in the immune response should not be vital, rather just an inflammatory condition should be sufficient to provide an environment that is not conducive with OPC survival and maturation.

2.1.2.2   Advantages of EAE over other models of demyelination

A number of other models of demyelination have been developed and are efficient for inducing and investigating demyelination and remyelination. Those most predominantly used are the cuprizone model (Blakemore, 1974; Torkildsen et al., 2008), the lysophosphatidyl choline/lysolethicin (LPC) model (Praet et al., 2014; Keough et al., 2015) and Theiler's murine encephalitis virus (TMEV) model (Torkildsen et al., 2008; Nathoo et al., 2014).

The cuprizone model uses the copper chelator, bis-cyclohexanone-oxaldihydrazone (cuprizone). Addition of cuprizone in the animals' drinking water is believed to lead to inhibition of copper dependent mitochondrial enzymes, which disproportional affecting oligodendrocytes. This is turn leads to an inhibition of myelin protein synthesis, myelin lipid metabolism and OL death, effectively inducing demyelination (Wergeland et al., 2012; Praet et al., 2014). The model observes consistent cortical demyelination and subsequent axonal loss. Spontaneous remyelination can then be reliably observed as early as 4 days after the toxin is no longer applied, with extensive remyelination by 4 weeks (Matsushima and Morell, 2001; Lindner et al., 2008; Torkildsen et al., 2008).

Although a number of advancements have been with the cuprizone model, it maintains its weakness in that the exact mechanism behind demyelination remains unclear. Although the mitochondrial disruption theory is likely, it is not clear why this would lead exclusively to OL disruption and not a more global effect. It is very possible that uncertain side effects could be interrupting results obtained from the model. Additionally, as the model is more akin to toxic demyelination rather than autoreactive demyelination (Torkildsen et al., 2008) in that T cells are negligible to disease progression (Matsushima and Morell, 2001), and the BBB remains undisrupted (McMahon et al., 2002), the model cannot be viewed in relation to a neuro-inflammatory disease.

The LPC model requires precise injection of LPC into the white matter tracts of the spinal cord (Jeffery and Blakemore, 1995). This produces reliable focal demyelination, akin to MS plaques. This is thought to be brought about by a direct toxic effect due to the detergent properties of LPC (Denic et al., 2011; Lassmann and Bradl, 2017). An immediate response of demyelination, accompanied by acute inflammation is produced, followed by OPC migration and proliferation (Denic et al., 2011; Lau et al., 2012; Keough et al., 2015). One of the main advantages of the LPC model over EAE is that the site of demyelination is precisely where the injection was administered. This is also advantageous over EAE as although the sites of demyelination are predictable, they are not precise and require searching for following tissue collection. However due to the nature of the LPC injections, only larger rodents can be used and therefore mice, and the extensive genetic resources already developed, are excluded, complicating research (Keough et al., 2015).

Additionally, the inflammation is rapidly cleared thus remyelination therapies developed through this model may not be translatable, especially in the case of MS, as a similar environment to that observed in human demyelination, is unlikely to be found.

TMEV takes advantage of the RNA viruses' ability to induce demyelination in a monophasic or biphasic manner, after intracerebral injection (Nathoo et al., 2014). Intracerebral injections of this virus induce reproducible chronic demyelination which only affects the CNS and affects the animal for the remainder of its lifespan. It is not exactly clear how demyelination occurs, whether it introduces autoimmunity, directly attacks OLs, or through indirect effects due to CNS inflammation (Denic et al., 2011).

Despite the advantages of these models for easily and reproducibly inducing demyelination, it was decided that in this investigation, EAE would be used. This is primarily so that we could compare the demyelination and remyelination processes to that of a major human disease and therefore hopefully investigate a more translatable disorder. Additionally, due to our LINGO1 co-interaction hypothesis, we wanted to utilise the same models to directly compare our investigations to those involving LINGO1 based therapies.

2.1.2.3   EAE protocol

Two models of EAE were used for this project. Firstly, an acute disease model was used in our facilities to investigate the role of AMIGO3 in the acute stages of demyelination. Additionally, a monophasic model of EAE was used to examine the progression of disease and responses in the chronic disease state.

2.1.2.3.1   Acute EAE and optic neuritis

For the acute model, C57BL/6 mice were maintained at the BMSU as previously described. Animals were injected subcutaneously with 100µl of MOG$_{35-55}$/CFA emulsion (1mg/ml; Hooke Laboratories). The animals received a clinical score based on progression of the disease (table 2.1). In the early stage disease, animals were euthanised at treatment day 10 (D10) for optic neuritis and D14/19 for early EAE samples. Daily clinical scores were taken from D14 up until date of collection.

2.1.2.3.2   Relapsing-remitting EAE

A relapsing-remitting model of EAE was also performed and samples generously supplied by Professor David Baker and Dr Gareth Pryce (Blizzard Institute, Barts and London Medical School, UK). The model used 6-8 week old, male and female ABH Biozzi mice. Mice were specific pathogen free. The mice were maintained in a 12 hour dark/light cycle at 21°C with 55% relative humidity. Food and water was available *ad libitum*, with moist food provided during clinical stages of the model to prevent undereating.

The animals were treated and collected as previously described (Al-Izki et al., 2012). Briefly, at 6-8 weeks, the mice received 2, 150µl subcutaneous injections of spinal cord homogenate/ complete Freund's adjuvant as defined by Al-Izka *et al* (2012). Injections were made subcutaneously on both left and right hand sides of the

Score	Clinical observation
0	Normal.
0.5	A limp tail, characterised by some tone but the mouse is unable to hold its tail upright. When the tail is lifted by a finger, it can partially curve around said finger.
1	Flaccid tail.
1.5	Difficulty with righting reflex. Mice when placed on their backs will struggle to right themselves and will do so slowly.
2	Impaired righting reflex. Mice are fully unable to right themselves when inverted.
2.5	Hind-limb gait disturbance. Mice demonstrate difficulty with their walk.
3	Hind-limb paresis. Clear signs of partial paralysis and weakness in the hindlimbs.
3.5	Effective paralysis of hind-limbs, although some minor movement.
4	Hind-limb paralysis. Usually with signs of fore-limb paresis.
5	Paralysis of all limbs

Table 2.1: EAE scores and their corresponding clinical observations.

mice. The first injection was deemed on D0, with a repeat injection following the same procedure on D7, however injections were made below and more posteriorly than the previous. The animals were maintained until progressing to a score of 4 for 2 consecutive days. At this stage, animals were euthanised and samples collected.

2.2 *Ex vivo* procedures

2.2.1 Cell culture

2.2.1.1 Primary OLG

2.2.1.1.1 Preparation of primary OPC

Primary mixed glial cultures were obtained from C57BL/6 mice at postnatal day 0-2 (P0-2). P2 pups are the optimum collection age to obtain the highest number of OPCs before substantial differentiation occurs (O'Meara et al., 2011). Mixed glial cultures were obtained as previously described (O'Meara et al., 2011), with some modifications as described below.

Brains were dissected and isolated neocortices were disrupted physically by slicing, and enzymatically by trypsinisation containing DNAseI (0.2% v/v; Thermo Fisher Scientific) to prevent aggregation of cells. Cells were triturated and strained through a 70μm filter before centrifuging at 200xg, 10°C for 7 minutes. The cells were then seeded into 3 poly-L-lysine (PLL; Sigma-Aldrich) coated T25 flasks with 6ml Dulbecco's modified Eagle's medium (DMEM; Life Technologies) containing foetal bovine serum (FBS; Sigma-Aldrich) (10% v/v) and incubated at 37°C, 5% CO_2. Following 24 hours, the media was replaced to remove excess debris. The cells were

then maintained for two days before replacing 2/3 of the media with sterile N2 media, consisting of DMEM:F12 (Life Technologies), penicillin-streptomycin (1X; Thermo Fisher Scientific), L-glutamine (200mM; Sigma-Aldrch), insulin (50µg/ml; Sigma-Aldrich), apo-transferrin (100ng/ml; Sigma-Aldrich), putrescine (100µM; Sigma-Aldrich), progesterone (20nM; Sigma-Aldrich) and sodium selenite (30nM; Sigma-Aldrich). Every subsequent third day, a 2/3 media change with N2 media was repeated.

When the cells have reached confluency and OPCs can be observed propagating on top of the astrocyte monolayer at a reasonably high concentration (fig. 2.1), usually D8-10, pure OPCs were isolated and cultured. Mixed glial cultures were fastened securely to an orbital shaker at 37°C, 5% CO_2 and shaken at 160rpm for 30 minutes. This first shake is to remove weakly adhered microglia from the cultures. A full media change was performed to remove the floating microglia. For primary microglial cultures, this media can be centrifuged at 300xg, 10°C for 5 minutes and reseeded with DMEM containing FBS (10%). For primary OPC cultures, following the full media change, the mixed glial cultures were attached to the orbital shaker at 37°C, 5% CO_2 and shaken at 200rpm for 16 hours.

Following shaking, media was removed carefully to prevent dislodging of astrocytes. The media was then seeded in to 10cm tissue culture dish, 2 flasks worth of media per dish, and incubated at 37°C, 5% CO_2 for 30 minutes. This step was to remove any loose astrocytes/microglia that would have become dissociated in to the media during the shaking. As astrocytes and microglia are more adherent to plastic
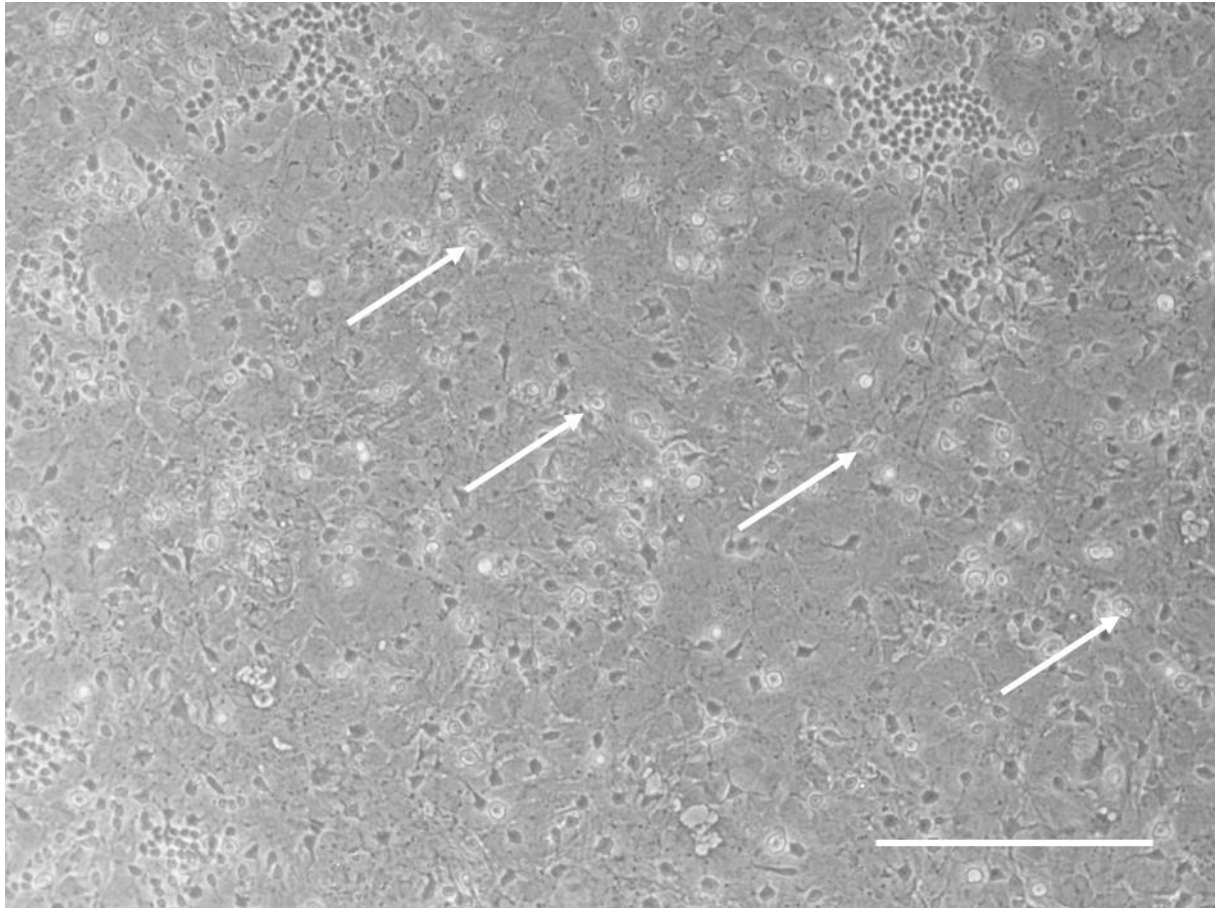
Figure 2.1: An example of the mixed glial cultures. The small circular cells with dual processes are OPCs, indicated by the arrows. A monolayer of large flat astrocytes can be seen coating the surface of the flasks which the OPCs are proliferating on top of. Scale bar represents 200μm.

than OPC, they will bind to the surface of the dish more readily than OPC so will not remain in solution. Every 10 minutes, the dishes were gently shaken to prevent the adhering of OPC to the base of the dish.

The media was then removed and centrifuged at 300xg, 10°C for 5 minutes. Supernatant was removed and cells were resuspended in 500µl of media. For OPC cultures, cells were resuspended in SATO media, consisting of DMEM supplemented with apo-transferrin (10µg/ml), insulin (10µg/ml; Sigma-Aldrich), putrescine (100µM), tri-iodo-L-thyronine (500nM; Sigma-Aldrich), sodium selenite (220nM), L-thyroxin (520nM; Sigma-Aldrich) and Horse serum (1%; Life Technologies), supplemented with bFGF (20ng/ml; Peprotech) and PDGF-AA (20ng/ml; Peprotech). OPCs were counted and seeded on Matrigel (Corning) coated surfaces and analysed following 24 incubation at 37ºC, 5%CO_2, as described per experiment. For mature OL, OPCs were suspended as for OPC cultures. After 24 hours incubation, media was replaced with SATO media, excluding the bFGF and PDGF-AA. Media was replaced on D3 and samples were collected on D5. Unless otherwise stated, OPC were dissociated from Matrigel coated surfaces by scraping with either a cell scraper or a 1000µl pipette tip if the wells were too small for a scraper. Scraping was performed with 500µl phosphate buffered saline (PBS) chilled to 4ºC. Following scraping, an extra rinse was performed with the PBS to ensure the maximum collection of cells possible. The solution was collected in a sterile Eppendorf tube which had been pre-chilled to 4ºC. This solution was then used for further processing.

2.3 *In vitro* procedures

2.3.1   Cell culturing

2.3.1.1   Oli-neu

Oli-neu cells are an immortalised murine cell line derived from primary mouse
OPCs. They are immortalised through the incorporation of a t-*neu* oncogene, leading
to the production of a constitutively active tyrosine kinase (Jung et al., 1995; Pereira
et al., 2011). These cells have been shown to express the OPC marker, NG2 (Jung
et al., 1995; Foale et al., 2014; Sakry et al., 2015). They also differentiate in to MAG
positive (an OLG marker) cells when treated with cAMP. Oli-neu also maintain the
ability to interact with axons both *in vivo* and *in vitro* (Jung et al., 1995). As such
these cells appear to express an OPC phenotype and as such Oli-neu cell cultures
are a useful tool for investigating OPCs. Despite this, Oli-neu do not appear to
produce dense, compacted myelin, indicating that they are not a perfect model and
that they lose some of their ability to fully differentiate in to mature OLs (Jung et al.,
1995). Finally as mouse EAE models were used in this investigation, mouse OPC
lines were chosen over other species. This ensured that our *in vitro* cell studies were
closely related to the *in vivo* experiments.

2.3.1.1.1 Collection and maintenance of Oli-neu cells

Oli-neu cells (originally provided by Prof Jacqueline Trotter, Johannes Gutenberg
University of Mainz) were stored at -80°C, with 500,000 cells in 400µl of freezing
media, which consisted of DMEM supplemented with FBS (20% v/v) and dimethyl

sulphoxide (DMSO) (10% v/v; Sigma-Aldrich). For experiments, Oli-neu cells were thawed at room temperature and suspended in SATO media. Following centrifugation at 150xg, 10°C for 5 minutes, the supernatant was removed and one sample of cells was seeded with 4.5ml of SATO in a T25 flask. The cells were then incubated at 37°C with 5% CO_2. When confluent, the cells were trypsinised and reseeded in a T75 flask with 10ml SATO and incubated at 37°C and 5% CO_2. When ~80% confluency is met, the cells were trypsinised and split as previously described.

2.3.2   Histology

2.3.2.1   Principles of Histology

2.3.2.1.1   Immunohistology

Immunohistology is used to localise specific antigens in either tissue samples, IHC, or cell cultures, immunocytochemistry (ICC). The technique utilises antigen specific antibodies, to highlight the localisation of specific proteins on a sample. A blocking protein such as bovine serum albumin (BSA) or non-immune serum is applied to coat the sample in non-specifically bound proteins and therefore prevent non-specific binding of the antibodies. A non-specific antibody will have a similar strength interaction to general proteins as the BSA, and thus is unlikely to displace bind and give incorrect signalling. This helps to reduce background staining. When examining intracellular antigen, a detergent is also applied to permeabilise the cells and allow infiltration of the antibodies (Polak and Noorden, 2003).

Following preparation of the samples, a primary antibody is applied which will only bind to the antigen of interest due to the blocking of non-specific interactions. This

primary antibody can contain a fluorescently probed tag or an enzyme, to produce signal directly. Alternatively, a fluorescently tagged secondary antibody targeted to the primary antibody, is used. The use of a secondary antibody step allows signal amplification since multiple secondary antibodies can bind to a single primary antibody (fig. 2.2) (Polak and Noorden, 2003).

Fluorophores will emit coloured light when excited by a specific wavelength of light. This can then be visualised and photographed for further analysis (fig. 2.2). An advantage of this system is that multiple antigens can be visualised independently on a single sample, providing that the fluorophores used are not excited by the same wavelengths of light. The antibodies used also have to be carefully chosen to ensure that they are not from the same/similar species and thus susceptible to crossover from the secondary antibodies (Polak and Noorden, 2003).

For fluorescent imaging, we also used 4', 6-diamidino-2-phenylindole (DAPI) as a counter stain. DAPI is a nucleic acid binding protein which greatly increases it fluorescent signal (at 461nm) when bound to regions of high adenosine-thymine interactions. As such, DAPI will only present signal when bound to DNA and thus highlights nuclei (Brisard and Rusling, 2007; Biancardi et al., 2013). As DAPI only binds to DNA, it is a useful tool for highlighting the nucleus and also for counting total cell numbers.
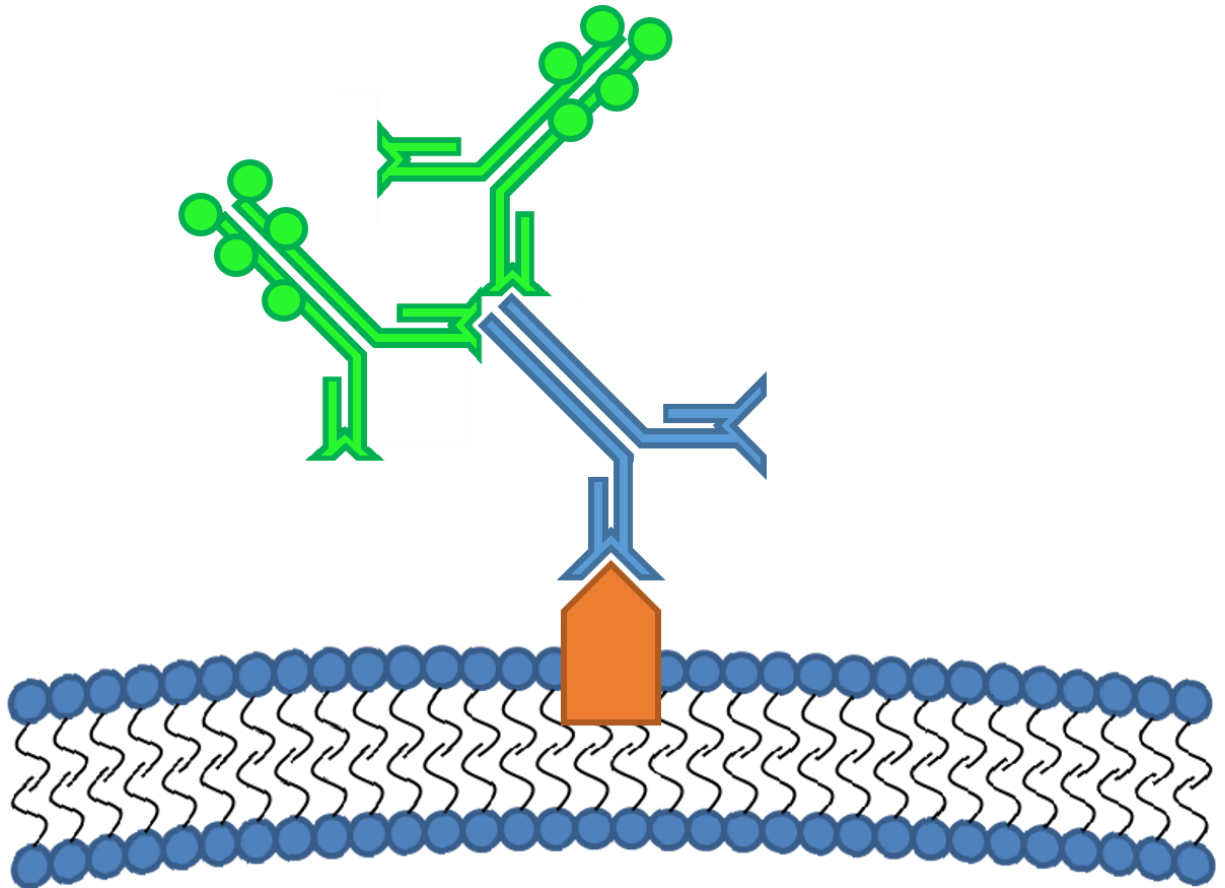
Figure 2.2: principles of Immunohistology. The primary antibody (blue) binds to the antigen of interest on the cell/tissue. Secondary antibodies (green) with labelled fluorescent probes can then bind to the primary antibody. Multiple secondary antibodies are then able to bind to the primary antibody and amplify the signal.

For enzymatic imaging, the secondary antibody contains a conjugated enzyme. When a certain compound is added, the enzyme will catalyse the conversion of said compound producing a colour change which can be visualised microscopically. In this study, diaminobenzidine (DAB) staining was used. The secondary antibody is biotinylated, meaning that when an avidin-biotin complex (ABC) is administered, the avidin will produce a strong interaction with the biotin. The ABC contains horseradish peroxidase which is able to oxidise DAB. When DAB is added to the ABC containing sample, the oxidation results in the generation of a brown colour which can be visualised under brightfield microscopy (Polak and Noorden, 2003). We used the nuclear staining compound, haematoxylin, in this study as a counterstain (Chan, 2014).

2.3.2.2   Processing of tissue for histology

Following dissection of tissue samples, as specified per tissue type, the samples were incubated in paraformaldehyde (PFA; TAAB laboratories) at 4°C. Incubation times varied for tissue samples as specified. Samples were then washed three times in PBS for 30 minutes. Following washing, samples were submerged in PBS with increasing concentrations of sucrose (10/20/30%). Samples were incubated for between 8-12 hours for cryoprotection. Tissue samples were submerged in optimal cutting temperature media (OCT) (TAAB Laboratories) and orientated upright. The samples were then snap-frozen with dry ice and stored at -20°C until use. The resultant frozen tissue blocks were then sectioned to 15μm using a cryostat microtome (Brights Instruments) and adhered to charged glass slides and stored at -20°C until required.

2.3.2.3   Processing of cell cultures for histology

Unless specified, cells were grown in 8 well chamber slides (Corning Falcon). Following treatment, cells were fixed with 4% PFA for 20 minutes. Fixed cells were then washed three times in PBS. Samples were then either used immediately or stored at 4°C for a maximum of 4 days.

2.3.2.4   Immunohistology Protocol

All stains were accompanied with a negative control, with no primary antibodies. Additionally, when more than one primary antibody was used, tests containing individual primary antibodies with all secondary antibodies were conducted to check that non-specific antibody interactions did not occur.

2.3.2.4.1.   Immunofluorescence

Immunohistology was performed as previously described unless stated otherwise (Ahmed et al., 2013). Slides were thawed for 30 minutes at room temperature before washing in PBS. After washing the sections were incubated in PBS-T (PBS containing 0.5% BSA and 0.5% Triton-X100) to permeabilise the tissue and block the sample from non-specific antibody binding. If all of the secondary antibodies used in the experiment were of the same species, 15% normal serum was also included, derived from the same species as the secondary antibodies (Burry, 2011). After incubation in a humidified chamber at room temperature for one hour, primary antibodies were applied at the stated concentrations in antibody diluting buffer (ADB). ADB consisted of PBS with 0.5% BSA (w/v) and 0.05% Tween 20 (v/v). Samples were incubated with 100μl of primary antibody/ADB solution for 14-16 hours at 4°C in

a humidified chamber. Following incubation, slides were washed in PBS. Secondary antibodies at the stated concentrations were applied in 100µl of ADB and samples were incubated in a humidified chamber at room temperature for 1 hour. Slides were washed in PBS and then a coverslip was mounted onto the slide using Vectashield mounting media (Vector laboratories). In some examples, this solution also contained DAPI.

2.3.2.4.2. DAB/ABC

For DAB/ABC staining, samples were prepared similarly to the protocol for immunofluorescence, however a biotinylated secondary antibody was incubated rather than the fluorescently labelled tag. This was performed in 100µl of ADB in the humidified chamber for 1 hour at room temperature. Following another PBS wash, samples were incubated for 30 minutes with ABC reagent (Vector Laboratories) and washed again in PBS. Sample were incubated with DAB solution (Vector Laboratories) for 5 minutes. A further wash in PBS was performed and then samples were incubated with Mayer's Haematoxylin (Thermo Fisher Scientific) for 1 minute and washed in PBS. The samples were dehydrated for in successive ethanol treatments (70%, 90% and twice in 100%, v/v), each for 5 minutes before being incubated in histoclear (National Diagnostics). This was performed 3 times for 5 minutes. Finally samples were mounted with Vectamount permanent mounting medium (Vector Laboratories).

2.3.2.5   Antibodies

The antibodies used in this study are listed below in table 2.2.

2.3.2.6　Imaging and analysis

Following labelling, sections were visualised using either a Zeiss Axioplan 2 epifluorescent microscope, equipped with an Axiocam HRc and imaged with the Axiovision software (all from Carl Zeiss Ltd), or a Zeiss Axiovert microscope equipped a differential spinning disc module (Revolution DSD1,Andor Technology) and a CCD camera (Andor Technology). Images were then thresholded and standardised using ImageJ (U.S.A. National Department of Health) to remove background staining and ensure that images could be compared fairly. Images were then randomised and anonymised to eliminate bias during analysis.

2.3.2.7　Semi-quantification of images

For the most part, histology was analysed qualitatively for localisation and expression patterns. In some cases it was possible to gain some quantification to examine the changing levels of expression. Multiple methods were used for semi-quantification; Total pixel counts, cell counts, and co-localisation cell counts.

Table 2.2: antibodies used for immunohistology and their sources.

Primary Antibodies		
Target	Source	Supplier (code)
AMIGO3	Rabbit polyclonal	Novus Biotech (NBP1-86405)
CC1	Mouse monoclonal	Calbiochem-Millipore (Cat. No. OP80)
CD4	Rabbit polyclonal	Novus Biotech (NBP1-19371)
CD8	Rabbit monoclonal	Novus Biotech (NBP1-79055)
GFAP	Rabbit polyclonal	Abcam (ab7260)
LINGO1 (C-15)	Goat polyclonal	Santa-Cruz (sc-48582)
LINGO1	Rabbit polyclonal	Abcam (ab23661)
MBP	Rat monoclonal	Millipore (MAB386)
Neurofilament-200 (NF200)	Mouse N52 clone, monoclonal	Sigma-Aldrich (N0142)
NG2	Rabbit polyclonal	Millipore (AB5320)
NG2	Mouse monoclonal	Abcam (ab20156)
NG2	Rat polyclonal	R&D (MAB6689)
NgR1	Rabbit polyclonal	Millipore (AB15138)
O1	Mouse polyclonal	Privately sourced
O4	Mouse monoclonal	R&D (Mab1326)
Olig2	Rabbit polyclonal	Millipore (AB9610)
OX42	Mouse monoclonal	Santa-Cruz (sc-53086)
Secondary Antibodies		
Target	Source	Supplier (code)
α-Goat Alexa Fluor (AF)488	Donkey	Molecular Probes (A11055)
α-Goat AF594	Donkey	Invitrogen [Molecular Probes] (A11058)
α-Mouse AF594	Donkey	Invitrogen (A21203)
α-Mouse AF594	Goat	Molecular Probes (A11032)
α-Mouse AF350	Donkey	Invitrogen (A10035)
α-Rabbit AF488	Donkey	Invitrogen [molecular Probes] (A21206)
α-Rabbit AF488	Goat	Molecular Probes (A11034)
α-Rat AF594	Donkey	Invitrogen (A21209)
α-Rat biotinylated	Rabbit	Vector laboratories (PK-6104)

2.3.3 Total pixel counts

Total pixel counts were used to examine the total distribution of a protein in a set area. Images were converted to display individual channels. A set sized region of interest (ROI) was applied to each image within a set anatomical region. This region was selected using the DAPI channel to prevent bias during ROI selection. Images to be quantified were then converted to binary images to only display only positive pixels over the threshold value. The total number of positive pixels within the ROI was then calculated and a percentage positive pixel count was analysed for quantification.

2.3.3.1 Pixel intensity

ROI were collected from samples as for pixel counts, however after thresholding, the average pixel intensity of positive pixels was measured.

2.3.3.2 Cell counts

ROIs and binary processing were applied as described above. Cells were then counted based on the number of areas with positive signal on the image. Automated counting was used attempt to minimise human error in the counting procedure. This was performed using the 'Particle Analysis/ITCN' plugin. This was predominantly used with DAPI, taking advantage of its nuclear expression.

2.3.3.3 Cell co-expression

Images and ROIs were generated as described above. The 'Colocalization' plugin on ImageJ was used to generate an image in which only pixels that were positive for

both proteins was displayed. The 'Particle Analysis/ITCN' plugin on ImageJ was then used to count the number of colocalised pixels.

2.3.4   Western Blot

2.3.4.1   Principles of Western Blot

Western blotting is a renowned technique for separating and visualising specific proteins from a mixture of proteins taken from a tissue or cell sample. In brief, a protein lysate solution is collected and heated with mercaptoethanol and sodium dodecyl sulphate (SDS). Heating causes denaturation of the proteins and disrupts the quaternary and tertiary structures, linearising the proteins. Mercaptoethanol breaks disulphide bonds between proteins, and SDS coats proteins in a negative charge. This results in unfolded proteins which have a net negative charge proportional to their size. The protein solution is inserted into a polyacrylamide gel, containing narrow pores which obscure the passage of proteins based on their size. As a result, when an electrical charge is supplied across the gel, short proteins migrate rapidly to the anode whereas large proteins migrate slower (Mahmood and Yang, 2012).

The proteins can then be transferred from the gel on to a membrane and visualised. Antibodies are used, similarly to that of Immunohistology, with a primary antibody against the protein of interest, and a secondary antibody to amplify the signal. Similarly to Immunohistology, immunofluorescence can be used, however in this study we used electrochemiluminescence (ECL). The secondary antibodies are conjugated with horse radish peroxidase (HRP), an enzyme which converts ECL agents to their luminescent form. This luminescence can then be recorded and

71

imaged, creating bands dependent on the quantity of the protein. Semi-quantification can be then performed on these bands (Mruk and Cheng, 2011).

2.3.4.2 Processing of samples for Western Blots

2.3.4.2.1 Cells

A protein lysis buffer (PLB) was used to disrupt the samples to obtain valid protein solutions. The protein lysis buffer was comprised of Tris-HCl (20nM; Sigma-Aldrich), NaCl (150mM; Sigma-Aldrich), ethylenediaminetetraacetic acid (EDTA) (1mM; Sigma-Aldrich), egtazic acid (EGTA) (0.5mM; Sigma-Aldrich), NP-40 (1% v/v; Thermo Fisher Scientific) and Protease inhibitor solution tablets (1 tablet per 10mls solution; Thermo Fisher Scientific). Two protocols were used, one for primary cells and one for immortalised cell lines.

Cell cultures were trypsinised and pelleted by centrifuging at 150xg, 10°C for 5 minutes. 50-100µl of ice cold PLB was added per sample. Primary cells had 50-100µl ice cold PLB added directly to the cell culture. The cells were then scraped and the resulting cell solution was triturated gently through a 27-gauge needle to disrupt the cell structure.

Following collection of the PLB-cell lysate solution for both primary and immortalised cell lines, the cell lysate solutions were vortexed at 1000rpm. The samples were then put on ice for 45 minutes and vortexed at 1000rpm every 10 minutes. After 45 minutes on ice, the samples were centrifuged at 8000xg, 4°C for 4 minutes. The supernatant was removed and the samples were stored at -20°C.

2.3.4.2.2   Tissue samples

Following dissection, samples were split in to roughly 25mg chunks and added to 500µl PLB. Samples were then homogenised with a mechanical homogeniser. Following homogenisation, the samples were vortexed at 1000rpm and put on ice for 45 minutes, being vortexed at 1000rpm every ten minutes. Samples were then centrifuged at 16000xg, 4°C for 20 minutes. The supernatant was removed and the samples were stored at -20°C.

2.3.4.3   Western Blot protocol

Gels were prepared with a resolving gel and a loading gel above which contained the loading wells. The resolving gel consisted of 2.75ml Protogel (Geneflow), 1.65ml Tris-HCl (1.5M, pH8.8), 2.2ml water, 66µl SDS (10% v/v;Sigma-Aldrich), 23.1µl ammonium persulphate (APS) (10% v/v; Sigma-Aldrich) and 9.9µl tetramethylethylenediamine (TEMED) (Sigma-Aldrich). The solution was then pipetted in to a 1mm cassette and ethanol was pipetted on top to prevent the formation of bubbles. This was then given 20 minutes to set at room temperature. The loading gel consisted of 0.4ml Protogel, 1.85ml Tris-HCL (0.5M, pH6.8), 0.75ml water, 30µl SDS (10% v/v), 15µl APS (10% v/v) and 7.5µl TEMED. This solution was similarly pipetted on top of the set resolving gel and given 30 minutes to set at room temperature.

A gel tank was filled with running buffer, which consisted of 3.03mg/ml Tris base (Sigma-Aldrich), 14.4mg/ml glycine as well as 5ml of 20% SDS/l of running buffer.

The western blot gel was submerged in running buffer in the chamber and connected to a power supply.

Cell/tissue lysis solutions were thawed on ice. Protein concentrations were then measured using the DC protein assay following the manufacturer's instructions (Bio-rad Laboratories), following the manufacturer's instructions. 5-30µg of total protein was mixed with a minimum of 5µl of lamelli blue buffer (Sigma-Aldrich) to make a total volume of 25µl. This solution was heated to 90°C for 4 minutes. Once heated, the samples were centrifuged at 8000xg for 5s.

Each protein lysis solution was then loaded into a well on the western blot gel, along with a protein ladder, and the samples were run at 150V, 45mA at room temperature for 110 minutes or until the proteins at the area of interest had separated sufficiently. Samples were run in running buffer, consisting of Tris Base (3.03g/L), glycine (14.4g/L; Geneflow) and SDS (0.01% v/v). Following electrophoresis, the bands were electrotransferred on to a methanol activated hydrophobic polyvinylidene difluoride (PVDF) membrane at 35V, 170mA for 110 minutes in transfer buffer, consisting of Tris Base (3.03g/L), glycine (14.4g/L), methanol (20% v/v) and SDS (0.01% v/v)

Following blotting, the membrane was removed, rinsed in TTBS solution for 5mintues at room temperature. TTBS consisted of Tris base (14g/L), Tris HCl (60g/L), NaCl (87.5g/L) and Tween 20 (500µl/L), pH 7.3. The membrane was then incubated with Marvel solution, consisting of TTBS with Marvel dried milk (5% w/v), for 1 hour at room temperature. The primary antibody was then applied to the membrane in Marvel solution overnight at 4°C.

Following incubation with the primary antibody, membranes were washed in TTBS before incubating with the secondary antibody in Marvel solution for 1 hour at room temperature. Finally the membranes were washed in TTBS before imaging. Membranes were imaged using ECL Western blotting reagents (GE Healthcare) following the manufacturer's instructions. Briefly, the ECL solution is applied evenly across the membrane and incubated in darkness for up to 1 minute. The membrane is dried, sealed inside a transparent plastic bag and then exposed to autoradiography film in darkness for the appropriate development time.

2.3.4.4 Antibodies

The primary antibodies used were the same antibodies for the Immunohistology studies. Housekeeper primary antibodies and secondary antibodies used for western blot analysis are listed in table 2.3.

Primary Antibodies		
Target	Source	Supplier (code)
Alpha-tubulin	Rabbit polyclonal	New England Biotechnologies (2144S)
HPRT1	Rabbit polyclonal	Enogene (E19-7463)
Secondary Antibodies		
Target	Source	Supplier (code)
α-Rabbit HRP	Goat	PI-1000
α-Rat HRP	Goat	PI-9400

Table 2.3: antibodies used for western blots and their sources

Gene	Forward primer	Reverse primer
α-tubulin	AAGCAGCAACCATGCGTGA	CCTCCCCCAATGGTCTTGTC
AMIGO3	AGACTTGGAGGATGTTCTGCC	TGAGTGCGTTGTGGCTCAAAT
HPRT1	TGCAGACTTTGCTTTCCTTGGTCAGG	CCAACACTTCGTGGGGTCCTTTTCA
LINGO1	CAAGAGAGACATGCGATTGG	TGGTTGAGTGTCTTGATGCG

Table 2.4: List of primers used in this study.

2.3.4.5   Semi-quantification of western blots

ImageJ was used to quantify the protein levels from the intensity and size of bands produced from the western blots. Briefly, imaged autoradiography film was scanned and images were imported to ImageJ. Integrated densities were measured for each band using the built-in gel plotting macros in ImageJ. Integrated densities from test samples were then normalised to the level of so-called 'house keeper' proteins chosen for their stable levels of expression (alpha-tubulin or β-actin).

2.3.5   PCR

2.3.5.1   Principles of PCR

The polymerase chain reaction (PCR) is an efficient technique for amplifying and measuring the concentration of DNA samples. In this study, only mRNA concentrations were measured, and thus needed to be converted to complementary DNA (cDNA) prior to PCR amplification. Reverse transcriptases are used to convert the mRNA samples to cDNA.

Thermosensitive synthetic oligonucleotides, DNA polymerase (Taq polymerase) and deoxynucleotide triphosphate bases are then combined with the cDNA sample in a thermal cycler to amplify the samples. The mixture is heated to 95°C, causing the cDNA strands to separate. The sample is then cooled to 50°C, allowing the primers to anneal before raising the temperature to 72°C, where Taq polymerase is activated and new DNA strands are replicated. This cycle can then be repeated to rapidly amplify the DNA samples (Eisenstein, 1990; Kramer and Coen, 2001).

For this study, we used SYBR green to quantify cDNA samples. SYBR green is able to bind to the minor groove within double stranded DNA (dsDNA), but is not able to bind to single stranded DNA. When bound to dsDNA, the dye emits a thousand fold greater fluorescence compared to when in solution (Tajadini et al., 2014). Therefore, as the reaction progresses and produces greater quantities of dsDNA, the greater the intensity of fluorescence from the sample. The number of cycles that are required to reach a set level of fluorescence, the threshold cycle (C_t), is inversely correlated to the concentration of original DNA.

2.3.5.2   Processing of samples for qPCR

RNA was collected from both cells and tissue for PCR analysis. For cell lines, the cell line was pelleted by centrifugation as per cell line. Supernatant was removed and the centrifugation was repeated twice with PBS to wash the cells. Following washing, RNA was collected from the samples using the RNeasy mini kit and Qiashredder kits (Qiagen) as directed on by the supplier.

For tissue samples, samples were cut in to 50mg chunks. These chunks were then loaded in to a cryotube with 500µl of Trizol and homogenised using a mechanical homogeniser for 1 minute, whilst incrementally increasing the speed of homogenisation. Samples were then incubated at room temperature for 5 minutes before adding 200µl chloroform and incubating for 5 minutes at room temperature. Samples were centrifuged at 10,000xg, 4°C for 15 minutes. The top layer of the subsequent solution (roughly 200µl) was removed and added to 700µl of 100%

ethanol. Samples were then briefly vortexed. These samples were then treated with the RNeasy mini kit (Qiagen) as directed by the supplier to collect pure RNA samples.

Concentrations of RNA samples from tissue and cells were measured using a Nanodrop spectrophotometer. Purity from contaminants was measured by examining the ratio of absorbance at 260/280nm. Readings of 1.8-2.1 were considered acceptable for use.

2.3.5.3 cDNA production

RNA was converted to cDNA using the SensiFAST cDNA synthesis kit (BIOline) as described by the supplier. Briefly, the RNA sample was added to 4µl of 5x Transamp buffer and 1µl reverse transcriptase as provided in the SensiFAST kit. DNase/RNase free water was added to the solution to make a final volume of 20µl. The samples were heated at 25°C for 10 minutes, 42°C for 15 minutes, 48°C for 15 minutes, 85°C for 5 minutes and finally held at 4°C for 5 minutes. Resultant cDNA samples were stored at -20°C until use.

2.3.5.4 qPCR protocol

Samples were amplified and analysed using SYBR green PCR master mix and IQ5 Optical System Software (BioRad Laboratories). A master mix solution was produced, containing 10µl SYBR green and forward/reverse primers at the optimised concentration per well used. cDNA was added at an equilibrated concentration and master mix/cDNA solution, topped up with RNAse free water to 20µl, was added in to

a 96 well plate on ice. The 96 well plate was centrifuged at 2000xg, 4°C for 5s. Following centrifugation, the 96 well plate was loaded in to the Biorad MyiQ PCR thermal cycler.

2.3.5.5 qPCR quantification

ΔCT values were calculated from SYBR green fluorescence by the BioRad IQ5 software. These values were then normalised against housekeeper genes and $\Delta\Delta$CT were calculated and converted to expression-fold changes.

2.3.5.6 Primers

Primers used for this study are listed in table 2.4.

2.4 Statistics

As all statistics were used between ordinal and continuous data, student t-tests, one way ANOVAs, Kruskal-Wallis tests or Mann Whitney U tests were used to analyse our samples. Prior to tests, samples were checked for both normal distributions and homogeneity of variances. If these assumptions were not met, samples were tested using the non-parametric, Kruskal-Wallis or Mann Whitney U tests. For ANOVAs, post-hoc Tukey tests were performed and for Kruskal Wallis tests, post hoc Bonferroni tests were performed. Significance was deemed when $p < 0.05$. All values are included with ± one standard error of the mean (SEM). All statistical analyses were performed using SPSS 22 (IBM).

Chapter 3

AMIGO3 expression during postnatal development

3.1 Rationale

As our preliminary data suggested that AMIGO3 is expressed in OLG, it was decided to examine whether AMIGO3 plays a role in OLG during development as well as if its expression has any relationship with the onset of myelination in postnatal mice.

3.1.1 Myelination during development

It was decided in this study to examine myelination in the corpus callosum (CC) since it provides a white matter region which is easily identified in multiple sections, and at multiple stages of development. It is therefore an ideal structure in which to visualise and analyse the development of myelin in the mouse CNS. The optic nerve is also a viable region for measuring the development of myelin during the same period, however it was considered less preferable to the CC since it is more difficult to extract at earlier developmental stages due to its size and its transparent appearance prior to myelination.

Myelination in the murine models appears to begin around P8-14, commencing laterally and progressing medially (Hamano et al., 1996; Shen et al., 2005; Calabrese and Johnson, 2013). Compact myelin is first observed around P17, with a rapid period of myelination between P14 and P21. By P21, the vast majority of myelination has occurred. The majority of the myelination of the corpus callosum can be seen from P35-40, although there is remodelling throughout life (Bjartmar et al., 1994; Hamano et al., 1996; Lodygensky et al., 2012). MRI images of whole murine and human brains show similar distributions, with myelination beginning after birth

and developing rostrally, with the frontal cortex receiving the last wave of myelination at around 18months (van Tilborg et al., 2018).

3.1.2 LINGO1 during myelination stages

LINGO1 expression appears very low during postnatal development. Its levels in the CNS rapidly increase around P4 and appear to decrease again during the main stages of myelination in mice. This led to the hypothesis that LINGO1 could be inhibiting myelination, and that its downregulation may enable myelination during development (Mi et al., 2004). Following this hypothesis, it would be valuable to examine whether AMIGO3 displays a similar pattern of expression as this would support a potential role in the mechanisms that suppress and promote OLG differentiation and myelination during postnatal myelination.

3.2 Aims

In this study we aim to examine the expression profile of AMIGO3 during development stages of myelination. Ideally we would like to examine the expression profiles in OLG to gain an insight in to the role of the LRRs during the early myelination stages. We also aim to determine the best antigens for analysing the changes in OPC maturation in the murine CC.

3.2.1 Hypothesis

We hypothesise that AMIGO3 expression will be high at the early stages of postnatal development however there will be a negative correlation between AMIGO3 expression and myelination. This would indicate that AMIGO3 will be reducing its inhibitory role on OPCs to allow OPC maturation and myelin production.

3.3 Experimental design and methods

3.3.1 Optimisation of IHC studies

Prior to embarking on the development study, antibodies were optimised on positive control tissue samples. Appropriate tissues were chosen based on a literature search. All mice used for the optimisation study were 6 weeks old as this meant that the animals had reached sexual maturity and were therefore likely to have reached full development, removing any variation based on age differences (Medina and Shepherd, 1981; The Jackson Laboratory, 2007; Yu et al., 2012).

3.3.2 Developmental studies

Coronal sections of mouse brains were collected which contained the CC as well as the lateral ventricles but did not include the hippocampi. This was to allow for a sufficient number of sections for all tests, but to limit any variation introduced by varying section position in the rostral-caudal axis. To determine the extent of myelination, the medial CC, immediately inferior to the cingulum, was chosen to be imaged. The medial CC rather than the lateral CC was chosen due to its more homogenous features in varying depths through the brain as well as the longer period for myelination to become completed, therefore a more gradual change in protein expression is likely to be observed (fig 3.1).

Incremental age groups were used for the development investigations. Mice were collected at P0, P7, P14, P21 and P28. This range was chosen to include the full range of myelination stages, P0 where myelination had not begun and (P8-14) with the initiation of myelination. It is not entirely clear when novel myelination finishes in

84

mice, considering that in a 'healthy' state, there is a constant turnover of mature OL from local OPC, therefore P28 was chosen as a terminal group when the majority of myelination and compaction has completed (Sturrock, 1980; Berger et al., 1991; Lodygensky et al., 2012; Chan et al., 2013; Yuen et al., 2014; Dai et al., 2015). For all developmental studies, n=4.

3.3.2.1   Immunohistochemistry

Due to the variation in volume and therefore time required to penetrate as well as saturate the tissue, the samples were left in 4% (v/v) PFA for varying times as shown in table 3.1. The choice of markers, and combinations to be used, in the main developmental study were dependent on the results obtained from these optimisation experiments. Total pixel counts observed in a uniform sized region of the medial CC (fig 3.1) were normalised against thresholds and quantified as previously discussed.

3.3.2.2   Western blots

Neocortices from neonate pups were isolated and dissected into 25mg chunks. Protein lysates were collected as previously described. Concentrations of primary antibody were as previously listed unless otherwise stated. Bands were visualised and analysed semi-quantitatively as previously discussed.

3.3.2.3   Experimental plan

A summary of the plan for the investigation, findings and experiments used is demonstrated in figure 3.2.
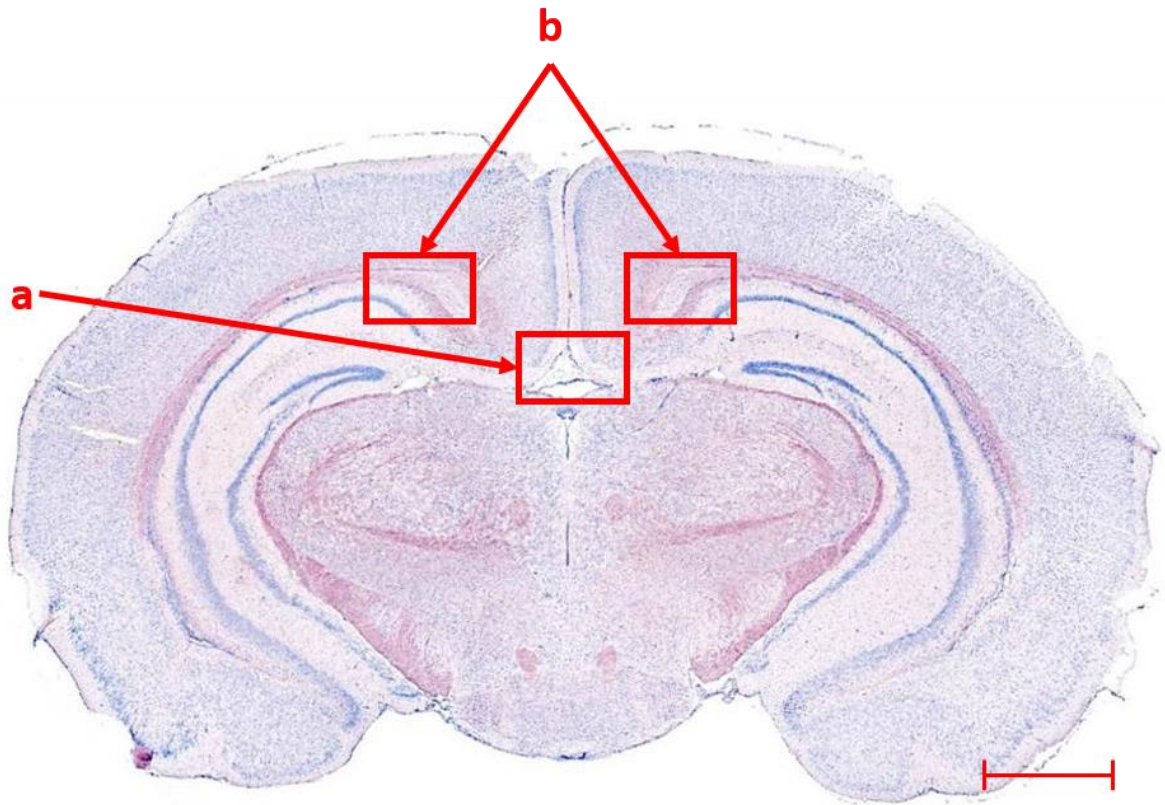
Figure 3.1: A coronal section of a mouse brain labelled with haematoxylin (blue) and Oil-Red-O (red). Images were taken at the medial and lateral corpus callosum as highlighted. Arrows indicate sites of imaging, where (a) is the medial CC and (b) is the lateral CC. Scale bar represents 1mm.

Age (postnatal day)	Length of fixation (hours)
0	2
7	4
14	6
21	18
28	24
Adult (6 weeks)	24

Table 3.1: length of fixation for dissected brains
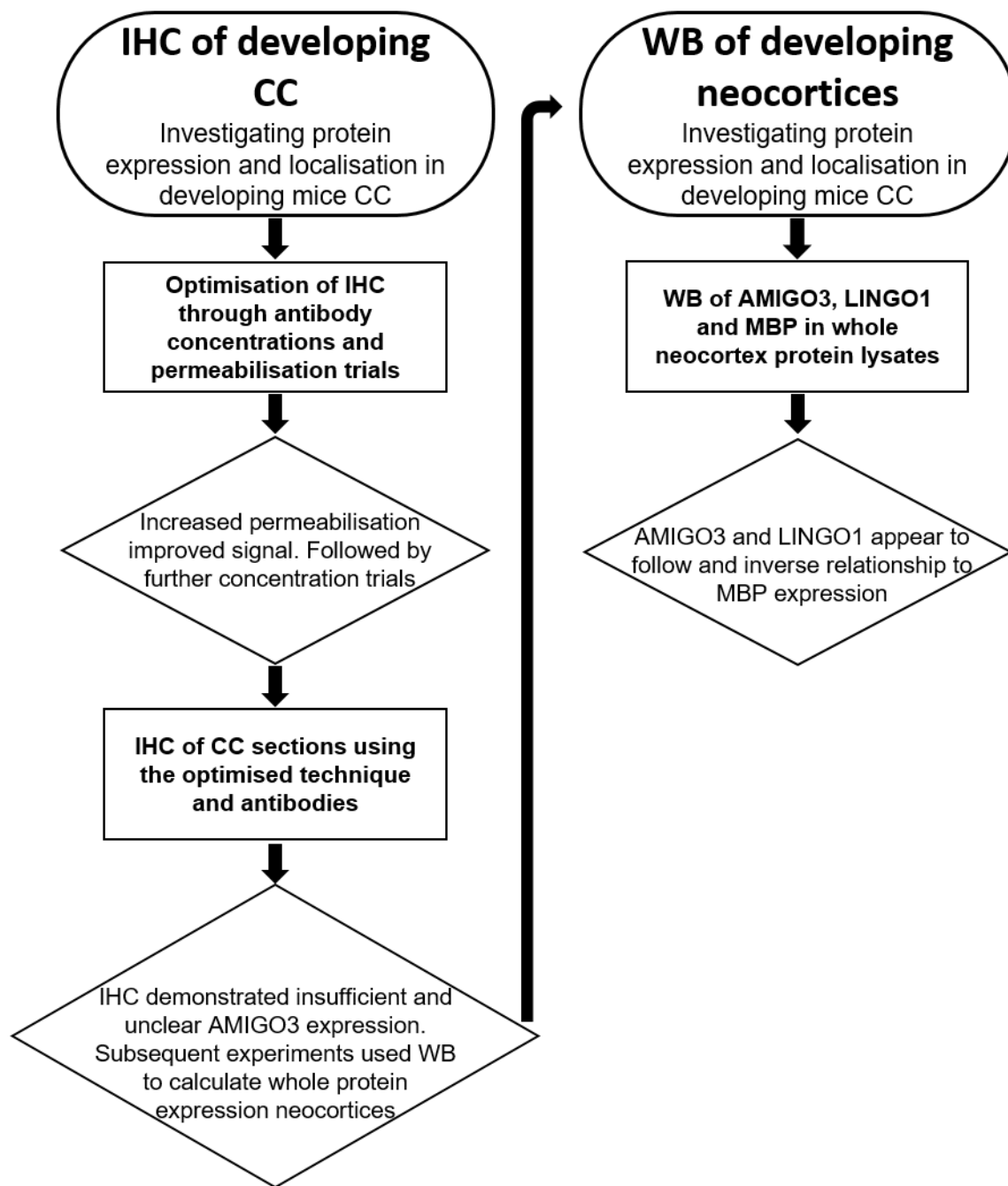
Figure 3.2: Flow chart demonstrating the plans and summarising the findings from chapter 3.

3.4 Results

3.4.1   Optimisation of immunohistochemistry

Immunohistochemistry for AMIGO3, CC1, LINGO1, MBP, NG2, NgR1 and Olig2 was performed using antibody dilutions previously used within this laboratory and as stated previously. Control tissues used for testing antibodies are listed in table 3.2. Where possible, samples for controls were collected using the same strains and dissection/preparation procedures as for the main studies.

Despite some signal being observed for AMIGO3, CC1, LINGO1 and NG2 (fig. 3.3A-D) the signal was weak and therefore it is likely that variation would be difficult to detect in the main developmental study. Signal was not observed in all tests, specifically NgR1 showed no signal (fig 3.3E). Furthermore, the minimal CC1 staining, as well as the LINGO1 staining, did not match previous studies, suggesting the staining observed may only be background (fig 3.3B & C). As a result, further optimisation was performed to improve the quality of the staining. OLIG2 and MBP antibodies however were observed to demonstrate reasonably strong signal (fig 3.3F &G)

3.4.1.1   Initial antibody concentration trials

Firstly, concentrations of antibodies used were tested to examine whether the lack of signal was simply due to a lack of available antibodies. Varying concentrations of CC1 antibodies were employed to test this whether the antibody was being used at sub-optimal concentration (fig 3.4). Qualitatively, 500 ng/mL and 1 µg/mL achieved a
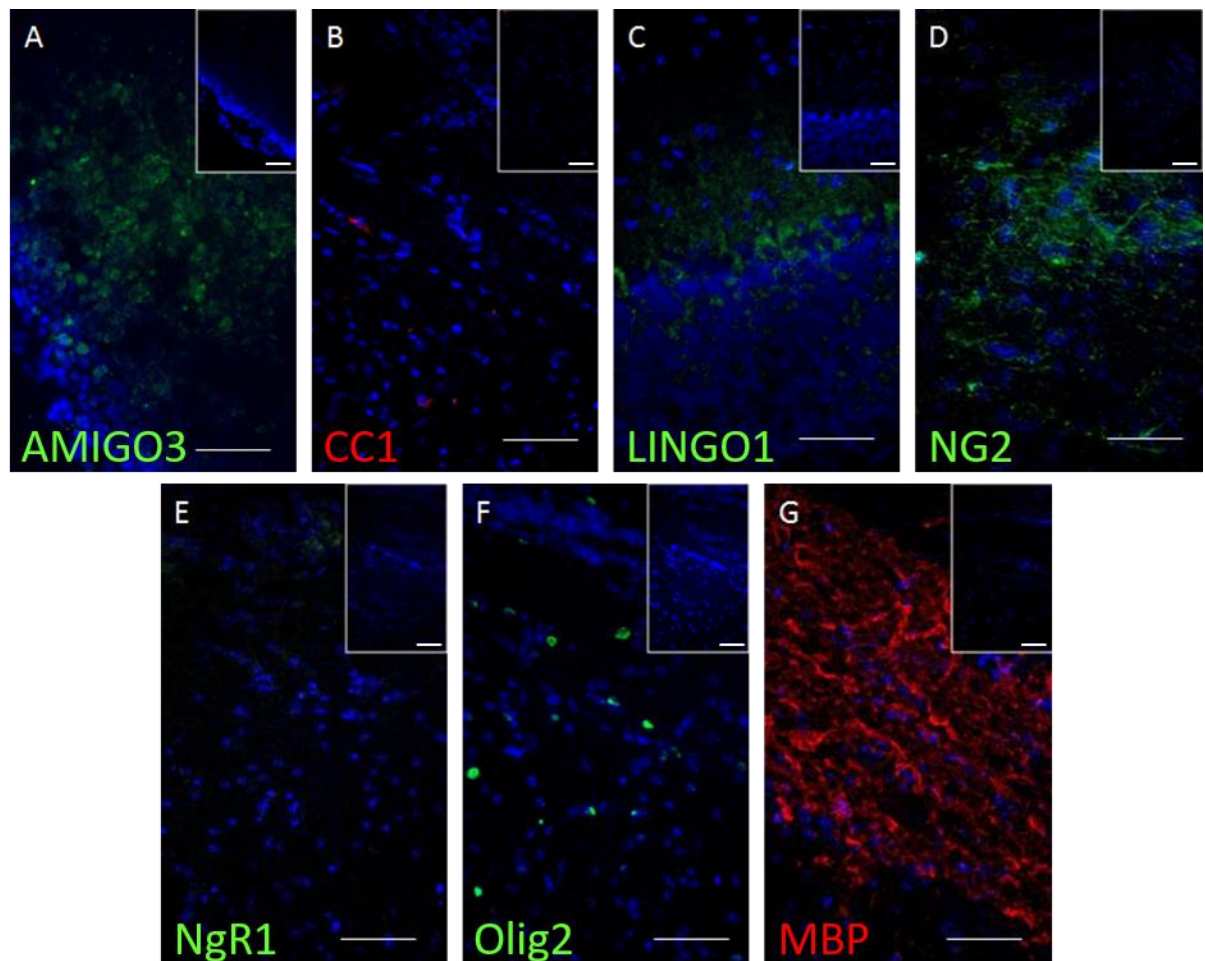
Figure 3.3: Representative positive control staining for (A) AMIGO3 in DRGs, (B) CC1 in the lateral CC, (C) LINGO1 in the cerebellum, (D) NG2 in the lateral CC, (E) NgR1 in the lateral CC, (F) Olig2 in the lateral CC and (G) MBP in the lateral CC. All sections were obtained from adult BALB/C mice. Blue shows DAPI staining and red/green shows the stated protein. Strong signal was observed with MBP, however all other markers showed limited signal. Scale bars represent 50μm, insets show negative controls, n=4 for each trial.
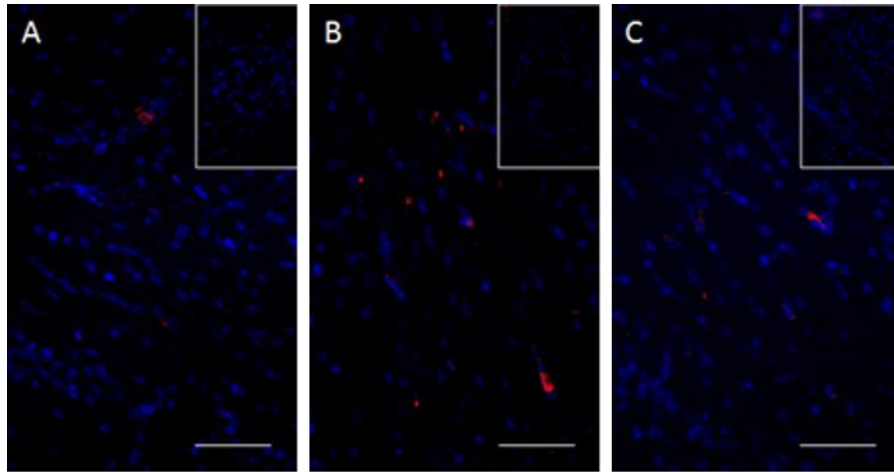
Figure 3.4: Representative staining for CC1 concentration trials. Images were taken of sections treated with anti-CC1 (red) antibodies at (A) 200ng/ml, (B) 500ng/ml and (C) 1µg/ml in the lateral CC. Blue shows DAPI staining. All image groups had a similar minimal intensity but maximum intensities were modified independently to produce the greatest qualitative signal. Scale bars represent 50µm, insets show negative controls, n=4.

minor improvement over the lowest concentration. However, overall fewer CC1^{+} cells were observed than expected for the CC which should contain a relatively high number of mature OLG. Due to the negligible improvements provided at higher concentrations of the antibody further optimisation was attempted.

3.4.1.2   Permeabilisation trials

We have previously found that a stronger permeabilisation treatment (2% (v/v)) Triton X-100 rather than 0.2%) is able to improve immunofluorescence signals in this system (Ahmed et al., personal communication). To assess whether the tissue samples were sufficiently permeabilised, samples were tested with a published technique previously used to stain thicker (300 µm) acute brain slices which involved a longer permeabilisation step (Fulton D et al., 2010). This method involved a single 4 hour block/permeabilisation step following the first wash. The blocking/permeabilisation solution consisted of 0.5% BSA (w/v), 0.1% or 2% (v/v) Triton X-100 and 15% normal serum (v/v). All subsequent steps followed the original protocol as previously described.

For this test, Olig2 was used due to the greater signal observed in the previous trials. It is apparent that there is a clear increase in the intensity of the Olig2 staining when treated with 2% (v/v) Triton X-100 (fig 3.5A-D). Furthermore, the extended blocking and permeabilisation treatment also permitted greater signal intensity (fig 3.5C-D & G-H). Although extended treatment with 0.1% Triton did improve the signal for Olig2, it was not as effective as treating with 2% Triton with the extended
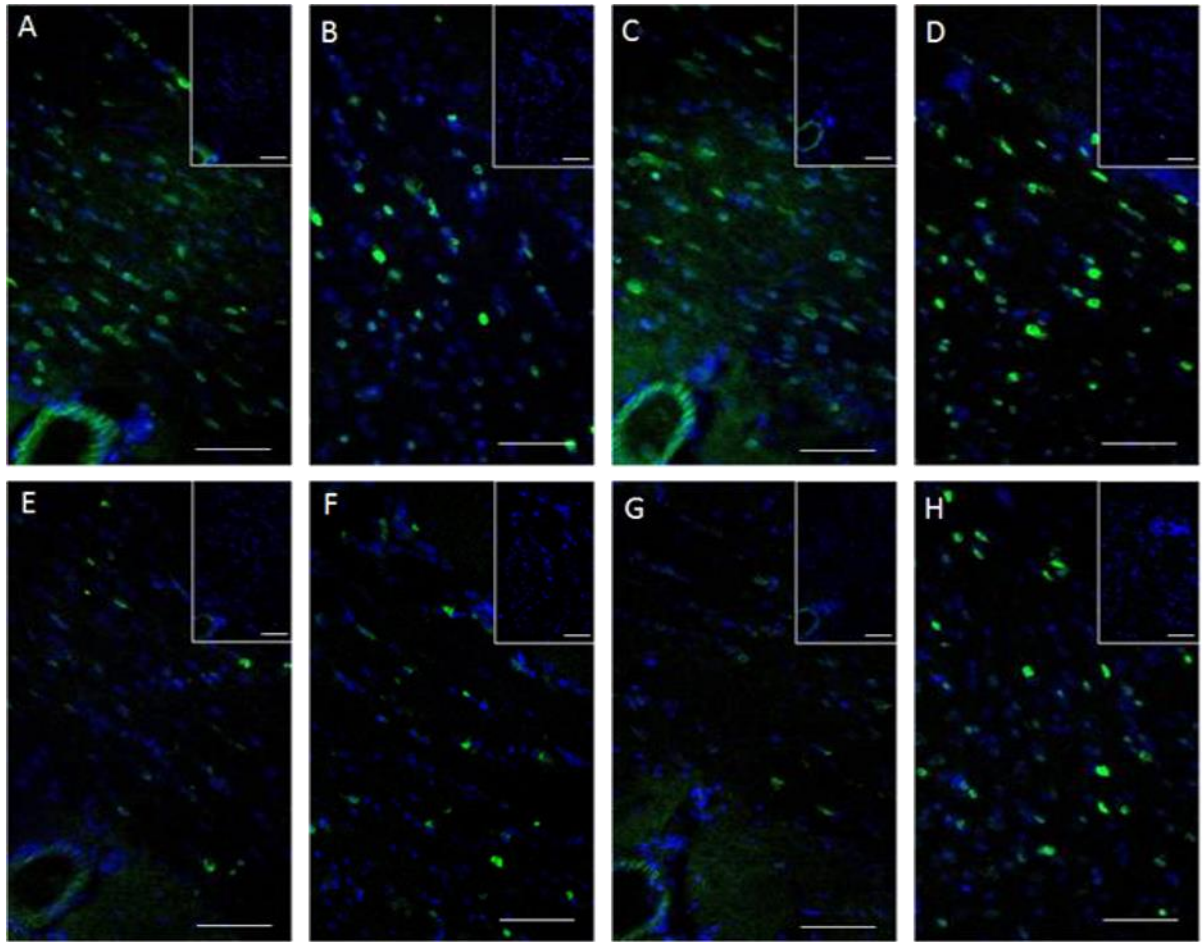
Figure 3.5: Representative 1/200 Olig2 staining (green) CC sections treated with the varying permeabilisation protocols. (A-D) Treatment with 2% (v/v) Triton following (A-B) the original protocol and (C-D) the new protocol. (E-H) Treatment with 0.1% (v/v) Triton following (E-F) the original protocol and (G-H) the new protocol. Images were either taken in the medial CC (A, C, E, G) or the lateral CC (B, D, F, H). Blue shows DAPI staining. For all images, varying minimal/maximal signal intensity adjustments were applied to produce the greatest qualitative signal. Increasing concentrations of Triton and treatment times appear to increase signal for Olig2 IHC. Scale bars represent 50µm, insets show negative controls, n=4.

incubation as well. As such it was decided that subsequent staining in this project would use a protocol involving permeabilisation in 2% (v/v) Triton X-100 for 4 hours.

To further optimise the staining, we tested whether further permeabilisation of the tissue would improve the signal. NG2 labelled sections were treated with the newly developed method of 2% (v/v) Triton X-100 for 4 hours to permeabilise the cells, or with 2% (v/v) Triton X-100 also in the ADB replacing Tween-20 as well as the permeabilisation step. Greater signal intensity was observed with the modified antibody incubation procedure, with Triton X-100 in the ADB (fig 3.6). Subsequent stains for all antibodies were therefore performed with 2% (v/v) Triton-X-100 in both the blocking/permeabilisation buffer as well as in the ADB.

3.4.1.3   Further antibody concentration trials

To further optimise the staining, concentration trials were performed.

3.4.1.3.1   AMIGO3

Due to the lack of signal, the anti-AMIGO3 antibody was trialled at a higher concentration. The antibody was tested at 1/100 (2µg/ml) and 1/50 (4µg/ml) (fig 3.7). In this study AMIGO3 was co-stained against anti-NF200 for reference. Interestingly, a degree of signal could be observed in all treatment groups, contradicting previous observations. It was determined that 1/50 would be used for subsequent studies.

Antigen	Tissue Sample	Source
AMIGO3	Dorsal Root Ganglion cells (DRGs)	A fairly widespread distribution with high levels observed in the DRG of mice (Ahmed et al., 2013) and preliminary data from our lab
CC1	Lateral CC	A monoclonal IgG recognising adenomatous polyposis coli protein in the cytoplasm of OLG. CC1 binding in the CNS are considered to be a specific marker for all differentiated OLs. The CC contains relatively high staining in mouse brains (Lin et al., 2006; Shen et al., 2008)
LINGO1	Cerebellum	Purely within the CNS, with high levels observed in the cerebellum (Llorens et al., 2008; Kuo et al., 2013)
MBP	Lateral CC	MBP is widespread within the brain, predominantly in the white matter. The CC contains relatively high levels (Mi et al., 2009; Guglielmetti et al., 2014; McQueen et al., 2014)
NG2	Lateral CC	NG2 positive cells are observed through the developing and adult brain, primarily in the CNS. The CC has relatively high levels (Clarke et al., 2012; Sullivan et al., 2013)
NgR1	Lateral CC	Present on most neurons, with levels being identifiable within the CC (Wang et al., 2006)
O1	CC	Presents clear staining within the CC of adult mice. O1 is expressed in the later stages of OPC differentiation, prior to full maturation (Sommer and Schachner, 1981; Liu et al., 2011)
O4	CC	Presents clear staining within the CC of adult mice. O4 appears to be a sign of OLG which have begun to differentiate, reaching a pro-OL stage (Gard and Pfeiffer, 1989; Sow et al., 2006)
Olig2	Lateral CC	Transcription factor present in all stages of OLG including OPC and differentiated OLG. Clear staining is observed in the white matter, including the CC of mouse brains (Cai et al., 2007; Maglione et al., 2010)

Table 3.2: Immunohistochemical markers used for examining OLG development are listed. Tissue sources used for positive controls are also included.
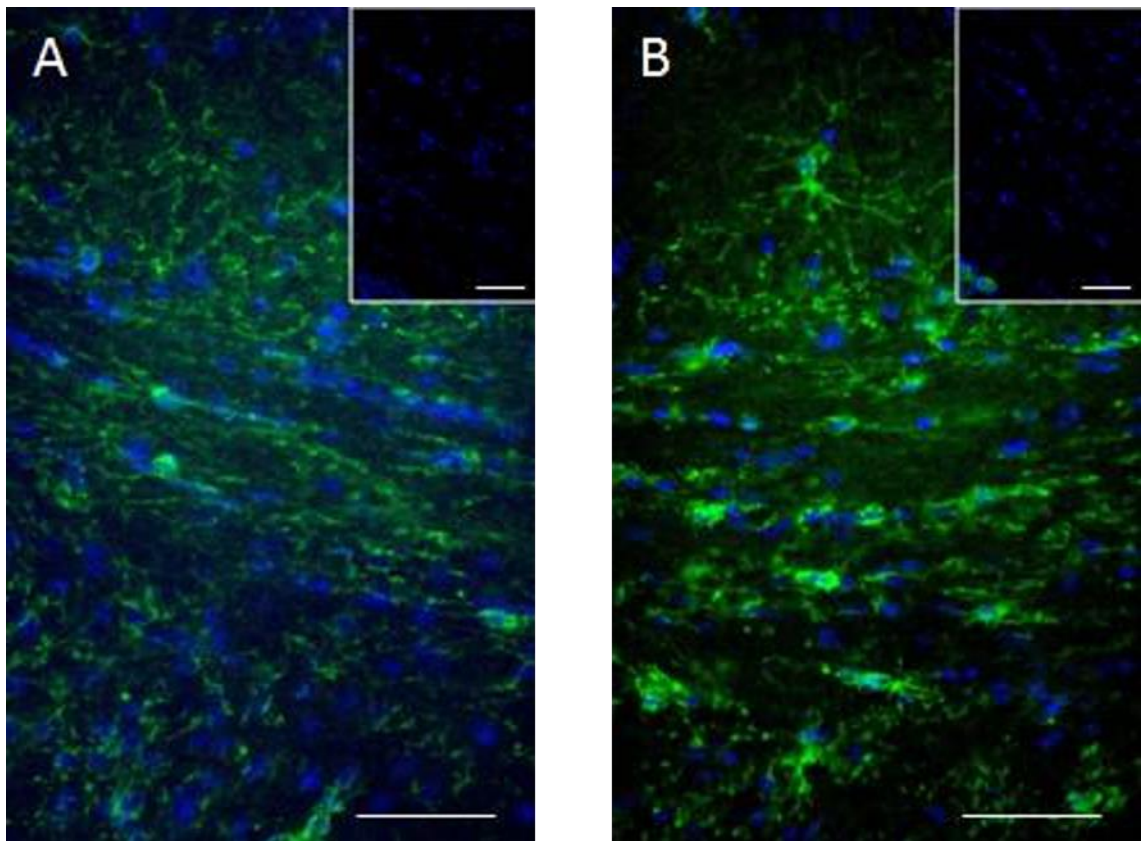
Figure 3.6: Representative NG2 staining (green) with DAPI (blue) of lateral CC sections. The ADB used for incubation of the sections either had the (A) described solution or (B) 2% (v/v) Triton X-100 replacing the Tween-20. Scale bars represent 50µm. For all images, varying minimal/maximal signal intensity adjustments were applied to produce the greatest qualitative signal. Insets show negative controls. 2 sections, with 2 images per section used per treatment group.
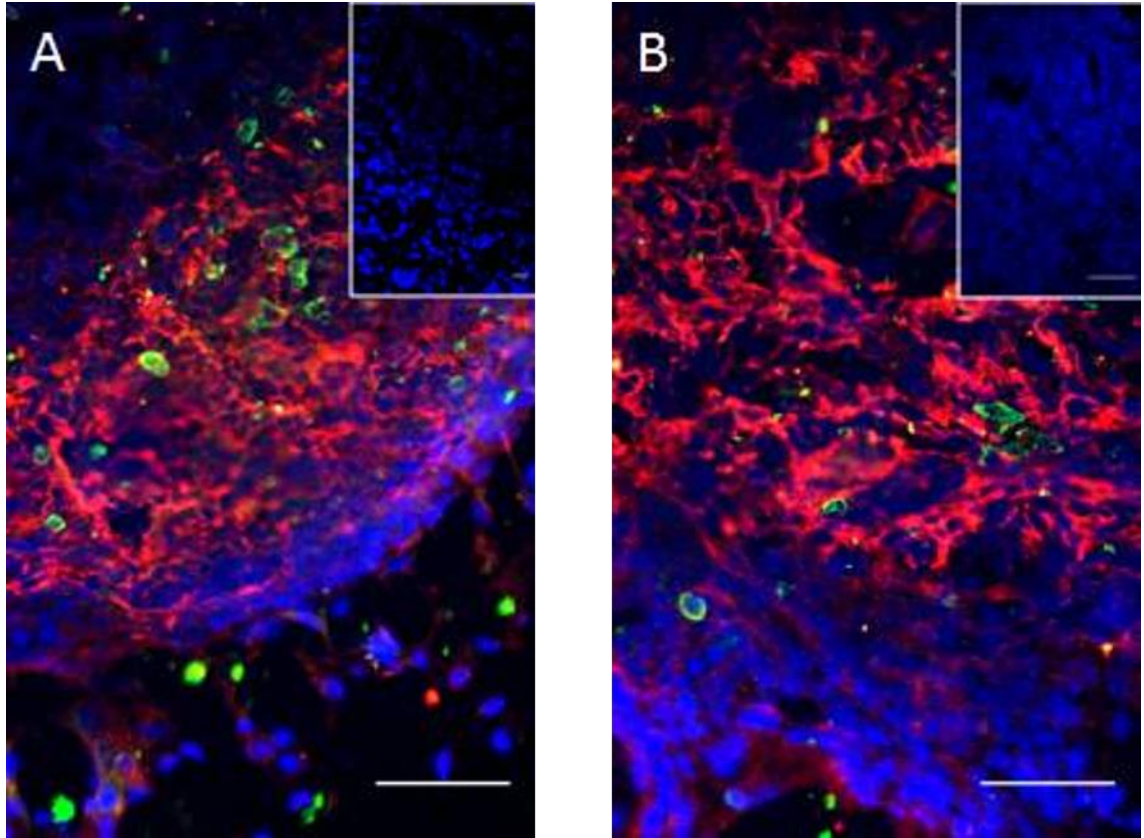
Figure 3.7: Representative staining for the AMIGO3 concentration trials. Images were taken of sections treated with anti-AMIGO3 antibodies at (A) 4µg/ml, and (B) 2µg/ml in the lateral CC. Blue shows DAPI and red shows NF200. Scale bars represent 50µm. For all images, varying minimal/maximal signal intensity adjustments were applied to produce the greatest qualitative signal. Insets show negative controls. 2 sections, with 2 images per section used per treatment group.

3.4.1.3.2   CC1

To improve the signal to noise ratio of the CC1 immunostaining, multiple concentrations of the primary antibody were tested with the new staining protocol. Anti-CC1 was tested at the original concentration as previously used in our lab (Fannon J et al., 2015), 1/500 (200ng/ml) as a control, as well as 1/200 (500ng/ml and 1/100 (1µg/ml) (fig 3.8). Interestingly high signal could be observed in all treatment groups. As signal was observed in all treatment groups, 1/200 (500ng/ml) anti-CC1 was selected for use in all subsequent experiments to ensure that sufficient signal could be observed, even if there is minimal expression.

3.4.1.3.3   LINGO1

The anti-LINGO1 antibody (Santa-Cruz Biotechnology, Wembley, UK) was tested at multiple concentrations in an attempt to improve the signal. Concentrations tested were 1/100 (2µg/ml), 1/50 (4µg/ml) and 1/25 (8µg/ml) (fig 3.9). Interestingly there was a lack of LINGO1 signal even with the highest concentration of the anti-LINGO1 Fc. Considering that even the highest concentration of this antibody failed to produce a positive signal, it was decided that a new anti-LINGO1 Fc would be tested. The alternative chosen was a rabbit anti-LINGO1 Fc (Abcam, Cambridge, UK). A subsequent titration was performed for optimisation. The anti-LINGO1 Fc was trialled at 1/100 (10µg/ml), 1/200 (5µg/ml), 1/400 (2.5µg/ml) and 1/500 (2µg/ml) (fig.3.10). We observed clear staining throughout the study, however the distribution did not follow previously observed patterns unless used at 10µg/ml (Llorens et al., 2008; Kuo et al.,
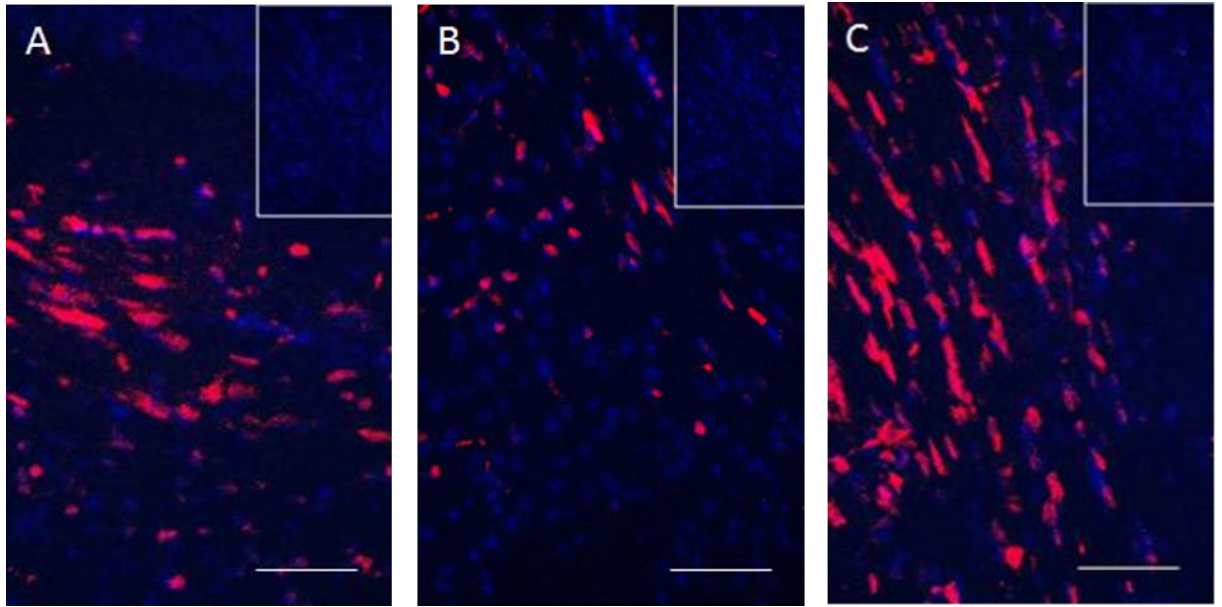
Figure 3.8: Representative staining for the CC1 concentration trials Images were taken of sections treated with anti-CC1 antibodies at (A) 1µg/ml, (B) 500ng/ml and (C) 200ng/ml in the lateral CC. Scale bars represent 50µm. For all images, varying minimal/maximal signal intensity adjustments were applied to produce the greatest qualitative signal. Insets show negative controls. 2 sections, with 2 images per section used per treatment group.
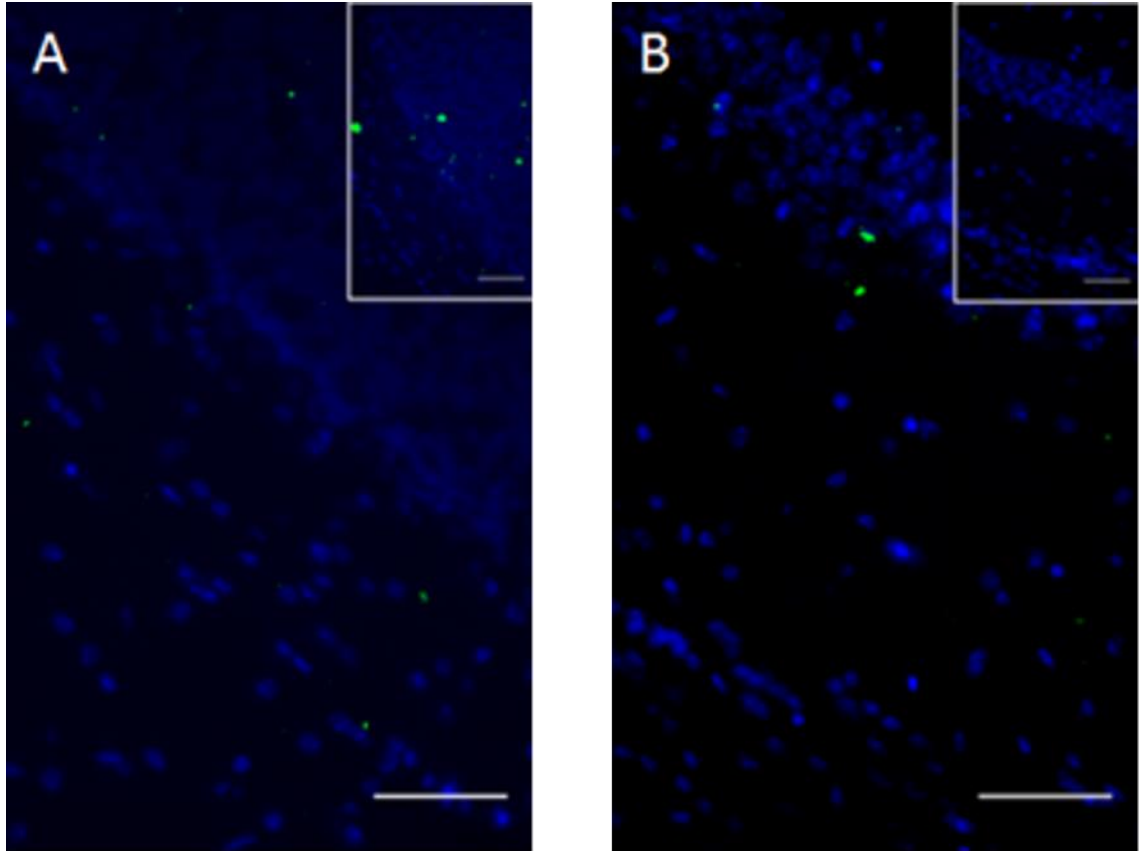
Figure 3.9: Representative staining for the Santa Cruz LINGO1 concentration trials. Images were taken of sections treated with anti-LINGO1 antibodies at its highest concentration, (A) 8µg/ml and (B) 4µg/ml in the cerebellum. Blue shows DAPI. Scale bars represent 50µm. For all images, varying minimal/maximal signal intensity adjustments were applied to produce the greatest qualitative signal. Insets show negative controls. 2 sections, with 2 images per section used per treatment group.
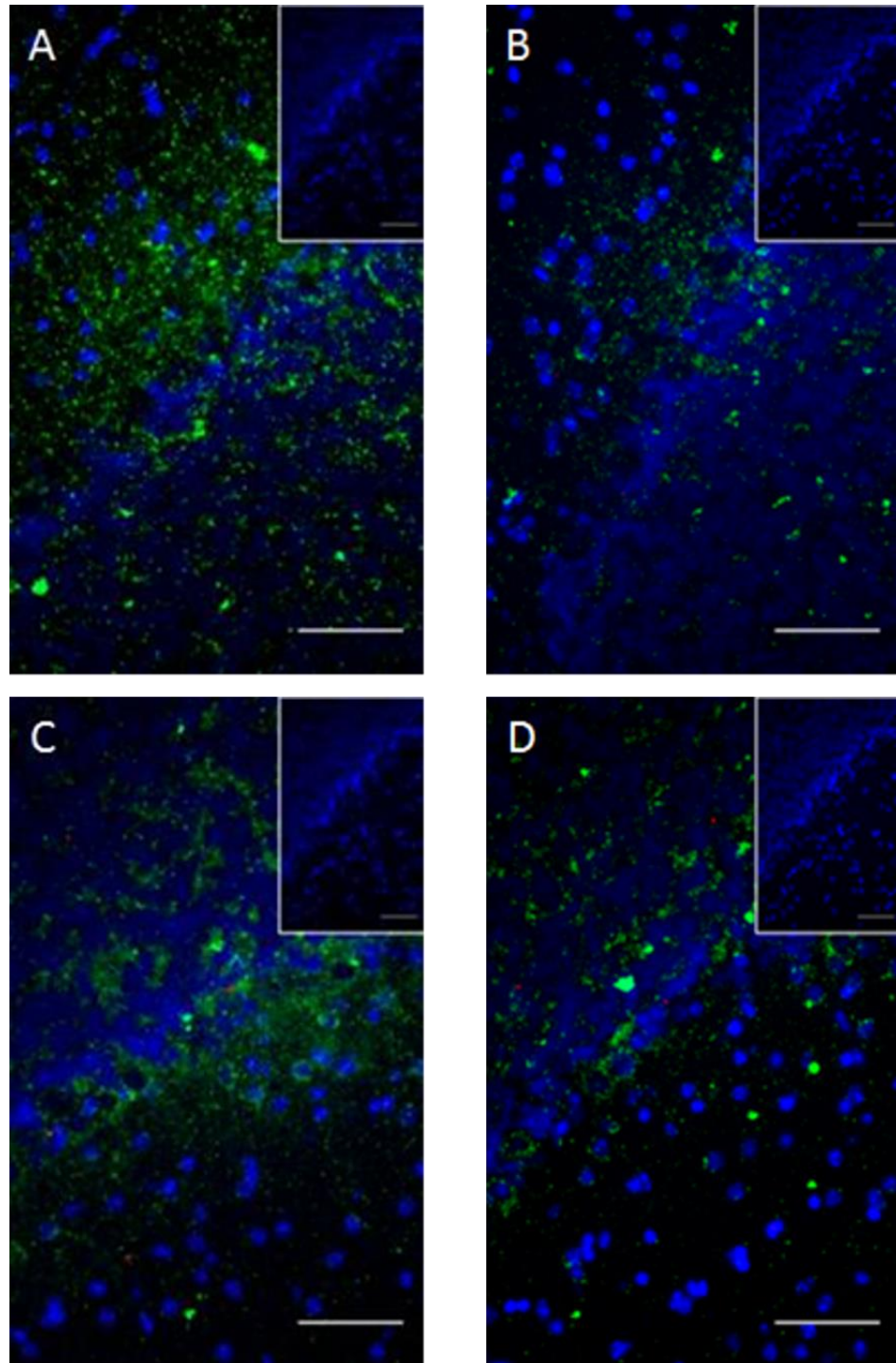
Figure 3.10: Representative staining for the Abcam LINGO1 concentration trials. Images were taken of sections treated with anti-LINGO1 antibodies at (A) 10μg/ml, (B) 5μg/ml, (C) 2.5μg/ml and (D) 1.25μg/ml in the lateral CC. Blue shows DAPI. Scale bars represent 50μm. For all images, varying minimal/maximal signal intensity adjustments were applied to produce the greatest qualitative signal. Insets show negative controls. 2 sections, with 2 images per section used per treatment group.

2013). It was therefore decided that the anti-LINGO1 Fc would be used at a dilution of 1/100 for subsequent studies.

3.4.1.3.4   MBP

MBP staining was repeated using the new protocol (2% v/v Triton, 4 hour permeabilisation, 2% v/v Triton in ADB). The concentration of antibodies was unaltered due to the successful staining using the original procedure. MBP staining with the optimised staining procedure showed a clear signal following the expected expression patterns in the CC (fig 3.11). Subsequent immunolabelling was therefore performed using anti-MBP at 1/200 (100µg/ml).

3.4.1.3.5   NG2

Although the conditions for the anti-NG2 antibody examined in section 3.3.1.1.2 (Fig. 3.6) appeared successful from the previous trials, the rabbit anti-NG2 Abcam was no longer useful as it was derived from the same source (rabbit) as the new LINGO1 antibody. Further trials were therefore performed with multiple concentrations using a mouse derived antibody (Millipore, Nottingham, UK). The mouse anti-NG2 was trialled at 1/800 (1.375µg/ml), 1/400 (2.75µg/ml) and 1/200 (5.5µg/ml) (fig 3.12). None of the samples showed any staining over background. It should be noted that there was excessive background staining in most cases when mouse antibodies were used, although this was acceptable when exceptionally strong signals were observed, such as with CC1 (fig 3.8).
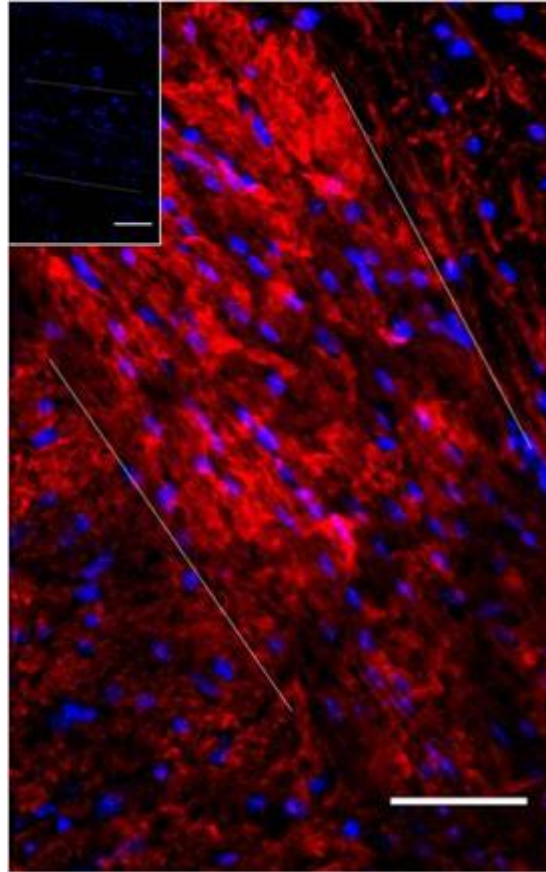
Figure 3.11: Representative staining for the anti-MBP trial. Blue shows DAPI. Scale bars represent 50µm. The image was adjusted through minimal/maximal signal intensity adjustments to produce the greatest qualitative signal. Insert shows a negative control. 2 sections, with 2 images per section used.

Figure 3.12: Representative staining for the mouse anti-NG2 Fc concentration trials. (A-B) Only the highest concentration is shown, 1/200 (5.5µg/ml) from two different samples within the study. Blue shows DAPI. Scale bars represent 50µm. Images were adjusted through minimal/maximal signal intensity adjustments to produce the greatest qualitative signal. 2 sections, with 2 images per section used per treatment group. Note the signal observed with anti-NG2 is equivalent with that in the negative controls (insets).

As no positive signal above the background staining was observed with the mouse anti-NG2, even at the highest used concentration, it was decided that a new antibody should be used. The replacement antibody was a rat anti-NG2 Fc (R&D, Abingdon, UK). Ultimately time constraints prevented the use of this antibody. However, if time had permitted, concentration titrations would have been performed using dilutions of 1/20, 1/50, 100, 1/200 and 1/500 based on the supplier's specifications.

3.4.1.3.6   NgR1

NgR1 antibodies were tested in the CC as previously discussed. The anti-NgR1 Fc was trialled at 1/200 (5µg/ml), 1/100 (10µg/ml) and 1/50 (20µg/ml) (fig 3.13). No signal was observed with 5µg/ml of anti-NgR1 Fc. Signal however became apparent when using a concentration of antibody of at least 10µg/ml, with increasing signal observed at the highest concentration tested. Subsequent studies would use 20µg/ml of NgR1 Fc.

3.4.1.3.7   O1

The mouse monoclonal O1 antibody, which recognises OLG specific glycolipid GalC is used as a marker of post-mitotic OL lineage cells (Gard & Pffeifer 1989) so was considered as a potential marker for colocalisation with anti-AMIGO and anti-LINGO1 IgG. O1 antibodies were trialled for its potential use in this investigation. The O1 antibody was obtained from the laboratory of Anthony Campagnoni (University of California, Los Angeles, USA). The concentration of anti-O1 Fc within our sample is not known. The following dilutions were tested with the O1 antibody; undiluted, 1/25,
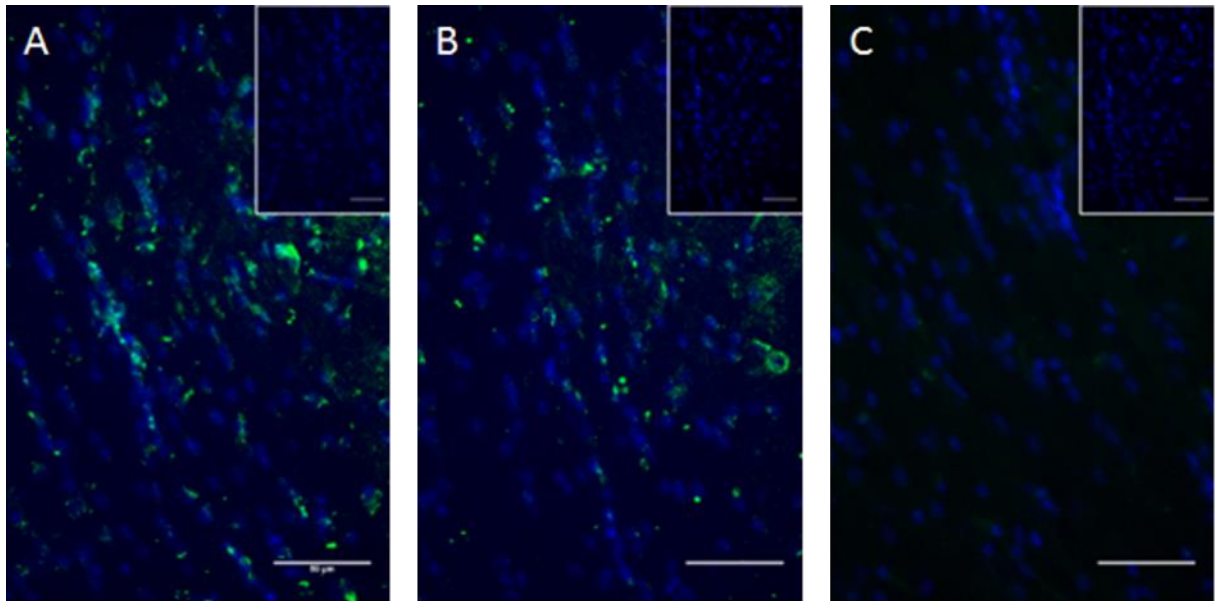
Figure 3.13: Representative staining for the mouse anti-NgR1 Fc concentration trials. Images were taken of sections treated with anti-NgR1 Fc at (A) 20µg/ml, (B) 10µg/ml, (C) 5µg/ml. Blue shows DAPI. Scale bars represent 50µm. Images were adjusted through minimal/maximal signal intensity adjustments to produce the greatest qualitative signal. Insets show negative controls 2 sections, with 2 images per section used per treatment group.

1/50, and 1/100 (fig 3.14). A clear signal could be observed with all treatment groups, although it appears excessive in the, 'neat', antibody treatment group, possibly indicating background staining due to a high concentration. Despite the abundant staining, the expression appears vesicular, in small patches, rather than labelling the whole cell. This is similar to previously observed, low powered images (Liu et al., 2011), therefore it was decided that O1 would be an inappropriate marker for this investigation.

3.4.1.3.8   O4

The glycoprotein O4, a surface antigen, is considered to be a marker of late OPCs (Back et al., 2001), so could potentially be a useful marker for undifferentiated oligodendroglia. A concentration trial was tested using 1/100 (5µg/ml), 1/200 (2.5µg/ml), 1/400 (1.25µg/ml) and 1/500 (1µg/ml) (fig 3.15). A reasonable signal was observed with all treatment concentrations, however the intensity was low even at 5µg/ml. Additionally, and similar to O1, a vesicular expression pattern was observed, with signal being localised to small patches, rather than across the entire cell. Based on the limited signal with this antibody it was decided that O4 would not be used in this investigation.

3.4.1.3.9   Olig2

Despite the satisfactory staining that we previously observed for the Olig2 (fig. 3.5), a concentration trial was conducted to try to optimise its staining. The antibody was trialled at 1/500 and 1/200 (fig 3.16). Despite staining observed in both trials, it
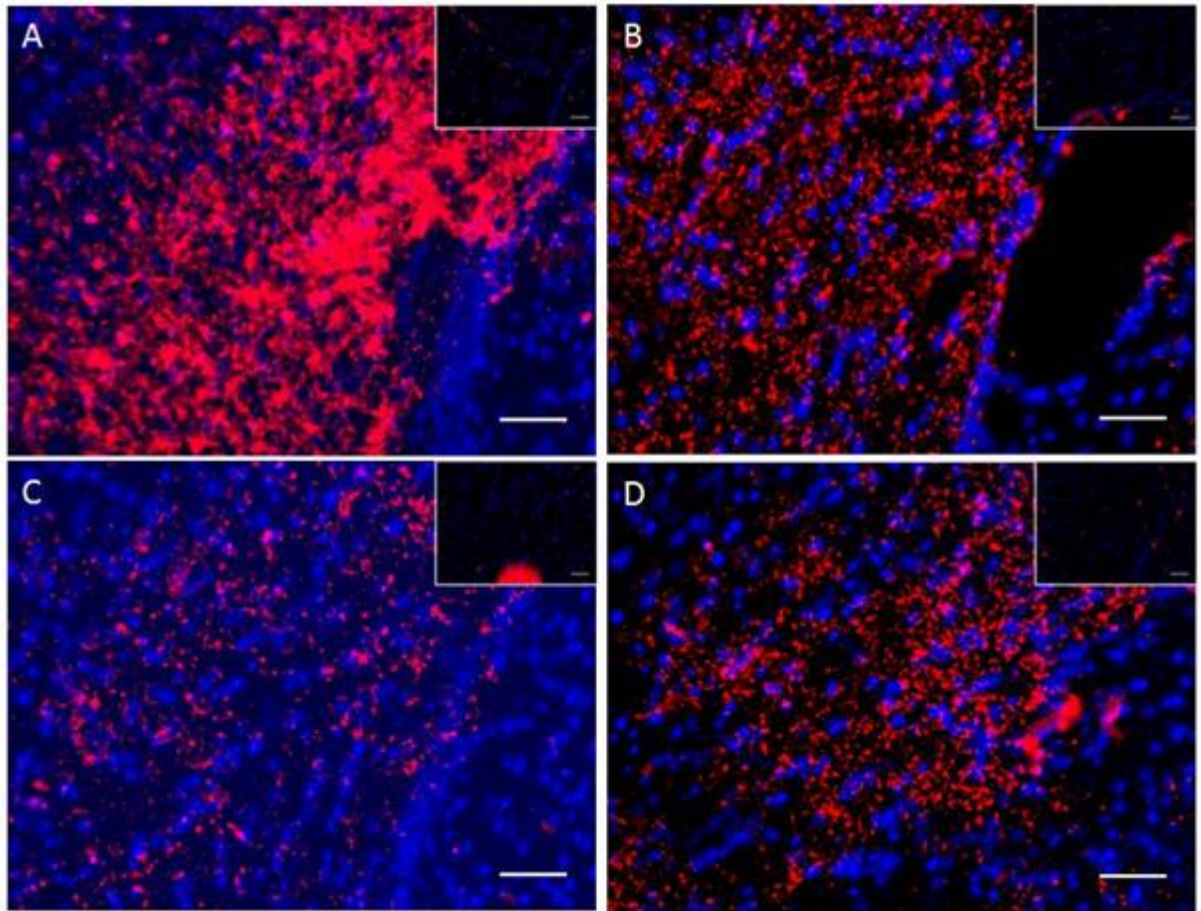
Figure 3.14: Representative staining for the O1 concentration trials. Images were taken of sections treated with anti-O4 antibodies at (A) undiluted, (B) 1/25, (C) 1/50 and (D) 1/100 in the lateral CC. Blue shows DAPI. Scale bars represent 50μm. For all images, varying minimal/maximal signal intensity adjustments were applied to produce the greatest qualitative signal. Insets show negative controls. 2 sections, with 2 images per section used per treatment group.
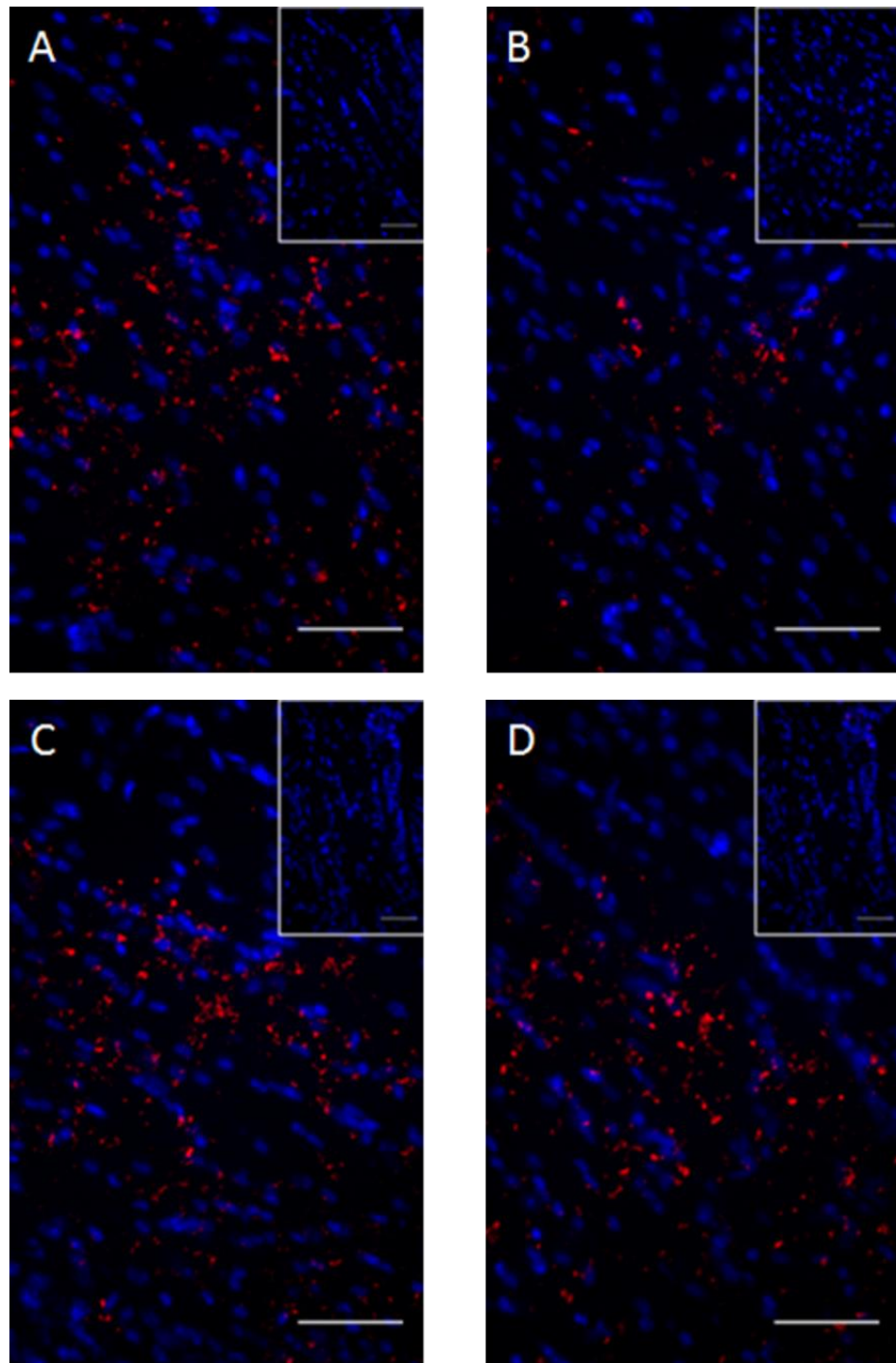
Figure 3.15: Representative staining for the O4 concentration trials. Images were taken of sections treated with anti-O4 antibodies at (A) 5µg/ml, (B) 2.5µg/ml, (C) 1.25µg/ml and (D) 1µg/ml in the lateral CC. Blue shows DAPI. Scale bars represent 50µm. For all images, varying minimal/maximal signal intensity adjustments were applied to produce the greatest qualitative signal. Insets show negative controls. 2 sections, with 2 images per section used per treatment group.
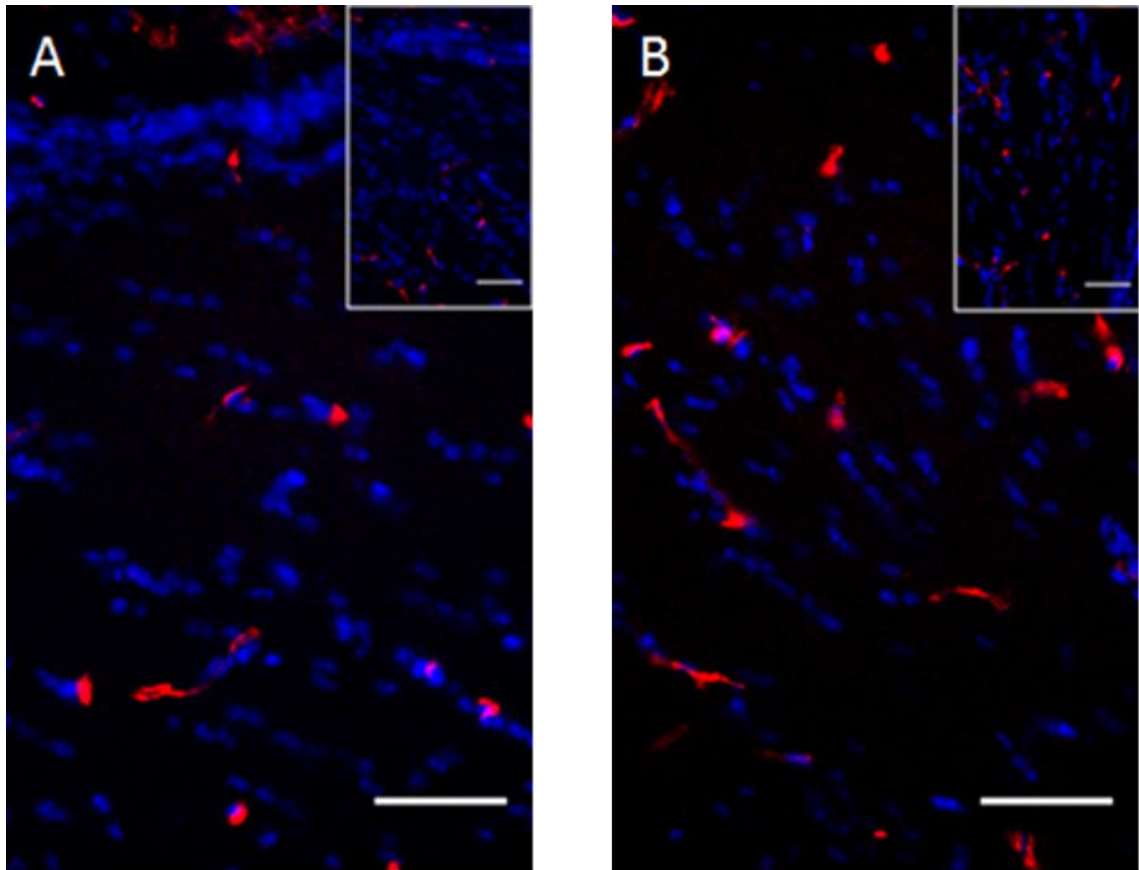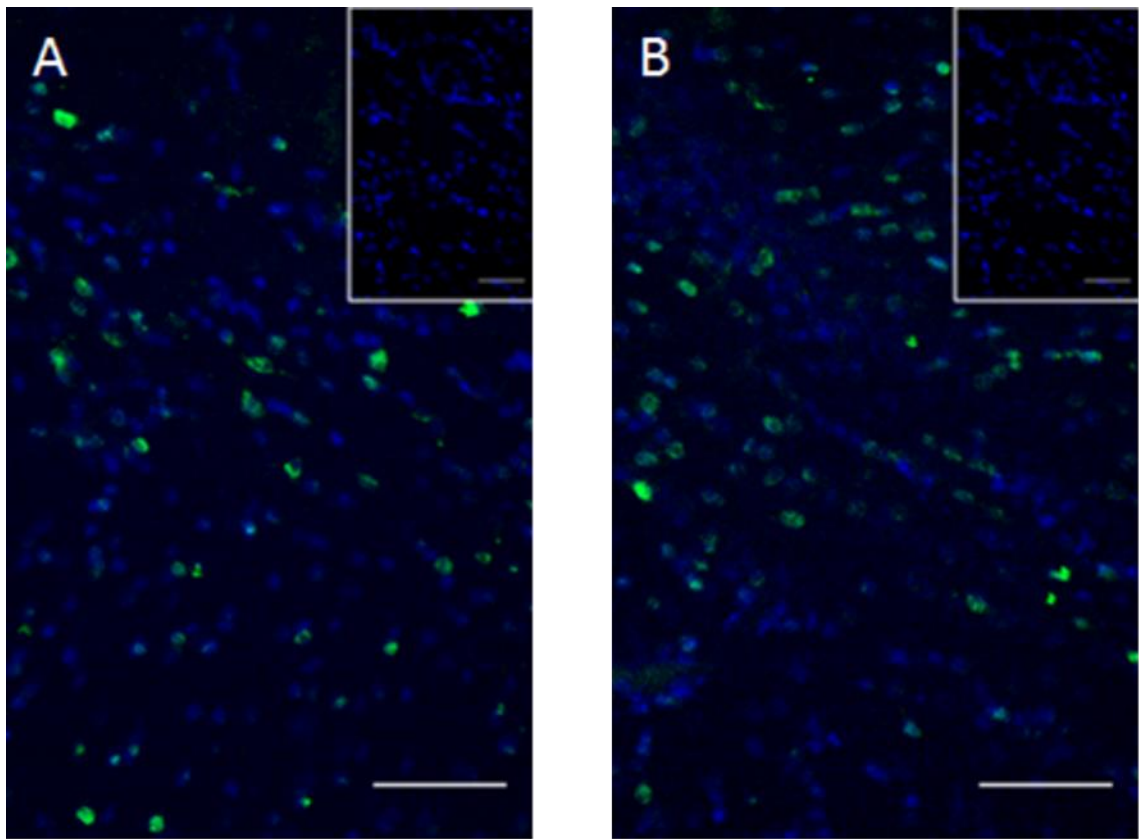
Figure 3.16: Representative staining for the Olig2 concentration trials. Images were taken of sections treated with anti-Olig2 antibodies at dilutions of (A) 1/200 and (B) 1/500. Blue shows DAPI. Scale bars represent 50μm. For all images, varying minimal/maximal signal intensity adjustments were applied to produce the greatest qualitative signal. Insets show negative controls. 2 sections, with 2 images per section used per treatment group.

was clear that greater levels were observed in the higher antibody (1/200) trial. The anti-Olig2 Fc was therefore used at a 1/200 dilution for subsequent studies.

3.4.1.3.10   Mature OL staining

CC1 is cytoplasmic so does not provide a signal which covers the entire OL. It was decided that a triple stain with CC1, MBP and the test marker (e.g. AMIGO3) would be useful for a comprehensive OL localisation study. To achieve effective spectral separation of the secondary antibody fluorophores in this triple stain, CC1 antibodies were tested with an AF 350 (blue) secondary antibody that could be used with the AF488 and AF593 labels (fig 3.17A-B). The spinning disc confocal system used for imaging in this study lacks a filter set compatible with the AF350 dye, thus it was not possible to perform confocal imaging on triple labelled sections. However, the staining was successful as shown by imaging of the AF350 signal on a wide-field fluorescent microscope (Axioplan-2, Carl Zeiss Ltd, Herefordshire, UK) (fig 3.17C-D). Since the available confocal system could not detect the AF350 signal, and because confocal imaging was desirable, it was decided that a double stain involving CC1 or MBP would be used for future localisation studies on mature OL.

3.4.1.4   Conclusions of optimisation studies

The preceding stages of this chapter focussed on optimising the IHC protocol so that a reliable analysis of the degree of myelination and AMIGO3/LINGO1 expression can be obtained during the early stages of development. We first observed that for many of the markers, there was a lack of signal due to insufficient permeabilisation of
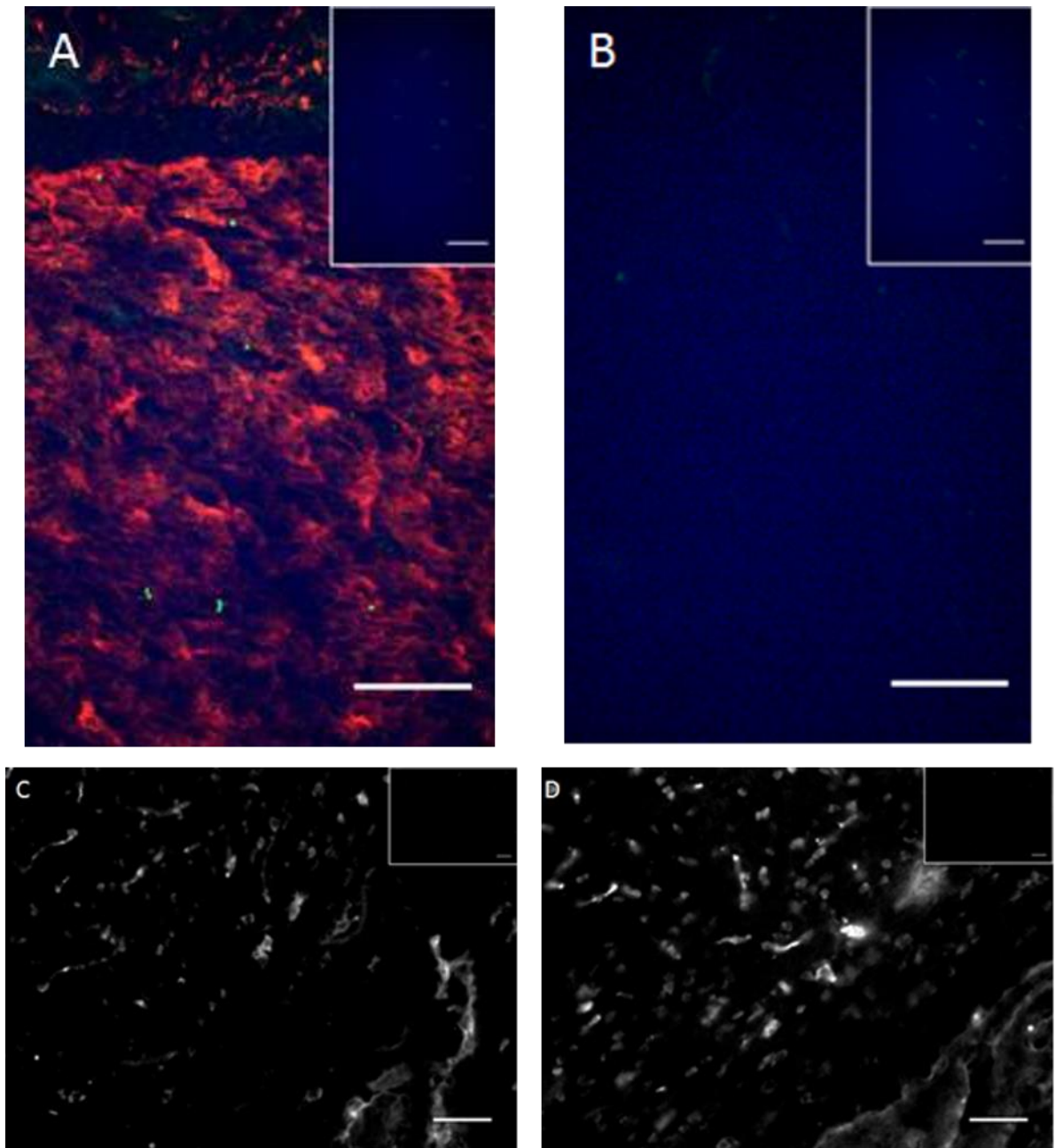
Figure 3.17: Representative staining for the mature OL test. (A) A triple stain for AMIGO3 (green), MBP (red) and CC1 (blue). (B) A single stain for CC1 alone (blue). No modifications were made to the CC1 signal. (C-D) Wide-field imaging of singe stained CC1 staining with AF350 secondary antibodies. Images were modified, with minimal/maximal signal intensity adjustments to produce the greatest qualitative signal. The same adjustments were applied to image pairs (A-B) for MBP and AMIGO3 and (C-D) for CC1. Scale bars represent 50μm. Insets show negative controls. 2 sections, with 2 images per section used per treatment group.

the tissue. Following a more extensive permeabilisation treatment protocol with higher concentrations of Triton X-100, as well as extended incubation with the detergent, and its inclusion in the ABD we observed improved staining. A limitation with this method is that Triton X-100 is a non-selective detergent, with overuse potentially resulting in removal of proteins (Goldenthal K et al., 1985; Jamur M and Oliver C, 2010). Our data, when using high concentrations of Triton X-100, showed improved signal, although it is possible that some protein has been lost during the preparation.

The subsequent aims of the immunohistochemistry experiments were to examine the expression of AMIGO3, LINGO1 and NGR1 proteins in oligodendroglia at various developmental stages. As AMIGO3, LINGO1 and NgR1 are all membrane bound proteins, it was decided that membrane proteins for the varying stages of OLG differentiation would provide the best target for colocalisation with the proteins of interest. A number of markers were considered for use in the identification of oligodendroglia at distinct points in their development. NG2 is a marker of undifferentiated OPC (Clarke et al., 2012). Other markers of OPC include platelet PDGFαR and anti-O4 (Fancy et al., 2004), although anti-O4 binding is retained in OLs thus this marker requires the use of a second OLG marker, such as anti-MBP to distinguish OPC from differentiating OLG.

Both PDGFαR and NG2 have been widely used as a reliable marker of OPCs. Previous success with anti-NG2 labelling of OPC in our lab influenced our decision to use NG2 as a marker of OPC in the present work (Fannon J et al., 2015). Anti-O4 Fc has similarly been observed to label both OPC processes and soma (Baccarini M et

al., 2008; Buzby J et al., 2010). Conversely, after our trials, we observed O4 staining in small nodules, possibly following a vesicular expression profile. Previous studies have used O4 antibodies in immunocytochemistry, rather than IHC (Baccarini M et al., 2008; Buzby J et al., 2010). It is possible that in our investigation the signal from the anti-O4 Fc was not clear enough over the background signal observed *in vivo*, despite being used at a high concentration. Additionally, O4 is not expressed during the early stages of OPC development, but rather expression begins when the cells begin to differentiate (Baumann N and Pham-Dinh D, 2001; Neman J and de Vellis J, 2008). Based on these observations and our data, O4 would not be appropriate for our investigation. Furthermore, NG2 staining provided positive results, displaying an expression pattern which appears to mark the entire OPC.

To examine the mature development stages, we examined the expression patterns of mature OL markers using IHC, including CC1 and O1. O1 staining has previously been observed in a nodular arrangement within the CC of wild-type mice, however these conclusions were obtained from low power images and thus may not be representative of the true staining pattern (Liu et al., 2011). We observed a similar staining pattern, indicating that the O1 is unlikely to be a useful marker for these studies, as there will likely be a significant portion of the cell which is not labelled.

CC1 can be seen to be a reliable marker of mature OLs from our data, however the antigen is cytoplasmic and so only the soma of the cell is labelled. To overcome this, we considered that co-staining with MBP to capture staining across the soma and processes. MBP is expressed on the processes of mature OLs, and within the myelin sheath where it plays an important structural role (Kotter M et al., 2005;

Quarles R et al., 2006). This method however required the use of a third fluorescent label (AF350) with adequate spectral separation from AF488 and AF594. Our data showed signal from this combination when imaged on a wide-field system, but due to technical limitations described above (section 3.3.1.3.10) it was not possible to acquire confocal images from sections with this triple label. Since confocal imaging was preferable for detecting colocalisation it was decided that a double stain involving CC1 or MBP would be used for the studies on mature OLs.

Based on the data obtained, we have determined the antibodies and their concentrations that will be used in subsequent studies (table 3.3). The subsequent studies will also look at combinations of the test markers (AMIGO3 and LINGO1) with the developmental markers. We intend to analyse whether there is a correlation between the intensity of test marker staining with the various development markers as well as to examine if this correlates with the extent of myelination, as determined from MBP staining, and differentiation, as indicated by the ratio of CC1$^+$ mature OLs within the total Olig2$^+$ oligodendroglia population (including OPCs and OLs) (Fannon J et al., 2015).

3.4.2   IHC analysis of AMIGO3 and myelination during development

Our first studies examined the frequency of AMIGO3 staining in relation to the CC1/Olig2$^+$ ratios, with a high ratio representing a high proportion of total oligodendroglia (Olig2$^+$) having matured to OL (CC1$^+$), and MBP pixel proportion, representing the degree of myelination. Qualitatively, both MBP and CC1 are not present, or are expressed at very low levels at P0 (fig 3.18F & K). It does not appear that OLIG2$^+$ cells increase up to P28, in fact qualitatively there appears to be a

Target protein	Source species	Supplier (code)	Original concentration	Working dilution
Polyclonal AMIGO3 (human C-terminus)	Goat	Santa-Cruz (sc-49881) (Lot no: JO511)	200µg/ml	1/50 (4µg/ml)
CC1 (APC) recombinant *E. coli* expressed in mouse myeloma cells	Mouse	Calbiochem (Cat. No. OP80)	100µg/ml	1/200 (500ng/ml)
Polyclonal LINGO1 (human C-terminus)	Rabbit	Abcam (ab23631)	1mg/ml	1/200 (5µg/ml)
Monoclonal to Bovine MBP	Rat	Millipore-Chemicon (MAB386)	2mg/ml	1/200 (100µg/ml)
Polyclonal NG2	Rabbit	Millipore-Chemicon (AB5320)	1mg/ml	1/200 (5µg/ml)
Polyclonal to NgR	Rabbit	Millipore-Chemicon (AB15138)	1mg/ml	1/50 (20µg/ml)
Polyclonal to Olig2	Rabbit	Millipore-Chemicon (AB9610)	100µl	1/500

Table 3.3: List of the antibodies to be used in subsequent experiments for the IHC during development study. Concentrations used and their sources are listed.

decrease in total OLG. A much greater CC1^{+} staining can be seen as early as P7 (fig3.18K-O). MBP also appears to increase with strong signal being observed throughout the CC as of P21 (fig 3.18F-J). Qualitative analysis of the AMIGO3 IHC is more difficult to interpret, there are only low levels observed throughout the observation period within the medial CC. Although there is some evidence to a change in the levels at P14 with IHC appearing more frequent, the observation was not consistent between all samples. Generally, AMIGO3 appears in a globular formation without any clear distribution within the CC.

Following qualitative analysis, pixel counts above the normalised threshold was used to semi-quantify the extent of myelination and AMIGO3 and MBP expression. Ratios of CC1^{+}/OLIG2^{+} cells were also calculated (fig 3.18P). Again, it is clear that both the mature OLG percentage and the extent of MBP expression start at negligible levels at P0 ($1.7\%\pm0.5\%$ and $1.4\times10^{-3}\pm1.2\times10^{-3}$ respectively) and rise during the observed periods of postnatal development.

MBP expression appears to reach a peak at P14 of 96.3 ± 1.4, and plateau for the rest of the examined period. As all samples were normally distributed, an ANOVA was used to determine if the level of anti-MBP signal increased significantly over the time-points. One-way ANOVA detected a significant source of variation between the 5 ages that were examined (ANOVA, $F(4,10)= 533.458$, $P<0.05$). Post-hoc comparisons revealed significant differences between MBP signals ($P<0.05$) between P0 and all other groups, as well as P7 and all other groups. Significance was not

Postnatal day	AMIGO3	MBP	CC1/OLIG2
0	A	F	K
7	B	G	L
14	C	H	M
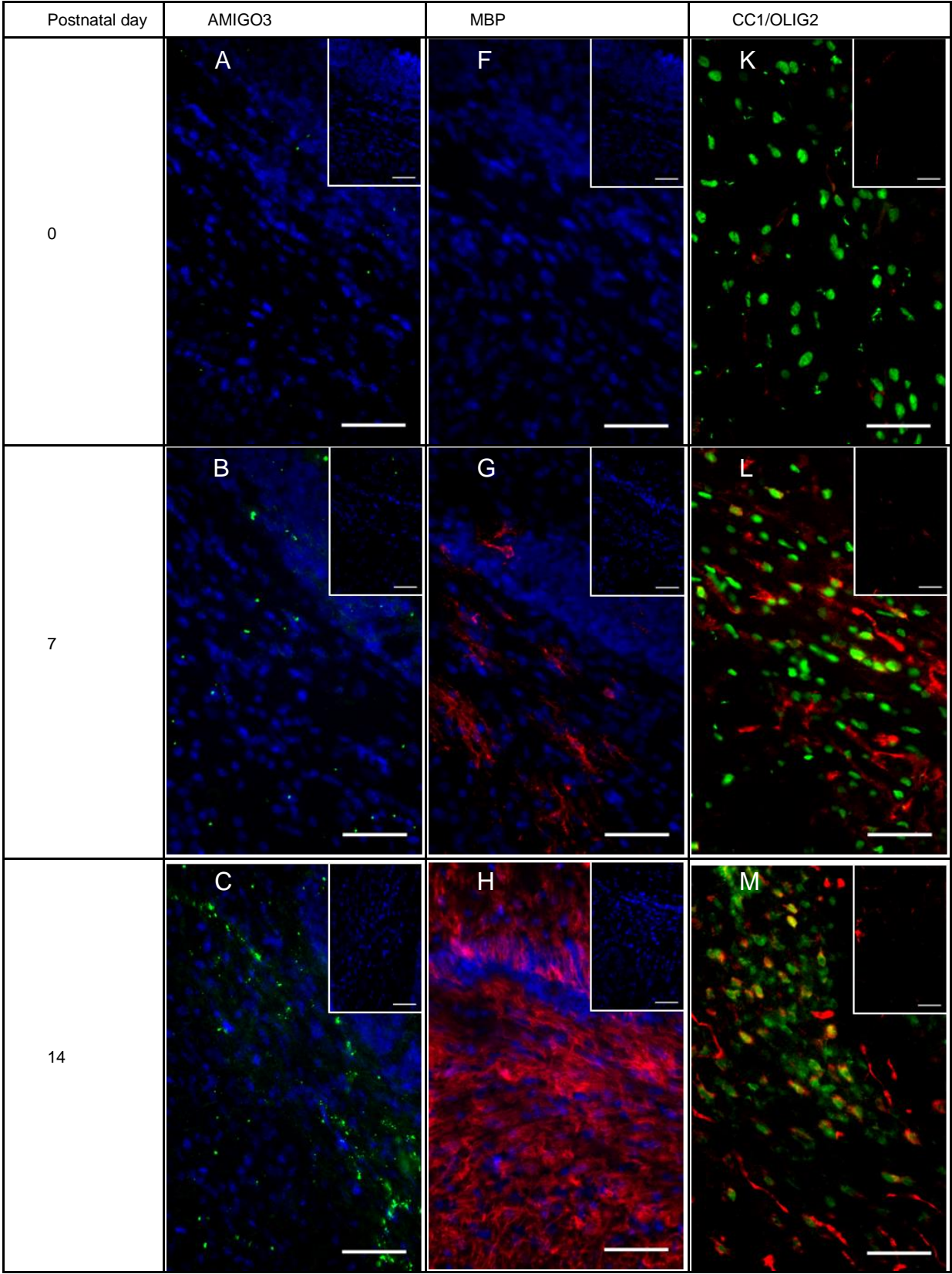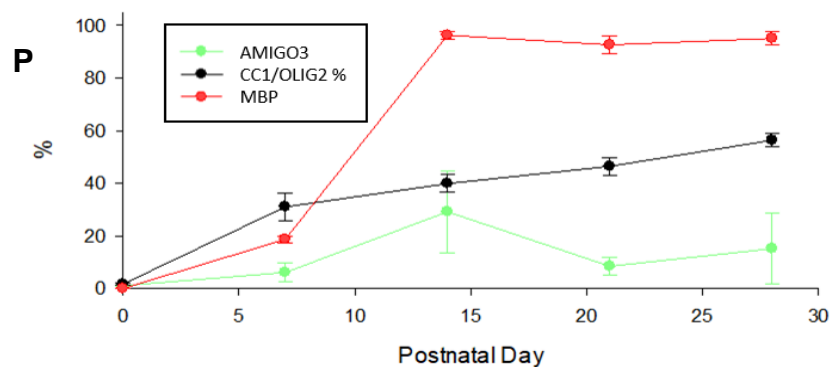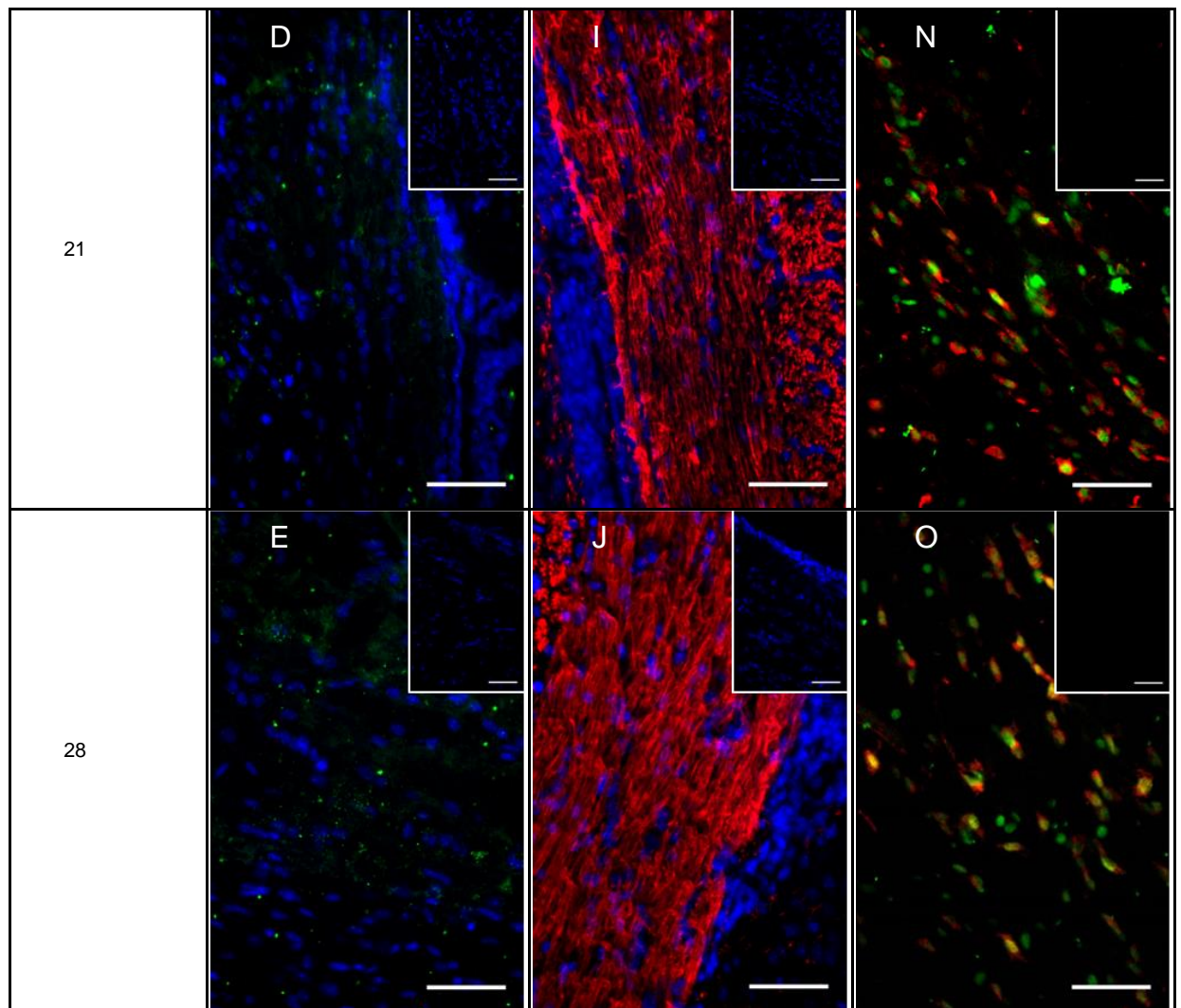
Figure 3.18: Representative staining for the development study for AMIGO3 (A-E, MBP (F-J) and Olig2//CC1 (K-O). AMIGO3 and MBP were counterstained with DAPI in blue. Olig2 is shown in green and CC1 in red. Scale bars represent 50μm. Insets show negative controls. Quantitation shown graphically (P), with AMIGO3 percentage positive pixels (green), MBP percentage positive (red) and the percentage of Olig2^{+} cells that are also CC1^{+} (black). Error bars represent one SEM, n=4.

found between P14, P21 and P27. $CC1^+/OLIG2^+$ ratios also increased from negligible levels at P0 however the rise is steadier and does not surpass ~60% even at P28 which reaches 56.4%±2.5%. As all samples were found to be normally distributed, ANOVAs were used to test the significance in the changing levels, with significance found within the groups (ANOVA, $F(4,10)=37.259$, $P<0.05$). P0 levels were found to be significantly different from all other samples following post-hoc tests ($P<0.05$). All subsequent groups did not show significance from their immediate neighbour (specifically P7 to P14, P21 to P14 and P28), however significance was found between every other group. This demonstrates that there was a significant increase over time in the $CC1^+/Olig2^+$ ratios, demonstrating a rise in the proportion of mature OLG.

AMIGO3 data was difficult to interpret. Despite starting at negligible levels (1.1±0.4) there appeared to be a small increase in the AMIGO3 positive pixel percentage. A peak was observed at P14 (29.2±15.6) before dropping but still being raised compared to original levels (8.5±3.4) at P21 and 15.2±13.3 at P28). Despite these observations, there was a high variability beyond P7 therefore it is unlikely that any definitive observations can be made from this analysis. Kruskal-Wallis analysis of the data failed to find significance between the groups ($P>0.05$).

3.4.3   Western Blot analysis of AMIGO3 expression in developing mouse neocortices

Following on from IHC analysis, Western blots were performed to test the expression of AMIGO3/LINGO1 and OLG proteins in whole neonatal pup neocortices. Due to the variability observed with the AMIGO3 IHC, we checked a

number of different AMIGO3 antibodies for western blot analysis. The Santa-Cruz, anti-AMIGO3 Ab was checked with Oli-neu cells, as well as cerebellum samples from BALB/c mice (fig 3.19). Clear bands were observed at 55kDa, indicating that AMIGO3 is present in CNS samples as expected, as well as within OPC derived cell lines.

Following optimisation, AMIGO3, LINGO1 and MBP were examined by western blot in the developing mouse neocortex. Two bands were observed for AMIGO3, one at 55kDa and one at 45kDa (fig 3.20). The integrated density level for the 55kDa band, the expected species for AMIGO3, started relatively low at P0 (0.26±0.02) before rising to its peak at P7 (1.91±0.13). An immediate drop is observed (0.46±0.11) by P14 which remains level at P21 (0.80±0.11) before dropping to negligible levels by P28 (0.06±0.01). The 45kDa band stays relatively constant throughout the development period (0.19±0.03, 0.45±0.06, 0.28±0.07 and 0.36±0.04 for P0, P7, P14 and P28 respectively), however there is a sharp rise at P21 (1.12±0.04) which immediately drops by P28. Only the 55kDa band was analysed statistically as this is the expected sized band for the functional protein (Ahmed et al., 2013). Not all of the samples were normally distributed so a Kruskal-Wallis test was used to test for statistically significant sources of variation, with significance found within the data ($P < 0.05$). Following post-hoc tests, a significant difference ($P < 0.01$) was found between P7 and P28, although there was a trend towards significance between P0 & P7, as well as P28 & P21 ($P = 0.057$ & $P = 0.083$ respectively).
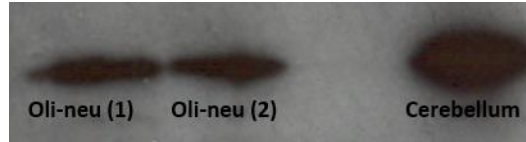
Figure 3.19: Representative Western blot bands observed with the Santa-Cruz anti-AMIGO3 Ab. Both Oli-neu samples as well as whole cerebellum samples demonstrated positive staining for AMIGO3 at 55kDa.
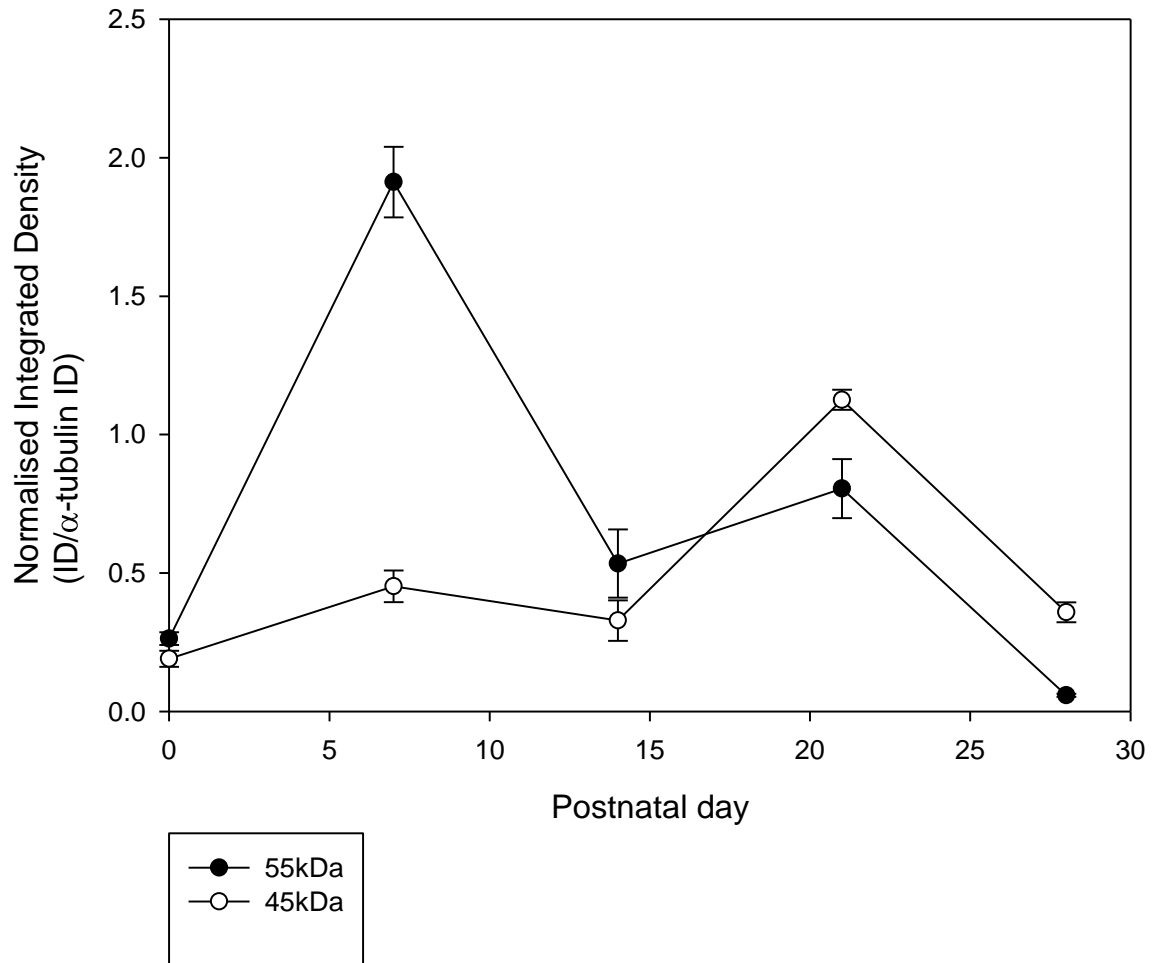
Figure 3.20: Quantification of AMIGO3 bands, normalised against α-tubulin, from whole neocortices of BALB/c mice during postnatal stages. Two bands were observed, one at 45kDa (white) and one at 55kDa (as expected, black). The largest and expected band showed an initial increase before dropping down to negligible levels by P28. Error bars represent one SEM, n=4.

A number of bands were observed for LINGO1 expression within the neocortex. Bands were observed at 87kDa (expected), 45kDa, 28kDa, 23kDa and 17kDa (fig 3.21). All of the bands start at relatively low integrated density levels at P0, 0.43±0.06, 0.32±0.07, 0.27±0.07, 0.25±0.07 and 0.37±0.05 respectively. For both the 18kDa and the expected 87kDa bands showed an immediate increase in integrated density to 2.89±0.06 and 2.28±0.05 respectively. Both samples showed a brief decline in expression at P14, 1.26±0.10 and 1.24±0.10 respectively, before increasing at P21, 3.13±0.39 and 2.62±0.17 respectively. A final decline was observed at P28 for both bands as well, although integrated density levels were maintained at greater levels than at P0, at 1.57±0.10 and 0.97±0.07 respectively. A similar pattern was observed for the 45kDa band, as it increased at P7 to 1.80±0.05 before decreasing at P14 to 0.57±0.06. Following this stage though, a steady increase in integrated density levels was observed for the remaining treatment period, 0.80±0.05 at P21 and 0.95±0.08 at P28. The 28kDa band showed an increase from P0, peaking at P14 0.94±0.07 before a steady decrease to P28 0.20±0.03. Finally, the 23kDa band showed an initial increase at P7, reaching 1.55±0.16. Subsequent levels were undetectable at P14 and P21 but a final modest increase was observed at P28, 0.79±0.07.

Only the 87kDa band was analysed statistically as this is the expected sized band for the functional protein (Jepson et al., 2012). As not all of the samples were normally distributed, a Kruskal-Wallis test was used to detect any variation. Following post-hoc tests, a significant difference was only found between P0 and P21 (P<0.01). Although no more groups showed a significant difference (P<0.05), a trend towards
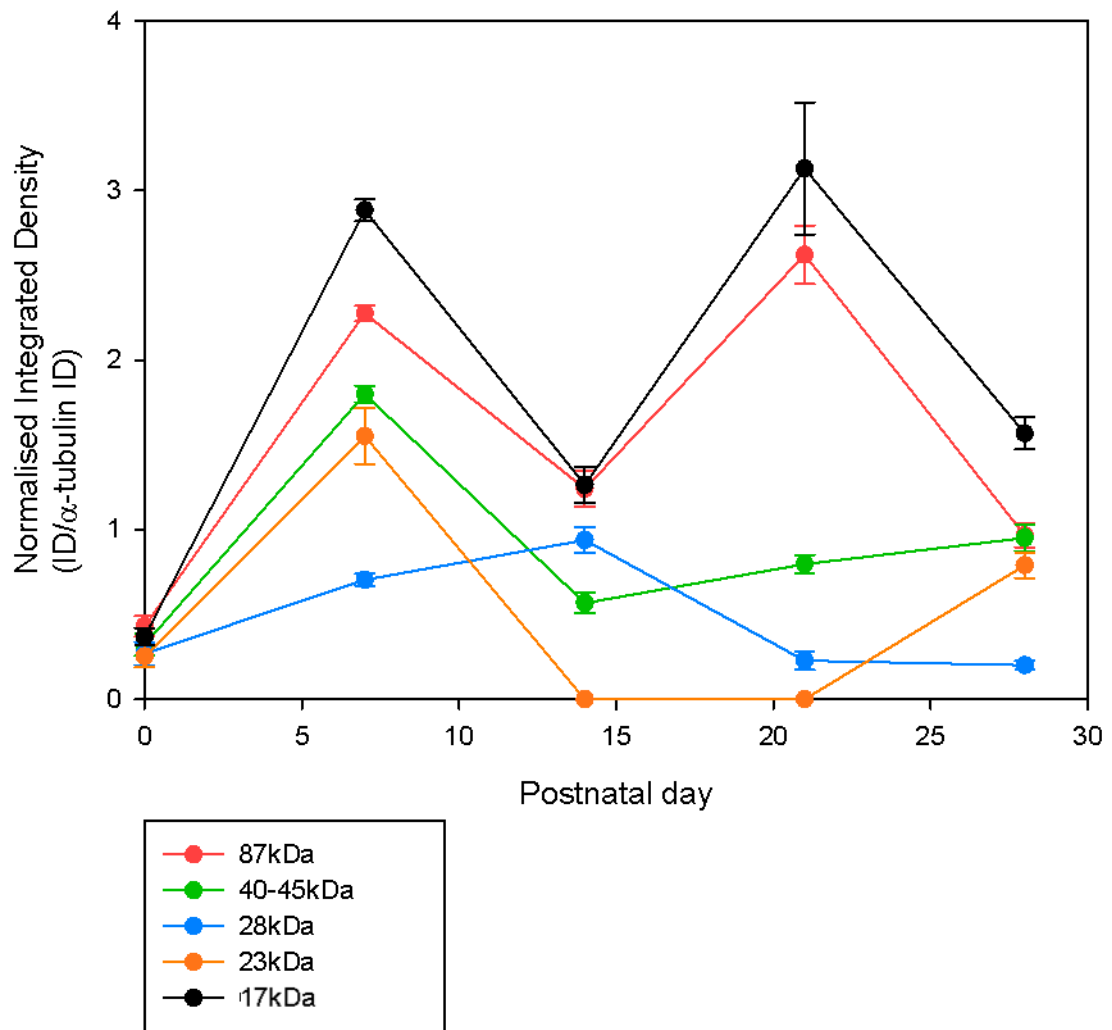
Figure 3.21: Quantification of LINGO1 bands observed from whole neocortices of BALB/c mice during postnatal stages. Five bands were observed, 87kDa (red), 45kDa (green), 28kDa (blue), 23kDa (orange) and 17kDa (black). The largest and expected band (red) demonstrated two peaks at P7and P21 before dropping but maintaining relatively high levels at P28. Error bars represent one SEM, n=4.

significance was observed between P0 & P7 (P=0.075) and PP21 & P28 (P=0.083) when looking at the adjusted significance values.

One band was observed for MBP at 18kDa. No signal was observed from P0-P14, 0.02±0.002 at P0, 0.03±0.003 at P7 and 0.02±0.002. A minor rise was observed at P21, 0.12±0.03 before a subsequent rise at the end of the observed period, reaching 1.21±0.10 (fig 3.22).

Figure 3.23 demonstrates the proportion of maximum integrated density signal for AMIGO3, LINGO1 and MBP, during the observed developmental stages so that comparison can be made between expression profiles. When compared against the signal for MBP in the neocortex, total levels of AMIGO3 appear to drop prior to the appearance of significant MBP expression. MBP expression rose to significant levels at P28 when AMIGO3 levels dropped to negligible levels. Similarly, LINGO1 levels were generally high when MBP levels were negligible, although the rise of MBP levels precedes the final decline in LINGO1 levels.
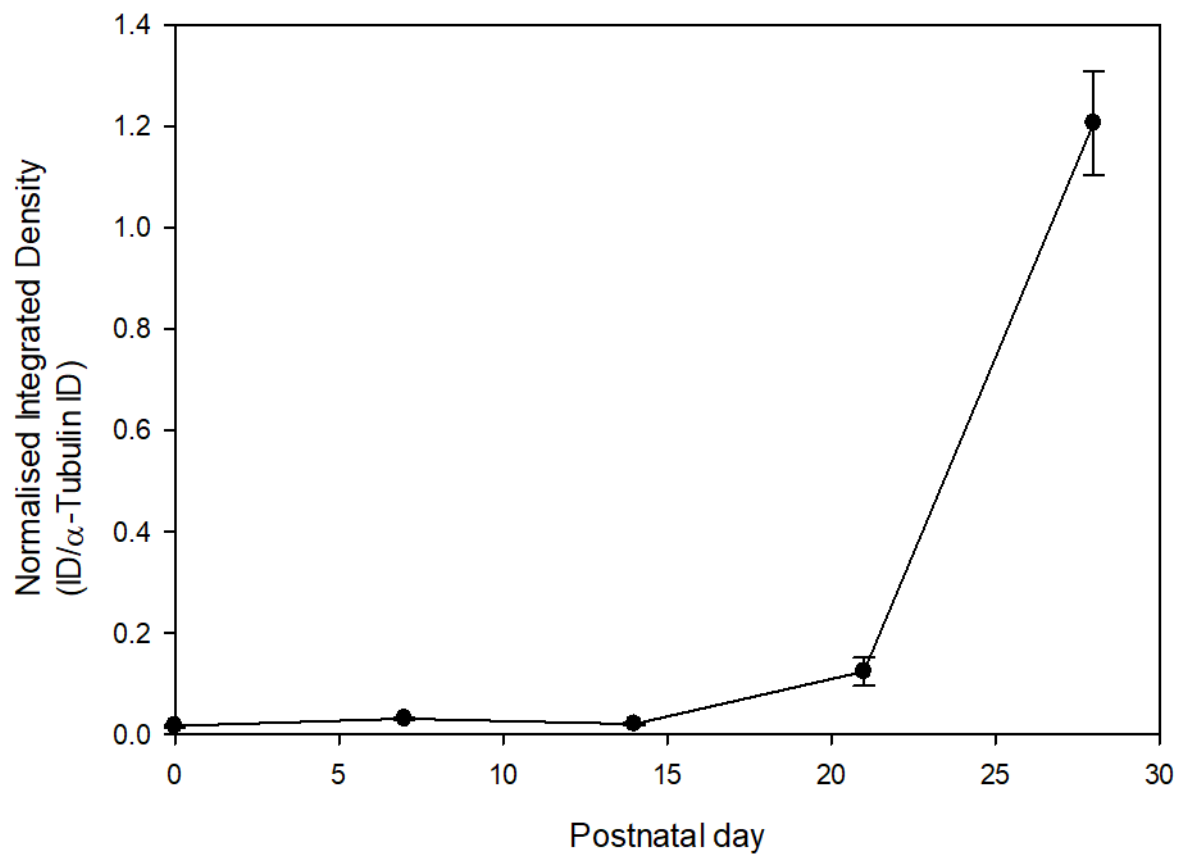
Figure 3.22: Quantification of the MBP band observed from whole neocortices of BALB/c mice during postnatal stages. One band was observed at 18kDa. Low levels of MBP were observed throughout the development stages until a sharp rise at P28. Error bars represent one SEM, n=4.
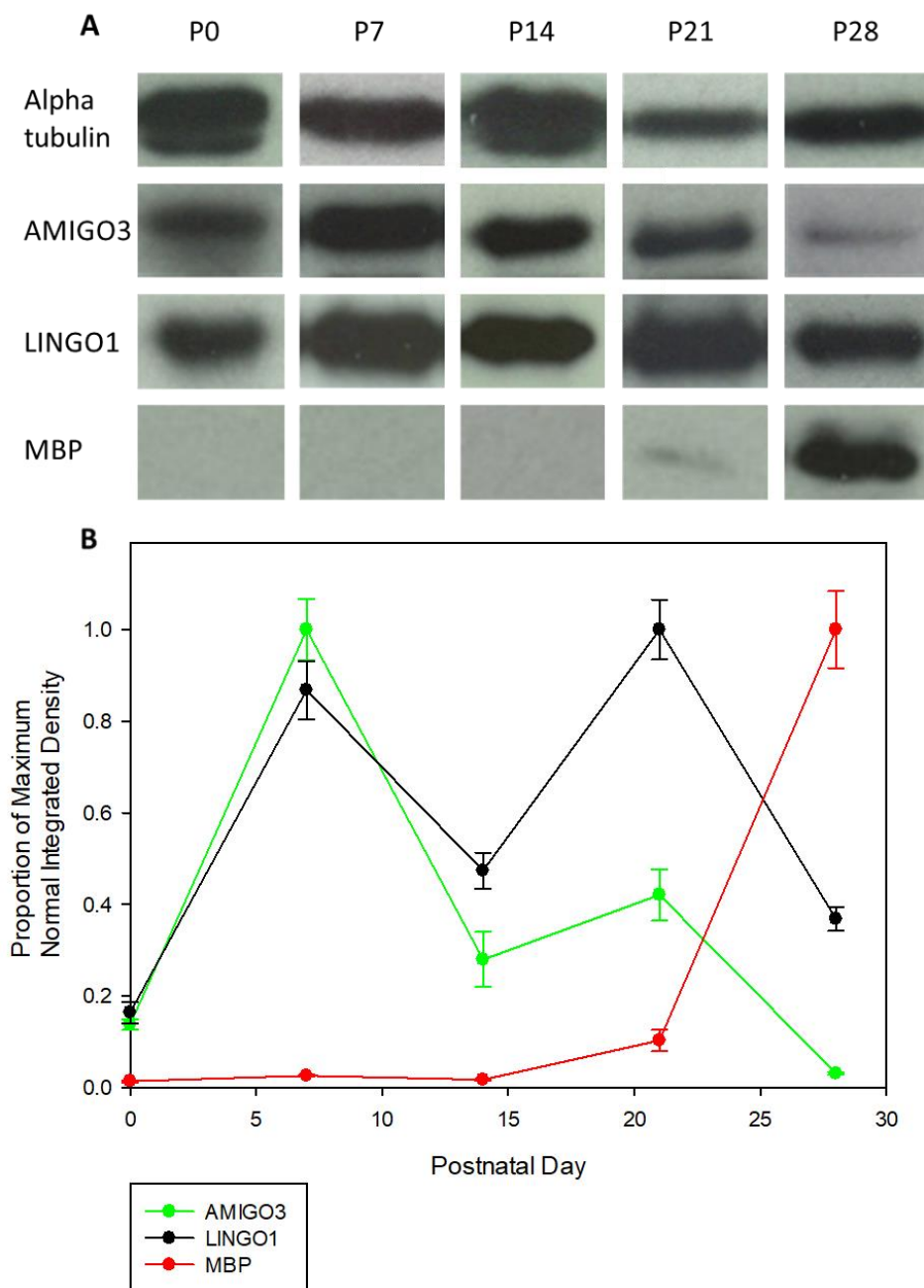
Figure 3.23: (A) representative western blots for AMIGO3 (green, LINGO1 (black) and MBP (red). (B) Proportion of the maximum normalised integrated density recorded for the various markers to highlight proportional changes and relationships. Both AMIGO3 (green) and LINGO1 (black) increase substantially at P7. Both demonstrate a rapid drop at P14, with LINGO1 increasing again at P21. A rise is also observed with AMIGO3 although levels stay relatively similar before both proteins demonstrate a final drop at P28, although LINGO1 levels remain raised. MBP (red) stays reduced until the end of the development period, coinciding with the final drops of AMIGO3 and LINGO1 expression. Error bars represent one SEM, n=4.

3.5 Discussion

3.5.1 Analysis of myelination during postnatal development

From our data it is clear that substantial myelination occurs in the CNS during P0-P28. This conclusion is supported by observations from both IHC of the CC and from western blot of whole mouse neocortices. Our IHC data matches with previous data from mouse models where the majority of myelination within the CC occurs between P8-P30 (Lodygensky et al., 2012; Chan et al., 2013; Dai et al., 2015). Interestingly there appears to be a variation between IHC and western blot data. As our dissection procedure included all structures above the lateral ventricles, the corpus callosum should have been included within the neocortex. As such, it would be expected that MBP should rise in the neocortex as detected by western blot at the same time as it does within the CC as detected by IHC. It should be highlighted that this variation may simply be a result of the variation in the techniques used. It is possible that the dissection and lysis procedure used in the western blot preparation resulted in damage or loss of the corpus callosum or myelin proteins therefore removing some of the signal. It is more likely however that the western blot protocol is simply less sensitive than IHC. Considering that IHC will be able to detect signal in individual cells rather than in whole tissue samples, it would be expected to have a higher sensitivity and therefore be able to detect smaller changes than western blot is able to. It has been reported previously that MBP levels in the telencephalon/forebrain of embryonic and postnatal OF1 mice become significant by P15, with some detectable levels by P10 (Gil et al., 2010). Our data show a later expression of MBP, whereas

the data from Gil *et al* 2010 more closely matches our IHC data, albeit, with a

potential lag behind the CC. These data show that myelination in the CC precedes

the rest of the neocortex although it is not clear why this would be the case. There

may be variation between our western blot data and that of Gil *et al* 2010 simply due

to sensitivity of the antibodies or due to variations in MBP expression between the

strains of mice. As the murine neocortex is predominantly grey matter (Zhang and

Sejnowski, 2000), it is likely that myelin will not be as prevalent proportionally when

compared to the CC alone. Although myelination levels out from P21 in mouse

forebrains (Gil et al., 2010), it would have been interesting to examine whether there

would have been any further changes beyond P28 for the BALB/c mice.

Interestingly, when looking at OLG maturation in the CC, there appears to be a

steadier rate of increase than the rate of myelination. The percentage of mature OL

to total OLG (CC1$^+$ and Olig2$^+$ against all Olig2$^+$ cells) increased from negligible

levels at P0 to almost 40% by P7 however this increase slows to almost 60% by P28

although our data do not show a levelling off suggesting that OPC maturation

continues beyond this stage. Previous studies have also shown an increase in total

CC1+ cells as well as a greater proportion of Olig2+ cells that are also CC1+ in other

murine CNS/white matter samples, albeit only at the early stages P7-P12 .

Expectedly, this shows that maturation of OPC precedes the onset of myelination.

3.5.2 AMIGO3 in the murine CC during postnatal development

The levels of AMIGO3 during development are more difficult to interpret from our

IHC data. Firstly, AMIGO3 in the CC appears to be largely variable when semi-

quantified through IHC. A non-significant increase in AMIGO3 signal was observed at

P14 despite a considerable degree of variability in this data and a relatively low sample size (n=4). It is likely that due to our low sample size, anomalous data has led to unrepresentative increases. Additional replicates would be desirable to provide further confidence in this finding. Similarly, AMIGO3 co-localisation with CC1 (data not shown) did not produce any meaningful and reproducible data due to the variability in the AMIGO3 signal. If the results are correct however, the IHC data suggests that AMIGO3 levels rise when myelination reaches its peak and just after the main onset of OPC maturation, coinciding with a slowing of the rate of maturation. This could suggest that AMIGO3 plays a role in the postnatal inhibition of OPC maturation and myelination, helping to slow the rate of OPC maturation and myelination when sufficient levels have been reached, potentially to prevent an excess of myelin being produced, and also to maintain an OPC population in the CNS. It should be highlighted that these data do not show AMIGO3 expression exclusively in OLG.

The distribution of AMIGO3, as viewed qualitatively, shows a light distribution across the CC with small clusters. Although there is very limited previous examples of AMIGO3 IHC in OLG, AMIGO3 has been found localised to the somas of retinal ganglion cells (RGCs) as well as the somas of Oli-neu cells (Ahmed et al., 2013; Foale et al., 2014). AMIGO3, being a homodimer, could make small clusters on the membranes of cells within the CC (Kuja-Panula et al., 2003). However, it is very possible that the extended blocking and permeabilisation steps that were required to get sufficient staining in the positive controls, may have removed too much of the membrane and therefore removed a lot of the protein as well. It would have been

interesting to compare the expression of AMIGO3 in both OPCs and OLs in developing brains. Our original plan was to use IHC double staining with AMIGO3 and CC1 or NG2 similarly to the CC1/Olig2 study. Due to the variability observed with AMIGO3 IHC it was deemed that this would not valuable. One method that could have been used would have been to isolate and separate OLG from developing mice using fluorescence-activated cell sorting (FACS) based on makers of differentiation and maturation and make an analysis of the AMIGO3 levels in the separated populations (Robinson et al., 2014a). This would allow detailed analysis of the expression of AMIGO3 in the OLG subpopulations at various stages of development, although large numbers of samples would be required for this study. Unfortunately, resource and time constraints meant that this was not possible.

3.5.3   AMIGO3 and LINGO1 in the murine neocortex during postnatal development

As previously discussed, to overcome the limitations with the AMIGO3 IHC, western blots were performed. Following our preliminary studies, it was clear that our antibodies were sufficient at detecting AMIGO3 in CNS samples. Similar results have already been shown in our group with the Abcam LINGO1 antibody (Ahmed et al., 2013).

From our data both AMIGO3 and LINGO1 protein expression in the mouse neocortex is high prior to the onset of myelination but decreases as myelination progresses. Interestingly the onset of myelination appears immediately following the reduction in AMIGO3 with the highest levels of myelin observed when AMIGO3 has reached negligible levels. Interestingly LINGO1 protein levels appear to drop and rise

again as myelination begins. If LINGO1 is the predominant inhibitor of developmental myelination, then its raised expression at P21 poses a dilemma. It is possible that AMIGO3 has a more crucial role during the developmental stages and that its expression is reduced earlier to ensure that AMIGO3 does not provide its inhibition to OPC development and myelination.

Considering that AMIGO3 has shown to be able to interact with the same receptors as LINGO1 (Ahmed et al., 2013), it is possible that the drop in expression of both AMIGO3 and LINGO1 is not sufficient as both proteins are still expressed at relatively high levels. I conclude that both proteins may be able to inhibit myelination through the same pathway. It is not until both LINGO1 levels have dropped and AMIGO3 has become absent that myelin increases by any significant amount, indicating that until low levels of both AMIGO3 and LINGO1 are present, myelination is still inhibited. As such it would be interesting to observe whether levels of LINGO1/AMIGO3 rise again as the rate of myelination decreases. Furthermore it should be noted that a number of other pathways have been indicated in the regulation of myelination such as the mTOR pathway, Wnt pathway and ERK pathway (Gaesser and Fyffe-Maricich, 2016), therefore it is likely that even though both LINGO1 and AMIGO3 levels are being altered, further changes from other pathways are required to properly regulate the state of myelination and OPC development.

One interesting point is that both AMIGO3 and LINGO1 are not expressed at high levels a P0. This shows that neither of the proteins are involved with any inhibition prior to birth in murine models. There are a number of pathways that are involved

with regulating the maturation of OPCs, therefore it is likely that other pathways are involved in the early stages of development. Recent data shows LINGO1 mRNA is expressed in embryonic day dpf13-17 mouse brains, specifically in the hippocampus and cortical plate and thalamus when labelled with digoxigenin-labelled antisense probes. AMIGO3 however only showed very faint levels in the ventricular zone and subventricular zone (Chauhan and Egea, 2014). Considering that our data shows low LINGO1 protein expression at P0, this suggests that, or the gene is expressed but there is a blockade on translation until early postnatal days. This could be examined by assaying total mRNA levels by PCR for LINGO1 during this period. Such an approach would help to determine if the levels of LINGO1 mRNA drop at P0 before a rise for P7, or whether there is a further blockade of translation.

The data from Chauhan and Egea (2014) and our study show that AMIGO3 is not being produced at the protein or mRNA level until P7. This could suggest that AMIGO3 is not involved with regulating OPC maturation process. If AMIGO3 is involved with limiting the maturation of OPCs, then there must be an alternative method being used in the prenatal stages of development. Alternatively, these data indicate that AMIGO3 may be more relevant in the myelination blockade, therefore AMIGO3 is not translated until mature OLs are present.

3.5.4   Limitations

There are a number of limitations associated with this study that need to be taken in to account for the analysis. As previously discussed, in both the IHC and western blot studies, it was not possible to analyse the expression of AMIGO3 or LINGO1 in exclusively OLG. Both AMIGO3 and LINGO1 have been indicated in the inhibition of

axonal growth, as well as being expressed in astrocytes and in the case of LINGO1 immune cells (Mi et al., 2004; Satoh et al., 2007; Ahmed et al., 2013). Therefore, it is possible that changes in expression could be related to the role of these proteins in the various cell types. This could be an area of further interest regarding OLG behaviour. AMIGO3 is both a heterodimer and homodimer and expressed on the external membrane, therefore it is possible that AMIGO3 signals between neurons, astrocyte and OLG as also proposed for LINGO1 (Kuja-Panula et al., 2003; Kajander et al., 2011; Jepson et al., 2012; Ahmed et al., 2013). This idea is also supported by the observations that neuronal signalling is essential for proper myelination, therefore there must be a method for neurons to interact with local OPCs to stimulate or inhibit their maturation and ensheathment (Bradl and Lassmann, 2010). This is not surprising as regulation of myelination is important to ensure proper timing of the onset of ensheathment, as well as to determine sheath length so that the neuronal circuits can function appropriately (Klingseisen and Lyons, 2018). This would mean that AMIGO3 expression on neuronal and astrocytic external membranes during development could signal to neighbouring OLG. If our hypothesis for the role of AMIGO3 is correct, this intercellular signalling could in turn have an impact on OLG maturation and myelination. Notably though, it is possible that these major changes in expression at P14 may represent changes in expression of the proteins in cells other than OLG or in specific grey matter regions where OLG are limited or absent.

It should also be pointed out that due to the time and financial constraints associated with this project, a limited sample size had to be used. With a larger sample size, it is likely that a normal distribution would have bene identified for the

studies and ANOVAs would have been appropriate to examine and significant differences in the data. Additionally, a number of the groups showed trends towards significance when analysed with the Kruskal-Wallis test. It is likely that a larger sample size would have reduced the SEM, helping to further identify minor variations, and allowing greater confidence in the results. Performing a power calculation would be beneficial to determine the number of animals that would be required. A similar study with LINGO1 was performed and could have been used as a basis for power calculations. However this study is not a direct preliminary study and therefore could have only been a guide rather than direct indication of the numbers required (Mi et al., 2004).

Another potential limitation with our work is the antibodies that were used. Multiple bands were observed for both AMIGO3 and LINGO1. For AMIGO3, bands were observed at 55kDa and 45kDa. The 45kDa likely represents a breakdown product of the original protein. Multiple bands were observed from the LINGO1 western blot. Again, all of the extra bands were at a reduced band size compared to the expected band therefore are likely breakdown products but again this does raise a limitation in that there is a small chance of non-specific binding. It also raises the possibility that there has been some degradation of the samples which may lead to unrepresentative results. Non-specific binding with antibodies could also lead to incorrect expression in our IHC providing false positives, however our controls should minimise this risk.

3.5.5   Future studies

A number of further questions have been posed by these data. Firstly, as previously discussed, it would be interesting to analyse the expression profile of

these proteins at both the protein and mRNA level in individual cell types. This would provide a better analysis of the role that AMIGO3 and LINGO1 have specifically in OLG. Although this would be difficult for mRNA analysis due to degradation during the fixation process, microarray following FACS has been performed and could provide an interesting further analysis (Iglesias-Ussel et al., 2013). Alternatively, a co-staining process could be developed for mRNA as well as OLG proteins markers to provide qualitative analysis.

It would also be very interesting to examine whether AMIGO3 is in fact able to interact between cells or even in solution. Although unlikely, it would be interesting to examine whether AMIGO3 is expressed in solution and in sufficient levels in the interstitial fluid, and whether altering levels would affect cultured OLG populations *in vitro* or even *in vivo*. Cellular interactions could also be investigated through co-cultures of neuronal/astrocytic populations with OLG. Increasing or decreasing expression of AMIGO3 through transfections in the neurons/astrocytes would then allow any changes in OLG behaviour to be attributed to intercellular interactions from neighbouring neurons/astrocytes.

Another avenue of investigation would be to investigate whether OLG exhibit an underlying expression of AMIGO3 both when reaching maturity and during their lifespan. It is known that both local OL and media from cultured OL inhibit the maturation of OPC therefore it would be interesting to observe whether AMIGO3 is potentially involved in this process (Miller, 2002). Finally, it still remains to be answered whether AMIGO3 is able to interact in OLG. Although we have data showing trends of AMIGO3 expression inversely correlating with myelination, as well

as data showing AMIGO3 expression in OLG (unpublished), there is yet to be any

evidence examining molecular interactions or changes in cell behaviour after altering

AMIGO3 expression.

Chapter 4

AMIGO3 expression in models of

oligodendrocyte trauma

4.1 Rationale

4.1.1 MS and OLG trauma

For the context of this study, I hereby shall be using the term 'trauma' in reference to all forms of injury including, but not limited to; inflammatory insults, excitotoxicity and hypoxia, rather than only physical injury.

MS shares a number of characteristics with simple CNS trauma, in that OLG are lost, albeit due to differing mechanisms, with an autoimmune response being the most likely cause in MS compared to mechanical injury in CNS trauma. Furthermore, CNS axons following both chronic and traumatic injury and MS demonstrate the ability for remyelination, however this becomes impaired due to environmental factors (Patani et al., 2007; Alizadeh et al., 2015). As such, the molecular mechanisms involved in OLG trauma are of value to remyelination therapies and should be relatable to MS.

As previously discussed, a number of OPCs survive even in developed MS plaques, and it is thought that these cells lose their innate ability to differentiate or their differentiation is inhibited, which results in the inefficient remyelination following demyelination (Patani et al., 2007). With this in mind, it would be valuable to develop an *in vitro* model to replicate the trauma that OPC receive during a bout of demyelination. Both LINGO1 and AMIGO3 are upregulated following CNS trauma and both molecules have been shown to some degree to be present in OLG. Based on this we wanted to investigate how conditions in the diseased CNS, such as in MS,

may affect the expression of AMIGO3 in OPC (Mi et al., 2004; Mi et al., 2005; Mi et al., 2007; Ahmed et al., 2013).

There are a number of potential processes that could be involved in the blockade of remyelination in MS. The simplest hypothesis is that due to repeated bouts of OL trauma, the amount of myelination-inhibiting, myelin-derived products increases, thereby inhibiting the maturation and myelin production capability of OPCs (Kotter et al., 2006; Zhao et al., 2006). A number of other inhibitory pathways have been suggested including the Notch-jagged signalling pathway (John et al., 2002), hyaluronan-TLR2 signalling (Sloane et al., 2010) and type IV collagen signalling with OPCs (You and Gupta, 2018), as well as the proper release of pro-regenerative factors from the immune system, such as TGF-β, Activin-A and IGF-1 as well as others.

Overall, it is believed that inhibition to OPC differentiation or OLG myelination is increased in MS plaques, therefore it is important to examine the inhibition process so that effective therapies can be developed to promote remyelination. As LINGO1 and AMIGO3 have been identified as potential inhibitors of remyelination, we decided to investigate whether there is a change in their expression following trauma to OLG.

4.1.2   Models of demyelination and OLG trauma

A number of models have been developed to investigate OLG trauma and demyelination. Most of these models have been used *in vivo*, namely cuprizone, ethidium bromide and LPC and the inflammatory based models of EAE (Merrill, 2009; Miron et al., 2011). Cuprizone is a copper chelator which is administered orally

preferentially affecting oligodendrocytes and leading to mitochondrial dysfunction and OLG death. LPC is an effective focal demyelination agent, which when used at the correct concentration (usually 1% v/v), results in localised demyelination followed by complete remyelination within four weeks (Jeffery and Blakemore, 1995; Lu et al., 2018). Ethidium bromide is similarly used as a focal demyelinating agent, which leads to more extensive and rapid demyelination than LPC (Squire, 2009). Ethidium bromide is a DNA intercalating agent which leads to the death of local astrocytes and OLG, requiring action of the immune system to clear debris before proper remyelination can occur (Merrill, 2009; Squire, 2009; Miron et al., 2011).

Although these models are useful techniques for examining demyelination in the whole system, we decided that an *in vitro* homogenous cell culture model would be beneficial as a way to quickly and reliably get an idea of AMIGO3 OLG responses independently that can then be related to a larger system. This also avoids the time constraints and expense associated with using animal models. We decided to examine two models for our *in vitro* OLG injury investigation. An excitotoxic model of OPC injury involving application of α-amino-3-hydroxy-5-methyl-4-isoxazolepropionic acid (AMPA) with cyclothiazide (CTZ) (Begum et al., 2018), and LPC induced OPC injury. Due to the expense and time-constraints involved in generating large numbers of primary OPC, the Oli-neu cell line was used for our models. As previously discussed, and shown by ourselves and others, Oli-neu cells are Olig2 and NG2 expressing and demonstrate a number of characteristics of OPC, having been immortalised from murine OPC (Jung et al., 1995; Pereira et al., 2011; Foale et al., 2014). Therefore, these cells will be a relevant model for our studies.

140

4.1.3 AMPA-CTZ

CTZ is a positive allosteric modulator of AMPA receptors. After binding with AMPA receptors, CTZ increases the receptor sensitivity to AMPA and blocks desensitisation. This results in the channel opening more readily and increases the length of time that the channel is open for, causing a much greater influx of ions (Fucile et al., 2006). This has then been correlated to an influx in Ca^{2+}, an increase in Ca^{2+} levels in mitochondria and subsequent mitochondrial damage, ultimately leading to cell death in a method that mimics excitotoxicity (Chen et al., 2007). Glutamate excitotoxicity has been presented to be a mechanism of lesion progression in MS. Inhibiting AMPA receptors with AMPA antagonists, as well as inhibiting other glutamate receptors, in EAE models reduces the clinical score (Werner et al., 2000; Gentile et al., 2018). This demonstrates that using AMPA receptor-induced excitotoxicity mimics some of the features observed in the cell degradation in MS. Furthermore, OLG have been identified to be extremely vulnerable to AMPA mediated excitotoxicity (McDonald et al., 1998) and the AMPA-CTZ model has been established in our lab (Begum et al., 2018). As such, it is highly likely that the excess release of glutamate into the extracellular space in MS lesions will cause over-activation of receptors on OPC, resulting in trauma to the cells (Kostic et al., 2013). As such, we believe that treating OPC with AMPA-CTZ will be an effective model for investigating some of the traumatic events observed in MS.

4.1.4 LPC

As already mentioned, LPC traditionally has been used to induce demyelination *in vivo* or *ex vivo*, and is believed to predominantly affect OLs, rather than OPCs

(Fressinaud et al., 1996; Zhang et al., 2011). However, examples exist of LPC being used to induce OL and OPC trauma *in vitro*, where the count of viable cells reduces following incubation (Ou et al., 2016). LPC is believed to function as a detergent, which leads to the disruption of the myelin membrane by inducing blebbing and disruption of the membrane (Seyedsadr and Ineichen, 2017). Recent work has demonstrated that LPC treatment leads to a detrimental over-activation of Olig2 in mature OL which leads to demyelination and appears to inhibit the OL survival mechanisms in a Gpr17 regulated manner. This is contrast to Olig2's role in OPCs where it promotes their differentiation (Ou et al., 2016; Lu et al., 2018). Although the exact mechanism that LPC functions through to induce damage to OPC is unclear, LPC has shown to be an effective agent for inducing damage to OLG (Jeffery and Blakemore, 1995; Keough et al., 2015; Ou et al., 2016; Lu et al., 2018). It was decided that this model would be interesting to examine the effects of trauma on OPCs.

4.1.5   AMIGO3 in CNS trauma

As previously discussed, AMIGO3 has been shown to be upregulated more rapidly than LINGO1 in SCI trauma (Ahmed et al., 2013). Furthermore, as LINGO1 experiences a lag before its protein expression is raised in EAE, it appears likely that LINGO1 does not have a role in acute diseases. AMIGO3 on the other hand has been shown to be upregulated, at least at the transcript level, immediately after trauma in murine SCI (Ahmed et al., 2013). As such, it is likely that AMIGO3 is also raised acutely in OLG disease.

4.2 Aims

Specifically, we wanted to examine whether we could develop effective models of CNS trauma and whether these models could be used to demonstrate changes in LRR protein expression. This could be used as evidence to back up a role for LRR proteins in the pathogenic blockade of remyelination in demyelinating diseases.

4.2.1 Hypothesis

We hypothesise that:

- AMIGO3 is upregulated following trauma to Oli-neu cells.
- AMIGO3 is upregulated to a higher degree than LINGO1 in the acute stage following trauma to Oli-neu cells, indicating its role in acute demyelination.

4.3 Experimental design and methods

4.3.1 AMPA-CTZ induced Oli-neu trauma

The AMPA-CTZ model has previously been tested and optimised within our group (Begum et al., 2018). Cell viability dropped to between 75-40% when treated with concentrations of AMPA ranging from 1-1000µM AMPA (with CTZ fixed at 100µm), demonstrating effective cell trauma. Previously our group used 100µM AMPA with 100µM CTZ as this demonstrated reliable and sufficient cell trauma to Oli-neu cells to measure responses to excitotoxicity.

500,000 Cells were seeded in a 6 well plate and cultured for 24 hours in SATO media at 37ºC with 5% CO_2, to allow them to adhere. After 24 hours, media was fully

replaced with SATO media containing 100μM AMPA and 100μM CTZ. Control groups were also prepared with either SATO containing 100μM CTZ as well as SATO alone shams. The samples were then incubated for 5 hours. Following incubation, samples were collected and processed as previously described, to detect AMIGO3 and LINGO1 protein and mRNA by western blot and RT-qPCR.

4.3.2   Optimisation of LPC induced Oli-neu trauma

To enable comparison with the AMPA-CTZ studies, incubations in LPC were designed initially planned as 5 hour treatments. However, since previous experience of the effects of LPC on Oli-neu was not available optimisation of the concentration of LPC was necessary. For this work 500,000 Cells were seeded into the wells of a 6 well plate and cultured for 24 hours in SATO media at 37ºC with 5% CO_2, to allow them to adhere. After 24 hours, LPC was applied at varying concentrations. Cell cultures were then analysed in a number of ways:

- Qualitative analysis was performed by imaging the cells directly.
- Brightfield images were taken and cells were analysed for morphological and density changes to determine whether trauma had been induced.
- Cell counts and viability assays through trypan blue analysis.

Cells were trypsinised and centrifuged as described (see section 2.3.1). Samples were then resuspended in equal volumes of SATO and 0.04% trypan blue. Samples were counted for total cells and viable cells in a haemocytometer.

4.3.3 LPC induced Oli-neu trauma

Once an appropriate concentration and time period of LPC incubation was decided, analysis of AMIGO3 and LINGO1 expression was performed in this model. 500,000 Cells were seeded in a 6 well plate and cultured for 24 hours to allow them to adhere. After 24 hours, LPC was applied in SATO media and incubated. Two tests were performed; firstly, samples were collected immediately after incubation. Secondly samples had media replaced with SATO media and left for a total period of 24 hours. After either the 5 hours or 24 hours, samples were collected and processed for AMIGO3 and LINGO1 expression by western blot.

4.3.4 Experimental plan

A summary of the plan for the investigation, findings and experiments used is demonstrated in figure 4.1.

4.4 Results

4.4.1 AMIGO3 and LINGO1 expression in Oli-neu cells following incubation with AMPA-CTZ

Our first model of Oli-neu cell trauma was the AMPA-CTZ model. AMIGO3 protein expression, normalised to α-tubulin, increased almost twofold following incubation with AMPA-CTZ compared to both CTZ alone and sham treated cells, reaching 0.92±0.07 compared to 0.52±0.09 and 0.59±0.02 respectively (fig 4.2). Significance (ANOVA, $F_{(2,8)}=9.577$, $P<0.01$) was found within the samples, therefore variation in the mean AMIGO3 protein level existed. The increase in AMIGO3 expression in AMPA-CTZ treated Oli- neu cells was found to be significant between both the CTZ

145
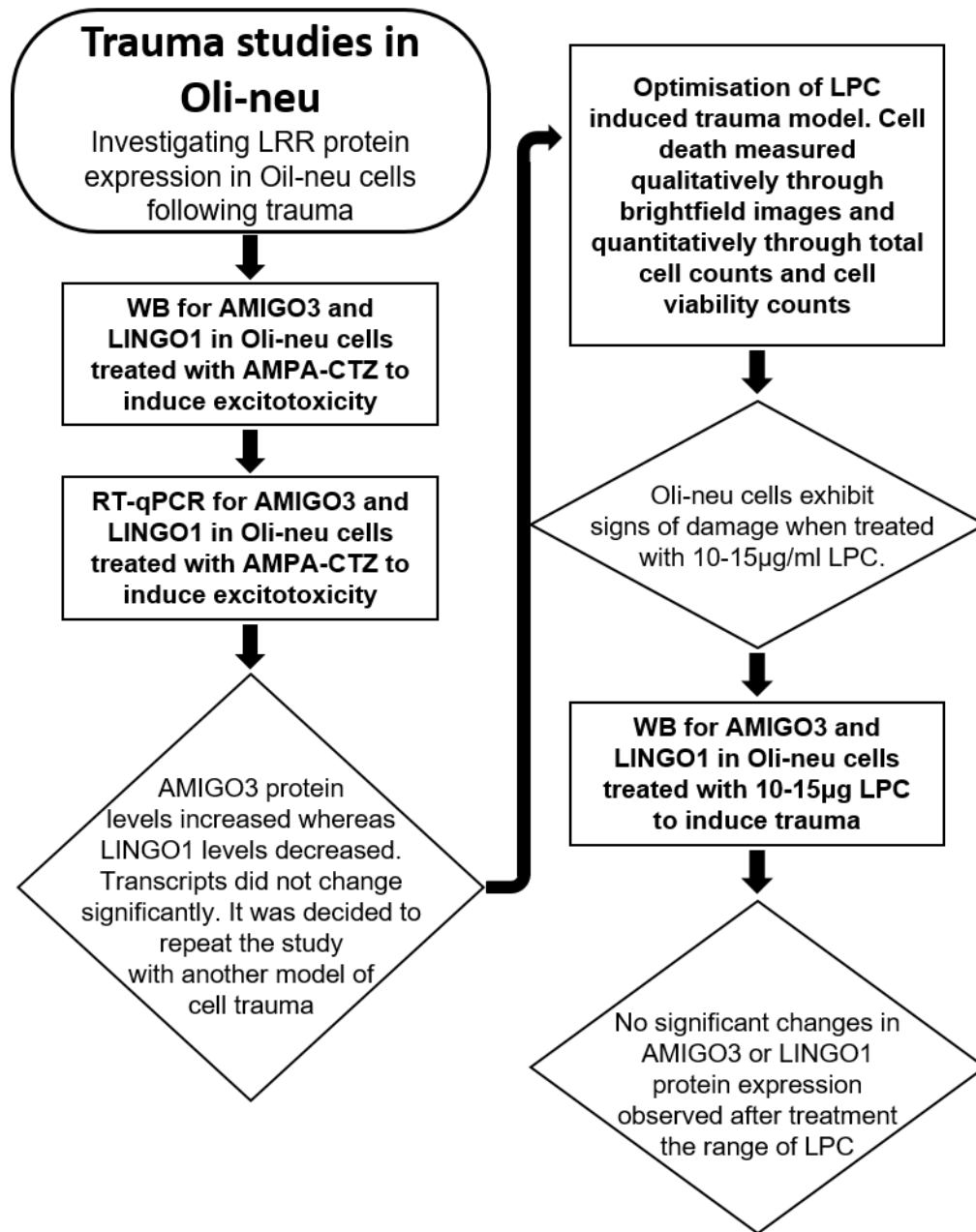
Figure 4.1: Flow chart demonstrating the plans and summarising the findings from chapter 4.
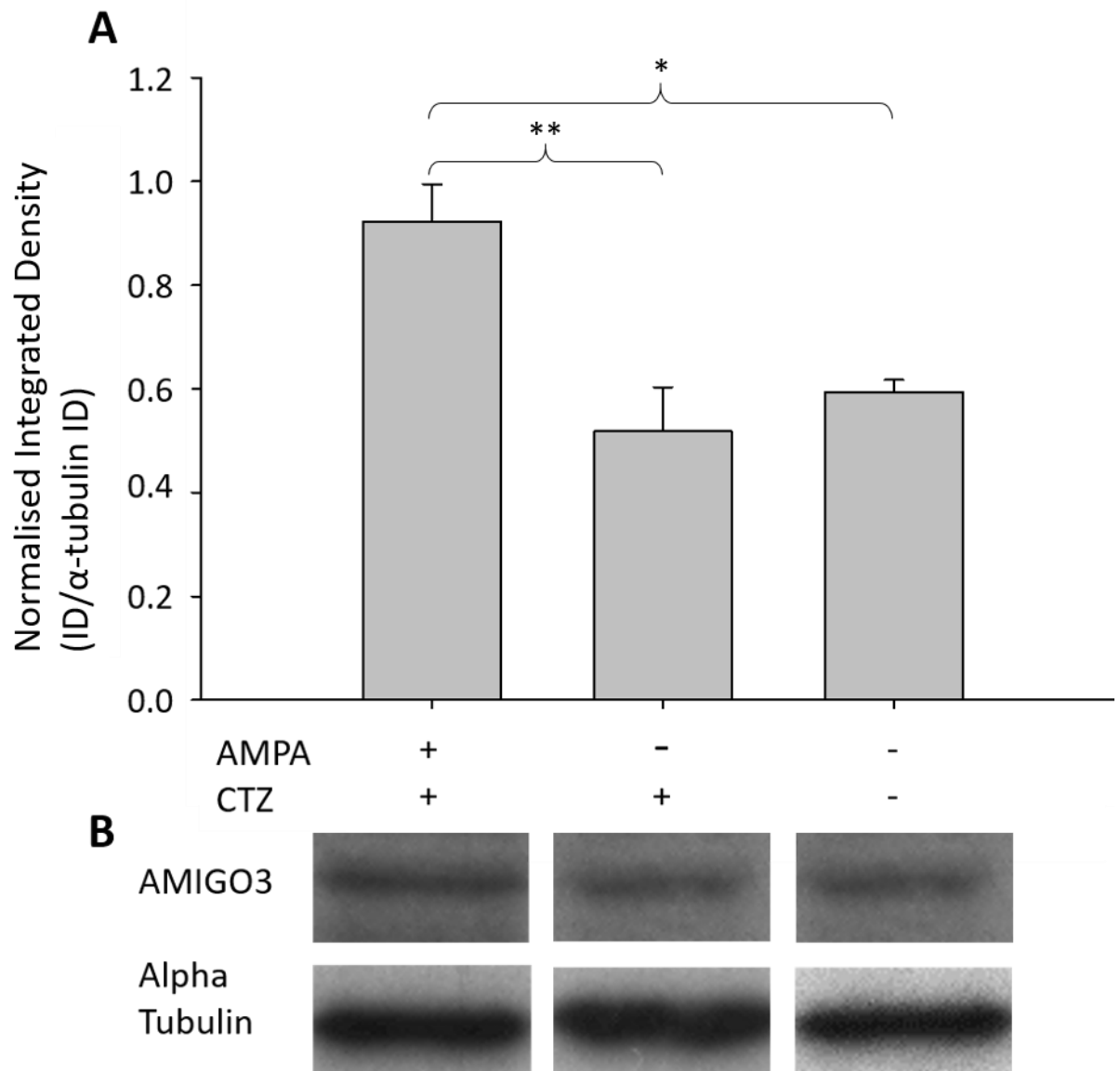
Figure 4.2: (A) AMIGO3 protein expression in Oli-neu cells treated with 100μg/ml AMPA and 100μg/ml CTZ, 100μg/ml CTZ or sham for 5 hours. (B) Representative Western blots for the treatments. AMIGO3 levels were found to rise, only when treated with both AMPA and CTZ, indicating that levels of AMIGO3 have risen following the induction of trauma in this model. Error bars represent one SEM, n=4 for each group (* p<0.05, **p<0.01).

alone and sham treated cells (p<0.01 and p<0.05 respectively). No significant variation was detected between the sham and CTZ alone treated samples.

Interestingly our first studies showed an inverse reaction to the LINGO1 protein levels. Integrated density readings of LINGO1 protein levels were relatively high in both the sham treated and CTZ treated (1.13±0.14 and 1.07±0.06 respectively). ANOVA analysis showed significance between the mean LINGO1 expression in the groups (ANOVA, $F_{(2,9)}=8.195$, P<0.01). No significance was detected between sham and CTZ alone treated groups (P>0.05). However the levels of LINGO1 protein dropped reaching 0.62±0.08 following incubation with AMPA-CTZ (fig 4.3), showing a significant decrease compared to both of the control groups (P<0.05).

RT-qPCR was subsequently used to analyse the expression of AMGO3 and LINGO1 mRNA following incubation with AMPA-CTZ. Changes in expression were normalised against the expression of the proteins in sham samples. Both AMIGO3 and LINGO1 mRNA levels showed a modest relative increase in expression levels compared to untreated samples, with relative changes of 1.32±0.09 and 1.28±0.30. These were compared against the relative fold changes for the CTZ alone treated groups and both groups did not display a significant increase in the relative fold changes in expression when analysed by a Mann Whitney U test (p<0.05) (fig 4.4).
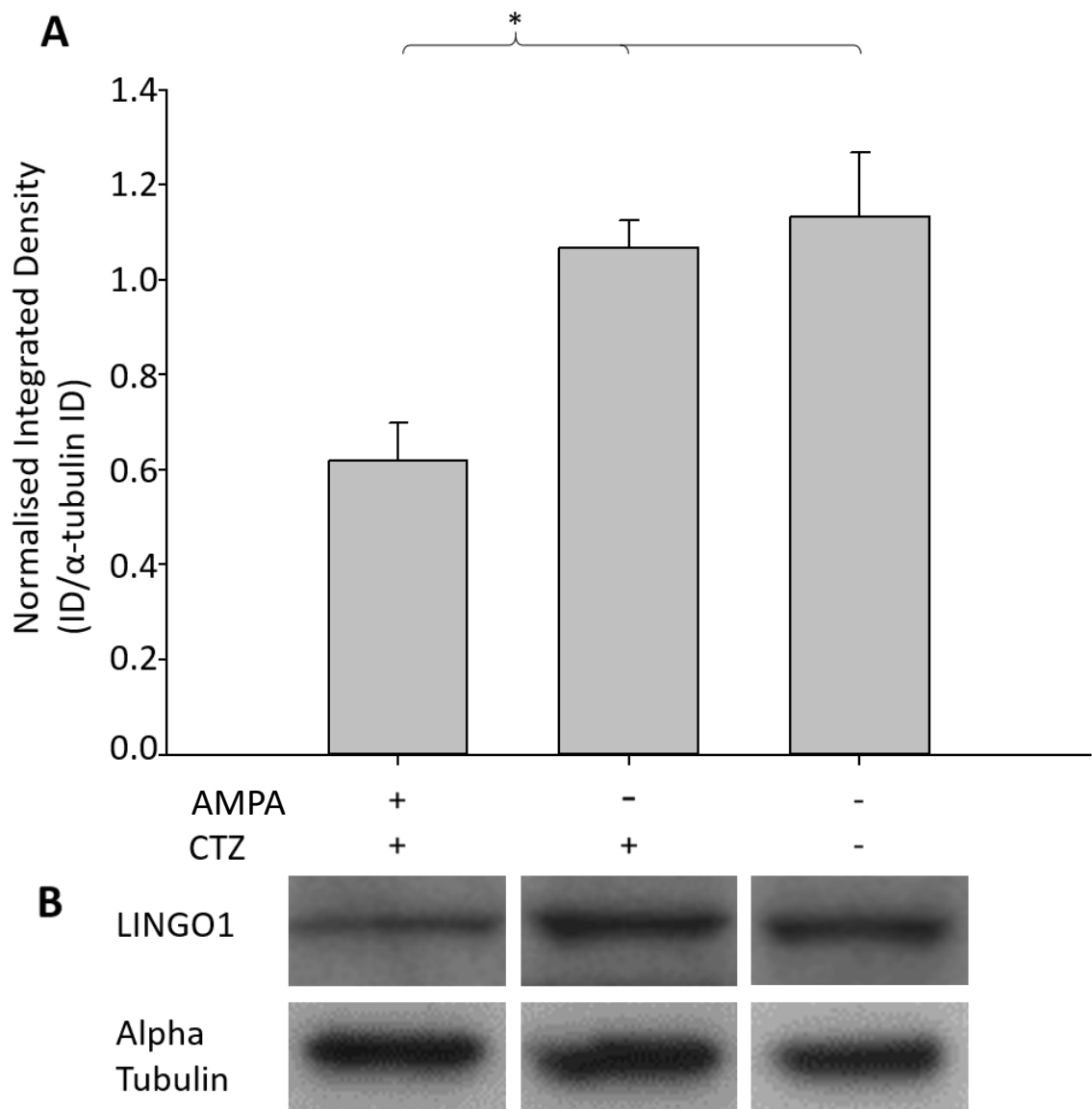
Figure 4.3: (A) LINGO1 protein expression in Oli-neu cells treated with 100µg/ml AMPA and 100µg/ml CTZ, 100µg/ml CTZ or sham for 5 hours. (B) Representative Western blots for the treatments) LINGO1 levels were found to decrease when treated with both AMPA and CTZ. This indicates a reduction in LINGO1 expression following trauma in this model. Error bars represent one SEM, n=4 for each group (* p<0.05).
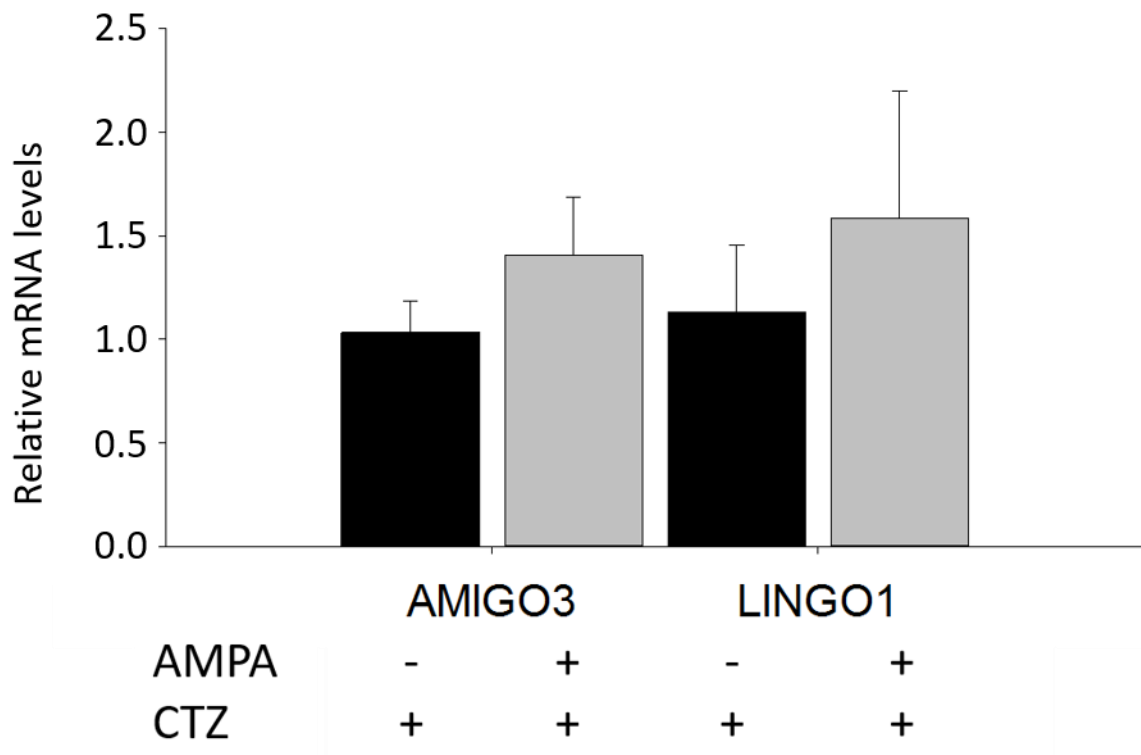
Figure 4.4: RT-qPCR analysis of AMIGO3 and LINGO1 mRNA expression in Oli-neu cells treated with 100μg/ml AMPA and 100μg/ml CTZ or 100μg/ml CTZ alone. Data is displayed as fold-changes compared against untreated controls. Although a rise in the mRNA levels of AMIGO3 and LINGO1 is observed, it is not significant when compared to the relative change in mRNA levels in cells treated with CTZ alone. Error bars represent one SEM, n=4 for each group.

4.4.2 Optimisation of LPC induced Oli-neu cell trauma

Various concentrations of LPC were tested in Oli-neu cell incubations to determine an optimal concentration and treatment period for inducing cell trauma. Cells were then visualised at the varying time points to get a qualitative analysis of the effects on cell viability. Treatment with concentrations of LPC ranging from 0.5-2.5mg/ml induced rapid and comprehensive cell death in Oli-neu cell cultures. Some residual cells were still present in the group receiving 0.5mg/ml when incubated for 40 minutes, however the cells were shrunken and spherical, having lost their characteristic bipolar phenotype (fig 4.5). It is clear from this data that the 0.5mg/ml treatment was too severe.

Due to the severe level of cell death observed with concentrations of LPC from 0.5mg/ml and above, levels of LPC were reduced to 0-50µg/ml and treatment periods examined between 5 minutes and 5 hours. Treatment with 5 and 10µg/ml LPC did not induce any clear phenotypical alterations in the Oli-neu cells morphology or density for up to 5 hours (fig 4.6). However, increases in LPC concentration above this level induced drastic results. A modest reduction in the density of Oli-neu cells was observed following addition of 25µg/ml LPC to the media following 5 minutes incubation. By 30 minutes incubation, most of the cells had retracted their processes and the density of the cells was drastically reduced. Following 5 hours, few cells remained and all cells were spherical with no processes visible. Treatment with 50µg/ml LPC showed more drastic changes, with a drastic reduction in cell density following 5 minutes of incubation. Minor processes were still visible in a few cells at

151
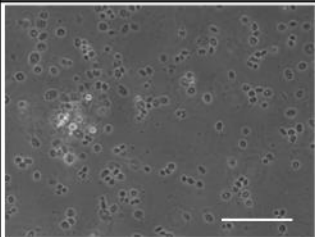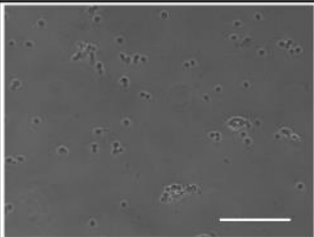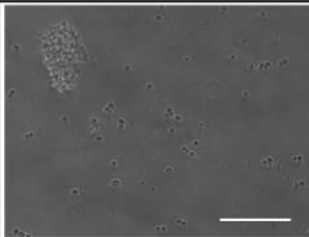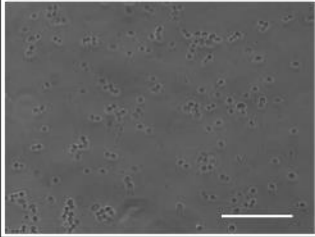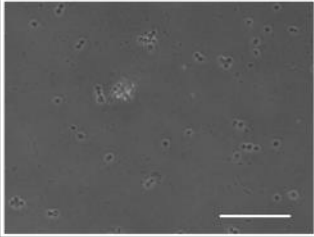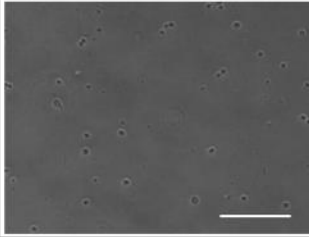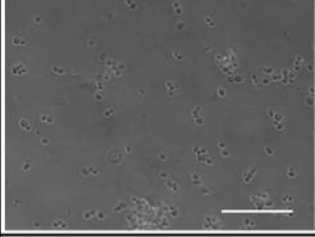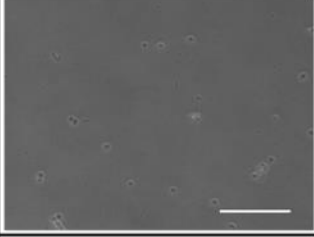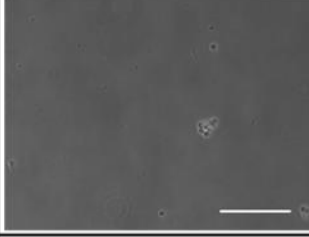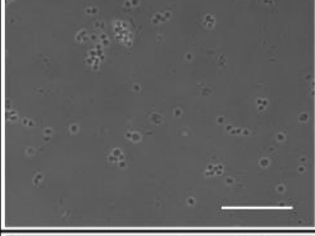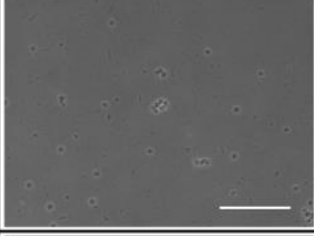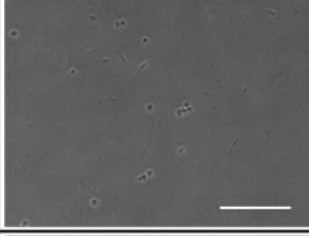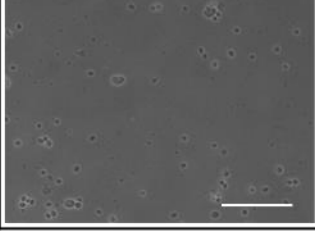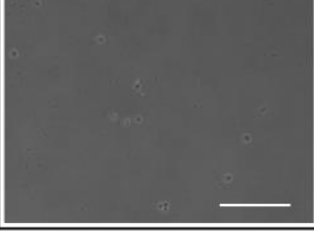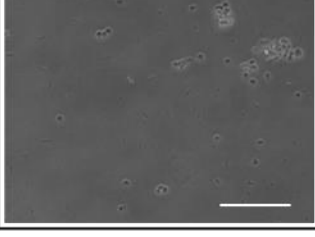
LPC concentration	Treatment time		
	40 minutes	4 hours	17 hours
0.5mg/ml			
1mg/ml			
1.5mg/ml			
2mg/ml			
2.5mg/ml			

Figure 4.5: Representative images of Oli-neu cells treated with varying concentrations of LPC. Concentrations tested vary from 0.5-2.5mg/ml. LPC at this concentration appears to cause marked cell death even at the lowest time point and concentration. Scale bars represent 100µm.
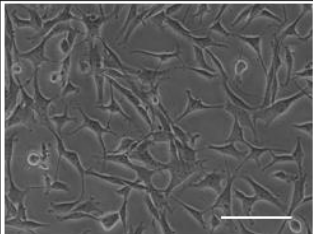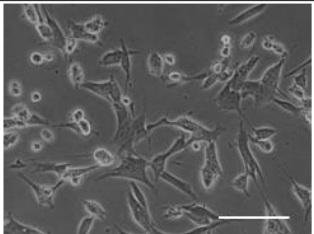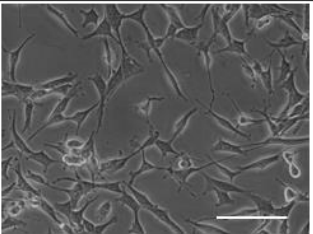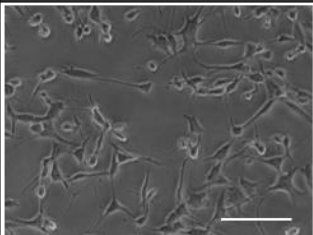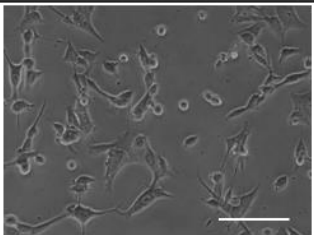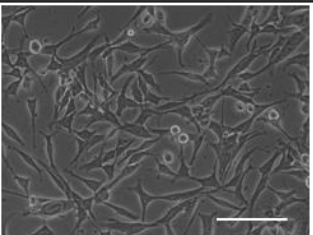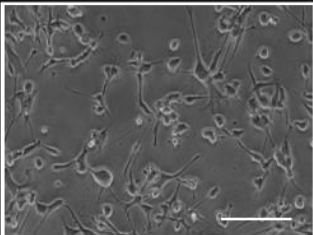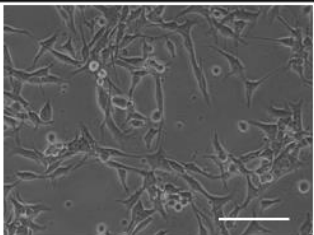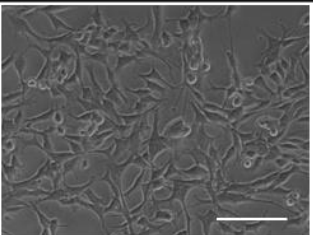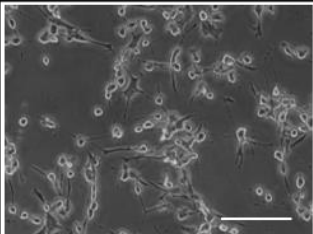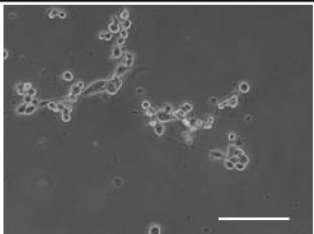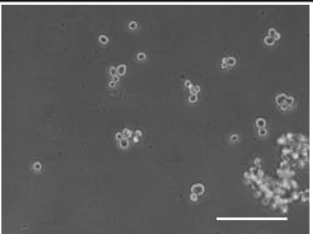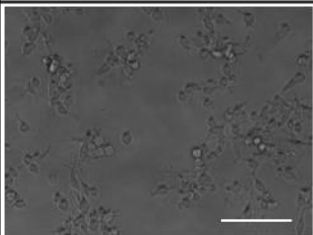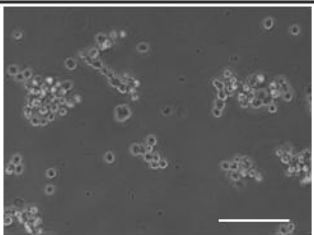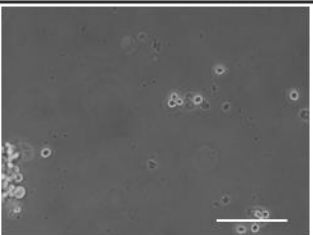
LPC concentration	Treatment time		
	5 minutes	30 minutes	5 hours
0µg/ml			
5µg/ml			
10µg/ml			
25µg/ml			
50µg/ml			

Figure 4.6: Representative images of Oli-neu cells treated with varying concentrations of LPC. Concentrations tested vary from 0-50µg/ml. very little phenotypical changes can be observed qualitatively with up to 10µg/ml LPC with any time point, however further increases lead to a marked reduction in cell density, with very few cells appearing to survive treatment with 50µg/ml LPC. Scale bars represent 100µm.

this time point. Further incubation showed a greater reduction in the cell density as well as a loss of all visible processes, with barely any cells present following 5 hours incubation (fig. 4.6).

Further tests were performed on Oli-neu in the range of 10-15µg/ml, where cells were still observed to survive following treatment for 5 hours. Total cell counts and the proportion of cells that take up the trypan blue (cell viability) were used to examine the extent of trauma to cells with LPC at this range. Counts of the total cell numbers following treatment with LPC showed no reduction after 5 hours with all concentrations (fig 4.7A). Interestingly, significance was found in the mean population of cells (ANOVA, $F(3,8)=7.833$, $P<0.01$). Post-hoc tests revealed that there was a significant increase ($p<0.05$) in the total cell population in cells which had been treated with 15µg/ ml ($1.31x10^6 \pm 9.4x10^4$ cells) when compared to Sato treated sham controls ($9.2x10^5 \pm 2.4x10^4$ cells), 10µg/ml ($8.8x10^5 \pm 6.7x10$ cells) and 12.5µg/ml ($9.5x10^5 \pm 7.5x10^4$) (fig 4.7A).

Proportions of cells that took up trypan blue were also measured. The control group did not show a normal distribution, therefore a Kruskal-Wallis and subsequent Dunn-Bonferroni post-hoc tests were used to analyse the proportion of Oli-neu which incorporated trypan blue following incubation with LPC. Qualitatively, it can be observed that the proportion of trypan blue positive cells does not increase until at least 12.5µg/ml, where a minor increase from 0.076±0.007 and 0.070±0.001 in sham controls and 10µg/ml respectively, to 0.131±0.006 was observed. A more substantial increase to 0.322±0.015 was seen when 15µg/ml LPC was used. Significance was
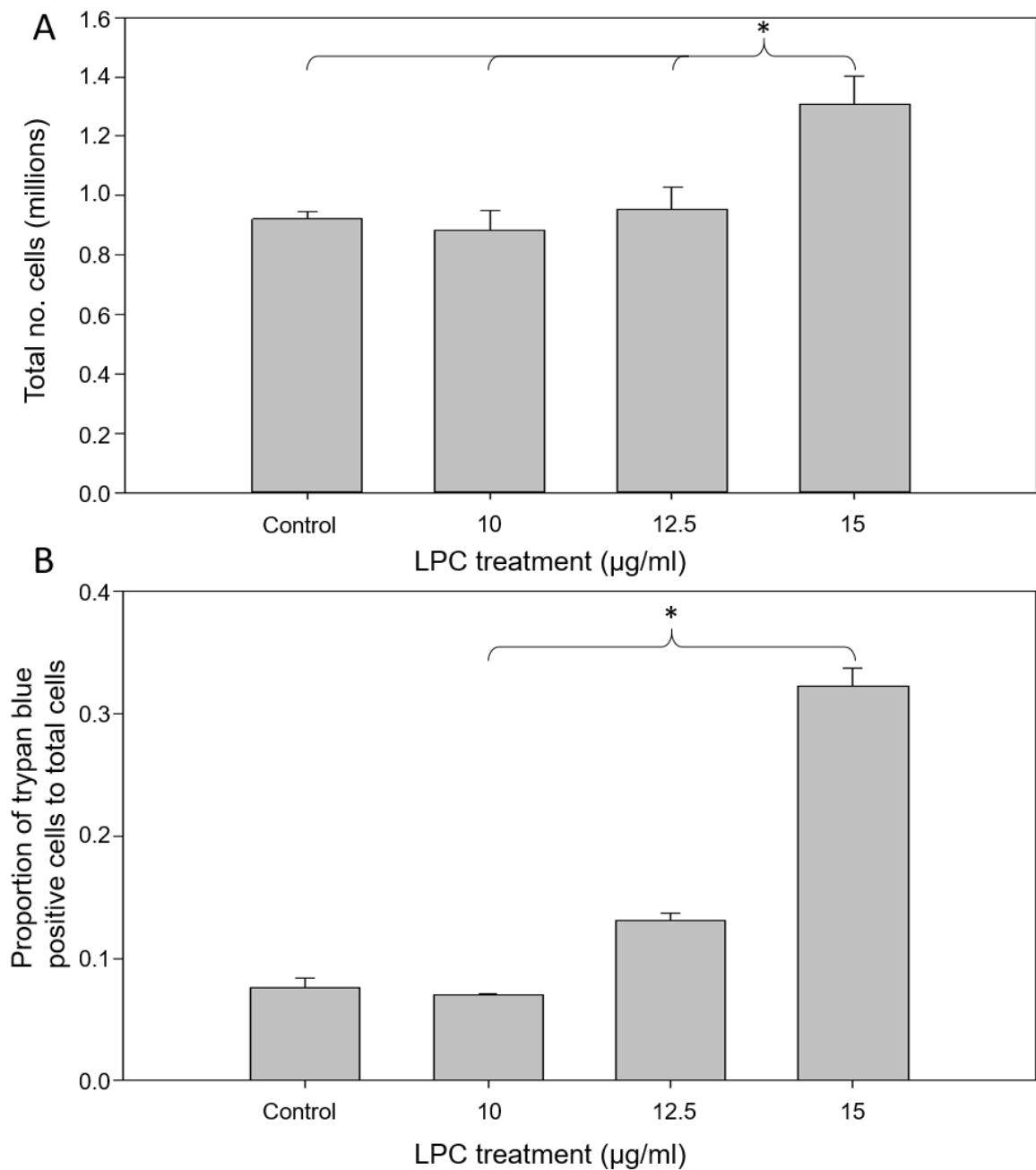
Figure 4.7: Optimisation of LPC induced Oli-neu cell trauma. Cells were treated with varying concentrations of LPC for 5 hours. (A) Total cell counts. Cell numbers increased at the highest levels of LPC, suggesting that cells were replicating. No other groups showed any significant change in cell population after treatment with LPC. (B) Proportion of trypan blue positive cells. There was an increase in the number of cells taking up trypan blue in the higher concentrations of LPC treated cells, although only significant at 15μg/ml. This indicates that a number of the cells had started to lose viability. Error bars represent one SEM, n=4 for each group (* $p < 0.05$).

155

only found (p<0.05) between the mean proportions of trypan blue incorporated cells treated with 15µg/ml and 10µg/ml, although a trend towards significance was observed between control and 15µg/ml LPC treated groups (p=0.105) (fig 4.7B).

4.4.3 AMIGO3 and LINGO1 expression in Oli-neu cells following incubation with LPC

An initial preliminary study looked in to the levels of AMIGO3 following treatment with LPC between 10-15µg/ml for 5 hours. A modest increase in expression was observed at both 10µg/ml and 15µg/ml LPC samples, reaching 0.50±0.08 and 0.51±0.13 respectively from 0.38±0.13 in controls. However, this trend did not reach statistical significance, and indeed ANOVA did not detect a significant source of variation within the groups' means (ANOVA, $F_{(3,8)}$=1.409, P>0.05). Interestingly a small drop in AMIGO3 expression was observed in the 12.5 µg/ml LPC group, to 0.24±0.05, although again significance was not found between this sample and any of the other samples (fig 4.8).

LINGO1 protein levels were analysed for cells treated with 10µg/ml LPC (fig 4.9). LINGO1 protein expression levels were normally distributed and had equal variance following incubation with 10µg/ml LPC for 5 hours, therefore a t-test was used to analyse variation in the mean compared to control samples. Similar to AMIGO3, a small and minor increase in LINGO1 expression was observed following incubation with 10µg/ml, raising LINGO1 integrated density levels from 0.26±0.05 in controls, to 0.34±0.05. Significance was not observed between the groups however (p>0.05).
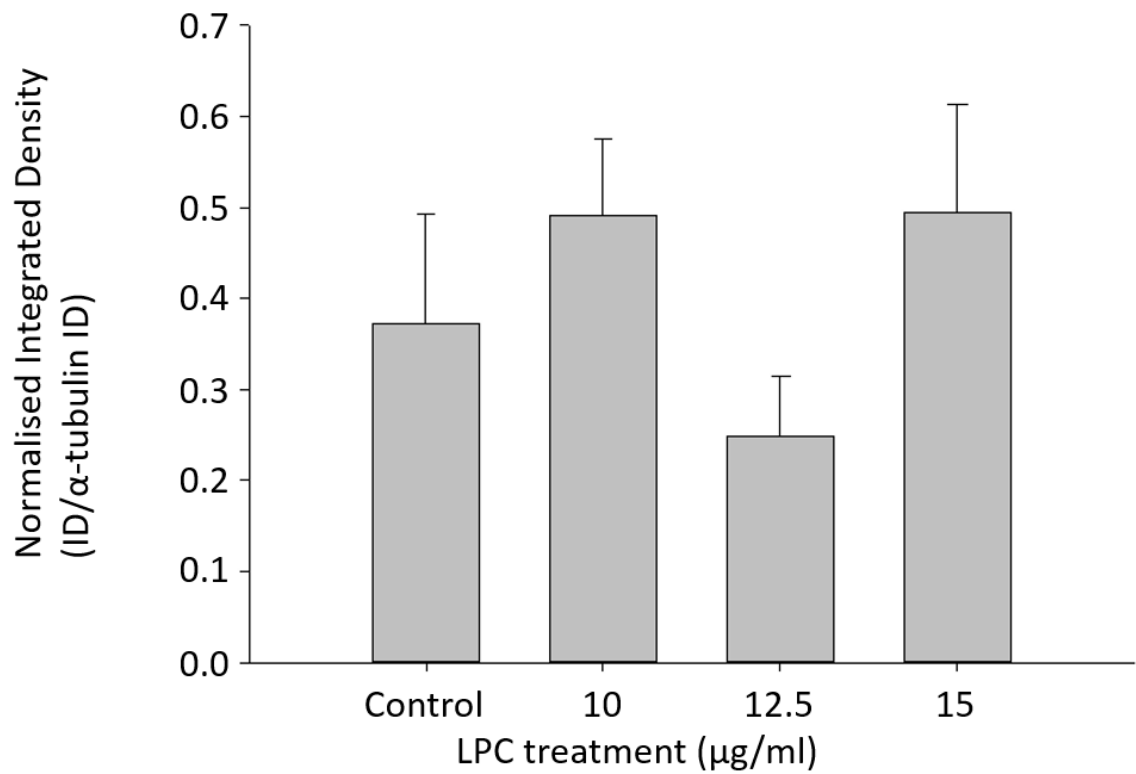
Figure 4.8: AMIGO3 protein expression in Oli-neu cells following treatment with LPC for 5 hours. Although significance was not observed, levels of AMIGO3 appear to rise following treatment with LPC, except in the 12.5µg/ml group, where a reduction can be observed. Error bars represent one SEM, n=4 for each group.
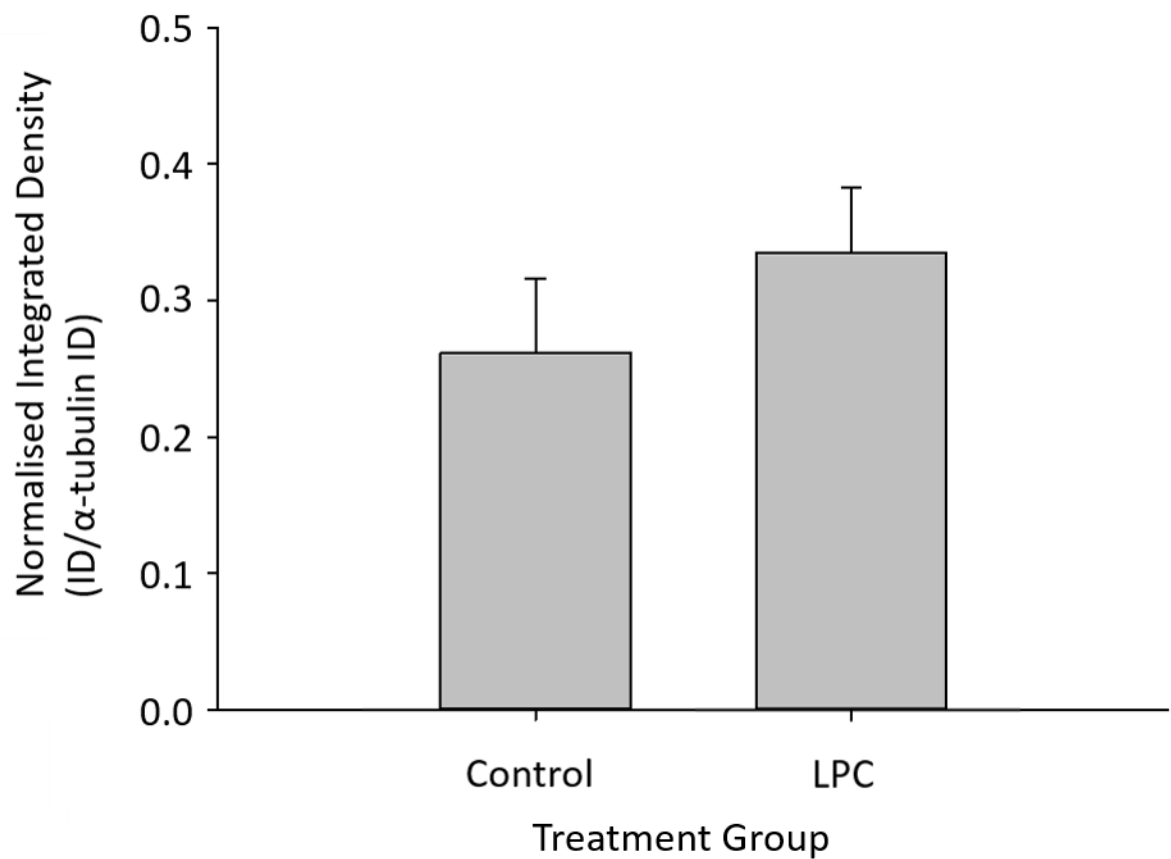
Figure 4.9: LINGO1 protein expression in Oli-neu cells following treatment with LPC for 5 hours. A minor and non-significant increase in LINGO1 protein levels was observed after treatment with 10µg/ml LPC for 5 hours. Error bars represent one SEM, n=4 for LPC treated, n=3 for controls.

4.4.3.1 AMIGO3 protein expression following 5 hour and 24 hour LPC

A further repeat with a larger size (n=12) was performed with cells exposed to 15µg/ml LPC for 5 hours. In this experiment protein samples were taken either immediately (5 hours), or 19 hours later (24 hours since incubation began). Both LPC treated and controls were found to be normally distributed with equal variance therefore samples were analysed using a t-test. A large variation in integrated density levels were observed for AMIGO3 levels in the LPC treated group, ranging from 0.7 to 1.3, with a mean normalised integrated density of 0.96 ± 0.04. This was found to be an increase compared to untreated control samples which had a mean normalised integrated density of 0.83 ± 0.08, however significance was not observed between the means of the groups (p=0.175, therefore p>0.05) (fig 4.10).

The 24 hour treatment data (5 hours LPC, 19 hours recovery) were analysed to examine AMIGO3 protein levels at a later time after trauma. Both LPC treated and controls were found to be normally distributed with equal variance therefore samples were analysed using a t-test. Again a large variation in normalised integrated density levels was observed in both the LPC treated and control groups, ranging from 0.64-1.70 and 0.50-1.45 respectively (fig 4.11). Similarly, no significance was observed between the means of the two groups (p=0.662, therefore p>0.05) and qualitatively, it appears that the mean normalised integrated density levels are equal, 1.07 ± 0.10 for LPC and 1.00 ± 0.11 for controls.
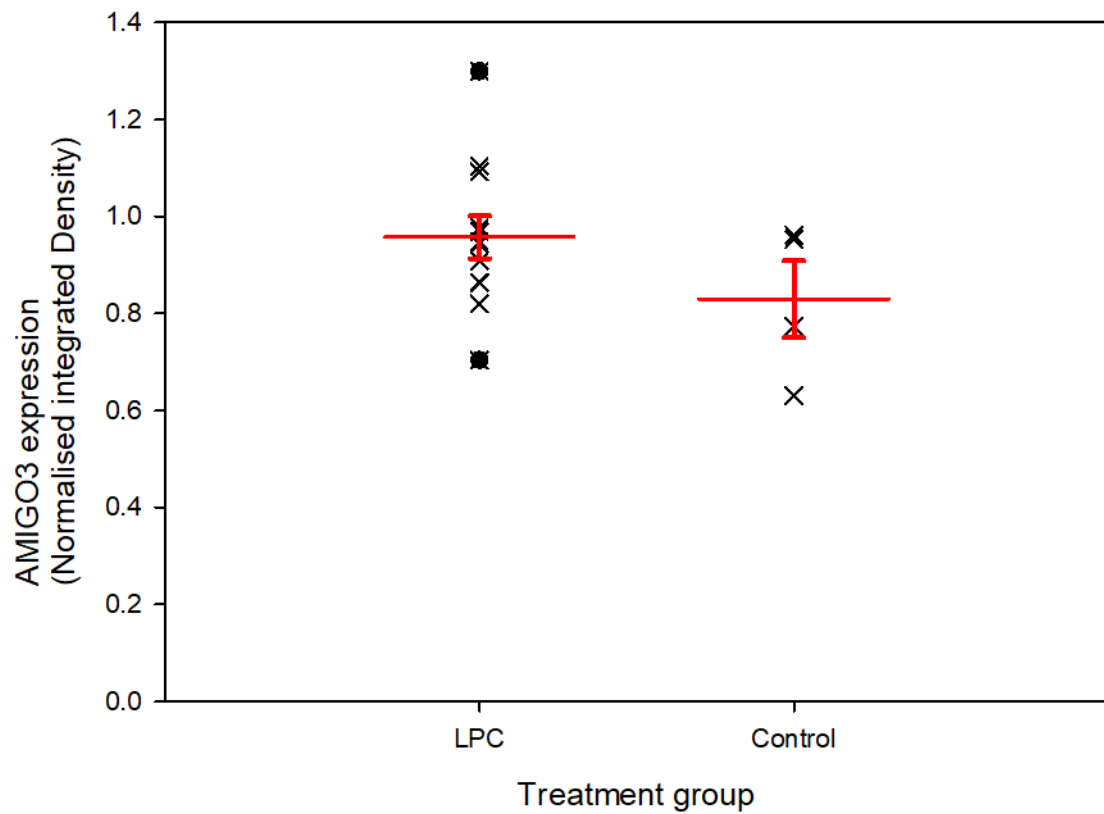
Figure 4.10: AMIGO3 protein expression in Oli-neu cells following treatment with 15μg/ml LPC for 5 hours. A larger repeat trial observed a large variation in levels of AMIGO3 following treatment with LPC. A minor although not significant increase in protein expression was observed. Error bars represent one SEM, n=12 for LPC treated, n=4 for controls.
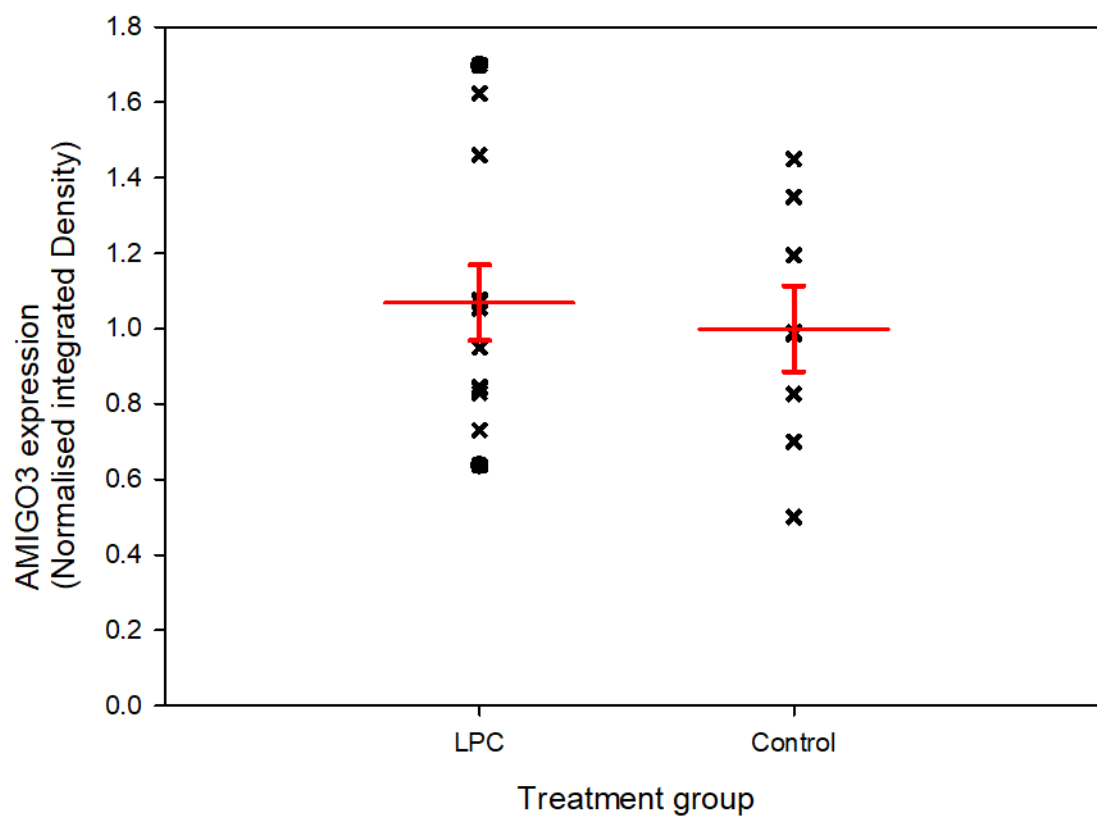
Figure 4.11: AMIGO3 protein expression in Oli-neu cells following treatment with 15μg/ml LPC for 5 hours, followed by 19 hours in normal growth media. AMIGO3 levels show high variation in both treated and controls with no clear change in the mean levels. Error bars show one SEM, n=12 for LPC treated, n=8 for controls.

4.5 Discussion

4.5.1 AMIGO3 and LINGO1 expression in OLG trauma: AMPA-CTZ

From the results of CTZ, it is useful to note that the levels of AMIGO3 and LINGO1 do not alter when treated with CTZ alone. This is expected as CTZ is not able to activate AMPA receptors in its own right. However, as levels of both AMIGO3 and LINGO1 are not altered between sham controls and CTZ alone incubation, this helps to validate our model. Interestingly in the acute stages of excitotoxic trauma, our model indicates that AMIGO3 is significantly upregulated within 5 hours of trauma, raising to over 80% in its protein expression. This matches our hypothesis and indicates that AMIGO3 is having a role in the acute stages of trauma. However, it is not clear exactly what role AMIGO3 is playing in this stage as, in contrast to the literature (Jung et al., 1995), our preliminary data was unable to elicit Oli-neu differentiation in response to cAMP treatment, thus we were unable to test the effects of differentiation on AMIGO3 expression. AMIGO3 mRNA levels are also observed to increase, albeit only qualitatively, after 5 hours of AMPA-CTZ induced excitotoxicity to Oli-neu cells. This agrees with our results from the western blot analysis, however it is unclear why significance was not observed. The most likely reason for this is the large degree of variation we observed in the data, hence a larger sample size is probably needed to detect the minor changes in the AMIGO3 mRNA expression.

Interestingly in this acute model of OPC trauma, LINGO1 levels are actually seen to decrease, reducing by around 30%. This appears to go against the *in vivo* trauma

data for LINGO1, where in demyelination and spinal cord injury, LINGO1 is observed to increase in protein expression (Ahmed et al., 2013; Wang et al., 2014; Theotokis et al., 2016), however it should be noted that these are all viewing LINGO1 levels after a longer time delay. It is interesting to note that the LINGO1 mRNA appears to increase during the 5 hour treatment period with AMPA-CTZ, opposing the protein levels, however this was not found to be significant. This actually matches data obtained *in vivo*, where multiple regions of the brain demonstrate increases in LINGO1 mRNA following kainic acid induced excitotoxicity (Karlsson et al., 2017). Similarly though, most anatomical regions analysed did not show a significant increase in expression until after 4 hours (Karlsson et al., 2017). This suggests that LINGO1 protein is being broken down at a rapid rate during the acute stages of trauma. It is possible that LINGO1 is simply broken down due to the trauma itself or it is being used up rapidly during this acute stage.

From this data however, it appears that AMIGO3 is upregulated more rapidly than LINGO1 following excitotoxic trauma. We propose that this indicates that just as with neurons in spinal cord injury (Ahmed et al., 2013), OPCs also upregulate AMIGO3 preferentially to LINGO1 during the early stages of disease. If both of these proteins are involved in the pathogenic inhibition of remyelination in MS and other demyelinating diseases, then our results suggest that AMIGO3 would be a more beneficial therapeutic target than LINGO1 as remyelination would be encouraged at an earlier stage of the disease. Earlier repair of myelin would allow neurons to be protected at an earlier stage so that less long-term damage would develop.

Interestingly, the excitotoxic model of trauma seems especially relevant as NgRs have been shown to play a role in protecting hippocampal neurons from excitotoxic damage (Lopez et al., 2011). This suggests that a signalling pathway that both AMIGO3 and LINGO1 are associated with, could be involved with mediating the effects of excitotoxic damage in OLG as well as limiting maturation and myelin production. As AMIGO3 is upregulated, whereas LINGO1 is downregulated following excitotoxicity in our model, it demonstrates that any NgR1 signalling that occurs in the OPCs must be utilising AMIGO3 preferentially over LINGO1 in the acute stages of trauma. Admittedly, the present data only investigates a single cell line so it possible that the OPCs and other OLG cell lines have variations in the downstream effects of NgR1 signalling. Furthermore, as already discussed, there is speculation to the presence and role of NgR1 on OLG (Bourikas et al., 2010; Mei et al., 2013). However if NgR1 is present and providing a protective role in excitotoxicity then further questions are raised as to why this signalling would also lead to an inhibition of OPC maturation and OL myelin production, assuming this hypothesis is correct.

4.5.2   AMIGO3 expression in OLG trauma: LPC

4.5.2.1   Optimisation

From our results, it is clear that relatively high concentrations of LPC (>25µg/ml) induced rapid and extensive cell death. When levels of LPC were at least 50µg/ml, none of the cultured cells maintained a bipolar morphology when viewed after 5 minutes of incubation. This indicates that the treatment was too severe and was inducing cell death. Although some cell survival was observed after incubation with 25µg/ml LPC for 30 minutes, the number of cells had appeared to reduce drastically

when viewed qualitatively. This means that it would be difficult to collect enough samples for protein analysis and that the treatment is likely causing such a severe reaction that it would not be relatable to disease. The range of treatments below 25µg/ml in the imaging studies showed relatively minimal variation. There appeared to be a minor reduction in cell density after 5 minutes with both 5µg/ml and 10µg/ml which appeared to recover following 5 hours treatment. Despite signs of initial cell death, the cells appear to maintain their bipolar expression throughout.

Further optimisation of the model focussed on concentrations of LPC ranging between 10-15µg/ml. We used trypan blue to provide cell counts and cell viability to get an insight in to the level of trauma that the cells were receiving. Interestingly, there was no sign of a reduction in the total number of cells at any of the time points, indicating that, although there was likely to be some degree of trauma, the cells were capable of surviving the treatment. Interestingly there was a significant increase in the total cell number when the cells were treated with 15µg/ml LPC for 5 hours. Why this would occur is not clear, but it could suggest that the treatment of LPC at this level actually encourages some cell division. The 15µg/ml LPC treatment was also the only time group where the proportion of cells positive for trypan blue, increased. Intriguingly, although at this level of LPC cells are starting to lose their viability, they seem to be replaced with new cells. It is likely that as the cells lose viability, their volume would decrease as their processes retract. Theoretically if the cells hadn't died fully and were not releasing products which encouraged apoptosis or death of neighbouring cells, then they will provide more space for new cells to colonise and thereby allow the cell numbers to increase. This however also suggests that there is

165

heterogeneity in the cells, as some are losing their viability and being replaced with cells that are less susceptible to LPC.

It is interesting to note that previous models of LPC in OLG have used much higher concentrations to induce a reduction in cell viability (Ou et al., 2016). Previously LPC has been used at between 400-600 times more concentrated than in our studies, well into the levels that induced full cell death. This could possibly indicate that the Oli-neu cells are far more susceptible to LPC treatment than primary rat OPCs. It is not clear why this would be the case but it does raise questions as to the why there is variation and could potentially suggest some variation in phenotypes between the primary cells and the Oli-neu cell line.

To confirm these findings, it would be useful to repeat with another analysis method. Another method that could have been used to investigate the cell death/degradation would have been to examine levels of lactate dehydrogenase (Merrill, 2009). Despite the potential concerns in the model due to the cell number changes, it was decided that further studies would use 10µg/ml LPC, as well as higher concentrations where time permitted.

4.5.2.2   AMIGO3 and LINGO1 following LPC incubation in Oli-neu cells

Following treatment with LPC at 10 and 15µg/ml, there appears to be a small increase in the levels of AMIGO3, albeit not significant. This suggests that AMIGO3 may be raised following treatment with LPC, although only at a low level. The means were only observed to increase by ~25-30% therefore it is not clear whether this would lead to a substantial change in activity even if the results are accurate.

Furthermore, there appears to be a small reduction in AMIGO3 expression at 12.5µg/ml, again not significant, therefore it is possible that AMIGO3 levels do not actually change following treatment with LPC between 10-15µg/ml for 5 hours. It is likely that more confidence could be obtained for the results if a higher sample size was used. A large variation was observed within the data for all groups which could have prevented our ability to detect significance between the means of the AMIGO3 levels. Western blots are only semi-quantitative, thus it is likely that a larger sample size is required to provide sufficient data to examine the means of AMIGO3 expression in Oli-neu cells following treatment with LPC.

To test this possibility we repeated the LPC treatment study with a larger sample size and only using LPC at a concentration (15µg/ml)where significant reductions in cell viability had been observed. Despite using a larger sample size, we again found that although a qualitative increase in the mean AMIGO3 protein expression was observed after the 5 hour LPC incubation, this was not found to be significant. Furthermore, repeating the tests and allowing the cells a further 19 hours following LPC incubation for further AMIGO3 translation, resulted in a similar minor increase in the mean that was not significant. Interestingly, the variation in AMIGO3 expression in both control and treated groups increased considerably in the 24 hour extracted samples when compared to the samples collected after 5 hours.

From these data it would appear that AMIGO3, and LINGO1, do not increase their protein expression significantly following LPC induced trauma. Even after 24 hours, AMIGO3 levels stilled remained relatively low indicating that this form of trauma did not induce the expression of either LRR proteins.

4.5.3   Comparison of OLG trauma models

The variations between the models of cell trauma may explain the variation that was observed. Depending on the method of trauma, different mechanisms will be activated and therefore the cells will react in a different manner (Kroemer et al., 2009). As LPC has been shown to promote Olig2 in mature OLs, it is possible that Olig2 is similarly promoted in OPC following LPC induced trauma. Olig2 expression has been demonstrated to encourage OPC maturation (Ou et al., 2016; Lu et al., 2018). Furthermore, it is also clear that LPC treatment results in efficient and complete remyelination in a relatively short period (Vereyken et al., 2009). As such, this model may not provide a true comparison to MS and demyelinating systems as it may directly encourage the maturation of OPC unlike the human diseases. If AMIGO3 is involved in inhibiting OPC maturation, then it would be expected to be downregulated when remyelination is occurring. Therefore, it is possible that LPC treatment may actually prevent an increase in AMIGO3 protein expression, whether directly or indirectly, through its potential stimulation of Olig2, and OPC maturation.

It could also be argued that excitotoxicity is more likely to have a more controlled destruction of OPC than LPC treatment due to the build up of calcium in the cells that is expected with this treatment (Chen et al., 2007). The LPC model however appears to produce a more direct and rapid break down of cell structures, therefore necrosis may occur rather than the more regulated apoptosis pathway. Indeed, it may be considered that LPC damages the cells from the outside in, while excitotoxicity is likely to induce injuries that proceed from inside to out (e.g. Ca^{2+} induced apoptosis). This variation of course raises questions to the validity of the models as they will only

be investigating one aspect of the OPC trauma response that would be observed *in vivo*. These models do however provide an invaluable insight which can help explain the responses in the animal models.

4.5.4   Limitations

There are a number of limitations associated with this study. Firstly, experimentally, our sample sizes were not always large enough to detect significance between variations in data. Furthermore, on the experimental procedures, further repeats of the data would have been beneficial to confirm our findings.

Our models, although able to address specific types of trauma to OPCs also contain limitations. Firstly, when comparing to MS or other demyelinating diseases, our models are limited in that they only examine one specific form of OPC trauma. MS is a multi-faceted disease and the environment within the lesion can become detrimental to OPC survival and maturation for a number of reasons. As the exact cause of MS is unknown, it is not clear if there is another unknown contributor which inhibits OPC development which we are not able to model. Furthermore, the models also are only able to examine OPCs in isolation. Although this is an advantage to examine the responses in the cell line alone, it does not represent the true environment where multiple cell types are present and may react to the disease conditions. However, as our experiments are simply looking at a potential mechanism for OPC inhibition, they remain relevant despite these limitations. Another limitation to these experiments is the narrow range with which we were able to use LPC. Minor increases in the LPC concentration caused dramatic changes in the proportion of Oli-neu which were no longer viable. This is likely to introduced variability to the data.

Finally, it is also possible that the reactions that we observed may be a specific behaviour of the Oli-neu cell line. It would have been beneficial to use a number of cell lines, for example the MO3.13 (McLaurin et al., 1995) or N19 (Paez et al., 2007) OLG lines, or preferably primary cells, to ensure that the behaviours are representative of OPCs. It also is possible that there could be variation between murine cell lines and human cell lines. Unfortunately, due to the cost of other primary cell lines and the difficulties associated in setting up primary cultures, we were not able to perform these experiments in this study.

4.5.5 Future studies

Following on from our data, there are a number of studies which could provide fascinating insights in to the role of AMIGO3 in OPC differentiation and myelination. It would be very interesting to repeat these studies with cells that have been encouraged to mature. This would provide an idea of whether changes in AMIGO3 expression following trauma correlate with its predicted inhibitory effects on OPC maturation. Furthermore, co-culture studies would provide a useful method to examine whether cultured OPCs or OPC cell lines, would be able to engage in some level of neuronal ensheathing. Co-culturing systems could also be examined through electron microscopy to get detailed images of the ensheathment of neurons, thereby giving a greater idea of the effects on the OLG development in correlation with AMIGO3 expression (Mi et al., 2005; Pang et al., 2012; Shao et al., 2017). An alternative would be using *ex vivo* cultured brain slices (Goebels, 2007). Our lab, as well as others, have previously modelled anti-MOG and complement induced demyelination in these *ex vivo* slice cultures (Fulton et al., unpublished; Goebels,

2007; Berg et al., 2017). These experiments would be invaluable to provide a more translatable view of the effects of inflammation induced demyelination in a whole system.

It should be noted that there are a number of potential methods of CNS trauma associated with MS and as such it would be valuable to repeat these experiments using a number of various models. It would be useful to repeat the trauma experiments with a different injury model, for example, a complement mediated (Alberdi et al., 2006), or free radical induced injury (Whittemore et al., 1995), or simply another excitotoxic model to confirm our findings (Karlsson et al., 2017). Repetitions in numerous models may help to identify where variations exist and potentially give an insight as to why recovery occurs in some cases but not in all, such as long term plaque development in MS compared to early stages of the disease (Patani et al., 2007). Furthermore, although we examined a small range for the LPC treatments, it would be interesting to examine the changes of AMIGO3 in our AMPA-CTZ model both over a varying time course and after varying degrees of trauma. This could help to get a better understanding of when and why AMIGO3 is expressed in traumatic injury to OPCs.

Another area of interest is that following LPC induced OPC trauma with 15μg/ml LPC, we observed an increase in the total number of cells. It would be interesting to note if there has been an increase in the cell proliferation following the trauma. This could be easily measured through BrdU counts, or flow cytometric cell cycle analysis, following LPC incubation (Chen et al., 2014). Furthermore, it would be interesting to note if there is any correlation between AMIGO3 expression and rate of proliferation.

171

It is possible that differentiation of OPC is initially inhibited following demyelination as a way to ensure sufficient OPC are present for full myelination, although it is known that this is not the limiting step in remyelination (Nakahara et al., 2009). It should be noted here that different degrees of demyelination may require different responses. For example, if there is only a small traumatic event, which has predominantly affected OLs, while high numbers of OPC are still present, then active remyelination would be the first process required. Although it would still need to be determined to what degree of OL/OPC loss is required for OPC proliferation to be more important than OPC differentiation, it would be interesting to determine whether AMIGO3 is linked to the control of these processes.

Another area of interest would be to examine the exact pathways that AMIGO3 is signalling through. It is possible that although AMIGO3 levels are changing, they may not be having any more of an effect. AMIGO3 cellular localisation may be the important factor, and therefore higher levels of AMIGO3 may not correlate with increased signalling following trauma if AMIGO3 is not present with its signalling partners. Based on this hypothesis, it would be interesting to examine the cellular distribution of AMIGO3 following trauma to OLG. Furthermore, as a pathway has not been elicited for AMIGO3 in OLG, it would be very interesting to observe if AMIGO3 interactions with itself or other proteins vary following OLG trauma. This could be easily investigated with ICC at a high power of magnification. Unfortunately, as we observed variability in AMIGO3 expression when visualising in IHC, it is unlikely that this approach would provide valuable data at this time. Such studies must wait until an efficient antibody and imaging system has been developed for visualising

172

AMIGO3. Alternatively, in terms of protein interactions, co-immunoprecipitation or Forester resonance energy transfer (FRET) analysis would be a useful tool to investigate the interactions of AMIGO3 at various stages in OLG lifecycles and in traumatic conditions. This however was not possible due to time constraints, but would be interesting for further research.

4.5.6   Conclusions

In conclusion, we have demonstrated that under an excitotoxic condition, both the mRNA levels and the protein levels of AMIGO3 rise in OPC cell lines in the first 5 hours following trauma. Further repeats both in Oli-neu cells, and in other cell lines, or primary cells, would be valuable to back up our *in vitro* data. This raise in AMIGO3 protein levels does not replicate in LPC induced OPC trauma, presumably due to the more direct cell destruction, or due to potential activation of Olig2 induced maturation pathways in the OPC. This demonstrates that AMIGO3 is likely to be raised following trauma to OPC in traumatic demyelination. It is still unclear what role AMIGO3 is having in this state, however it is possible that this represents a mechanism for inhibition of remyelination form local OPC following demyelination.

Chapter 5

AMIGO3 expression in demyelinating

disease

5.1 Rationale

Current research for LRRs in demyelinating disease has focussed squarely on the role of LINGO1 in inhibiting the development of mature OPCs (Foale et al., 2017). As previously discussed LINGO1 has been identified in models of demyelination (section 1.4.2.2), as well as in MS lesions (Mi et al., 2013), and its inhibition has led to *in vivo* remyelination. However, as already highlighted in (section 1.4.2.2.2) there are concerns with LINGO1 as a target for the development for treatments for MS, in that recent clinical trials did not demonstrate positive outcomes when optic neuritis patients were treated with opicinumab, an anti-LINGO1 antibody, compared to placebos (Cadavid et al., 2017). Visual evoked potentials appeared to improve slightly however there was no significance found when analysed. Furthermore, there was no evidence for any change in the thickness of RGC layers in the retina between treatment groups. The authors argue that these results are indicative of longer studies being required, or that an earlier imminent administration of opicinumab is warranted. Alternatively, these observations may indicate that, while LINGO1 plays a minor role in encouraging remyelination, these actions may be eclipsed by compensatory inhibition by AMIGO3. As a result, OPC maturation and remyelination may still be inhibited despite therapeutic blockade of LINGO1. A lack of improvement would then be observed in patients given anti-LINGO1 therapies to encourage remyelination, at least in the acute stages following demyelination.

We have demonstrated that AMIGO3 is present during postnatal development, and that its protein concentration alters substantially during the main stages of postnatal

myelination. In addition we have shown that trauma to OPC alters the levels of AMIGO3. Based on these findings we decided to examine the expression profile of AMIGO3 during inflammatory demyelination in the brains of animal models and in human MS. Although minor preliminary evidence exists demonstrating expression of AMIGO3 in MS lesions and in OPC (Ahmed et al., personal communication), no data exists correlating any changes in expression, therefore this data will be invaluable in examining the role of AMIGO3 in demyelinating disorders.

5.1.1 EAE as a model of MS

EAE is the primary model used for examining immune related demyelination and is the most commonly used animal model for examining MS (Kipp et al., 2012). A number of varieties of EAE have been developed which can provide insight to various stage of inflammatory related demyelination (Baker et al., 2011; Constantinescu et al., 2011). EAE has been induced in multiple species, including primates, highlighting the translatability of the model, however the majority of studies have investigated it in mouse models (Kap et al., 2010; Robinson et al., 2014b). Similarly most LINGO-1 based studies have used mouse models, therefore for direct translatability we chose to use mouse models as well (Sun et al., 2015; Zhang et al., 2015a; Foale et al., 2017).

A number of variants of the EAE model have been developed allowing models to be chosen depending on the aspect of the disease under investigation (Constantinescu et al., 2011). As AMIGO3 mRNA expression rises at a faster rate compared to LINGO1 in spinal cord following trauma (Ahmed et al., 2013), and because we observed a rise in AMIGO3, but not LINGO1, protein expression in our

acute excitotoxic model (section 4.4.1), we predict that AMIGO3 expression will be higher compared to LINGO1 in the acute stages of EAE induced demyelination. As such we decided to examine AMIGO3 in an acute EAE/optic neuritis model (section 2.1.2.3), as well as in a more developed relapsing-remitting model which better represents the most common form of MS disease progression (Al-Izki et al., 2012).

5.1.1.1   EAE progression

As EAE is an ascending disease, progression begins in the inferior spinal cord with inflammation occurring in the lumbar region and progressively ascending through the spinal cord (Miller and Karpus, 2007). As a result, EAE begins with paralysis of the hind limbs, correlating with demyelination in the lumbar spinal cord. Therefore the loss of myelin proteins such as MBP, as well as an infiltration of CD4^{+} T helper cells would commence in the lumbar region of the spinal cord (Miller and Karpus, 2007). CD4^{+} cells appear to then have an integral role in the ensuing pathogenic demyelination through inducing CNS inflammation as well as priming of phagocytes for myelin derived proteins. This is further demonstrated by the fact that EAE can be induced in healthy naïve mice by transfer of CD4 cells primed for myelin derived proteins from myelin immunised mice (Elyaman et al., 2008; Constantinescu et al., 2011; McGinley et al., 2018). Although MS and EAE are thought to be predominantly a CD4^{+} T-helper cell mediated disease, there is also evidence that cytotoxic T-cells, or CD8^{+} cells, play an important role in progression of the disease (Robinson et al., 2014b). In fact, CD8^{+} cells are the predominant T cell in developed MS lesions (Rangachari and Kuchroo, 2013; Steckner et al., 2016). As a result, CD8^{+} cells are a prime target for indicating inflammation in the spinal cord in EAE.

There are a number of other signs that describe the progression of EAE. OX42 (CD11b or α-integrin M) is a marker of microglia, with some small levels of expression reported on macrophages as well. During acute stages of EAE, whilst inflammatory related demyelination is occurring, an increase in the number of CD11b$^+$ is observed indicating the increased role of local inflammatory cells in phagocytosing cellular debris (Crocker et al., 2006; Alrehaili et al., 2018). Furthermore, as the disease progresses and increased neurodegeneration occurs, an increase in the levels of GFAP is observed. GFAP is expressed normally at low levels in astrocytes, but then marked increases are observed following CNS trauma due to the resultant reactive gliosis and scar formation (Paintlia et al., 2008; Kundi et al., 2013). We intend to use these markers to determine the progression of disease in our models to correlate the expression of AMIGO3 with levels of the disease

5.2 Aims

The aim of this study is to examine the expression profile of AMIGO3 during the stages of demyelination. We wanted to characterise the extent and level of demyelination in our models to choose an effective stage to evaluate the expression of AMIGO3. These models will be used to evaluate the levels of AMIGO3 following demyelination. The aim of this investigation is therefore to gain a better understanding of the expression of AMIGO3 following demyelination, and to determine any correlations with disease progression.

5.2.1 Hypothesis

We hypothesise that AMIGO3 levels will be raised in the acute stages of demyelination. This will amount to higher AMIGO3 protein levels in EAE induced animals compared to controls.

5.3 Experimental design and methods

5.3.1 Demyelinating models

As AMIGO3 is believed to be the more significant LRR molecule in the acute stages of demyelination, we decided to examine early stage models of demyelination. As such we used our acute EAE model which has a minimal demyelination so that we can examine the first stages of the disease, as well as a relapsing-remitting model where further progression will have occurred.

5.3.2 Optic neuritis

Optic neuritis was induced as previously described (section 2.1.2.3). For optic neuritis, optic nerves were dissected at D10 following disease induction. IHC was then use to analyse MBP and AMIGO3 expression profiles compared between optic neuritis induced and untreated controls. Expression levels of AMIGO3 were analysed by total pixel counts and pixel intensity from AMIGO3 IHC images.

5.3.3   EAE

5.3.3.1   Acute EAE

Acute EAE was induced using the same protocol as optic neuritis, however mice were allowed to progress until D14 and D19 so that further disease progression could be observed. Clinical scores and IHC were used to analyse the model before further tests. For IHC, transverse lumbar sections were prepared as described (section 2.3.2.2). Sections were then labelled with markers of myelin (MBP), inflammation (OX42, CD4 and CD8) and reactive gliosis (GFAP), to determine the extent of disease progression. DAPI counts were also performed on the sections to analyse whether cell numbers had changed during disease progression. Samples were compared against untreated healthy controls. Unless stated otherwise, images from transverse lumber sections were taken at the posterior fasciculus to analyse changes in the white matter (fig 5.1). Lumbar sections were used as EAE is an ascending disease, which begins with infiltration of immune cells at the lumbar region of the spinal cord (Miller and Karpus, 2007). Furthermore, MBP has been shown to be expressed highly in the lateral spinal cord within the white matter tracts, with high levels seen in the posterior fasciculus (Mei et al., 2012). Due to the high levels of MBP in the posterior fasciculus as well as lumbar segments being affected foremost in EAE, there should be a greater development of the disease in the lumbar region of the spinal cord. As such, we focussed our analysis on this area of the spinal cord.
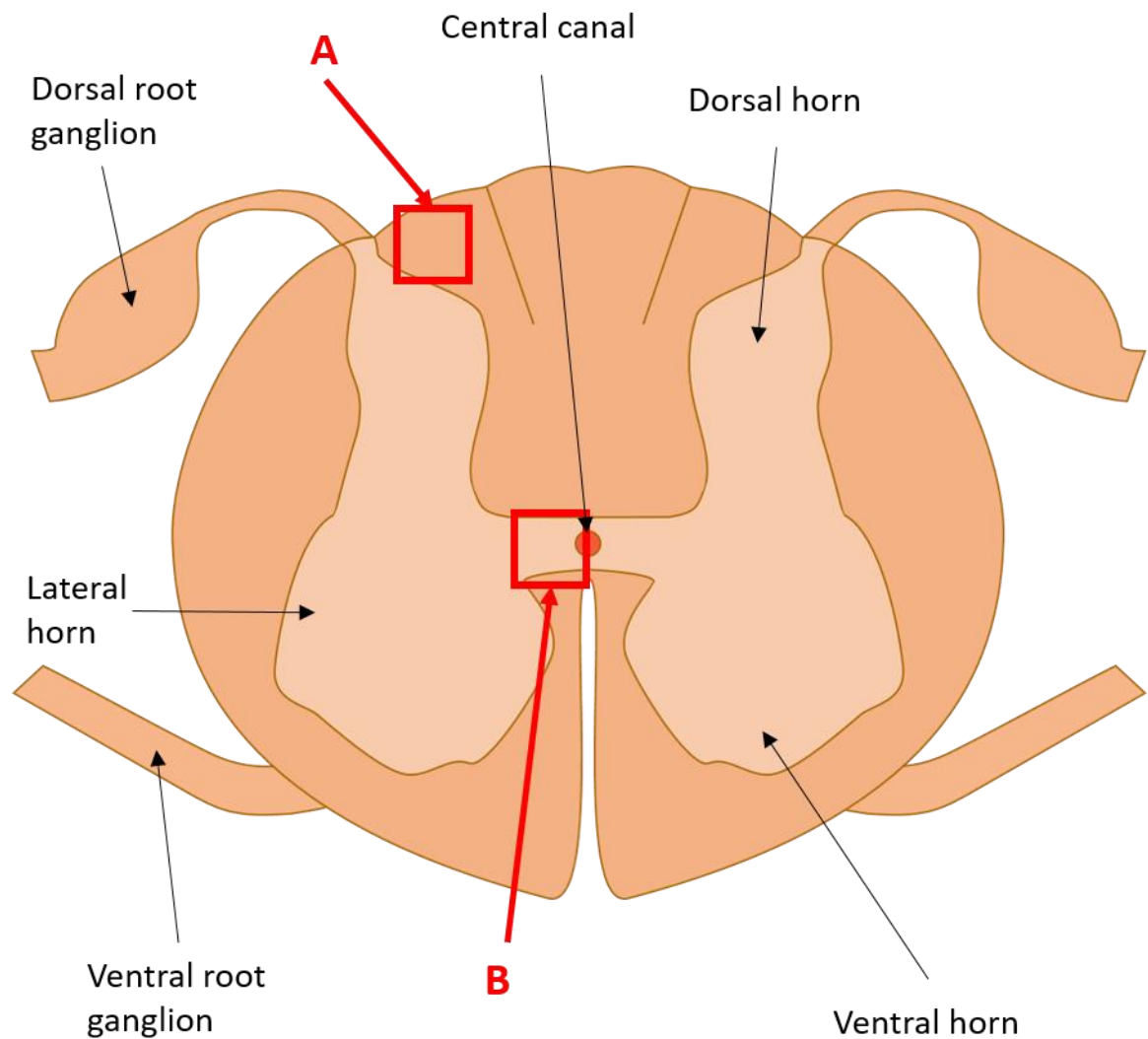
Figure 5.1: Diagram of the spinal cord and regions used for IHC. Images were obtained predominantly, and unless otherwise stated, alongside the dorsal horn on the lateral edge of the spinal cord. Specifically, in the white matter of the posterior fasciculus (A). For CD4 and CD8 analysis, some images were obtained in grey matter, at the anterior commissure alongside the central canal (B)

5.3.3.2   Relapsing-remitting EAE

Relapsing-remitting EAE was induced as previously described (section 2.1.2.3). As samples were collected once a clinical score of 4 had been reached, monitoring of clinical score disease progression over time was not performed. Transverse lumbar spinal cord sections were prepared for IHC analysis of the samples. Due to issues with immunofluorescence on samples that had been stored for an extended period of time, samples were only analysed for MBP expression through DAB staining.

5.3.3.3   AMIGO3 protein analysis

For analysis of AMIGO3 expression, protein lysates were collected from superior lumbar spinal cords from EAE and untreated control samples. Samples were then analysed by western blot to semi-quantitatively assess levels of AMIGO3.

5.3.4   Multiple sclerosis

White matter brain samples of chronic lesions from MS patients (MS white matter, MSWM), normal appearing white matter (NAWM) and healthy controls were gratefully obtained from the Multiple Sclerosis and Parkinson's Tissue Bank, UK. Samples were flash frozen prior to collection. Protein lysates were obtained from the samples for semi-quantitative western blot analysis of AMIGO3 and LINGO1 protein levels in the chronic human disease.

5.3.5   Experimental plan

A summary of the plan for the investigation, findings and experiments used is demonstrated in figure 5.2.
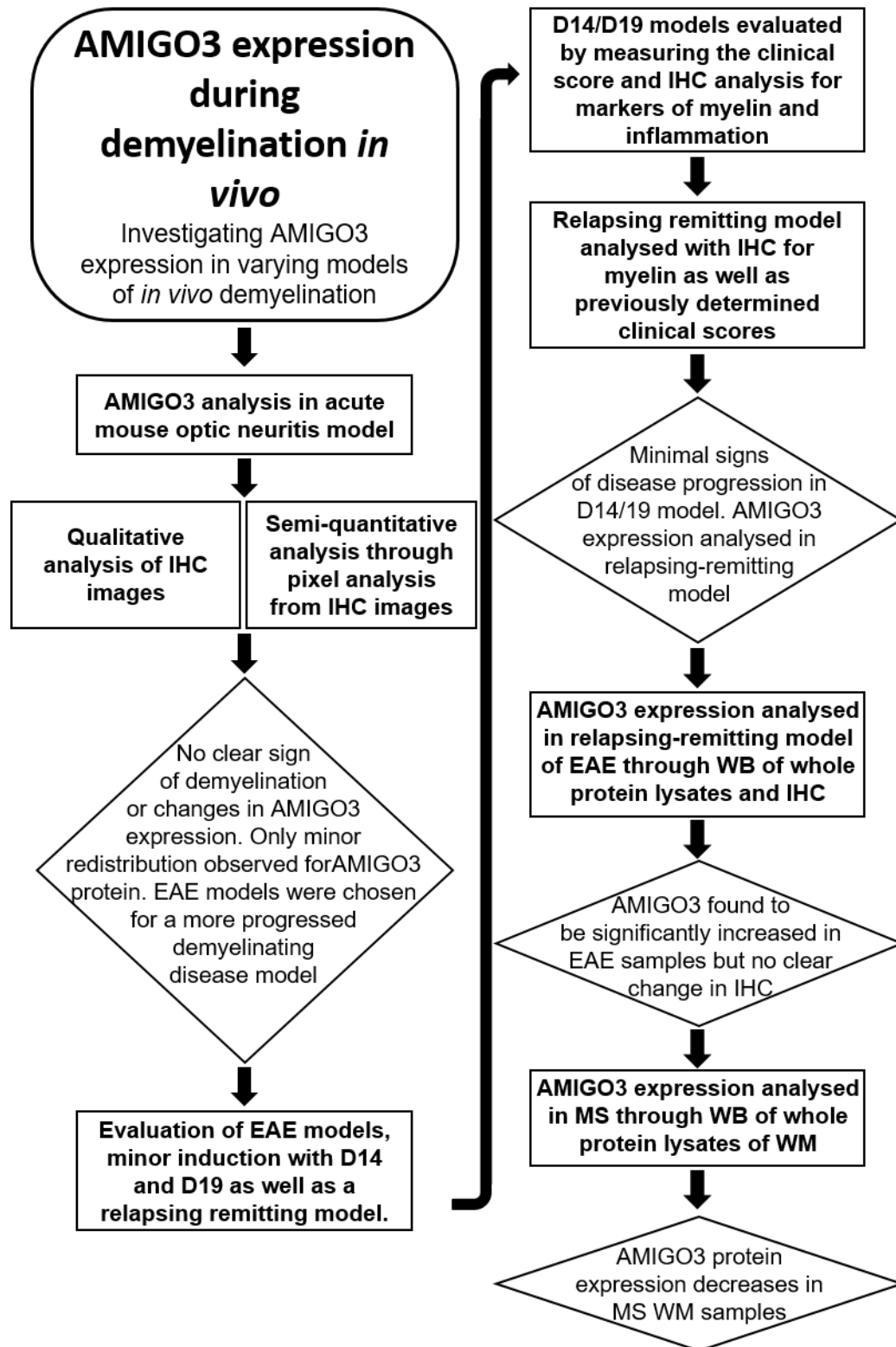
Figure 5.2: Flow chart demonstrating the plans and summarising the findings from chapter 5.

5.4 Results

5.4.1 Optic Neuritis

Following the induction of optic neuritis in C57BL/6 mice, samples were obtained of optic nerves to examine the extent of demyelination and AMIGO3 expression (fig 5.3 & 4). Firstly, examining AMIGO3 staining, there is no qualitative evidence of any increase or decrease in AMIGO3 levels (fig 5.3). Interestingly though, the distribution of AMIGO3 in optic nerves from optic neuritis induced samples displayed a tendency to redistribute more to the external surface of the nerve. Our images also suggest that AMIGO3 appears to arrange in long strips running along the nerve, potentially redistributing along axons. This is opposed to a more globular arrangement which is more prevalent in the control samples.

MBP distribution was also analysed qualitatively in the optic neuritis samples. As with AMIGOs, there is no major variation that can be observed qualitatively between the sham control and optic neuritis samples and it is not clear if there is a change in total MBP levels. Both controls and optic neuritis samples show a relatively even distribution across the optic nerve (fig 5.4).

The intensity and percentage of positive pixels were analysed following IHC for AMIGO3 in the optic neuritis samples to determine semi-quantitatively if there was any change in AMIGO3 expression in this model of demyelination (fig 5.5). Firstly, the average pixel intensity was measured for AMIGO3 positive IHC. Although a larger variation was observed in the sham treated animals, both the sham and optic neuritis
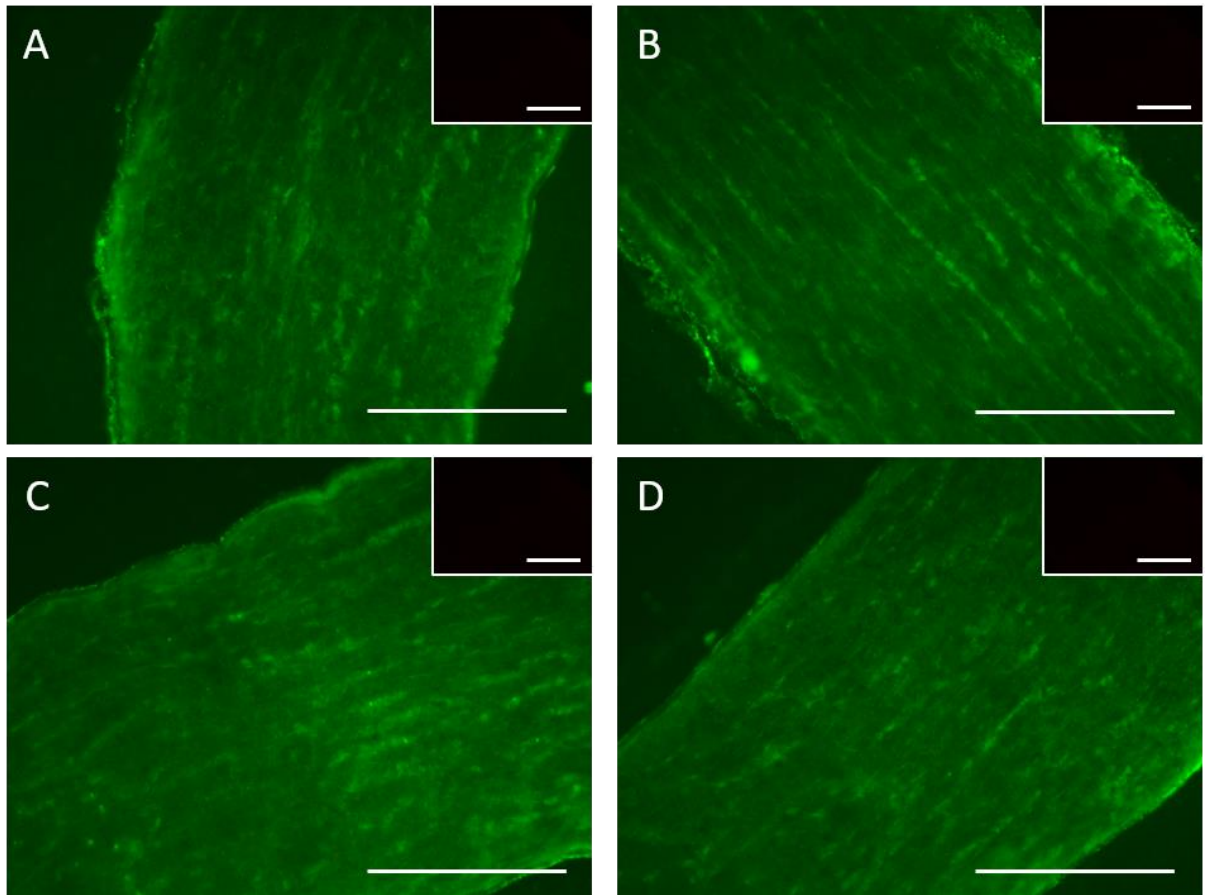
Figure 5.3: Representative AMIGO3 staining in C57BL/6 mice optic nerves for the optic neuritis study. (A-B) optic neuritis and (C-D) normal controls. No major variation can be seen between treated and sham samples although a small retribution of AMIGO3 to the external membrane of the nerve as well as to axons is seen in optic neuritis samples. Scale bars represent 100µm, n=3. Insets show negative controls.
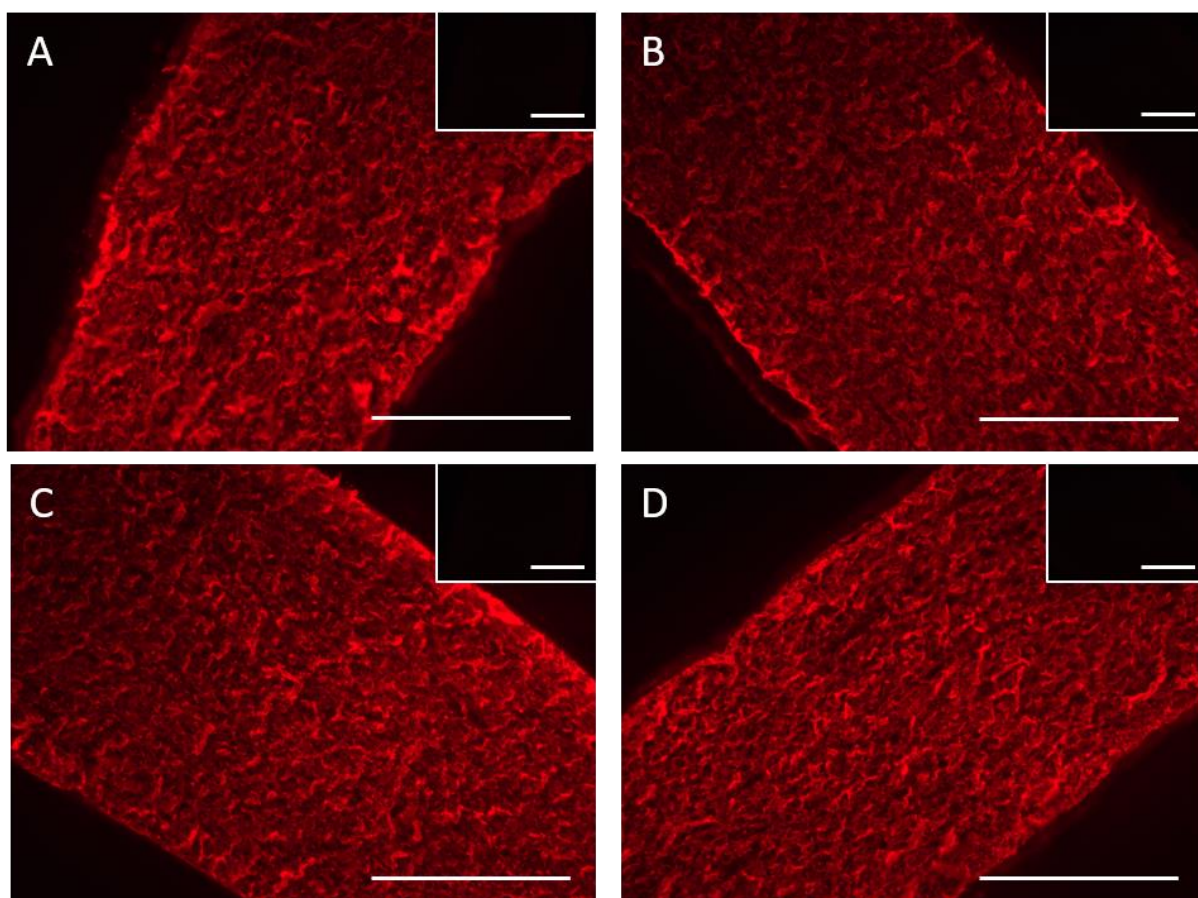
Figure 5.4: Representative MBP staining in C57BL/6 mice optic nerves for the optic neuritis study. In both (A-B) optic neuritis and (C-D) normal controls. MBP distribution and staining intensity stays relatively constant between the groups. Scale bars represent 100μm, n=3. Insets show negative controls.
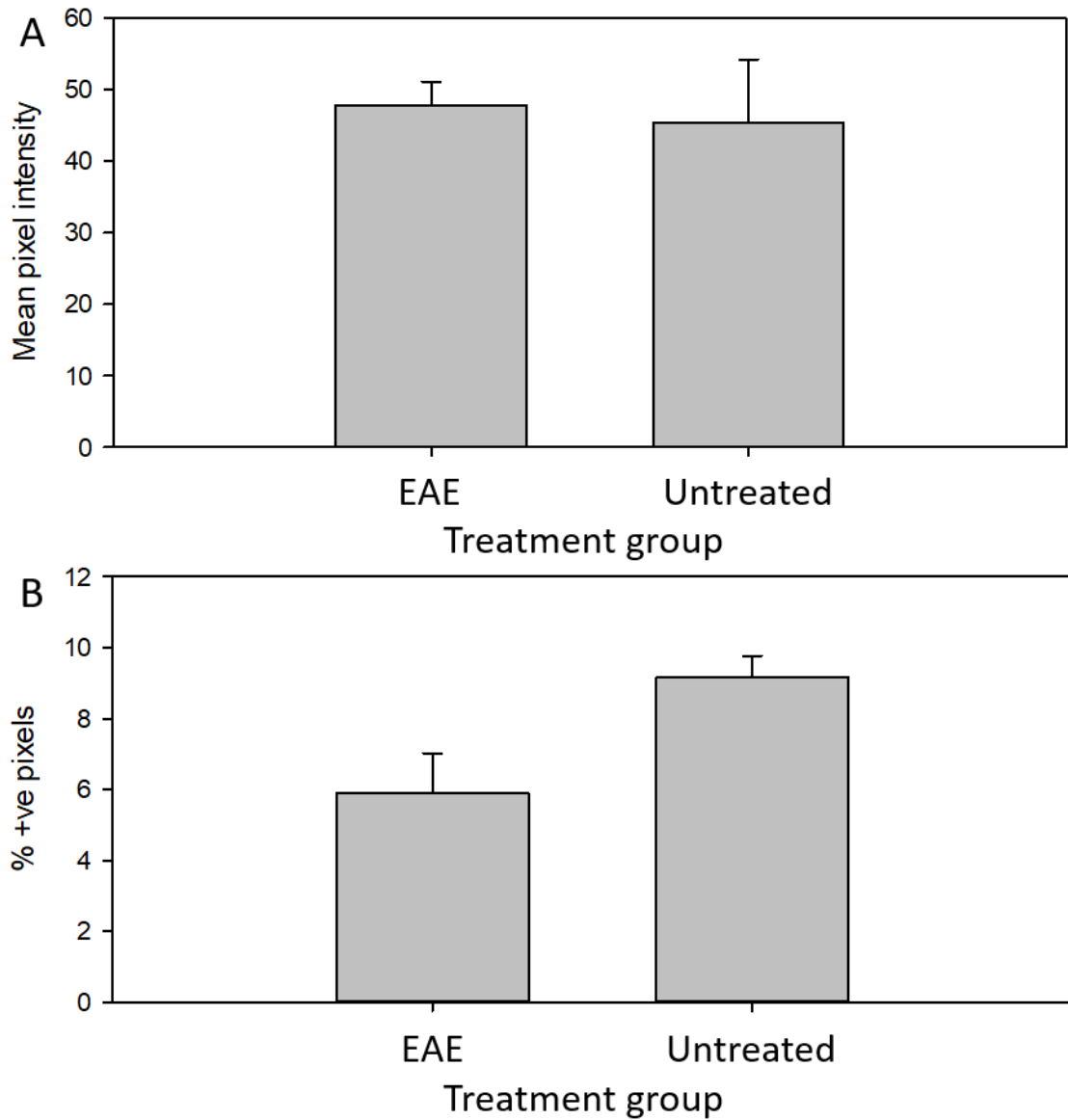
Figure 5.5: Semi-quantitative AMIGO3 pixel analysis from optic neuritis samples. (A) The average pixel intensity was analysed and (B) the percentage of pixels positive above threshold for AMIGO3. No clear difference can be seen in the pixel intensity after IHC against AMIGO3, however a decrease in the total percentage of positive pixels above threshold was seen for optic neuritis samples. Error bars represent one SEM, n=3.

samples showed a relatively equal mean pixel intensity, 45.4±8.9 and 47.8±3.3 respectively. Both samples were normally distributed and had an equal variance, therefore a t-test was used to analyse any variation in the mean pixel intensities. As expected from the qualitative results, no significant variation was observed (p>0.05). The percentage of positive pixels over the threshold value was then tested to observe if any variation existed based on areas of positive signal. Again the data for both groups was found to be normally distributed and have equal variance. T-tests did not find significance, although there was a potential trend towards significance (p=0.06) between the positive pixel percentages within optic nerves for AMIGO3. Interestingly, the sham group showed a higher mean level, with a mean positive pixel percentage of 9.16±0.60 compared to 5.90±1.11 in the optic neuritis samples, indicating a potential reduction in AMIGO3 following induction of optic neuritis.

5.4.2   Evaluation of EAE models

We evaluated two models of EAE to determine AMIGO3 expression, our D14 and D19 acute stage EAE and the relapsing-remitting model.

5.4.2.1   Day 14 and Day 19 Acute models of EAE

Clinical scores were measured during the study for the animals from D14 onwards (fig 5.6). D14 collected animals showed very limited disease progression with two animals reaching a score of 0.5, however the majority did not demonstrate signs of disease (fig 5.6A). Allowing the animals to progress further to D19 lead to animals reaching a clinical score of 1-1.5 within the evaluation period (fig 5.6B). Furthermore,

A

Animal #	Day 14
1	0
2	0.5
3	0
4	0
5	0.5

B

Animal #	Treatment Day				
	14	15	16	17	19
1	0	0	0	1	1.5
2	0	0	0.5	1	1.5
3	0	0	0.5	1	1
4	0	0.5	0.5	0.5	1
5	0	0	0.5	1	1

C
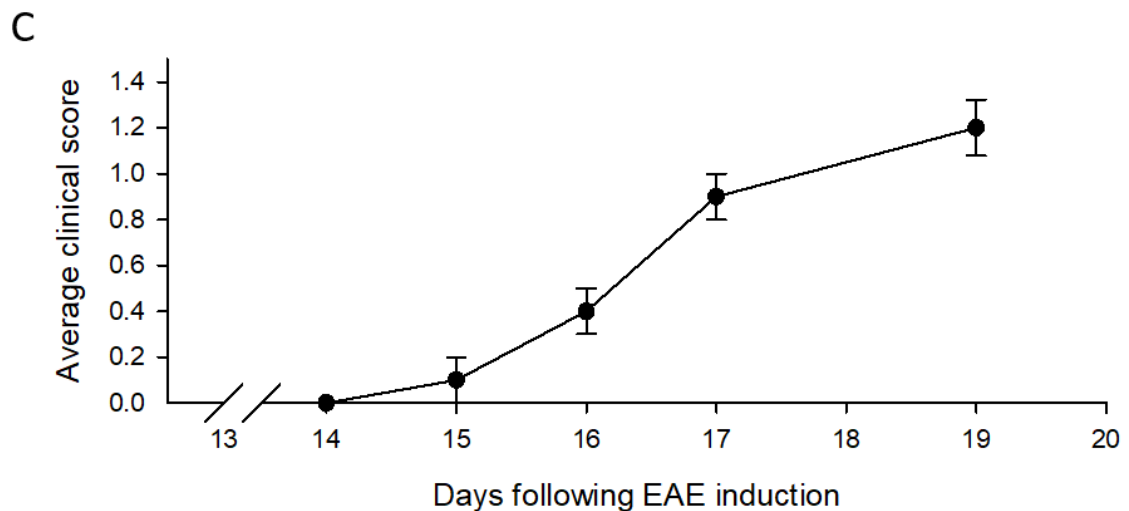
Figure 5.6: EAE scores for the D14 and D19 acute EAE studies. (A) EAE scores on D14 for the animals collected on D14. Minimal signs of EAE induction were observed by this time. (B) EAE scores from D14-D19 for animals collected on D19. Scores can be seen to increase during the period up to collection on D19. (C) Mean EAE scores (D14 to D19) for the animals collected on D19. Error bars represent one SEM, n=8.

a steady increase in the average clinical score was observed from 0.00±0.00 at D14 for the D19 collected animals, to 1.20±0.12 by D19 (fig 5.6C). A maximum score of 1.5 was observed in this model and timeframe.

Lumbar sections were analysed for signs of demyelination and inflammation, matching with the progression of EAE. MBP IHC was used to assess the extent of demyelination in the acute model. Interestingly, qualitatively a marked reduction in MBP positive staining was observed compared to untreated controls in D14 collected samples, indicating demyelination (fig 5.7). It should be noted however that some of the samples displayed greater levels of MBP (not shown) therefore there was a degree of variability within the EAE groups. A reduction in the MBP levels is also observed in the D19 samples (fig 5.8), however it did not appear to be as great as in the D14 samples. Despite the modest reduction in MBP levels at D19, the staining appeared more dispersed than untreated controls suggesting a loss of the myelin sheath architecture.

Both D14 and D19 samples were analysed for the expression of OX42. The majority of samples demonstrated very minimal numbers of OX42^{+} cells both in the untreated controls and the acute EAE (figs 5.9 & 10). Similar results were observed both in the white matter at the posterior fasciculus as well as the grey matter surrounding the central canal in the anterior commissure. Interestingly, there was one sample in the D14 acute EAE samples that responded at substantial levels with multiple OX42^{+} cells around the central canal. Despite being a clear development of inflammation, this was not representative of all of the animals.
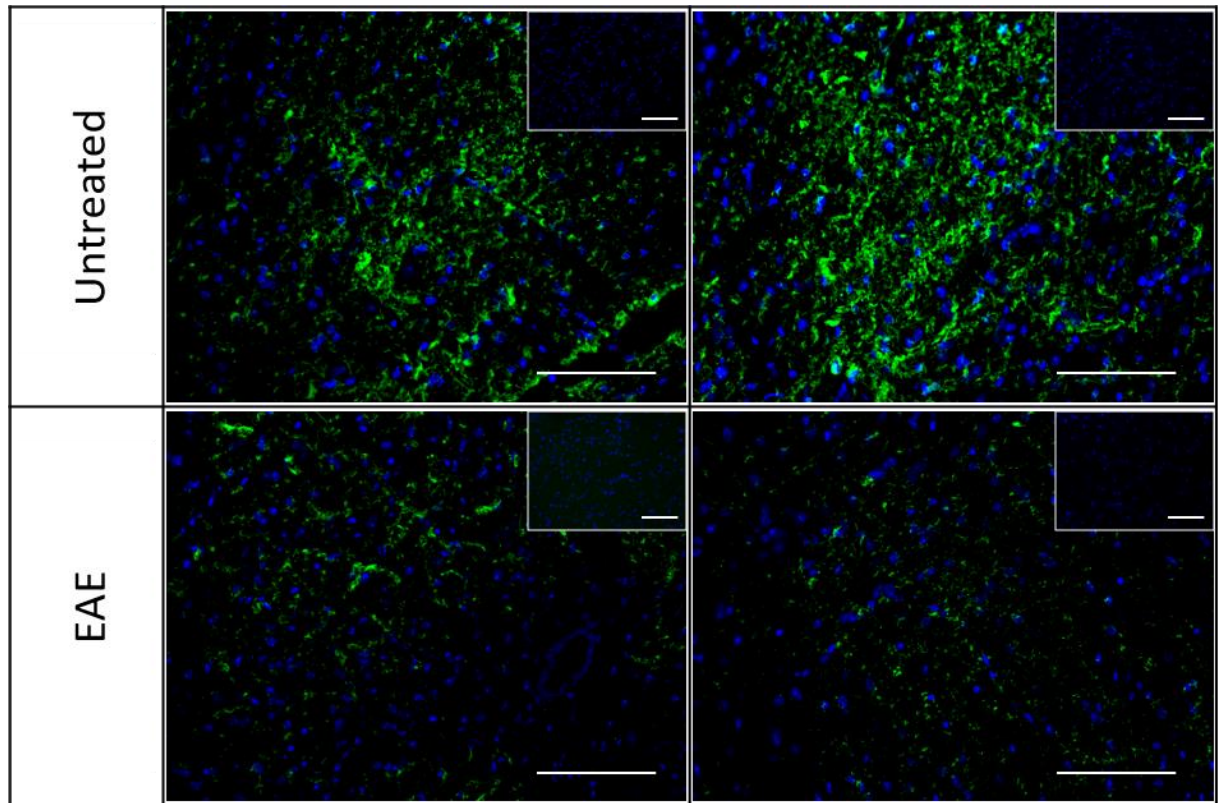
Figure 5.7: Representative MBP (green) IHC in D14 acute EAE samples. 2 images are shown, from different animals in the same group of the study. Samples were counterstained with DAPI (blue). MBP levels appear to drop substantially between the untreated controls and EAE induced groups, demonstrating that demyelination has occurred. Scale bars represent 100μm, n=5 for treated, n=3 for untreated controls. Insets show negative controls.
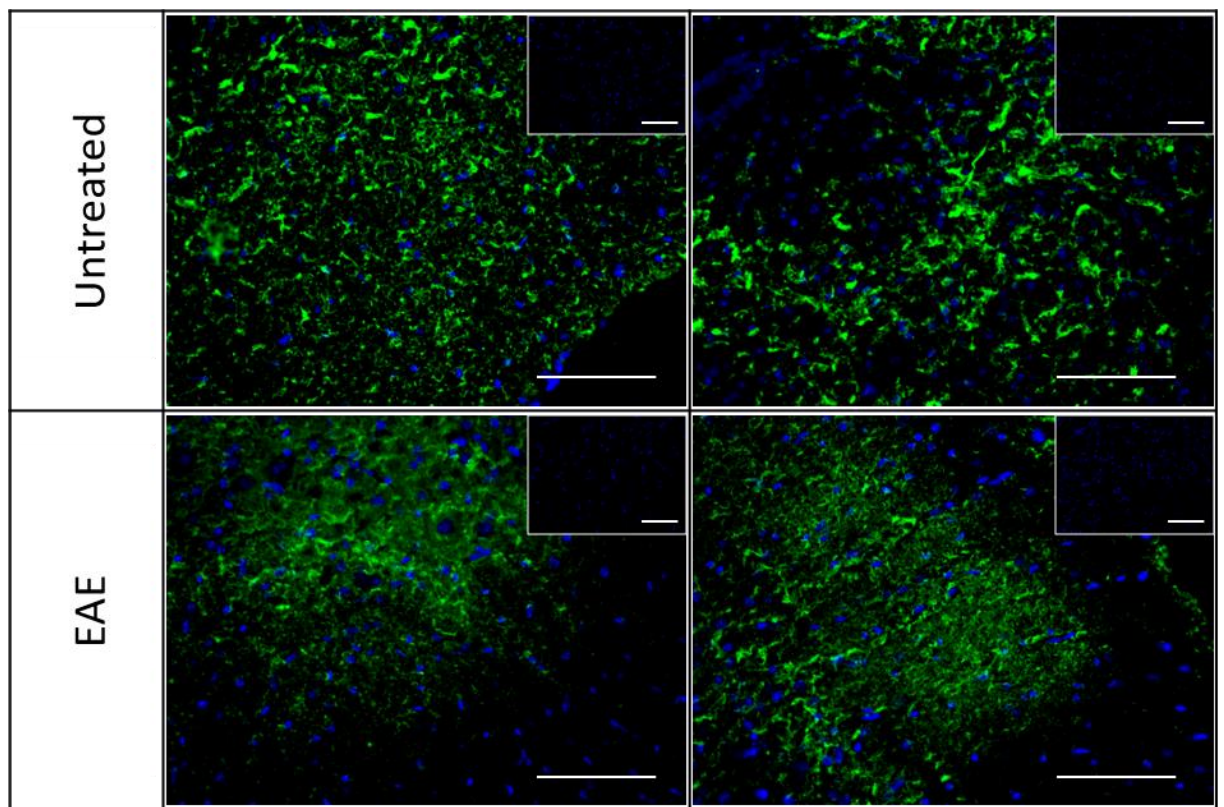
Figure 5.8: Representative MBP (green) IHC in D19 acute EAE samples. 2 images are shown, from different animals in the same group of the study. Samples were counterstained with DAPI (blue). A reduction in the intensity of the signal can be observed between untreated controls and EAE samples, however MBP can still be seen in a similar distribution throughout the white matter. Scale bars represent 100μm, n=5 for treated, n=3 for untreated controls. Insets show negative controls.
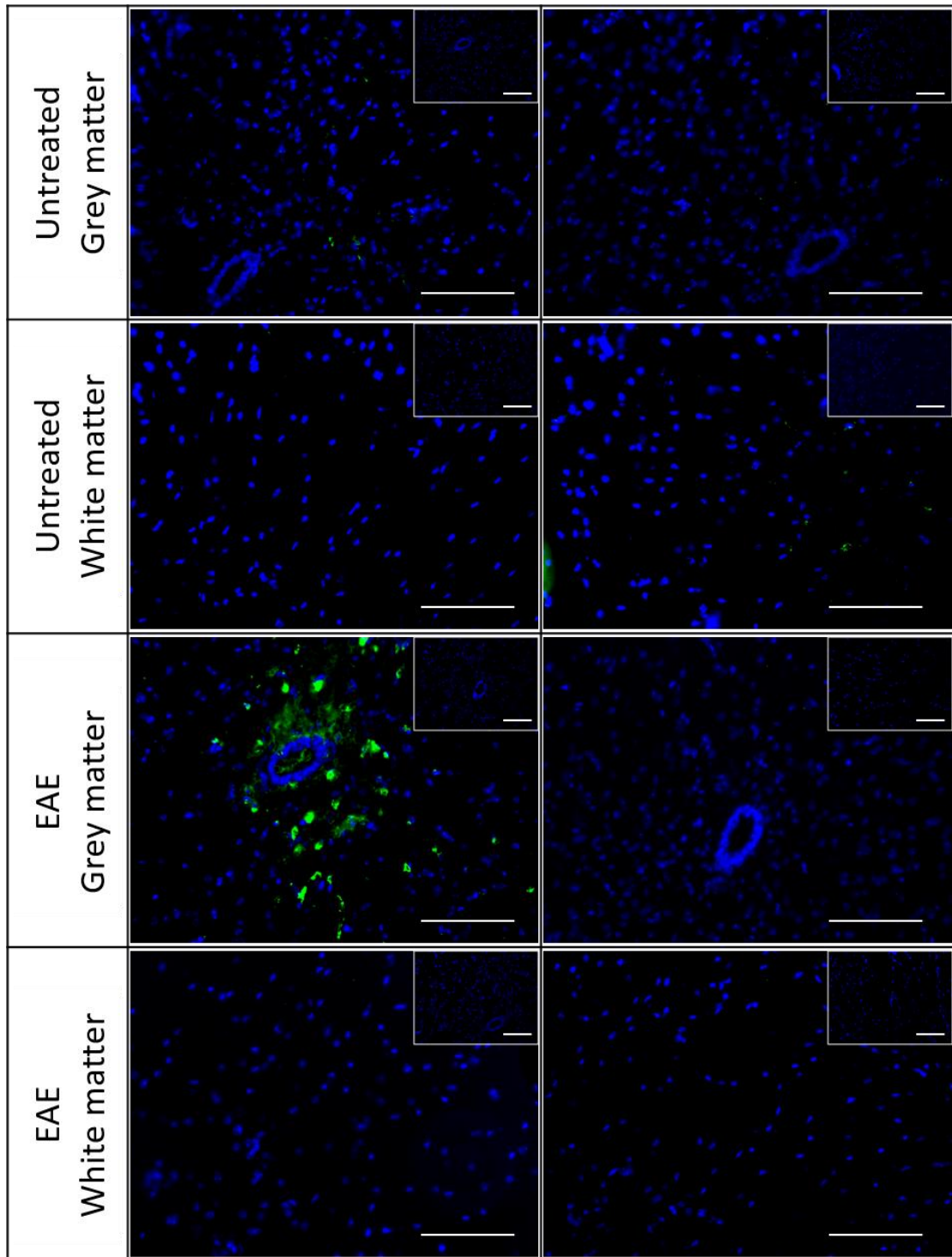
Figure 5.9: Representative OX42 (green) IHC in D14 acute EAE samples. 2 images are shown, from different animals in the same group of the study. Samples were counterstained with DAPI (blue). Minimal staining was observed for both EAE and untreated controls following 14 days after EAE induction, both by the central canal and at the posterior fasciculus of lumbar sections. One animal did show positive staining around the central canal but this was not representative of the samples. Scale bars represent 100μm, n=5 for treated, 3 for untreated controls.
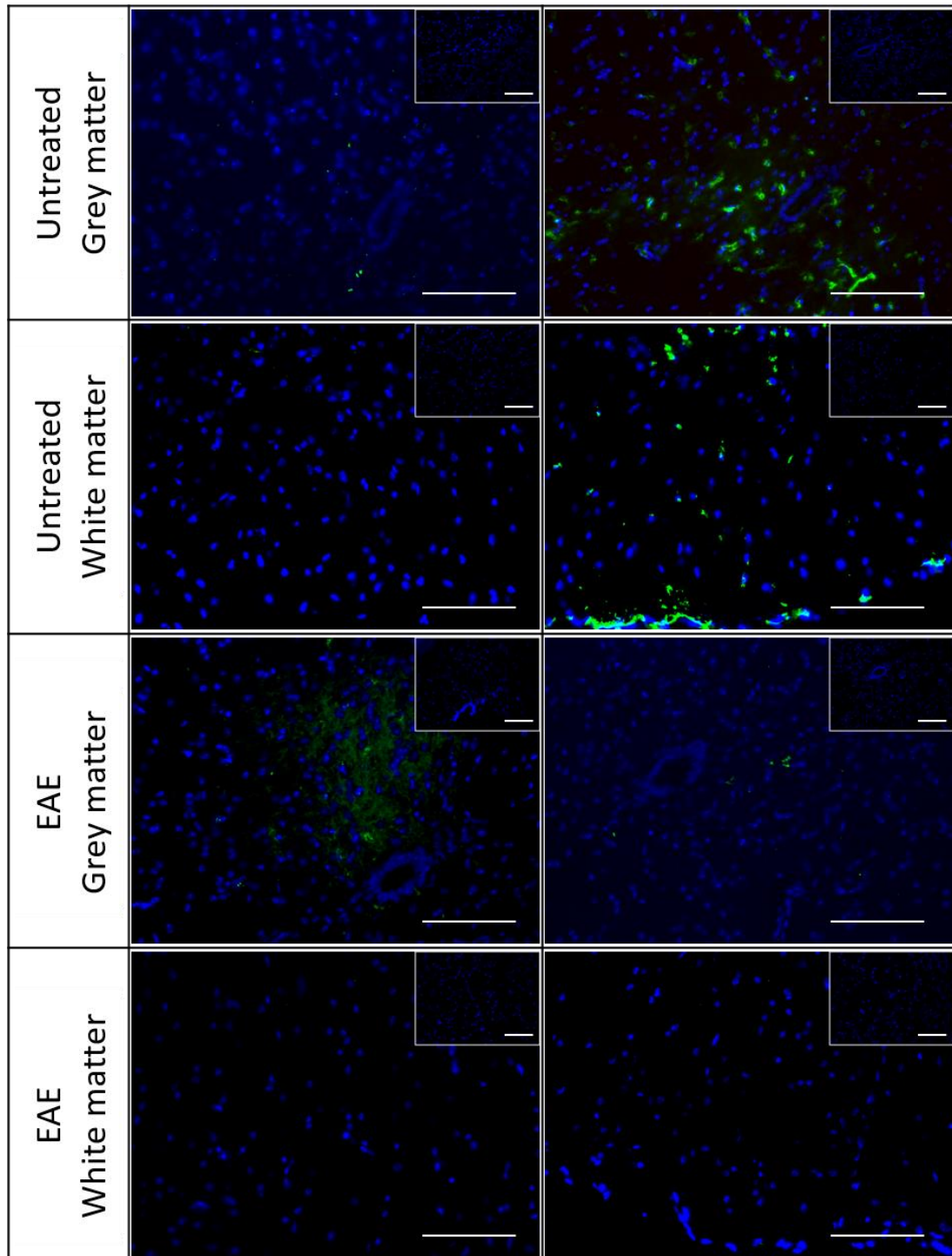
Figure 5.10: Representative OX42 (green) IHC in D19 acute EAE samples. 2 images are shown, from different animals in the same group of the study Samples were counterstained with DAPI (blue). Minimal staining was observed for both EAE and shams following 19 days after EAE induction, by the central canal and at the posterior fasciculus of lumbar sections. Minor staining was observed in some untreated control samples and EAE samples however most samples showed minimal or no staining. Scale bars represent 100µm, n=5 for treated, 3 for untreated controls.

GFAP was analysed to indicate signs of reactive gliosis in the lumbar spinal cords of D14 and D19 animals (figs 5.11 & 12). No GFAP[+] staining was observed in any of the groups, both untreated and acute EAE in D14 and D19 analyses. CD4 and CD8 IHC were only analysed in the D19 samples, where CD4^{+} IHC was similarly not observed (fig 5.13). CD8 positive staining was observed but only at very low levels and it was not seen in every sample either.

DAPI counts were performed in white matter of acute EAE and untreated control samples to provide an additional means to suggest inflammation (fig 5.14). A slight reduction in the DAPI counts was observed in both the D14 and D19 EAE samples, however neither of these were found to be significant (ANOVA, $F(3,11)= 1.061$, $P > 0.05$). Similarly, there was no significance in the DAPI counts between D14 and D19 EAE samples either.

5.4.2.2   Relapsing-remitting EAE

All animals in the relapsing-remitting EAE were allowed to progress to a clinical score of 4, therefore significant signs of disease progression had occurred with hindlimb paralysis. Due to difficulties examining the samples by immunofluorescence, DAB staining was utilised. We stained for MBP to probe for clear sign of demyelination. Qualitatively, although both EAE and untreated controls showed MBP[+] staining, it appeared that MBP levels reduced in the white matter of lumbar spinal cords, in the EAE samples (fig 5.15).
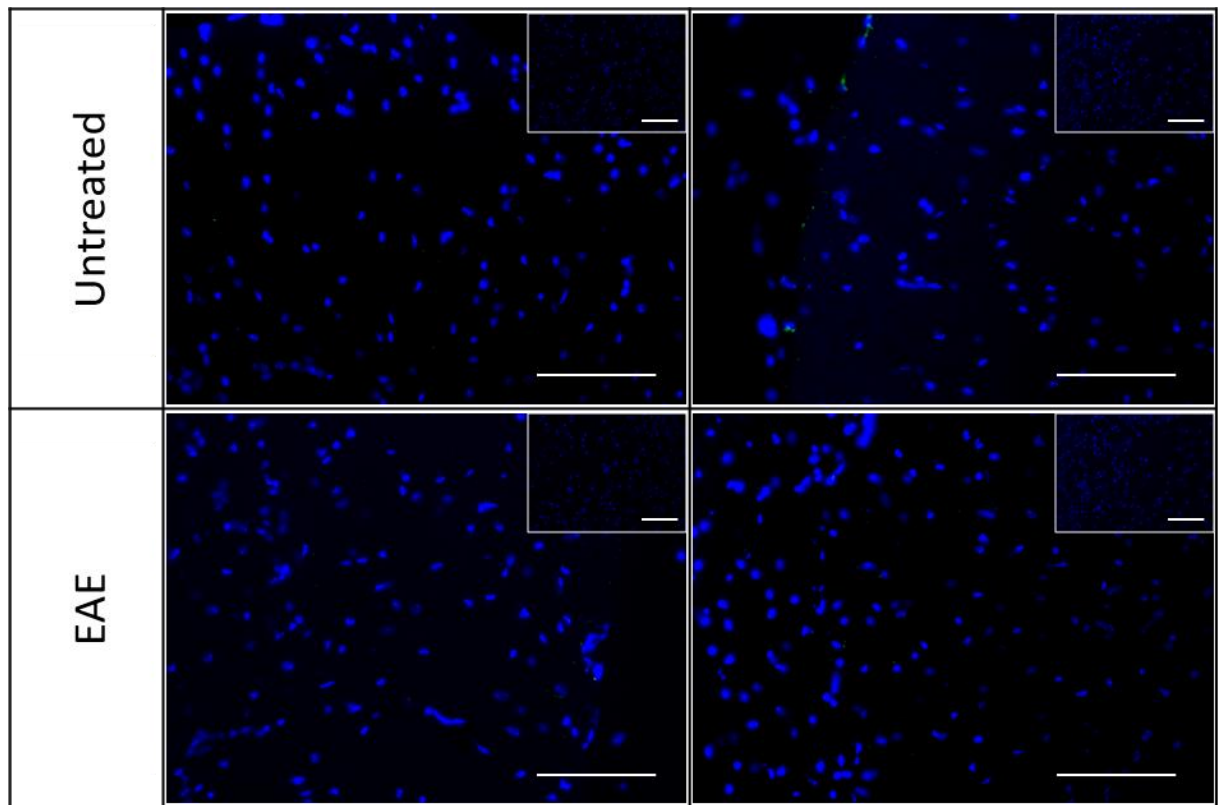
Figure 5.11: Representative GFAP (green) IHC in D14 acute EAE samples. 2 images are shown, from different animals in the same group of the study. Samples were counterstained with DAPI (blue). Minimal GFAP staining was observed in both untreated control and EAE groups. Scale bars represent 100µm, n=5 for treated, 3 for untreated controls.
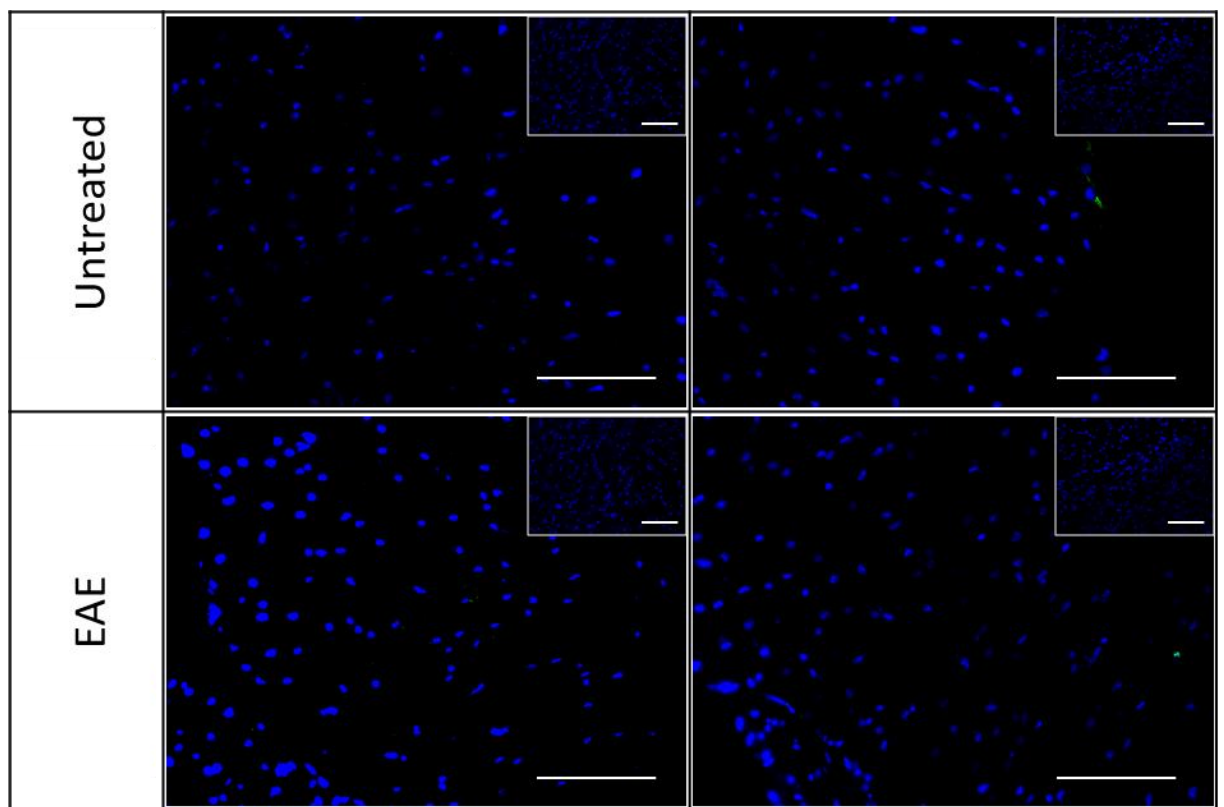
Figure 5.12: Representative GFAP (green) IHC in D19 acute EAE samples. 2 images are shown, from different animals in the same group of the study. Samples were counterstained with DAPI (blue). Minimal GFAP staining was observed in both untreated controls and EAE groups. Scale bars represent 100μm, n=5 for treated, 3 for untreated controls.
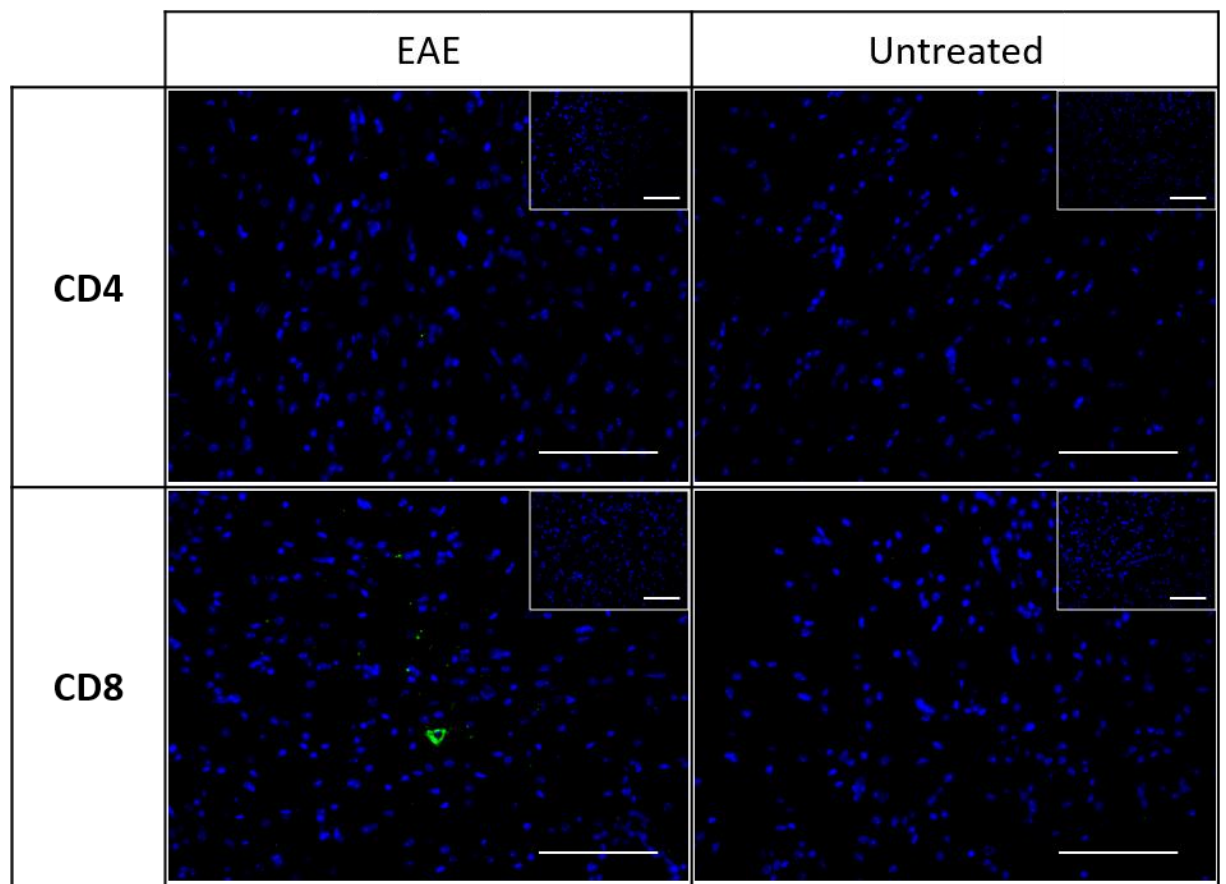
Figure 5.13: Representative CD4 and CD8 (green) IHC in D19 acute EAE samples. 2 images are shown, from different animals in the same group of the study. Samples were counterstained with DAPI (blue). No CD4 staining was observed in both untreated controls and EAE groups. Although minor, some EAE samples showed CD8 positive staining, however this was minimal and did not demonstrate a significant influx of CD8$^+$ cells. Scale bars represent 100μm, n=5 for treated, 3 for untreated controls.
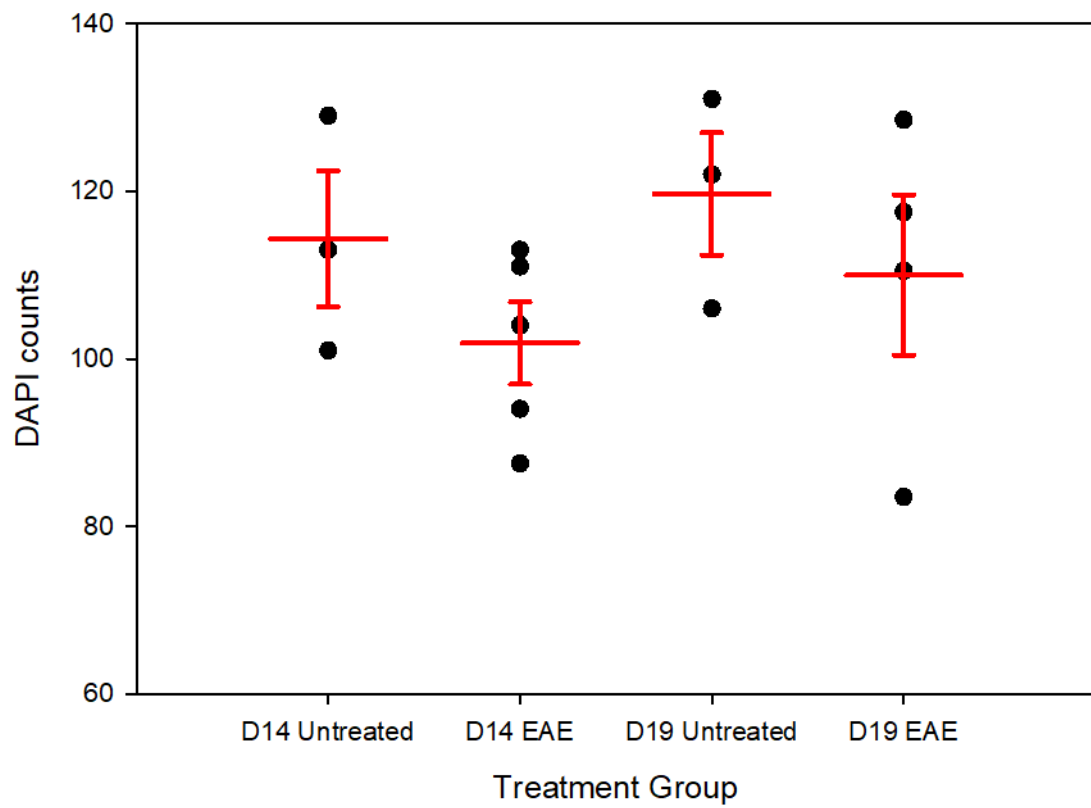
Figure 5.14: DAPI counts from lumbar posterior fasciculus of acute EAE mice and untreated controls at D14 and D19. A minor reduction in the DAPI counts was observed following EAE induction, compared to untreated control samples. This was however not found to be significant. Error bars represent one SEM, n=5 for D19 EAE, n=5 for D14 EAE and n=3 for untreated controls.
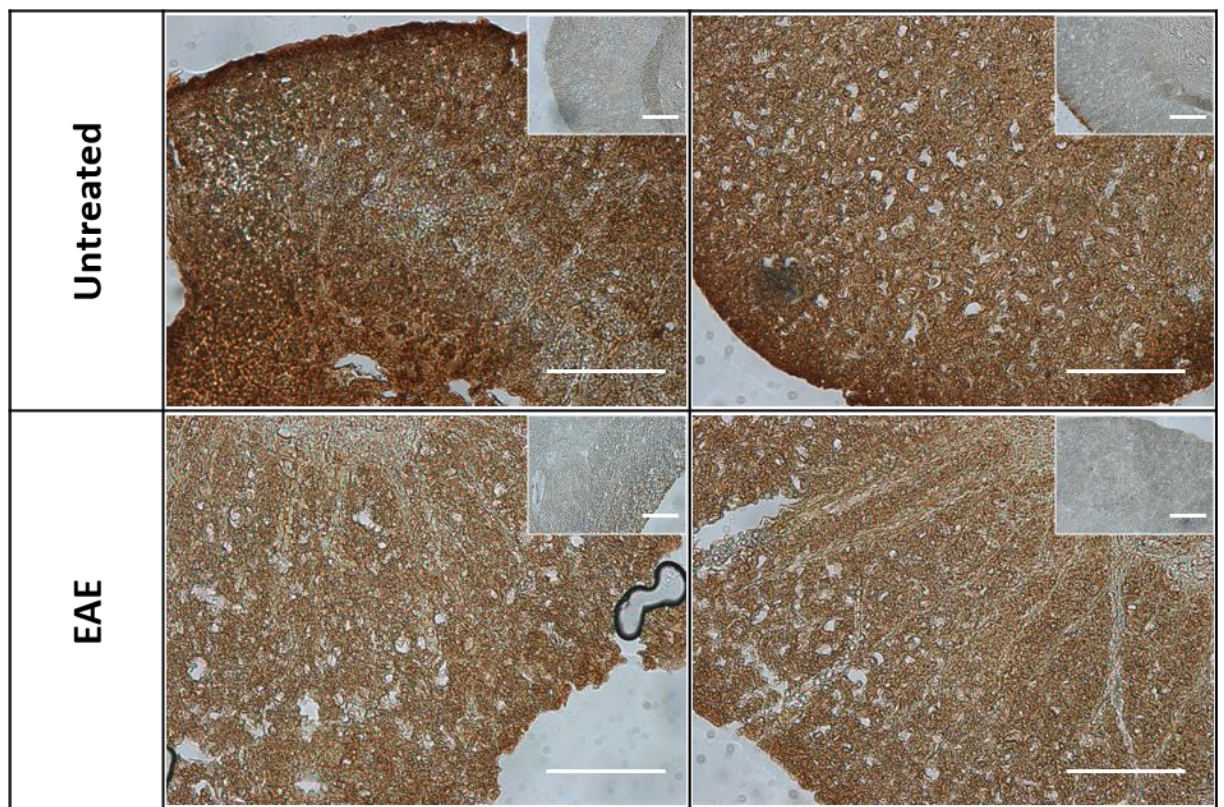
Figure 5.15: Representative IHC for MBP in relapsing-remitting EAE samples. 2 images are shown, from different animals in the same group of the study. The intensity of the DAB staining reduces in EAE samples, indicating that there has been a decrease in the level of MBP, therefore demyelination is likely to have occurred. Scale bars represent 100μm, n=6 for EAE samples, 4 for untreated controls.

5.4.3 Discussion of EAE models

Our D14 and D19 models of EAE showed low levels of disease progression as expected for this acute model of inflammatory disease. MBP levels appeared to reduce slightly in both D14 and D19 models, suggesting a very mild response. The low levels of EAE induction could also explain the variability as one minor change in one animal would appear significant compared to the remaining samples. Interestingly, a number of markers of inflammation and lesion development were unchanged with variable levels within the groups, raising questions to the level of inflammation achieved. In contrast, the relapsing-remitting model has been demonstrated previously to induce comparative and reproducible signs of demyelination combined with the secondary signs of neurodegeneration (Al-Izki et al., 2012). In agreement with this we observed a reduction in the MBP staining indicating that the model had induced demyelination. Due to the lack of signs of inflammation and the low signs of disease progression, as well as the high variability in MBP levels and signs of inflammation within groups in the acute models of EAE, we decided to focus on the relapsing-remitting model of EAE for the Western blot analysis of AMIGO3 and LINGO1.

5.4.4 AMIGO3 in relapsing-remitting EAE

We observed a 30% increase in the expression of AMIGO3 protein in protein lysate collected from the lumbar spinal cord samples of relapsing remitting EAE compared to healthy controls (fig 5.16). The integrated density rose from 0.97±0.06 in untreated controls to 1.30±0.09 in EAE samples. The increase was found to be
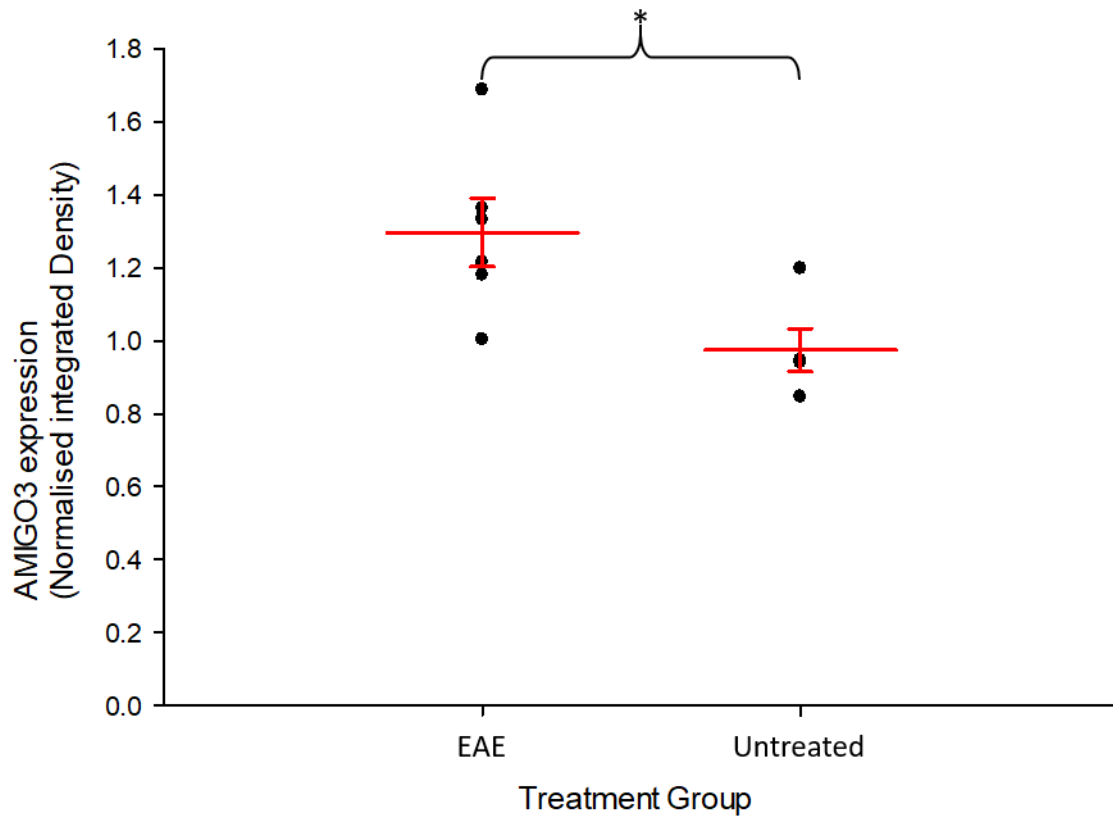
Fig 5.16: AMIGO3 expression in relapsing-remitting EAE samples. AMIGO3 expression can be seen to be significantly raised following induction of EAE in EAE spinal cord protein lysates. Error bars represent one SEM, n=4 for untreated controls, n=6 for EAE samples.

significant (P<0.05) when analysed via t-test. DAB staining for AMIGO3 showed

minimal clear staining, with no major observable difference between EAE and

controls (fig 5.17)

5.4.5 AMIGO3 in MS

Interestingly AMIGO3 showed a reduction in their proteins levels analysed from

MS samples, both in the lesion sites and in the normal appearing white matter,

compared to that of healthy tissue (fig 5.18). AMIGO3 protein normalised integrated

density readings dropped from 0.64±0.17 to 0.44±0.08 in MS lesions as well as a

decrease to 0.44±0.07 in NAWM samples from MS patients. None of these changes

were found to be significant however (ANOVA, $F_{(2,12)}=1.149$, P>0.05).

5.5 Discussion

5.5.1 Optic Neuritis

We first modelled an acute model of induced demyelination with our previously

developed optic neuritis model. Interestingly, there was no clear reduction in

AMIGO3 expression, except that the strongest staining appeared to redistribute to

some degree to appear in a linear distribution, presumably along axons, although it

should be noted that was a degree of variability between samples with some samples

not showing any change in the distribution. Furthermore, when pixel analysis was

performed, there was no clear sign of any increase in AMIGO3, however there was a

potential decrease at this stage, although this was minor and not found to be

significant. It is likely that due to the relatively small sample size and the semi-
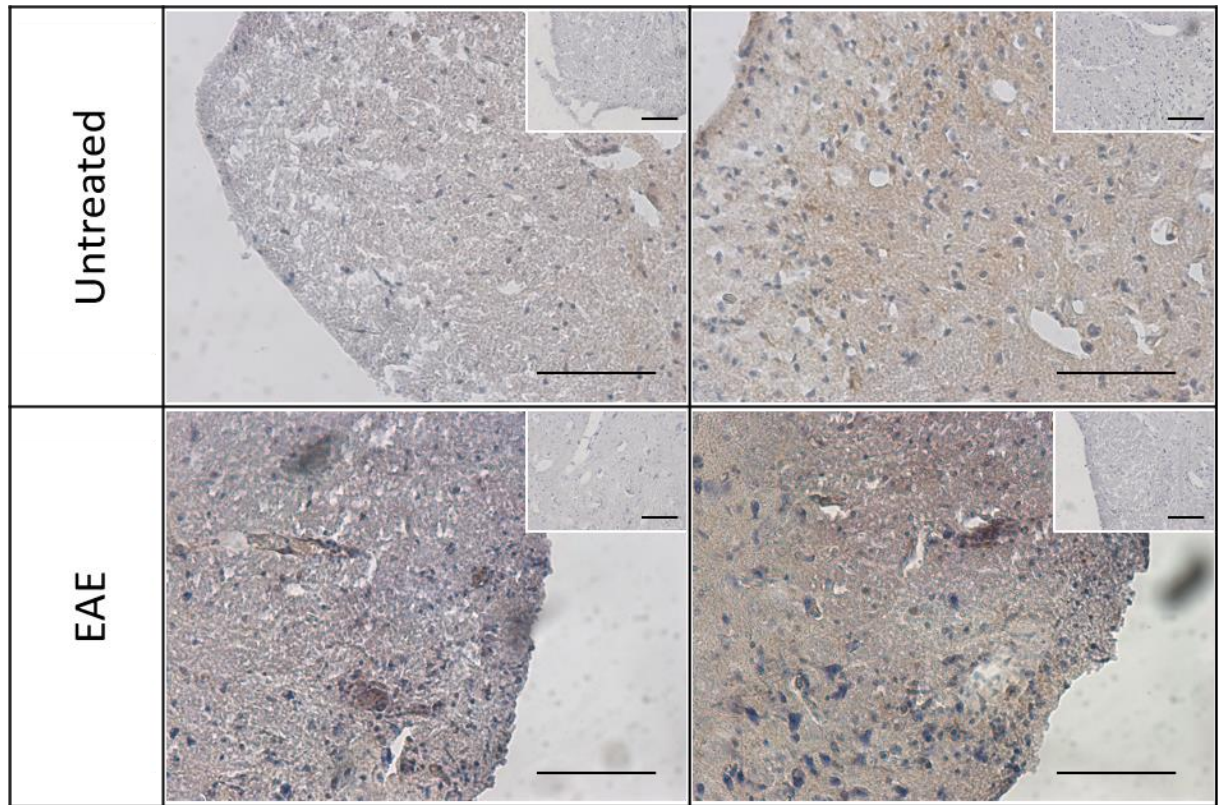
Fig 5.17: Representative DAB IHC for AMIGO3 in relapsing-remitting EAE samples. Samples were counterstained with eosin. The intensity of the DAB staining remains relatively low and constant in both EAE and untreated groups. Samples were counterstained with haematoxylin. Scale bars represent 100μm, n=6 for EAE samples, 4 for untreated controls.
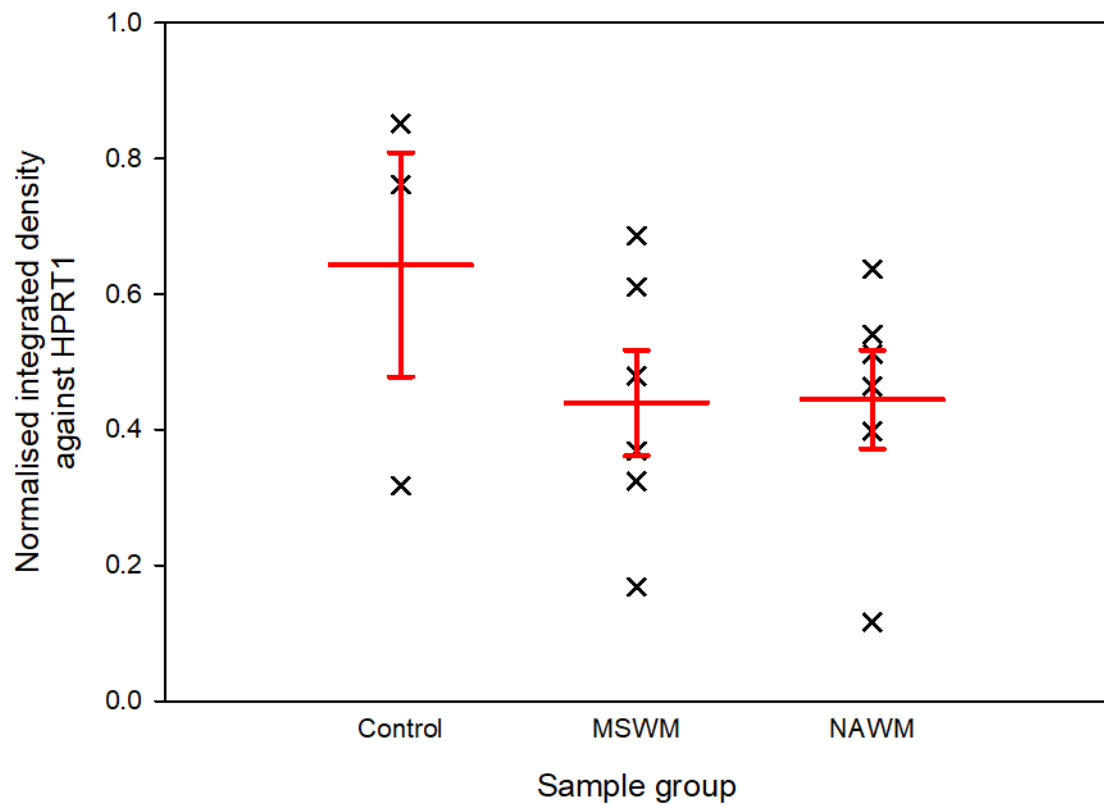
Figure 5.18: AMIGO3 protein expression in MS samples. AMIGO3 expression appears to reduce slightly in both tissue samples from MS patients, both in lesions and NAWM, although no significance was found between any of the groups. Error bars represent one SEM, n=6 for MSWM & NAWM groups, n=3 for healthy controls.

quantitative nature of our analysis methods that we were unable to identify these changes. Furthermore, when MBP was also analysed to examine the extent of demyelination, we did not observe any changes between the optic neuritis group and untreated controls. Although we were aiming to examine AMIGO3 in the acute stages of disease, prior to extensive demyelination, it appears that the model may have been insufficient to induce a significant disease state. It should also be noted that due to the low time course allowed for disease progression, it was not possible to examine how far the disease had progressed prior to sample collection. As such it is very possible that animals may have experienced variable disease progression which may not have been significant enough to induce a noticeable disease state. To further examine the expression profile of AMIGO3 in demyelinating disease, more progressed EAE models were examined.

5.5.2   Evaluation of EAE models

Due to the low level of demyelination observed in our optic neuritis model, we decided that it was prudent to examine AMIGO3 expression in a more developed model of EAE. Firstly we tested our acute model following a longer treatment period, specifically 14 and 19 days, which has previously been shown to develop low scores in EAE in our group (Ahmed et al., personal communication. As briefly discussed previously (section 3.4.3), we observed that there was a steady increase in the clinical score from a mean average score of treated animals of 0 at D14 to 1.2 at D19. At this stage flaccid tails were observed indicative of early EAE progression (Al-Izki et al., 2012). It should be highlighted however that scoring is subjective, therefore

206

although we did see a clear increase in the scores there is a risk of researcher bias in the scoring system.

It is interesting to note that there was a variation between the level of demyelination observed in the white matter of lumbar sections, between the D14 and D19 samples. At D14, there appeared to be relatively low levels of MBP in the EAE induced animals compared to the untreated controls. This reduction in MBP staining was much less marked in D19 samples. It is not clear why this would have been the case, however one explanation is that the model exhibited some recovery within the timeframe. The model was a mild form of acute inflammatory induced demyelination, thus it is possible that the demyelination may have stopped by D19. It is also possible that we observed some early stages of remyelination by D19, hence the increased MBP signal.

We further tried to examine other signs of EAE progression to determine whether the model demonstrated signs of disease progression. As discussed, EAE progression is demonstrated by an increase in the numbers of local microglia (OX42^{+} cells) as well as an increase in the numbers of invading T-helper cells (CD4^{+}). Although not considered the initiator, cytotoxic T-cells (CD8^{+}) are also present to some degree as the disease progresses. Additionally, as axons are lost, there is an increase in reactive gliosis as astrocytes fill in the damaged area, creating glial filaments and leading to the production of a glial scar (Correale and Farez, 2015).

We generally observed very minimal positive IHC signal for all of these markers, although some variability was observed. One sample did show strong staining for OX42 surrounding the central canal at D14 indicating that some of the animals did experience a degree of inflammation through activation and recruitment of microglia. This observation however was only detected in one of the groups, therefore it highlights that there is significant variation between groups. Furthermore, as only one sample in the earliest collection time point demonstrated this inflammatory marker, it supports the view that the model may be observing the remyelination period rather than the active demyelination period.

Again, as with OX42, CD4^{+} and CD8^{+} staining was not detected to any relevant degree, indicating a lack of T-cell recruitment to the spinal cord. These data indicate that there had been a minimal inflammatory response, or if it was present, that it was regressing by the time of collection. It is likely due to the increasing signs of MBP and the limited sign of inflammatory cells and reactive gliosis, that by the time of tissue collection, the samples had already experienced demyelination, and remyelination was occurring. Alternatively, the models had simply not experienced sufficient disease induction.

The lack of development may be a result of the variation in our procedure compared to similar studies. Pertussis toxin is traditionally injected subcutaneously with the Mog-35-55 to further elicit the immune response (Zeinali et al., 2018). We decided against this protocol based on our previous investigations as without the pertussis toxin our model should have lead to a less developed form of

demyelination. Although our scoring does appear reduced compared to the traditional method, the disease induction may have been too light to provide a sufficient response for examining the expression of AMIGO3 during demyelination. Due to the lack of clear and consistent signs of demyelination as well as the minimal signs of disease progression within the groups in both D14 and D19 samples, it was decided that we would employ another model of EAE to examine a more progressed form of the disease.

We decided to examine the relapsing-remitting model of EAE, with samples gratefully received from Professor David Baker and Dr Gareth Pryce (Blizzard Institute, Barts and London Medical School). Due to the samples being fixed with formal saline (containing 4% formaldehyde and 8.5g/L sodium chloride) for multiple days before processing, it was not possible to perform immunofluorescent IHC due to the high amount of background signal created by the fixation process. As a result, myelination was analysed by examine MBP$^+$ signal through DAB staining. A clear reduction in the MBP levels was observed between the relapsing-remitting EAE induced samples when compared to the untreated controls.

It should be noted however that EAE, and MS, do not demonstrate even demyelination across the spinal cord, instead having focal regions of demyelination (Barnett and Prineas, 2004; Linker and Lee, 2009; Boyd et al., 2013). This might explain why different degrees of demyelination were observed in the relapsing-remitting model of EAE. Time constraints meant that it was not possible to examine the entirety of the spinal cord. It is very possible that despite our efforts to select

sections where demyelination appeared, that we may have chosen sections where lesions were not developing. As such it was decided to analyse AMIGO3 expression via western blots, so that an average of the expression in the lumbar section of the spinal cord, both in MSWM and NAWM could be analysed compared to healthy levels. This approach should have helped to remove some of the variability between samples.

5.5.3   AMIGO3 in EAE

We observed in our relapsing-remitting model of EAE, that AMIGO3 levels were significantly raised compared to healthy controls. These data indicate that AMIGO3 is likely to be playing a role in the development of disease in this model of EAE. As the model is relapsing remitting, it is likely that animals at a score of 4 are experiencing a degree of acute inflammation in the spinal cord. As such, we can conclude that AMIGO3 levels are raised in lumbar spinal cords during bouts of inflammation induced demyelination.

Although not completed in this study, it would have been valuable to investigate whether LINGO1 levels were raised at a similar time point to AMIGO3, or if AMIGO3 increased expression precedes LINGO1 as it does in spinal cord injury (Ahmed et al., 2013). A recent study has analysed the levels of LINGO1 mRNA in acute and chronic forms of MOG_{35-55} induced EAE (Theotokis et al., 2016). They found that although a minor increase in LINGO1 was observed in spinal cords at the acute stage, this was not significant. It was not until the disease was deemed chronic, that a significant upregulation of LINGO1 mRNA was observed in the spinal cord samples. As this

form of EAE is a chronic progressive model, with a low clinical score, it is unlikely to experience major stages of inflammation. As such, our relapsing-remitting model, developed a score 4 after the second relapse (Al-Izki et al., 2012) and therefore sample collection is likely to have followed a large inflammatory response. Although this raises difficulties in directly comparing the results, it could be argued that the relapsing-remitting model would demonstrate a more severe acute response, therefore the rise in AMIGO3 expression is likely to correlate with the acute damage to the CNS, rather than a chronic build up. As such these data suggest that AMIGO3 is raised at an earlier stage than LINGO1. It should be stated again however that the different models and analysis techniques raise questions to this conclusion and it is essential to evaluate the levels of AMIGO3 and LINGO1 in our EAE model so that a direct comparison can be procured.

We were unable to confirm the localisation of AMIGO3 to a certain cell type, due to the variability in previous AMIGO3 immunofluorescence experiments and the lack of clear AMIGO3^{+} staining with our DAB staining protocol. It is likely that our anti-AMIGO3 antibodies were lacked the specificity to identify AMIGO3 levels through IHC as previously observed (chapter 3). As such, it still remains to be answered whether AMIGO3 expression is changed in specific cell types in demyelinating disease. It should be noted however that changes in expression in non-OLG cells could also lead to changes in activity in OLG due to potential homotypic interactions of AMIGO3, and its potential to signal intercellularly in a similar manner to LINGO1 (Kuja-Panula et al., 2003; Jepson et al., 2012).

5.5.4 AMIGO3 in MS lesions

From our investigation, we observed a non-significant decrease in AMIGO3 in both the MSWM and NAWM compared to healthy control white matter. It should be noted that this study had only a small sample size, therefore it is possible that significance would have been detected had a greater number of replicates been possible. This would be an interesting finding if correct. This could indicate that in developed MS, AMIGO3 based therapies may not prove beneficial due to the lack of expression. This of course ignores the concept that the proteins may be relocated to areas of higher activity in OLG following trauma so the reduced levels may not be indicative of reduced activity.

Interestingly, if the minor reductions in AMIGO3 in MS tissue that we observed are correct, then it is interesting to note that the reductions occur in both MSWM and NAWM. This is unexpected as 'healthy' white matter tissue in MS patients would not be expected to change levels as they have not received any direct trauma. Conversely however, axonal loss has been observed in NAWM suggesting that these expression changes may relate to the loss of axons (Constantinescu et al., 2011). As both LINGO1 and AMIGO3 are expressed within axons (Mi et al., 2004; Ahmed et al., 2013), it is possible that potential increases in protein expression in OLG, as suggested from our and other EAE studies, may be counteracted by a reduction in axonal expression due to this loss of axons (Theotokis et al., 2016). An alternative interpretation of this MS data is that AMIGO3 does not play a significant role in the human demyelinating disease. However, as stated above the sample sizes used in

this study were low, thus additional replicates would be required to confirm this interpretation.

5.5.5 AMIGO3 and LINGO1 in demyelinating diseases

Based on our data, it appears that AMIGO3 is upregulated following significant inflammation and trauma to the mouse CNS. It is still yet to be determined whether this increase is seen earlier than LINGO1, however the delay in LINGO1 mRNA displayed in both spinal cord and chronic progressive EAE is likely indicative that AMIGO3 is upregulated preferentially in early stages of disease (Ahmed et al., 2013; Theotokis et al., 2016).

Furthermore, it would appear that AMIGO3 has a more active role in acute stages, and potentially is no longer relevant in chronic disease, due to the relatively reduced or similar expression levels between human healthy and MS lesions in brain white matter. Direct comparisons between our MS and EAE data should be taken with caution due to the differing white matter regions and models examined though.

5.5.6 Limitations

A number of limitations are present from this study. Firstly, relatively low sample sizes were used due to time and financial constraints. Further repeats would be valuable to confirm our findings.

In the terms of our models, it has to be noted that although EAE is considered a valuable animal replication of MS, there have been a number of therapeutic approaches that have proven successful in EAE but have not translated into MS

therapies. This indicates that there must be a significant difference between the human disease and disease progression in the EAE models (Baker and Amor, 2015). Despite these issues, the results still provide an insight in to the potential role of AMIGO3 in demyelinating disorders.

Although in our MS study there was selection between lesion sites and NAWM, this was not possible in our EAE studies due to time constraints. As a result, we were unable to compare whether the increased expression of AMIGO3 that we observed in our EAE samples is specifically located within lesion site, within the unaffected white matter, or a general change across the whole matter.

It is also pertinent to mention that our relapsing-remitting samples were not analysed in this study to determine the extent of inflammation. Previous studies have shown that inflammation is significant and that due to the development of the disease, that significant immune infiltration will have occurred, however it would be valuable to define this for our own study (Al-Izki et al., 2012).

One major limitation is that our EAE studies used untreated controls rather than sham treated controls. It is possible, although unlikely, that some of the responses that we observed were due to treatment procedure alone, rather than the induction of EAE itself. This has been the traditional approach for EAE studies, however it would be valuable for repeats to re-examine the results with sham treated subjects to remove this variability.

5.5.7   Future studies

Firstly, it would be interesting to repeat the experiments in a number of different EAE models to confirm whether our findings are indicative of a general change in demyelinating states or whether it is specific to the models that we used.

Despite our progression in understanding the expression profile of AMIGO3 in demyelinating disease, we are still to determine the potential methods through which AMIGO3 could act *in vivo* and in MS. It would be very interesting to firstly repeat these experiments but analyse the level of expression with particular cell lines. This could be done through FACS to separate cell lines prior to analysing the levels of mRNA or protein, however it is possible that the FACS process could alter expression or limit the number of cells available for further analysis.

Furthermore, a study altering the levels or action of AMIGO3 *in vivo* would be fascinating to gain an insight into potential roles for AMIGO3 in disease. This could be done through genetic modifications, through addition of active AMIGO3, or through inhibiting the action of AMIGO3 through antibody therapies. Despite being an important part of our experimental design, the cost of providing an effective inhibitor of AMIGO3 for the full period of an EAE study was not viable. Therefore it was not possible to investigate the effects of inhibiting AMIGO3 on a model of demyelination. This would be an invaluable piece of information as it would present whether AMIGO3 based therapies would have any direct impact on demyelination *in vivo*.

Interestingly, Theotokis et al (2016) noted that there was a shift between TROY and P75 mRNA expression between acute and chronic forms of EAE in C57BL/6 mice. TROY was expressed at higher levels in the acute stages, with P75 levels increasing whereas TROY levels decrease in chronic form of the disease. It is possible that these change in co-receptor molecules could show preferential binding to either LINGO1/AMIGO3, thus potentially indicating a method for AMIGO3 to act with the NgR1 receptor complex over LINGO1 in different stages of EAE development. This raises an interesting further study to determine whether there is any competition between the proteins in OLG responses to demyelination. This hypothesis is reliant on NgR1 being expressed in OLG, therefore further work is required to confirm this concept.

5.5.8   Conclusions

We conclude from this study that AMIGO3 levels rise following inflammatory induced demyelination in murine EAE. A significant inflammatory response is required however before AMIGO3 expression is upregulated. It is likely that the elevated levels of AMIGO3 have an effect on OLG. However, it still remains to be answered exactly what impact AMIGO3 will have on the cells. Chronic MS lesions showed reduced AMIGO3 expression, potentially due to the loss of neural cells, predominantly neurons, but OLG as well. Further work is required to confirm whether this reduction is related to the differentiation potential or level of OPC in chronic stages of demyelination.

Chapter 6

AMIGO3 and NgR1 during OPC maturation

6.1 Rationale

In this project so far, we have predominantly been investigating the expression profile of AMIGO3 during models of disease states, however there has yet to be any evidence published which analyses the potential pathways through which AMIGO3 could function, the levels of AMIGO3 during myelination and the potential effects of altering AMIGO3. As we have discussed, AMIGO3 has been identified in OLG and we have identified that AMIGO3 is raised during excitotoxic trauma to the cells.

AMIGO3 shares a number of attributes with LINGO1, and has been shown to be able to interact with the NgR1 receptor in both neurons and COS7 cells transfected to express both AMIGO3 and the NgR1 receptor complex proteins. Therefore it is likely that AMIGO3 shares a similar mechanism of action in OLG (Mi et al., 2004; Ahmed et al., 2013). There is some debate as to whether LINGO1 is able to function through the NgR1 receptor in OLG as traditionally, LINGO1 was shown to be able to function through the NgR1 receptor in both COS-7 cells and neurons leading to growth cone collapse in regenerating axons in a RhoA dependent manner. More recent evidence has been found suggesting that in OPC LINGO1 is able to function via interactions with a number of proteins, including ErbB2, gelsolin and PI3K (Foale et al., 2017).

As previously discussed (section 1.4.2.2) there is some debate about whether NgR1 is present on OLG. Data supporting NgR1 expression on OLG tends to be generated from OPC cells derived from neural stem cell lines or entirely different cell lines altogether (Jepson et al., 2012; Mi et al., 2013; Kwon et al., 2014). Furthermore,

it has been reported that OL do not express NgR1, albeit without evidence (Mei et al., 2013), and studies with a human hybrid oligodendrocyte hybrid cell line, MO3.13, demonstrate P75 expression, but a lack of NgR expression at both the transcript and protein level (Bourikas et al., 2010). The MO3.13 data demonstrates evidence of a lack of OLG expression of NgR1, however it should be highlighted that these cells are a hybrid line with human rhabdomyosarcoma cells, and have been shown to also express the astrocyte marker GFAP, therefore they do not exhibit a purely OLG phenotype (McLaurin et al., 1995). Despite this data there is no clear consensus as to whether the NgR1 receptor complex is expressed on OLG, therefore it is of value to examine the expression of the proteins in primary OLG cell lines.

Furthermore, despite our repeated findings of changes in AMIGO3 levels in various models of myelination, there has yet to be a direct link to OLG maturation or myelin production. As such, it was deemed necessary to examine the expression profile of AMIGO3 in primary OPC cultures following and during the maturation process.

6.2 Aims

The aim of this study is to investigate whether any of the proteins of the NgR1 complex are present in primary OLG to determine whether NgR1 signalling could be a mechanism through which AMIGO3, and LINGO1 could function. We also aim to examine the levels of AMIGO3 before and after encouraging the primary to mature.

6.2.1 Hypothesis

We hypothesise that:

- NgR1 receptor proteins will be expressed on OPCs to allow for AMIGO3 signalling in the immature cells.
- NgR1 will not be present on mature cells as its role in inhibiting maturation and myelin production will no longer be relevant.
- AMIGO3 will also be downregulated following maturation.

6.3 Experimental design

6.3.1 NgR1 expression in OLG

Primary OPC were collected and grown as previously described (section 2.2.1.1). These cells were used for ICC studies to examine for markers of OLG and to characterise the cells for NgR1 receptor complex proteins.

6.3.1.1 IHC in OLG cultures

For ICC imaging of OPC cultures, following collection and resuspension of OPCs as described (section 2.2.1.1), the cells were then seeded at 25,000 cells per well on Matrigel coated, 8 well chamber slides (Corning Falcon). Cells were incubated at 37ºC, 5% CO_2 for 24 hours. Following incubation, cells were fixed and IHC was performed as described (section 2.3.2.3). OPCs were labelled for the OLG marker Olig2 (Cai et al., 2007; Maglione et al., 2010), the OPC marker NG2 (Clarke et al., 2012), the microglia marker OX42 (Alrehaili et al., 2018), the astrocyte marker GFAP (Kundi et al., 2013) and NgR1 and P75.

For mature OLs, OPCs were similarly seeded on 8 well chamber slides for 24 hours. However maturation treatment was performed as described (section 2.2.1.1). On D5, cells were fixed and IHC was performed as described (section 2.3.2.3). OLG were then labelled for Olig2 & CC1 and NgR1.

6.3.2 AMIGO3 expression during maturation

AMIGO3 and PLP levels were analysed at the transcript level by qPCR to examine the expression of AMIGO3 during maturation. Following collection of primary OPCs, cells were seeded at 25,000 cells per well in a Matrigel coated 48 well plate as previously described (section 2.2.1.1). At D1 post-shaking, primary OPCs were collected with a cell scraper and mRNA/cDNA collected and generated as previously described.

OPC were treated to induce maturation and mRNA/cDNA samples were similarly collected and generated on D5 post-shaking. For transfections, on D11 when maturation was encouraged, SATO media was supplemented with Opti-MEM (8% v/v) containing lipofectamine (8% v/v) and 40nM siRNA. Samples were incubated with the siRNA for 6 hours at 37ºC, 5% CO_2 before a full media change with SATO. Normal maturation treatment was continued from this step and samples were collected on D5 post-shaking.

6.3.3 Experimental plan

A summary of the plan for the investigation, findings and experiments used is demonstrated in figure 6.1.
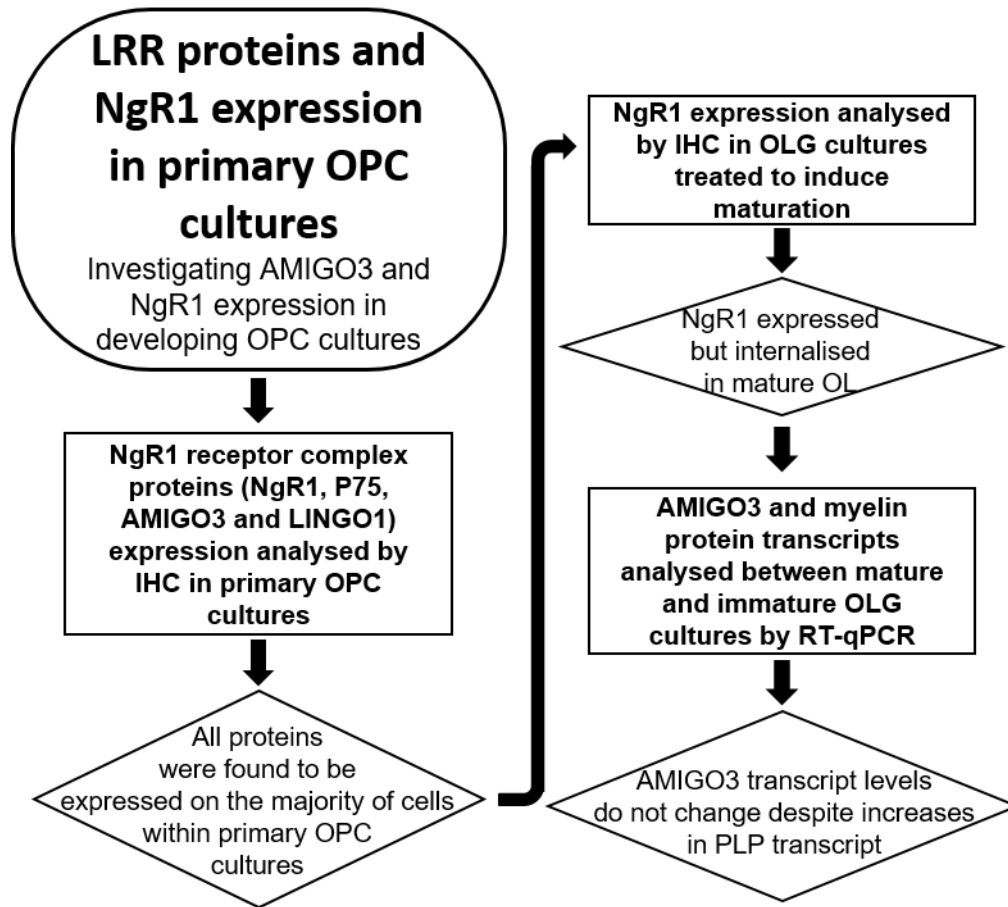
Figure 6.1: Flow chart demonstrating the plans and summarising the findings from chapter 6.

6.4 Results

6.4.1　　　NgR1 in OLG

6.4.1.1　　Characterising primary OPC

We first attempted to characterise our primary OPC cultures to confirm their OLG identity. Olig2$^+$ staining could be seen in the majority of cells, with DAPI$^+$ and Olig2$^+$ matching for the majority of cells in our samples (fig 6.2). We then attempted to characterise the maturity of the cells through NG2 and CC1 ICC (fig 6.3). Although not clear in all of the imaged cells, NG2$^+$ was observed surrounding the majority of DAPI$^+$ nuclei (fig 6.3A & B). In a number of cells, NG2$^+$ staining demonstrated clear staining across the cell, with the soma and processes highlighted. Interestingly, multiple processes could be seen from these cells. CC1$^+$ staining was also observed in some cells, but the signal was relatively weak and centred immediately around the nucleus in the soma (fig 6.3 C & D). Just under half of the cells appeared to present some CC1$^+$ staining, however this was not quantified.

Having confirmed the OLG identity of these cultures, OX42 and GFAP IHC was performed to identify if there was any contamination in our primary OPC cultures (fig 6.4). OX42$^+$ staining was not observed in any of our samples (fig 6.4A & B). GFAP did show small levels of positive staining above the threshold value, however this did not localise to cells or demonstrate the expected staining profile, therefore this likely represents a contamination of proteins of structures rather than a major infiltration of
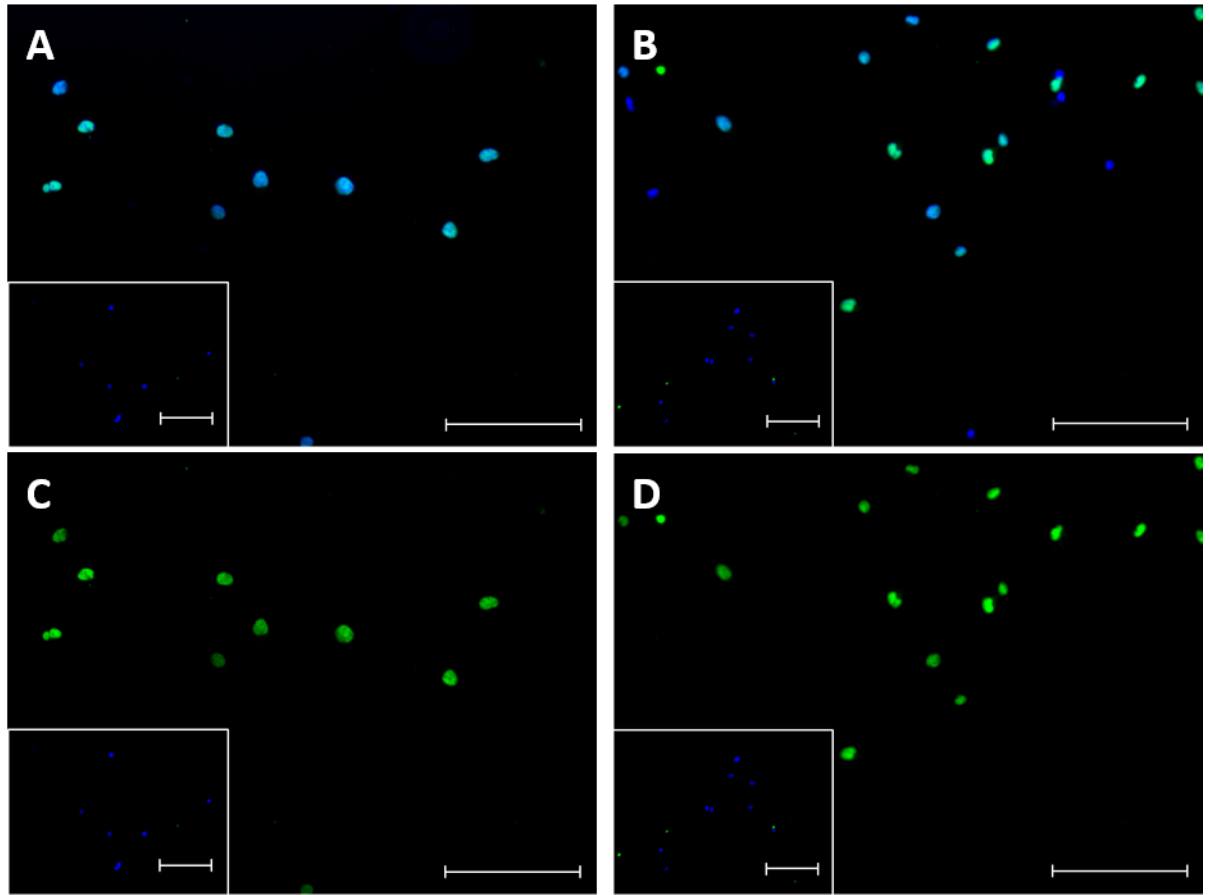
Figure 6.2: Representative Olig2 ICC in cultured primary OPC. 2 images are shown, from different cultures within the same group of the study. (A & B) Samples were counterstained with DAPI (blue). Olig2 and DAPI are colocalised in the majority of cells. The majority of cells demonstrate Olig2$^+$ staining in the nucleus. (C & D) the same images are shown however without DAPI signal was removed. Scale bars represent 100µm, n=3. Insets show negative controls.
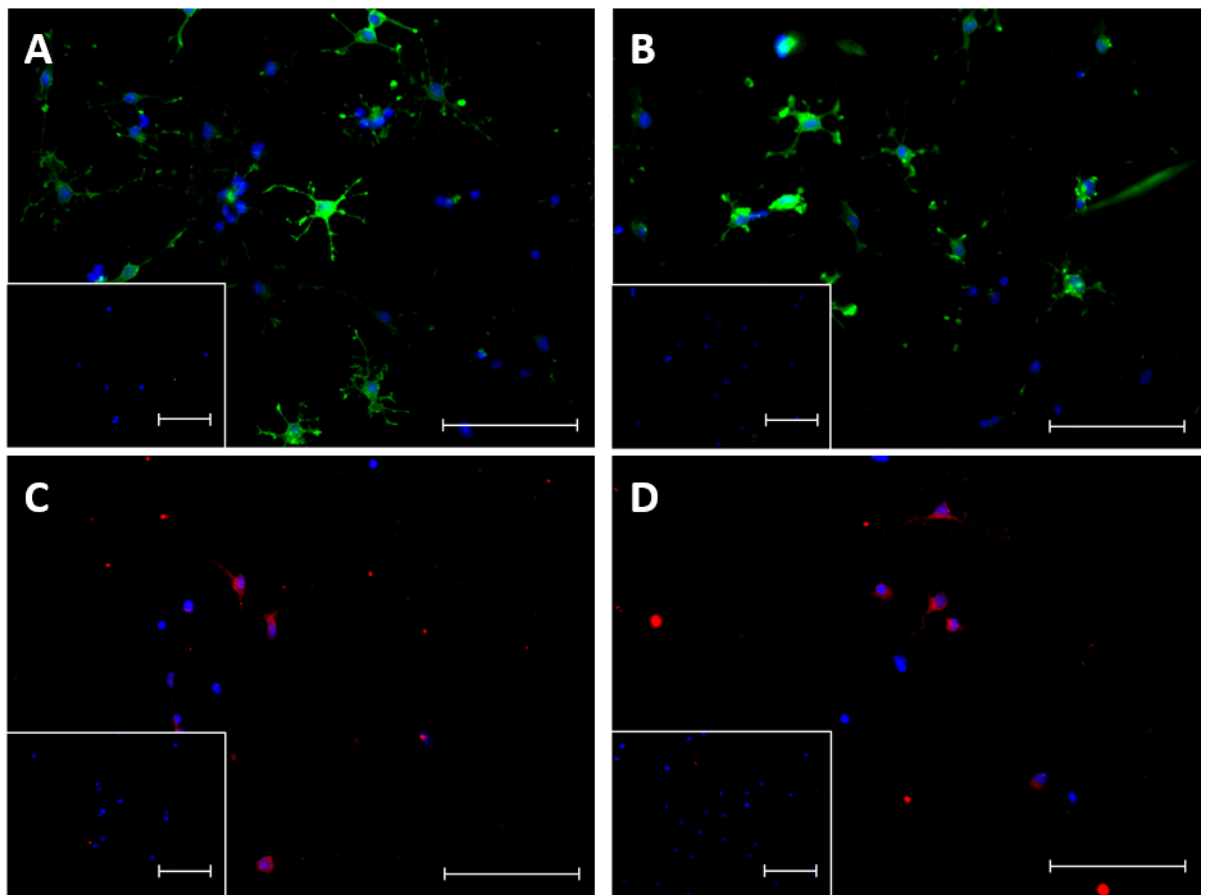
Figure 6.3: Representative NG2 (A & B) and CC1 ICC (C & D) in cultured primary OPC. 2 images are shown, from different cultures within the same group of the study. Samples were counterstained with DAPI (blue). (A & B) NG2$^+$ (green) is seen in a number of the cells and appears to label the soma and processes of the cells, indicative of OPC. (C & D) CC1$^+$ (red) is present, however only a few of the cells demonstrate positivity, indicating that some of the cells have, at the least, begun to differentiate. Scale bars represent 100μm, n=3. Insets show negative controls.
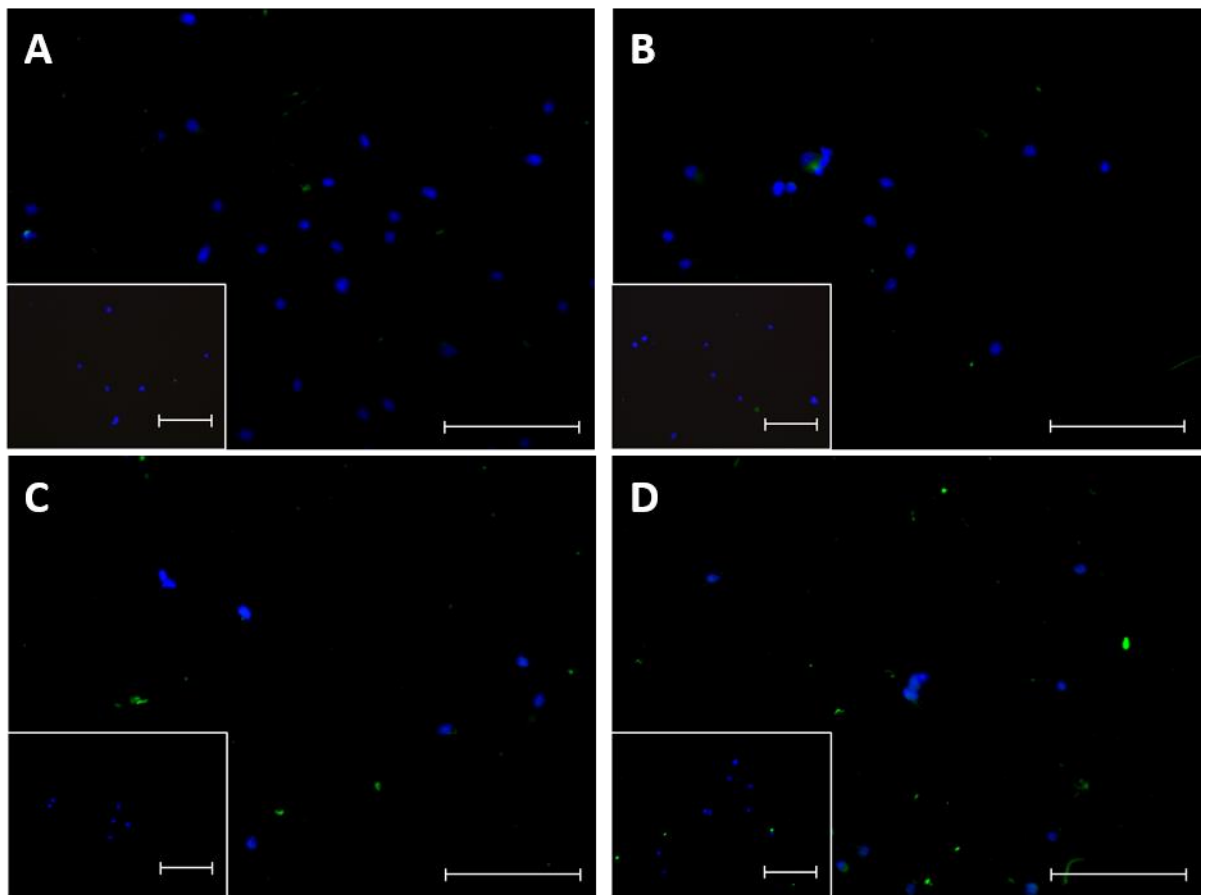
Figure 6.4: Representative OX42 (A & B) and GFAP (C & D) ICC in cultured primary OPC. 2 images are shown, from different cultures within the same group of the study. Samples were counterstained with DAPI (blue). (A & B) OX42^{+} (green) was not observed in any of the samples. (C & D) GFAP (green) was seen at low levels, likely representing minor contamination of astrocytes. Scale bars represent 100μm, n=3. Insets show negative controls.

GFAP$^+$ cells. It is also possible that GFAP$^+$ cells may have infiltrated the cultures but were not able to survive in the new media as well as the OLG.

6.4.1.2   NgR1 in immature OPCs

NgR1 and P75 expression was analysed in our OPC cultures (fig 6.5). We observed strong NgR1$^+$ ICC signals localised in a bipolar distribution as well as within the soma (fig 6.5A & B). Almost all DAPI$^+$ cells demonstrated NgR1$^+$ staining surrounding the nucleus indicating that the majority of cells are positive for the NgR1. P75 ICC was also performed (fig 6.5C & D) which showed similar results. Almost all cells demonstrated positive staining around the DAPI$^+$ nucleus suggesting a somal distribution. Interestingly, the signal was not as strong as NgR1 and images had to be enhanced to clearly identify positive staining over the thresholded value.

6.4.1.3   AMIGO3 and LINGO1 in OPCs

AMIGO3 expression was relatively limited within our OPC cultures (fig 6.6A & B). Not all of the DAPI$^+$ cells showed co-staining with AMIGO3$^+$ signal, however there does appear to be AMIGO3 staining within the soma of most cells to some degree. LINGO1$^+$ staining was also analysed in the primary OPCs (fig 6.6C & D). Similarly, LINGO1 was not observed in all cells however the majority of DAPI$^+$ nuclei also exhibited LINGO1$^+$ staining. Interestingly, the LINGO1$^+$ staining largely matched the DAPI$^+$ signal, with a small distribution immediately surrounding DAPI$^+$.
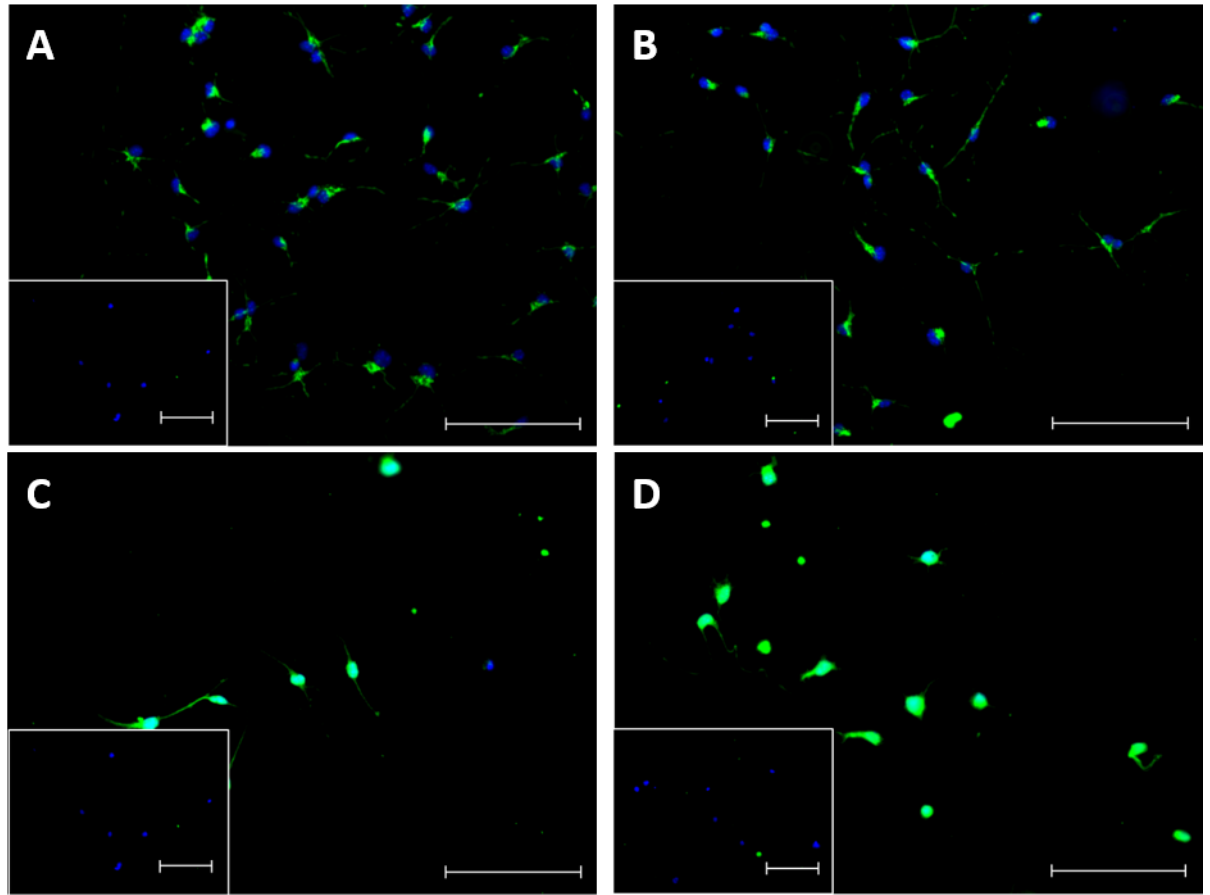
Figure 6.5: Representative NgR1 (A & B) and P75 (C & D) ICC in cultured primary OPC. 2 images are shown, from different cultures within the same group of the study. Samples were counterstained with DAPI (blue). (A & B) Clear images could be taken of NgR1 staining (green) in primary OPC, appearing to be distributed throughout the soma of the cells and in the processes. (C & D) P75+ (green) was observed in the majority of cells as well. P75 demonstrated localised staining to and immediately around the nucleus and in the soma. Scale bars represent 100μm, n=3. Insets show negative controls.
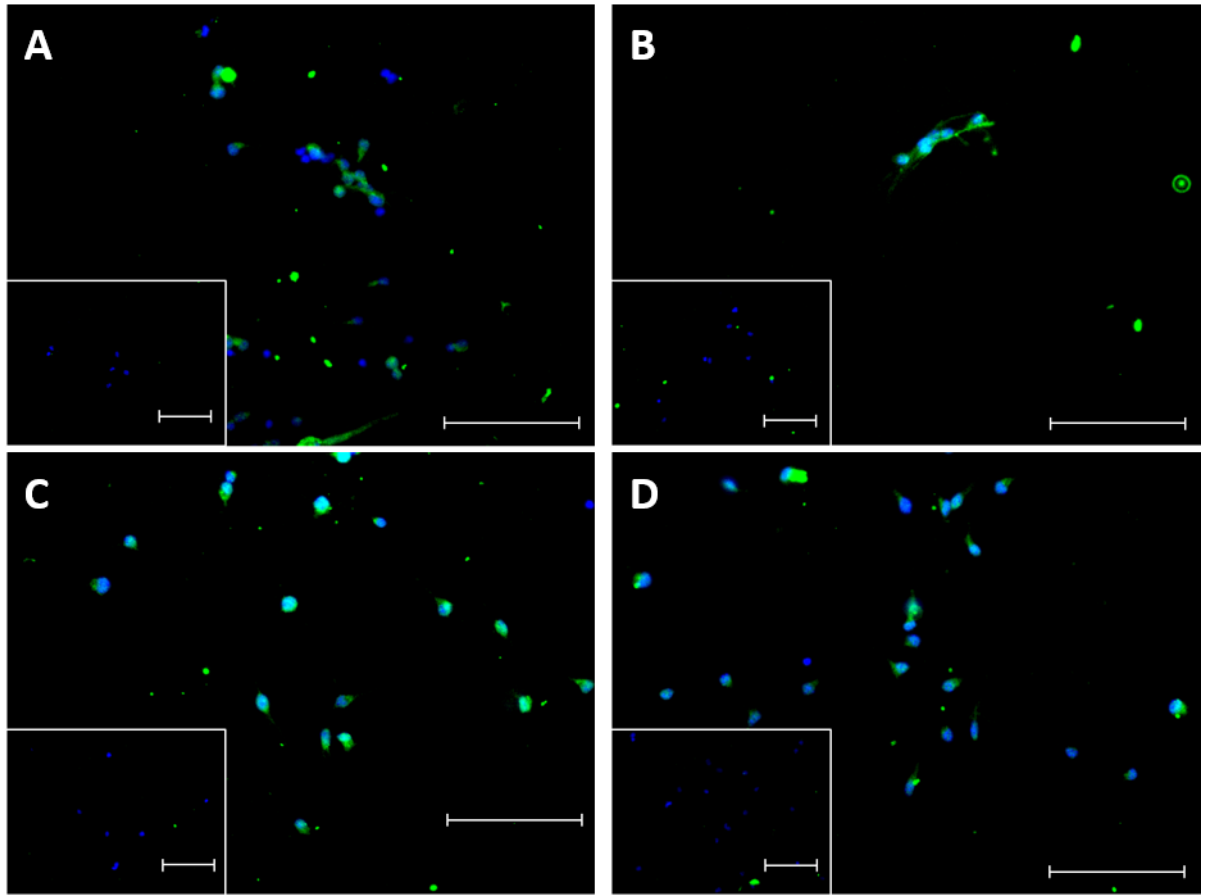
Figure 6.6: Representative AMIGO3 (A & B) and LINGO1 (C & D) ICC in cultured primary OPC. 2 images are shown, from different cultures within the same group of the study. Samples were counterstained with DAPI (blue). (A & B) A large number of the DAPI$^+$ cells demonstrated low levels of AMIGO3 in the SOMA of OPC. (C & D) Most cells demonstrated LINGO1$^+$ staining which tended to correlate with DAPI$^+$ nuclei, suggesting a lack of LINGO1 distribution across the soma and membrane of the cells. Scale bars represent 100µm, n=3. Insets show negative controls.

6.4.1.4   NgR1 in mature OL

Following incubation with maturation media to encourage maturation of the cells, we performed ICC for OLIG2 and CC1 (fig 6.7A & B) to confirm that the cells had an OL phenotype. Strong and extensive CC1$^+$ ICC signals surrounded the majority of Olig2$^+$ nuclei. Some cells expressed lower levels with minor signal, however generally the CC1 signal was more intensive and more extensively distributed than that observed in the untreated cultures (fig 6.3C & D).

The maturation media incubated cells were also stained for NgR1 (fig 6.7C & D). Most of the DAPI$^+$ regions demonstrated a region of NgR1$^+$ IHC in the immediate vicinity. Although not comprehensive, it is possible to see that the NgR1$^+$ staining appeared in small clumps, potentially a vesicular distribution, rather than the bipolar distribution observed in the primary OPC cultures (fig 6.5A).

6.4.2   AMIGO3 and primary OPC maturation

AMIGO3 mRNA expression was examined in primary OPC following incubation with maturation media (fig 6.8). Firstly, a large variation was observed with AMIGO3 expression in these primary cells before treatment was administered. The relative levels of AMIGO3 mRNA normalised to the untreated controls was 1.48±0.67. No significant change was observed following induction of maturation (P>0.05) , with the mature cells having a relative level of AMIGO transcript of 1.43±0.45. We also analysed the levels of PLP transcript expression to determine the extent of myelin production (fig 6.9). The mean of the relative normalised PLP mRNA levels could be
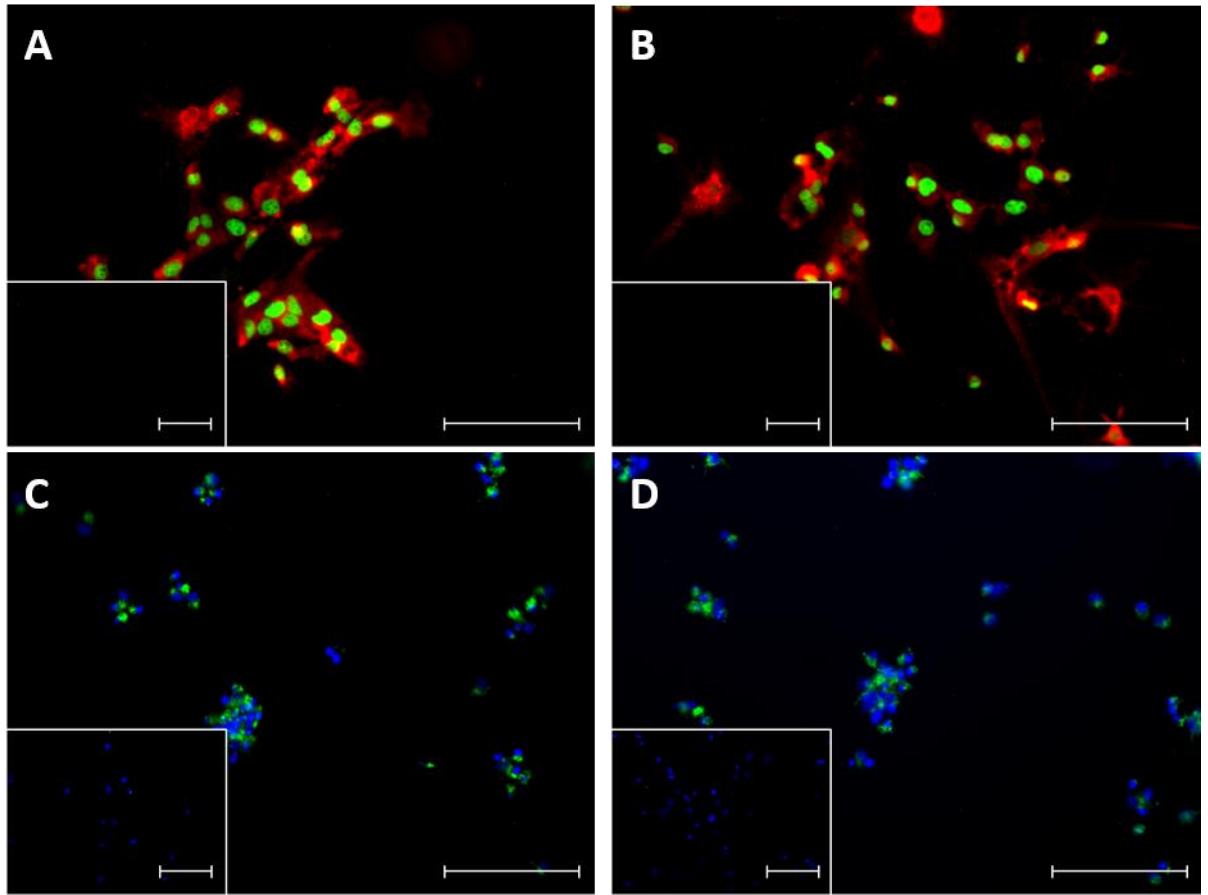
Figure 6.7: Representative CC1/Olig2 (A & B) and NgR1 (C & D) ICC in cultured primary OPC cultured in maturation media for 5 days prior to imaging. (A & B) CC1$^+$ (red) was observed clearly surrounding the majority of Olig2$^+$ (green) nuclei, demonstrating a high proportion of cells having matured. (C & D) samples were counterstained with DAPI (blue). NgR1$^+$ (green) staining was observed in small clusters immediately surrounding DAPI stained nuclei. Scale bars represent 100μm, n=3. Insets show negative controls.
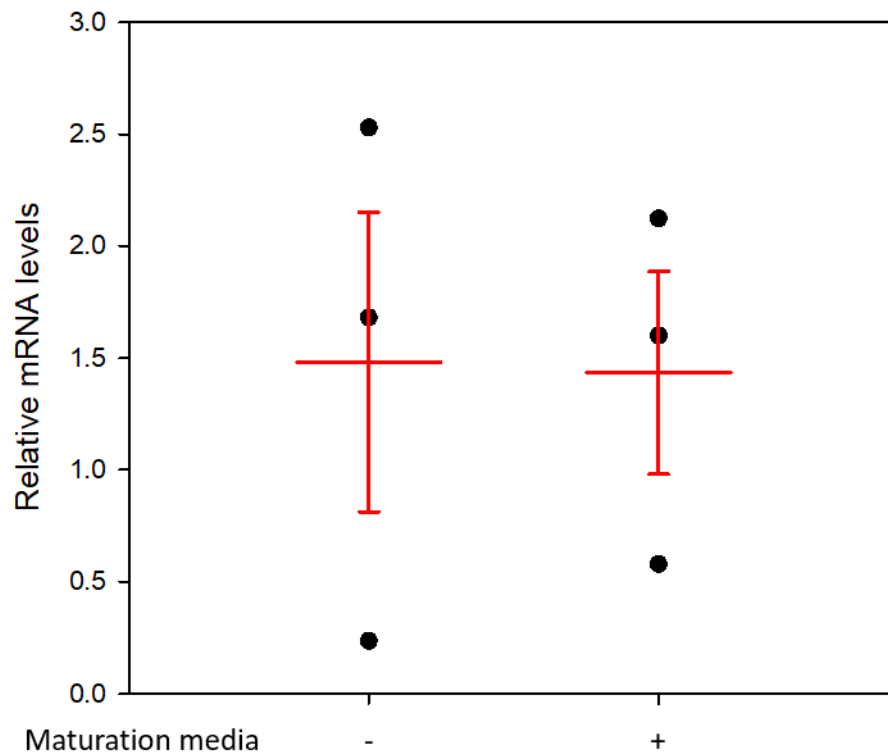
Figure 6.8: RT-qPCR analysis of AMIGO3 mRNA expression in primary OPCs in AMIGO3 maturation studies. Pure OPC cultures were examined for AMIGO3 expression prior to treatment (represented as maturation media negative), and following treatment with maturation media alone. A high variation was observed in AMIGO3 transcript levels, which do not appear to alter between OPC and OL. Error bars represent one SEM, n=3 for each group.
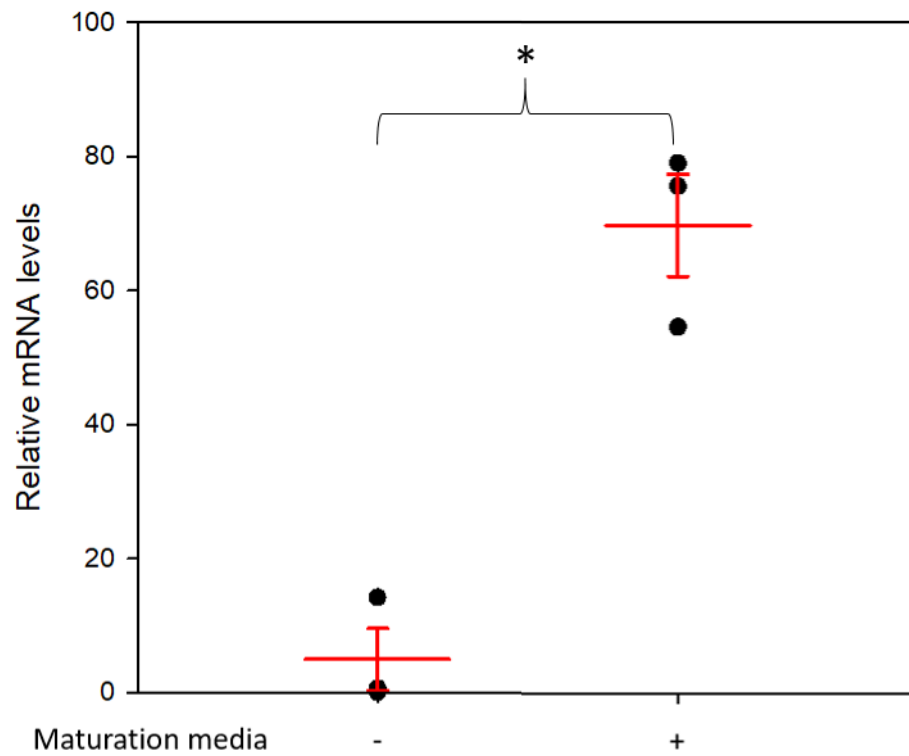
Figure 6.9: RT-qPCR analysis of PLP mRNA expression in primary OPCs in AMIGO3 maturation studies. Pure OPC cultures were examined for PLP expression prior to treatment (represented as maturation media negative), and following treatment with maturation media alone. PLP mRNA is observed to increase following incubation with maturation media. Error bars represent one SEM, n=3 for each group.

seen to significantly increase (P<0.01) over tenfold from 4.94±4.61 to 69.75±7.63

after 5 days of incubation in the differentiation medium.

6.5 Discussion

6.5.1 Characterisation of primary OLGs

Our data shows convincing evidence that the majority of our primary cells are in

fact OPCs. The majority of cells imaged clearly have Olig2^{+} and NG2^{+} staining,

indicating that they are of OLG descent and that they are immature in nature.

Unsurprisingly, there were minimal signs of contamination similar to previous reports

(O'Meara et al., 2011). We did not observe any OX42^{+} staining, demonstrating

negligible infiltration of microglia, and we also did not observe any clear definitive

GFAP[+] staining. The minor GFAP[+] staining that we did observe did not demonstrate

its normal phenotype (Cho and Messing, 2009) and appeared in small clusters that

did not associate with cells. This likely represents a small degree of infiltration, or it

could even represent that the astrocytes were not able to survive in the SATO media,

although as astrocytes are much more adept at surviving than OLG, this would

appear unlikely (Burman et al., 2014). Due to the cells demonstrating clear OPC

markers and there being minimal signs of infiltration of other glial cells, it is very likely

that these primary cultures will be a strong model for looking at AMIGO3 and NgR1

expression in OLG. Additionally, as they are primary cells, they are unlikely to

express additional markers outside of the OLG lineage as can be the case with

immortalized cell lines, such as the MO3.13 cells expressing the astrocytic marker GFAP (McLaurin et al., 1995).

Following characterisation of the OPCs, we encouraged primary OPCs to mature by removing bFGF and PDGF-AA from the media. Following maturation treatment we performed ICC analysis to determine the phenotype of the cells. Firstly we co-stained with Olig2 and CC1 to investigate the numbers of Olig2$^+$ OLG that also expressed the mature OL marker CC1. The vast majority of the Olig2$^+$ cells in the OPC that had received maturation treatment, demonstrated clear CC1$^+$ staining, with a bright stain surrounding the Olig2$^+$ nucleus, very similar to the staining observed *in vivo* in our previous studies (section 3.3.2). Significantly clearer staining was observed for CC1 in the maturation treated cells compared to the primary OPC cultures. Furthermore the vast majority of OLIG2$^+$ cells in the matured cultures demonstrated CC1$^+$ ICC, indicating a high proportion of the cells had successfully matured or were maturing. These observations provide strong evidence that our protocol was effective at producing primary OPCs that rapidly mature following the removal of the mitogenic factors bFGF and PDGF-AA. The only limitation with the protocol was that we tended to generate relatively low overall numbers of cells, therefore it was difficult to perform analyses on large numbers of the samples.

6.5.2   The NgR1 receptor complex in OLG

We imaged primary OPCs and OLs to determine whether NgR1 receptor complex proteins were present. Interestingly the OPCs that we imaged demonstrated a clear sign of NgR1 signal. Furthermore, we also imaged our OPCs for P75, with positive

ICC signal as well. NgR1+ staining in OPCs appeared to generally follow a bipolar distribution, although in some samples NgR1 appeared concentrated in the soma or localised to one side of the cell, based on DAPI+ staining. P75 distribution was more centred around the nucleus. However P75 also displayed a bipolar distribution, albeit less defined. These data clearly show that in mice primary OPCs two of the proteins involved in the tripartite NgR1 receptor complex (Mi et al., 2004; Ahmed et al., 2013) are present. Although this may not be the case with human OPCs, or even rat OPCs, this demonstrates that AMIGO3 and LINGO1 are very likely to be able to able to signal the NgR1 receptor in mouse OPCs.

On top of our evidence of NgR1 and P75 in OPCs, we also demonstrated positive staining for NgR1 in differentiated OLs. However, the distribution did not follow the same pattern as in OPCs. NgR1 appeared in small globules which tended to be in small clumps, rather than spread throughout the soma as with the OPCs. It is possible that NgR1 appears in small collections on the membrane of OLs, however the data also points to a vesicular distribution. This suggests that NgR1 is being internalised and removed from the membrane, although more functional studies would be required to confirm this. Patch clamp analyses involving myelin derived proteins within the pipette internal solution would be interesting to examine whether the NgR1 complex functions similarly on mouse OLGs at different stages, and whether this function is similar to that observed in neurons (Morris et al., 2016; Zabala et al., 2018).

We also imaged our OPCs for AMIGO3 and LINGO1, with positive ICC signal for both proteins. AMIGO3 distribution was irregular and not spread evenly across cells, and LINGO1 was found to be located largely in the nucleus. It has to be highlighted however that neither AMIGO3 nor LINGO1 provided strong signal through ICC, with adjustments of minima and maxima pixel displays required to make the staining visible. It is possible that the antibodies do not show high signal in this model. However, this data also suggest that protein levels of AMIGO3 and LINGO1 were relatively low in our cells. Despite these issues, the data clearly shows that both AMIGO3 and LINGO1 are expressed in our cultured OLGs, demonstrating that all three components of the tripartite NgR1 receptor complex are present and presumably are able to function on mouse OLG.

It would not be surprising to find the functional NgR1 receptor complex on OLG as this would provide a mechanism to prevent excessive myelination from taking place, assuming our hypothesis that AMIGO3 inhibits myelination is correct. It is well established that cues from axons are involved in the regulation of where and how much myelin is produced (Arancibia-Carcamo and Attwell, 2014). Despite this, signalling between OLG is likely to play a role in limiting the amount of myelin being produced, and hence interfering with the nodes of Ranvier. As NgR1 is activated by proteins derived from myelin, it is likely that neighbouring myelinated OLG processes will prevent new unmyelinated processes from binding to axons alongside the already developed myelin sheath. Despite our evidence of NgR1, P75 and

AMIGO3/LINGO1 being present on OLG, specifically in OPCs, we have not analysed the potential functions of these proteins.

6.5.3 AMIGO3 in primary OPC development

We next analysed the levels of AMIGO3 during maturation. Due to the relative low numbers of cells, and therefore low amount of samples we could collect, we decided to analyse the mRNA expression of AMIGO3 before and following maturation treatment. PLP mRNA expression was also analysed as a marker for myelin gene expression. We did not observe any change in the levels of AMIGO3 between D1 (1 day after seeding primary OPCs and prior to maturation treatment) and D6 following the maturation treatment. This indicates that the levels of AMIGO3 transcripts do not alter during the maturation process. This presents an argument against the role for AMIGO3 in inhibiting the differentiation of OPCs. It is possible however that we have taken our observations at the wrong time point to observe this change. As such it would be interesting to observe if a similar trend occurs at earlier time points during the maturation process, rather than at a time point where most of the cells have become CC1^{+}. We would expect to see AMIGO3 levels drop immediately after D1 when the mitogenic factors, PDGF and bFGF, are removed, followed by a rise as the cells reach maturity. Our data may then suggest that AMIGO3 levels rise again after differentiation has occurred.

6.5.4 Limitations

Despite our attempts to reduce variability, there are a number of limitations with this investigation. Firstly, as discussed, our sample sizes were relatively small, as a

result of time and financial constraints. Repeats with larger sample sizes would help to provide a greater confidence with our results. It has to be noted that in our primary OPC studies, we were only able to maintain a sample size of 3 for each treatment group due to time constraints and limitations in the numbers of samples that we could obtain from one litter. To ensure that samples received the same treatment, studies were conducted with the cells grown from one litter of pups, therefore the number of cells and samples we received was directly correlated with the litter size. Ideally, we we would maintain a larger breeding colony and ensure a larger supply of pups however this was not possible for this study.

Furthermore, in regards to our ICC study, we have not provided quantitative results. Cell counts should be performed to provide quantitation of the findings in this chapter. It would be interesting to examine the expression of our proteins of interest cells whilst co-staining for cell specific markers, such as CC1 and NG2.

6.5.5   Further studies

As we have determined that NgR1 is in fact present on mice OLG, it would now be interesting to determine whether AMIGO3 and LINGO1 are able to interact with the receptor complex and whether this will produce the characteristic RhoA responses in OLG cells. This could be analysed through Co-IP with AMIGO3/LINGO1 and NgR1/P75/TROY. A RhoA G-LISA assay would also be beneficial to determine the response of inhibiting AMIGO3 in cultured OLG to determine whether the traditional RhoA signalling pathway is active in these cells.

Another interesting point is that we have discussed previously is that AMIGO3 is both a heterodimer and homodimer. Although AMIGO3 levels do not appear to alter much within our cells during the maturation phase, it is possible that levels alter on neighbouring glia or neurons. In addition, a more detailed time course examining the expression of AMIGO3 mRNA should be conducted during and following the initiation of OPC differentiation.

Finally, we have only examined the levels of AMIGO3 in during injury treatments (Chapter 4), or whilst encouraging primary OPCs to mature. As levels of AMIGO3 have been shown to rise following trauma, it would be interesting to examine how levels of AMIGO3 alter following trauma induced during the differentiation process. It would be interesting to examine how trauma affects the primary OPCs ability to differentiate. It is possible that AMIGO3 has relatively minor relevance in the healthy model, but becomes more significant in a disease/injury state. As such, OPCs encouraged to mature following trauma could potentially have altered AMIGO3 expression which could affect their ability to mature.

6.5.6   Conclusions

From this study, we can conclude that NgR1 and P75 are expressed on mouse primary OLGs, and that in OPCs, the NgR1 receptor complex is likely to be functional. In addition this work confirms that AMIGO3 is expressed by mouse OPC, and that LINGO1 appears to exhibit a nuclear localisation in these cells. Finally AMIGO3 levels did not alter during OPC differentiation although a finer temporal analysis is required to confirm these findings.

Chapter 7

General discussion

7.1 General conclusions

7.1.1 AMIGO3 in models of myelination

The purpose of this study was to determine the role of AMIGO3 in remyelination. As such, we examined the expression profile of AMIGO3 in models of myelination and remyelination. Namely, we examined the expression profile of AMIGO3 in the neocortex during postnatal development, following the stages of myelination, as well as in demyelinating disease models and *in vitro* cell cultures.

Our data suggests that in both developmental stages of myelination and in EAE, that AMIGO3 is upregulated. Specifically in development, this upregulation of AMIGO3 drops immediately prior to the production of MBP, whereas our EAE model did not show clinical improvements whilst AMIGO3 protein levels remained raised. Although it should be highlighted that we were unable to quantify AMIGO3 in OPCs alone, these data provide a strong correlation between AMIGO3 expression and a reduced sign of OPC maturation and myelin production.

Counter to our hypothesis, AMIGO3 levels did not change between primary OPCs and primary OPCs following maturation treatment. This suggests that AMIGO3 has no role in the maturation process, at least in this model as signs of maturation were observed. Furthermore, we observed a decrease in PLP mRNA when AMIGO3 was knocked down. This provides evidence of AMIGO3 actually playing a positive role in, at least, myelination and potentially maturation of OPCs. This particular experiment had a number of limitations in that we had a limited sample size which prevented

242

some of the control groups, most notably a sham treatment group, and that we did not observe a significant reduction in AMIGO3 transcript following KD treatment, therefore the data can only be deemed preliminary. If AMIGO3 actually promotes OPC maturation, then it is difficult to explain the increased expression prior to developmental maturation. This concept would also put it at odds with data from LINGO1 studies which demonstrate an inhibitory effect considering the similar mechanisms of action observed between the two analogous proteins (Chen et al., 2006; Sun et al., 2015; Zhang et al., 2015a). This is further highlighted by the presence of the NgR1 receptor on our primary OPCs which both AMIGO3 and LINGO1 are known to be able to interact with and aid with activation of the NgR1 receptor complex (Mi et al., 2004; Ahmed et al., 2013).

Furthermore, it is interesting to note that AMIGO3 levels were not increased in our acute stage optic neuritis model. We did however fail to observe any sign of demyelination when MBP was imaged by IHC. This suggests that this model, despite showing some clinical signs of disease progression, caused a limited response within the CNS. As discussed (section 5.5.1), it is possible that our model was too mild to induce significant damage to the CNS, and thus AMIGO3 may require a more significant input to induce a response.

7.1.2 The role of LRRs in trauma models

Our data does highlight the link between EAE disease progression and OPC excitotoxicity. Excitotoxicity has been well documented in regards to neurons in EAE but limited work has been done in regards to excitotoxicity to OLG in EAE (Mehta et

243

al., 2013). Interestingly, it is known that OPCs are able to respond to glutamate, one of the main signalling proteins involved with excitotoxicity, and excessive glutamate binding induces signalling which leads to apoptosis of the cell (Sanchez-Gomez et al., 2011; Begum et al., 2018). Despite this, there is still a need to examine the effects of this excitotoxicity in regards to demyelinating diseases. Our data showing that AMIGO3 is upregulated following AMPA-CTZ induced excitotoxicity could pose a potential pathway which affects OPC behaviour following this trauma. This is hypothesised to pathologically inhibit effective maturation of the affected OPCs. As excitotoxicity is linked with a number of neurodegenerative disorders including spinal cord injury, stroke and Alzheimer's disease, as well as MS and numerous others, our data highlights the potential damage and obstruction to OPC maturation that may be accompanying these diseases (Mehta et al., 2013). Our data also suggests that neuronal damage may be essential to induce the release of glutamate which in turn inhibits OPC differentiation (Pal, 2018).

It is unclear whether our primary OPCs can be deemed a traumatic model or not as the cells have been dissected, which in itself is trauma. Despite this, the extended period of culturing is likely to return the OPCs to a resting state and prevent activation of trauma induced pathways. Conversely, the procedure of shaking the cells to relieve the OPCs from mixed glial cultures could induce some degree of trauma. Despite these arguments, it appears that the primary culture model is not a model of trauma, and therefore the cells have not received the potentially necessary cues to promote AMIGO3 expression.

Finally, in terms of excitotoxic trauma, we observed that LINGO1 protein levels actually went down in the acute following 5hrs treatment. This further demonstrates that AMIGO3 appears to be more prevalent in the early stages of disease, matching previous reports following spinal cord injury (Ahmed et al., 2013).

We believe that these studies show that AMIGO3 is upregulated preferentially to LINGO1 following CNS and OPC trauma, potentially largely in the form of excitotoxicity. It is not until significant injury that AMIGO3 is upregulated in OPC. We suggest that this trauma induced upregulation of AMIGO3 then inhibits OPC development, whether directly or intercellularly between local neurons, OPC and other glia, resulting in the pathogenic inhibition of remyelination in demyelinating diseases. Furthermore, it appears that AMIGO3 plays a role in early stages of development, which we believe inhibits OPC maturation. At the onset of developmental myelination, AMIGO3 expression is reduced and does not play a role in OPC inhibition until significant injury has occurred. Our theory appears to have similarities with a recent theory that normal developmental regulators of myelination, such as PSA-NCAM, are re-expressed following trauma on stressed axons which repel and inhibit local OPCs (Podbielska et al., 2013).

7.1.3   AMIGO3 mechanism of action in OLG

There is yet to be any data demonstrating how AMIGO3 is able to signal within OLG. As discussed however, AMIGO3 has been previously shown to function via the NgR1 receptor complex in DRGNs as well as transfected COS7 cells containing all the machinery for the receptor complex (Ahmed et al., 2013). As such, our data

which demonstrated NgR1 and P75 protein expression in OPCs, two proteins involved with the NgR1 complex, as well as NgR1 in OLs present a possible mechanism. It was also interesting to note that NgR1 appeared to be internalised in the mature cells, presenting evidence that the receptor is no longer functional, or that it has a reduced function in mature cells. The receptor complex may still have a function whilst internalised, however our observations indicate that it would no longer be able to interact and therefore signal from interactions on the external surface of the cell.

7.1.4 AMIGO3 in multiple sclerosis

One of the interesting results from this study is the evidence that AMIGO3 protein levels actually appear to reduce, although not significantly, in MS lesion plaques and in the healthy white matter of MS patients. These data do however suggest that AMIGO3 may not be being expressed in the human disease, at least in the brain. Alternatively, it is still possible that levels of AMIGO3 would have been high in early stages of plaque formation, however due to the samples being post-mortem, we were only able to analyse healthy white matter or developed plaques. It should be noted that these samples were collected post-mortem and therefore there is a chance, albeit rather slim, that cell death and proteins degradation will have occurred prior to our analysis.

7.2 Limitations and further studies

7.2.1 Models of myelination

We used a number of models to examine myelination and remyelination however these models all had their limitations. Firstly, with our EAE models, we were only able to examine AMIGO3 expression before and after significant disease progression. As we hypothesised that AMIGO3 is likely to act in the acute stages of disease, we wanted to develop early stages models, however our attempts appeared to result in very mild induction of disease and were accompanied by minimal signs of demyelination. It would have been interesting to examine the levels of AMIGO3 throughout EAE progression when recovery was present. For example, as we observed AMIGO3 levels rise and then drop immediately before developmental myelination, it would be interesting to see if a similar pattern is observed in the remyelination stage after EAE induced demyelination. This was similarly the case with our OPC cultures, as by D6 when we analysed the levels of AMIGO3, cells were already demonstrating substantial CC1 expression, indicating their maturation. As O4 is arguably a marker of pro-OLs, it would have been interesting to observe levels of AMIGO3 in correlation with O4 expression (Baccarini M et al., 2008; Neman J and de Vellis J, 2008).

Due to our results appearing preliminary with our knock down studies, it would be essential to repeat these experiments to back up our results. Additionally, it would be interesting if the reduction in PLP transcript translates to a reduction in PLP and other

signs of myelination. Examining the production of myelin-sheets, an *in vitro* sign of myelin production through O4+ staining would be one example of how to examine the early stages of myelin production (Mi et al., 2005).

Another potential model would be to develop co-cultures with neurons, to examine OPC ensheathment in relation to AMIGO3 expression. This would allow a quick and effective model for examining remyelination *in vitro*. DRGN would be the most effective neurons for these models due to the low degree of contaminants associated with their dissection and culturing (O'Meara et al., 2011).

7.2.2   OPC trauma and AMIGO3 expression

One of the interesting conclusions from this study was the observation that AMIGO3 proteins levels are raised in EAE and that this matches a similar raise observed in excitotoxicity induced trauma to Oli-neu. Despite the clear rise in AMIGO3 protein expression in Oli-neu following excitotoxicity, AMIGO3 protein was not raised in our LPC model of OPC trauma. This shows that AMIGO3 is only upregulated due to specific traumatic events and signalling pathways. As EAE, and MS, are multi-factorial, questions arise to which forms of cell trauma are required to activate the expression of AMIGO3 *in vivo*. As such, further studies would be valuable to determine which forms of trauma induce AMIGO3 expression and why AMIGO3 is not upregulated in LPC induced OPC trauma. This could lead to interesting studies determining the pathways through which AMIGO3 expression is upregulated and provide us with a greater insight in to when AMIGO3 therapies would be beneficial.

248

7.2.3   Functional AMIGO3 studies

Although we have observed correlations between AMIGO3 transcript and protein expression in varying models of myelination and remyelination, we have failed to develop an effective causative study. Knock down or constitutively active studies of AMIGO3 expression *in vivo* would be instrumental in understanding the role of AMIGO3 in myelination and remyelination. For example, comparing the effects of altered AMIGO3 expression on the rate of myelination/MBP production in development, or on the ability of primary OPC cultures to differentiate. This would also be fascinating with our trauma models to definitively link the altered AMIGO3 expression profiles that we observed, to direct cellular responses.

The most effective and translational in terms of demyelination would have been to analyse the effects of the development of EAE when AMIGO3 levels have been altered or the protein has been inhibited. This could have been done again through genetic editing or similarly to LINGO1 studies, through developing an effective inhibitor for AMIGO3, presumably in the form of an anti-AMIGO3 antibody therapy. An inhibitor could be administered in disease models which would allow for direct comparisons to the human demyelinating diseases. As demyelination in MS and EAE is associated with breakdown of the BBB and AMIGO3 in CNS enriched (Kuja-Panula et al., 2003; Chen et al., 2006; Bennett et al., 2010), antibody therapies would be effective for localised CNS treatment. Additionally, as we expect AMIGO3 to be only expressed at low levels away from the sites of trauma, there is likely to be minimal side effects in healthy tissue associated with AMIGO3 inhibitors.

As we have discussed briefly before, it is possible that AMIGO3 is able to interact with itself or with NgR1 receptor complex proteins intercellularly in a similar way as that proposed for LINGO1 (Jepson et al., 2012). This could be investigated through incubation with soluble AMIGO3 with OPC cultures, as well as through altering expression profiles of AMIGO3 in co-cultures systems, for example knocking down AMIGO3 expression in DRGNs and using the KD neurons in co-cultures with our primary OPCs.

As we have identified NgR1 as a potential mechanism through which AMIGO3 signalling could occur in OPCs, it would be vital to determine whether this signalling results in the same characteristic RhoA activation observed in neurons (Mi et al., 2004; Ahmed et al., 2013). Furthermore, it would be interesting to investigate if there is any preferential binding for AMIGO3 or LINGO1 with the NgR1 complex, which could be easily tested through co-immunoprecipitation studies.

7.2.4 Translation to human demyelinating diseases

One of the major limitations with our studies is the use of murine OPCs and EAE to model remyelination in disease. Although EAE shares a number of similarities to MS, the majority of successful EAE designed therapies have proven to be ineffective as treatments for MS, most notably the results of the LINGO1 clinical trials for optic neuritis (Cadavid et al., 2017). Clearly, there must be significant variation between the model and the human disease. As we are purely examining the remyelination process, it could be argued that this is less relevant compared to inflammation and immune response research, however it still needs to be considered that more

translational models would be beneficial to determine that any responses that we observed are clinically relevant. As EAE has been developed in primates, this demonstrates a valuable further step in regards to developing AMIGO3 therapies (Slierendregt et al., 1995; Baker and Amor, 2014), however stronger data of the functional role for AMIGO3 is essential before progressing to these higher models of EAE.

A final point that has to be acknowledged with our studies is whether remyelination will be effective. Remyelination is known to produce thinner myelin sheaths than those prior to demyelination, raising the question as to how effective the new myelin sheaths can be (Duncan et al., 2017). Despite this limitation, encouraging remyelination will clearly provide some benefit in the form of axonal protection and restoration of saltatory conduction, therefore further investigations into the role of AMIGO3 in remyelination, and specifically following trauma induced demyelination, could be vital in developing effective treatments for demyelinating diseases.

7.3   Final conclusions

From our data, it is clear that AMIGO3 is expressed in OLG, and specifically in OPCs. We have shown that AMIGO3 levels are relatively low and do not become apparent until trauma has been received to the CNS, with AMIGO3 protein rising in both whole CNS extracts and in specifically in OPCs. The NgR1 receptor complex is shown to be present on mouse OPCs highlighting that AMIGO3 and LINGO1 would be able to function through this signalling pathway. It still is yet to be determined what

the direct effects of AMIGO3 expression are in both OPCs and demyelinating diseases, however our data raises AMIGO3 as a promising potential future therapeutic for treating demyelinating disorders. Further work is essential to determine the functional role for AMIGO3 following trauma and in EAE.

References

Abbaszadeh HA, Tiraihi T, Delshad A, Saghedizadeh M, Taheri T, Kazemi H, Hassoun HK (2014) Differentiation of neurosphere-derived rat neural stem cells into oligodendrocyte-like cells by repressing PDGF-alpha and Olig2 with triiodothyronine. Tissue Cell 46:462-469.

Aggarwal S, Yurlova L, Simons M (2011) Central nervous system myelin: structure, synthesis and assembly. Trends Cell Biol 21:585-593.

Ahmed Z, Douglas M, John G, Berry M, Logan A (2013) AMIGO3 Is an NgR1/p75 co-receptor signalling axon growth inhibition in the acute phase of adult central nervous system injury. PLOS ONE 8:e61878.

Ahmed Z, Dent R, Suggate E, Barrett L, Seabright R, Berry M, Logan A (2005) Disinhibition of neurotrophin-induced dorsal root ganglion cell neurite outgrowth on CNS myelin by siRNA-mediated knockdown of NgR, p75NTR and Rho-A. Molecular and Cellular Neuroscience 28:509-523.

Al-Izki S, Pryce G, O'Neill JK, Butter C, Giovannoni G, Amor S, Baker D (2012) Practical guide to the induction of relapsing progressive experimental autoimmune encephalomyelitis in the Biozzi ABH mouse. Mult Scler Relat Disord 1:29-38.

Alberdi E, Sánchez-Gómez M, Torre I, Domercq M, Pérez-Samartín A, Pérez-Cerdá F, Matute C (2006) Activation of Kainate Receptors Sensitizes Oligodendrocytes to Complement Attack. The Journal of Neuroscience 26:3220-3228.

Alharbi FM (2015) Update in vitamin D and multiple sclerosis. Neurosciences (Riyadh) 20:329-335.

Alizadeh A, Dyck SM, Karimi-Abdolrezaee S (2015) Myelin damage and repair in pathologic CNS: challenges and prospects. Front Mol Neurosci 8:35.

Alrehaili AA, Lee JY, Bakhuraysah MM, Kim MJ, Aui PM, Magee KA, Petratos S (2018) Nogo receptor expression in microglia/macrophages during experimental autoimmune encephalomyelitis progression. Neural Regen Res 13:896-907.

Anastasiadis P, Moon S, Thoreson M, Mariner D, Crawford H, Zheng Y, Reynolds A (2000) Inhibition of RhoA by p120 catenin. Nature Cell Biology 2:637-644.

Aranami T, Yamamura T (2008) Th17 Cells and autoimmune encephalomyelitis (EAE/MS). Allergol Int 57:115-120.

Arancibia-Carcamo IL, Attwell D (2014) The node of Ranvier in CNS pathology. Acta Neuropathol 128:161-175.

Baccarini M, Catalanotti F, Galabova-Kovacs G, Herbst R, Matzen D, Reyes G, Silva A, I W, Zezula J (2008) Essential role of B-Raf in oligodendrocyte maturation and myelination during postnatal central nervous system development. The Journal of Cell Biology 180.

Back SA, Luo NL, Borenstein NS, Levine JM, Volpe JJ, Kinney HC (2001) Late oligodendrocyte progenitors coincide with the developmental window of vulnerability for human perinatal white matter injury. J Neurosci 21:1302-1312.

Baker D, Amor S (2014) Experimental autoimmune encephalomyelitis is a good model of multiple sclerosis if used wisely. Mult Scler Relat Disord 3:555-564.

Baker D, Amor S (2015) Mouse models of multiple sclerosis: lost in translation? Curr Pharm Des 21:2440-2452.

Baker D, Gerritsen W, Rundle J, Amor S (2011) Critical appraisal of animal models of multiple sclerosis. Mult Scler 17:647-657.

Bakiri Y, Karadottir R, Cossell L, Attwell D (2011) Morphological and electrical properties of oligodendrocytes in the white matter of the corpus callosum and cerebellum. J Physiol 589:559-573.

Barnett MH, Prineas JW (2004) Relapsing and remitting multiple sclerosis: pathology of the newly forming lesion. Ann Neurol 55:458-468.

Baumann N, Pham-Dinh D (2001) Biology of oligodendrocyte and myelin in the mammalian central nervous system. Physiological Reviews 81:871-927.

Bear M, Connors B, Paradiso M (2007) Neuroscience: Exploring the brain, 3 Edition. USA: Lippincott Williams & Wilkins.

Begum G, Otsu M, Ahmed U, Ahmed Z, Stevens A, Fulton D (2018) NF-Y-dependent regulation of glutamate receptor 4 expression and cell survival in cells of the oligodendrocyte lineage. Glia.

Belin S, Zuloaga KL, Poitelon Y (2017) Influence of Mechanical Stimuli on Schwann Cell Biology. Front Cell Neurosci 11:347.

Bella J, Hindle K, McEwan P, Lovell S (2008) The leucine-rich repeat structure. Cellular and Molecular Life Sciences 65:2307-2333.

Bennett J, Basivireddy J, Kollar A, Biron KE, Reickmann P, Jefferies WA, McQuaid S (2010) Blood-brain barrier disruption and enhanced vascular permeability in the multiple sclerosis model EAE. J Neuroimmunol 229:180-191.

Bercury K, Macklin W (2015) Dynamics and Mechanisms of CNS Myelination. Developmental Cell 32:447-458.

Berg CT, Khorooshi R, Asgari N, Owens T (2017) Influence of type I IFN signaling on anti-MOG antibody-mediated demyelination. J Neuroinflammation 14:127.

Berger T, Schnitzer J, Kettenmann H (1991) Developmental changes in the membrane current pattern, K^+ buffer capacity, and morphology of glial cells in the corpus callosum slice. The Journal of Neuroscience 11:3008-3024.

Bergles DE, Richardson WD (2015) Oligodendrocyte Development and Plasticity. Cold Spring Harb Perspect Biol 8:a020453.

Beurel E, Kaidanovich-Beilin O, Yeh WI, Song L, Palomo V, Michalek SM, Woodgett JR, Harrington LE, Eldar-Finkelman H, Martinez A, Jope RS (2013) Regulation of Th1 cells and experimental autoimmune encephalomyelitis by glycogen synthase kinase-3. J Immunol 190:5000-5011.

Bhat R, Steinman L (2009) Innate and adaptive autoimmunity directed to the central nervous system. Neuron 64:123-132.

Bhatheja K, Field J (2006) Schwann cells: origins and role in axonal maintenance and regeneration. Int J Biochem Cell Biol 38:1995-1999.

Biancardi A, Biver T, Secco F, Mennucci B (2013) An investigation of the photophysical properties of minor groove bound and intercalated DAPI through quantum-mechanical and spectroscopic tools. Phys Chem Chem Phys 15:4596-4603.

Bittner S, Afzali AM, Wiendl H, Meuth SG (2014) Myelin oligodendrocyte glycoprotein (MOG35-55) induced experimental autoimmune encephalomyelitis (EAE) in C57BL/6 mice. J Vis Exp.

Bjartmar C, Hildebrand C, Loinder K (1994) Morphological heterogeneity of rat oligodendrocytes: electron microscopic studies on serial sections. Glia 11:235-244.

Blakemore WF (1974) Remyelination of the superior cerebellar peduncle in old mice following demyelination induced by cuprizone. J Neurol Sci 22:121-126.

Blakemore WF, Keirstead HS (1999) The origin of remyelinating cells in the central nervous system. J Neuroimmunol 98:69-76.

Boeschoten RE, Braamse AMJ, Beekman ATF, Cuijpers P, van Oppen P, Dekker J, Uitdehaag BMJ (2017) Prevalence of depression and anxiety in Multiple Sclerosis: A systematic review and meta-analysis. J Neurol Sci 372:331-341.

Bourikas D, Mir A, Walmsley A (2010) LINGO-1-mediated inhibition of oligodendrocyte differentiation does not require the leucine-rich repeats and is reversed by p75(NTR) antagonists. Molecular and Cellular Neuroscience 45:363-369.

Boyd A, Zhang H, Williams A (2013) Insufficient OPC migration into demyelinated lesions is a cause of poor remyelination in MS and mouse models. Acta Neuropathol 125:841-859.

Bradl M, Lassmann H (2010) Oligodendrocytes: biology and pathology. Acta Neuropathol 119:37-53.

Brisard G, Rusling J (2007) New Bioanalytical and Biomedical Methods: The Electrochemical Society.

Brosamle C, Halpern ME (2002) Characterization of myelination in the developing zebrafish. Glia 39:47-57.

Brown TL, Verden DR (2017) Cytoskeletal Regulation of Oligodendrocyte Differentiation and Myelination. J Neurosci 37:7797-7799.

Brück W (2005) Inflammatory demyelination is not central to the pathogenesis of multiple sclerosis. Journal of Neurology 252:V/10-V/15.

Burman J, Zetterberg H, Fransson M, Loskog AS, Raininko R, Fagius J (2014) Assessing tissue damage in multiple sclerosis: a biomarker approach. Acta Neurol Scand 130:81-89.

Burry R (2011) Controls for immunocytochemistry. Journal of Histochemistry and Cytochemistry 59:6-12.

Buzby J, Chen G, Chen H, He L, Qian L (2010) Curcumin protects pre-oligodendrocytes from activated microglia in vitro and in vivo. Brain Research 1339:60-69.

Cadavid D, Balcer L, Galetta S, Aktas O, Ziemssen T, Vanopdenbosch L, Frederiksen J, Skeen M, Jaffe GJ, Butzkueven H, Ziemssen F, Massacesi L, Chai Y, Xu L, Freeman S, Investigators RS (2017) Safety and efficacy of opicinumab in acute optic neuritis (RENEW): a randomised, placebo-controlled, phase 2 trial. Lancet Neurol 16:189-199.

Cai J, Chen Y, Cai W, Hurlock E, Wu H, Kernie S, Parada L, Lu Q (2007) A crucial role for Olig2 in white matter astrocyte development. Development 134:1887-1899.

Calabrese E, Johnson GA (2013) Diffusion tensor magnetic resonance histology reveals microstructural changes in the developing rat brain. Neuroimage 79:329-339.

Cao Q, He Q, Wang Y, Cheng X, Howard R, Zhang Y, DeVries W, Shields C, Magnuson D, Xu X, Kim D, Whittemore S (2010) Transplantation of CNTF-expressing adult oligodendrocyte precursor cells promotes remyelination and functional recovery after spinal cord injury. The Journal of Neuroscience 30:2989-3001.

Carroll SL (2017) The Molecular and Morphologic Structures That Make Saltatory Conduction Possible in Peripheral Nerve. J Neuropathol Exp Neurol 76:255-257.

Castro-Borrero W, Graves D, Frohman TC, Flores AB, Hardeman P, Logan D, Orchard M, Greenberg B, Frohman EM (2012) Current and emerging therapies in multiple sclerosis: a systematic review. Ther Adv Neurol Disord 5:205-220.

Chan C, Liu X, Zhao L, Liu G, Lee C, Feng Y, Ye K (2013) PIKE is essential for oligodendroglia development and CNS myelination. Proceedings of the National Academy of Sciences of the United States of America 111:1993-1998.

Chan JK (2014) The wonderful colors of the hematoxylin-eosin stain in diagnostic surgical pathology. Int J Surg Pathol 22:12-32.

Chang A, Tourtellotte WW, Rudick R, Trapp BD (2002) Premyelinating oligodendrocytes in chronic lesions of multiple sclerosis. N Engl J Med 346:165-173.

Chauhan D, Egea J (2014) Analysis of the Expression Pattern of Transmembrane proteins with extracellular leucine rich repeats (eLRRs) in the developing nervous system. In: Molecular and Developmental Neurobiology: Universitat de Lleida.

Chen H, Kintner DB, Jones M, Matsuda T, Baba A, Kiedrowski L, Sun D (2007) AMPA-mediated excitotoxicity in oligodendrocytes: role for Na(+)-K(+)-Cl(-) co-transport and reversal of Na(+)/Ca(2+) exchanger. J Neurochem 102:1783-1795.

Chen J, Zuo S, Wang J, Huang J, Zhang X, Liu Y, Zhang Y, Zhao J, Han J, Xiong L, Shi M, Liu Z (2014) Aspirin promotes oligodendrocyte precursor cell proliferation and differentiation after white matter lesion. Front Aging Neurosci 6:7.

Chen Y, Aulia S, Li L, Tang B (2006) AMIGO and friends: An emerging family of brain-enriched, neuronal growth modulating, type I transmembrane proteins with leucine-rich repeats (LRR) and cell adhesion molecule motifs. Brain Research Reviews 51:265-274.

Cho W, Messing A (2009) Properties of astrocytes cultured from GFAP over-expressing and GFAP mutant mice. Exp Cell Res 315:1260-1272.

Chrast R, Saher G, Nave KA, Verheijen MH (2011) Lipid metabolism in myelinating glial cells: lessons from human inherited disorders and mouse models. J Lipid Res 52:419-434.

Clarke L, Young K, Hamilton N, Li H, Richardson W, Attwell D (2012) Properties and fate of oligodendrocyte progenitor cells in the corpus callosum, motor cortex, and piriform cortex of the adult mouse. The Jounal of Neuroscience 32:8173-8185.

Compston A, Coles A (2008) Multiple sclerosis. Lancet 372:1502-1517.

Constantinescu CS, Farooqi N, O'Brien K, Gran B (2011) Experimental autoimmune encephalomyelitis (EAE) as a model for multiple sclerosis (MS). Br J Pharmacol 164:1079-1106.

Correale J, Farez MF (2015) The Role of Astrocytes in Multiple Sclerosis Progression. Front Neurol 6:180.

Cover KS, Vrenken H, Geurts JJ, van Oosten BW, Jelles B, Polman CH, Stam CJ, van Dijk BW (2006) Multiple sclerosis patients show a highly significant decrease in alpha band interhemispheric synchronization measured using MEG. Neuroimage 29:783-788.

Crawford AH, Tripathi RB, Foerster S, McKenzie I, Kougioumtzidou E, Grist M, Richardson WD, Franklin RJ (2016) Pre-Existing Mature Oligodendrocytes Do Not Contribute to Remyelination following Toxin-Induced Spinal Cord Demyelination. Am J Pathol 186:511-516.

Crocker SJ, Whitmire JK, Frausto RF, Chertboonmuang P, Soloway PD, Whitton JL, Campbell IL (2006) Persistent macrophage/microglial activation and myelin disruption after experimental autoimmune encephalomyelitis in tissue inhibitor of metalloproteinase-1-deficient mice. Am J Pathol 169:2104-2116.

Croxford AL, Kurschus FC, Waisman A (2011) Mouse models for multiple sclerosis: historical facts and future implications. Biochim Biophys Acta 1812:177-183.

Dai J, Bercury K, Ahrendsen J, Macklin W (2015) Olig1 function is required for oligodendrocyte differentiation in the mouse brain. The Journal of Neuroscience 35:4386-4402.

de Wit J, Ghosh A (2014) Control of neural circuit formation by leucine-rich repeat proteins. Trends Neurosci 37:539-550.

de Wit J, Hong W, Luo L, Ghosh A (2011) Role of leucine-rich repeat proteins in the development and function of neural circuits. Cell and Development Biology 27:697-729.

Denic A, Johnson AJ, Bieber AJ, Warrington AE, Rodriguez M, Pirko I (2011) The relevance of animal models in multiple sclerosis research. Pathophysiology 18:21-29.

Dickendesher T, Baldwin K, Mironova Y, Koriyama Y, Raiker S, Askew K, Wood A, Geoffroy C, Zheng B, Liepmann C, Katagiri Y, Benowitz L, Geller H, Giger R (2012) NgR1 and NgR3 are receptors for chondroitin sulfate proteoglycans. Nature Neuroscience 15:703-712.

Dienstmann R, Rodon J, Serra V, Tabernero J (2014) Picking the point of inhibition: a comparative review of PI3K/AKT/mTOR pathway inhibitors. Mol Cancer Ther 13:1021-1031.

DiLuca M, Olesen J (2014) The cost of brain diseases: a burden or a challenge? Neuron 82:1205-1208.

Dong Z, Brennan A, Liu N, Yarden Y, Lefkowitz G, Mirsky R, Jessen KR (1995) Neu differentiation factor is a neuron-glia signal and regulates survival, proliferation, and maturation of rat Schwann cell precursors. Neuron 15:585-596.

Duncan ID, Marik RL, Broman AT, Heidari M (2017) Thin myelin sheaths as the hallmark of remyelination persist over time and preserve axon function. Proc Natl Acad Sci U S A 114:E9685-E9691.

Eisenstein BI (1990) The Polymerase Chain-Reaction - a New Method of Using Molecular-Genetics for Medical Diagnosis. New Engl J Med 322:178-183.

Elyaman W, Kivisakk P, Reddy J, Chitnis T, Raddassi K, Imitola J, Bradshaw E, Kuchroo VK, Yagita H, Sayegh MH, Khoury SJ (2008) Distinct functions of autoreactive memory and effector CD4+ T cells in experimental autoimmune encephalomyelitis. Am J Pathol 173:411-422.

Fancy S, Zhao C, Franklin R (2004) Increased expression of Nkx2.2 and Olig2 identifies reactive oligodendrocyte progenitors cells responding to demyelination in the adult CNS. Molecular and Cellular Neuroscience 27:247-254.

Fancy SP, Kotter MR, Harrington EP, Huang JK, Zhao C, Rowitch DH, Franklin RJ (2010) Overcoming remyelination failure in multiple sclerosis and other myelin disorders. Exp Neurol 225:18-23.

Fannon J, Wysnavie T, Fulton D (2015) Neuronal activity and AMPA-type glutamate receptor activation regulates the morphological development of oligodendrocyte precursor cells. Glia 63:1021-1035.

Fields D (2014) Myelin-More than Insulation. Science 344:264-266.

Fitch MT, Silver J (2008) CNS injury, glial scars, and inflammation: Inhibitory extracellular matrices and regeneration failure. Exp Neurol 209:294-301.

Flores AI, Narayanan SP, Morse EN, Shick HE, Yin X, Kidd G, Avila RL, Kirschner DA, Macklin WB (2008) Constitutively active Akt induces enhanced myelination in the CNS. J Neurosci 28:7174-7183.

Foale S, Fulton D, Ahmed Z (2014) A role of AMIGO3 and related proteins in remyelination: An insight into multiple sclerosis pathology. In: Neurobiology Section, School of Clinical and Exprimental Medicine, p 6: University of Birmingham.

Foale S, Fulton D, Ahmed Z (2015) Characterising the role of amphoterin induced gene and open reading frame 3 (AMIGO3) in the pathogenesis of, and treatment for multiple sclerosis. In: Neuropharmacology and Neurobiology. Birmingham: University of Birmingham.

Foale S, Berry M, Logan A, Fulton D, Ahmed Z (2017) LINGO-1 and AMIGO3, potential therapeutic targets for neurological and dysmyelinating disorders? Neural Regen Res 12:1247-1251.

Foote AK, Blakemore WF (2005) Inflammation stimulates remyelination in areas of chronic demyelination. Brain 128:528-539.

Franklin R, Ffrench-Constant C (2008) Remyelination in the CNS: from biology to therapy. Nature Reviews Neuroscience 9:839-855.

Freeman SA, Desmazieres A, Fricker D, Lubetzki C, Sol-Foulon N (2016) Mechanisms of sodium channel clustering and its influence on axonal impulse conduction. Cell Mol Life Sci 73:723-735.

Fressinaud C, Vallat JM, Pouplard-Barthelaix A (1996) Platelet-derived growth factor partly prevents chemically induced oligodendrocyte death and improves myelin-like membranes repair in vitro. Glia 16:40-50.

Frühbeis C, Fröhlich D, Kuo W, Amphornrat J, Thilemann S, Saab A, Kirchhoff F, Möbius W, Goebbels S, Nave K, Schneider A, Simons M, Klugmann M, Trotter J, Krämer-Albers E (2013) Neurotransmitter-triggered transfer of exosomes mediates oligodendrocyte-neuron communication. PLoS Biology 11:e1001604.

Fucile S, Miledi R, Eusebi F (2006) Effects of cyclothiazide on GluR1/AMPA receptors. Proc Natl Acad Sci U S A 103:2943-2947.

Fujita Y, Yamashita T (2014) Axon growth inhibition by RhoA/ROCK in the central nervous system. Frontieers in Neuroscience 8:338.

Fulton D, Paez P, Fisher R, Handley V, Colwell C, Campagnoni A (2010) Regulation of L-type Ca++ currents and process morphology in white matter oligodendrocyte precursor cells by golli-myelin proteins. Glia 58:1292-1303.

Funfschilling U, Supplie LM, Mahad D, Boretius S, Saab AS, Edgar J, Brinkmann BG, Kassmann CM, Tzvetanova ID, Mobius W, Diaz F, Meijer D, Suter U, Hamprecht B, Sereda MW,

Moraes CT, Frahm J, Goebbels S, Nave KA (2012) Glycolytic oligodendrocytes maintain myelin and long-term axonal integrity. Nature 485:517-521.

Furlan R, Cuomo C, Martino G (2009) Animal models of multiple sclerosis. Methods Mol Biol 549:157-173.

Gaesser JM, Fyffe-Maricich SL (2016) Intracellular signaling pathway regulation of myelination and remyelination in the CNS. Exp Neurol 283:501-511.

Gard AL, Pfeiffer SE (1989) Oligodendrocyte progenitors isolated directly from developing telencephalon at a specific phenotypic stage: myelinogenic potential in a defined environment. Development 106:119-132.

Gentile A, Musella A, De Vito F, Fresegna D, Bullitta S, Rizzo FR, Centonze D, Mandolesi G (2018) Laquinimod ameliorates excitotoxic damage by regulating glutamate re-uptake. J Neuroinflammation 15:5.

Ghasemi N, Razavi S, Nikzad E (2017) Multiple Sclerosis: Pathogenesis, Symptoms, Diagnoses and Cell-Based Therapy. Cell J 19:1-10.

Gil V, Bichler Z, Lee JK, Seira O, Llorens F, Bribian A, Morales R, Claverol-Tinture E, Soriano E, Sumoy L, Zheng B, Del Rio JA (2010) Developmental expression of the oligodendrocyte myelin glycoprotein in the mouse telencephalon. Cereb Cortex 20:1769-1779.

Goebels N (2007) Organotypic CNS Slice Cultures as an In Vitro Model for Immune Mediated Tissue Damage and Repair in Multiple Sclerosis. Alternatives to Animal Experimentation 24 Spec:85-86.

Goldenberg M (2012) Multiple Sclerosis Review. Pharmacy and Therapeutics 37:175-184.

Goldenthal K, Hedman K, Chen J, August J, Willingham M (1985) Postfixation detergent treatment for immunofluorescence suppresses localization of some integral membrane proteins. The Journal of Histochemistry and Cytochemistry 33:813-820.

Graziano AC, Cardile V (2015) History, genetic, and recent advances on Krabbe disease. Gene 555:2-13.

Green AJ, Gelfand JM, Cree BA, Bevan C, Boscardin WJ, Mei F, Inman J, Arnow S, Devereux M, Abounasr A, Nobuta H, Zhu A, Friessen M, Gerona R, von Budingen HC, Henry RG, Hauser SL, Chan JR (2017) Clemastine fumarate as a remyelinating therapy for multiple sclerosis (ReBUILD): a randomised, controlled, double-blind, crossover trial. Lancet 390:2481-2489.

Gregath A, Lu RQ (2018) Epigenetic Modifications: Insight into Oligodendrocyte Lineage Progression, Regeneration and Disease. FEBS Lett.

Grigoriadis N, van Pesch V, Paradig MSG (2015) A basic overview of multiple sclerosis immunopathology. Eur J Neurol 22 Suppl 2:3-13.

Guest J, Hiester E, Bunge R (2005) Demyelination and Schwann cell responses adjacent to injury epicenter cavities following chronic human spinal cord injury. Experimental Neurology 192:384-393.

Haines B, Rigby P (2008) Expression of the Lingo/LERN gene family during mouse embryogenesis. Gene Expression Patterns 8:79-86.

Hamano K, Iwasaki N, Takeya T, Takita H (1996) A quantitative analysis of rat central nervous system myelination using the immunohistochemical method for MBP. Developmental Brain Research 93:18-22.

Hanafy KA, Sloane JA (2011) Regulation of remyelination in multiple sclerosis. FEBS Lett 585:3821-3828.

Harbo HF, Gold R, Tintore M (2013) Sex and gender issues in multiple sclerosis. Ther Adv Neurol Disord 6:237-248.

Harlow DE, Honce JM, Miravalle AA (2015) Remyelination Therapy in Multiple Sclerosis. Front Neurol 6:257.

Hemmer B, Archelos J, Hartung H (2002) New concepts in the immunopathogenesis of multiple sclerosis. Nature Reviews Neuroscience 3.

Hill RA, Li AM, Grutzendler J (2018) Lifelong cortical myelin plasticity and age-related degeneration in the live mammalian brain. Nat Neurosci.

Homma S, Shimada T, Hikake T, Yaginuma H (2009) Expression pattern of LRR and Ig domain-containing protein (LRRIG protein) in the early mouse embryo. Gene Expression Patterns 9:1-26.

Hossain S, Ahmed M, Alam S, Watanabe A, Harashima A, Yonekura H, Yamamoto H (2011) Expression and Roles of AMIGO Gene Family in Vascular Endothelial Cells. International Journal of Molecular Medicine and Advance Sciences 7:5-11.

Iglesias-Ussel M, Marchionni L, Romerio F (2013) Isolation of microarray-quality RNA from primary human cells after intracellular immunostaining and fluorescence-activated cell sorting. J Immunol Methods 391:22-30.

Inoue H, Lin L, Lee X, Shao Z, Mendes S, Snodgrass-Belt P, Sweigard H, Engber T, Pepinsky B, Yang L, Beal M, Mi S, Isacson O (2007) Inhibition of the leucine-rich repeat protein LINGO-1 enhances survival, structure, and function of dopaminergic neurons in Parkinson's disease models. Proceedings of the National Academy of Sciences of the United States of America 104:14430-14435.

Iobbi C, Korte M, Zagrebelsky M (2017) Nogo-66 Restricts Synaptic Strengthening via Lingo1 and the ROCK2-Cofilin Pathway to Control Actin Dynamics. Cereb Cortex 27:2779-2792.

Jadasz J, Aigner L, Rivera F, Kury P (2012) The remyelination philosopher's stone: stem and progenitor cell therapies for multiple sclerosis. Cell Tissue Research 349:331-347.

Jamur M, Oliver C (2010) Permeabilization of cell membranes. Methods in Molecular Biology 588:63-66.

Jeffery ND, Blakemore WF (1995) Remyelination of mouse spinal cord axons demyelinated by local injection of lysolecithin. J Neurocytol 24:775-781.

Jennum P, Wanscher B, Frederiksen J, Kjellberg J (2012) The socioeconomic consequences of multiple sclerosis: A controlled national study. European Neuropsychopharmacology 22:36-43.

Jepson S, Vought B, Gross C, Gan L, Austen D, Frantz J, Zwahlen J, Lowe D, Markland W, Krauss R (2012) LINGO-1, a transmembrane signaling protein, inhibits oligodendrocyte differentiation and myelination through intercellular self-interactions. The journal of Biological Chemistry 287:22184-22195.

John GR, Shankar SL, Shafit-Zagardo B, Massimi A, Lee SC, Raine CS, Brosnan CF (2002) Multiple sclerosis: re-expression of a developmental pathway that restricts oligodendrocyte maturation. Nat Med 8:1115-1121.

Jung M, Krämer E, Grzenkowski M, Tang K, Blakemore W, Aguzzi A, Khazaie K, Chlichlia K, Blakenfeld G, Kettenmann H, Trotter J (1995) Lines of Murine Oligodendroglial Precursor Cells Immortalized by an Activated neu Tyrosine Kinase Show Distinct Degrees of Interaction with Axons In Vitro and In Vivo. European Journal of Neuroscience 7:1245-1265.

Kajander T, Kuja-Panula J, Rauvala H, Goldman A (2011) Crystal structure and role of glycans and dimerization in folding of neuronal leucine-rich repeat protein AMIGO-1. J Mol Biol 413:1001-1015.

Kap YS, Laman JD, t Hart BA (2010) Experimental autoimmune encephalomyelitis in the common marmoset, a bridge between rodent EAE and multiple sclerosis for immunotherapy development. J Neuroimmune Pharmacol 5:220-230.

Karlsson TE, Wellfelt K, Olson L (2017) Spatiotemporal and Long Lasting Modulation of 11 Key Nogo Signaling Genes in Response to Strong Neuroexcitation. Front Mol Neurosci 10:94.

Keough MB, Jensen SK, Yong VW (2015) Experimental demyelination and remyelination of murine spinal cord by focal injection of lysolecithin. J Vis Exp.

Khan O, Williams MJ, Amezcua L, Javed A, Larsen KE, Smrtka JM (2015) Multiple sclerosis in US minority populations: Clinical practice insights. Neurol Clin Pract 5:132-142.

Kida E, Palminiello S, Golabek AA, Walus M, Wierzba-Bobrowicz T, Rabe A, Albertini G, Wisniewski KE (2006) Carbonic anhydrase II in the developing and adult human brain. J Neuropathol Exp Neurol 65:664-674.

Kipp M, van der Star B, Vogel DY, Puentes F, van der Valk P, Baker D, Amor S (2012) Experimental in vivo and in vitro models of multiple sclerosis: EAE and beyond. Mult Scler Relat Disord 1:15-28.

Klein R, Smeyne R, Wurst W, Long L, Auerbach B, Joyner A, Barbacid M (1993) Targeted disruption of the trkB neurotrophin receptor gene results. Cell 75:113-122.

Klingseisen A, Lyons DA (2018) Axonal Regulation of Central Nervous System Myelination: Structure and Function. Neuroscientist 24:7-21.

Kobe B, Kajava A (2001) The leucine-rich repeat as a protein recognition motif. Current Opinion in Structural Biology 11:725-732.

Komiyama Y, Nakae S, Matsuki T, Nambu A, Ishigame H, Kakuta S, Sudo K, Iwakura Y (2006) IL-17 plays an important role in the development of experimental autoimmune encephalomyelitis. J Immunol 177:566-573.

Korn T, Bettelli E, Oukka M, Kuchroo VK (2009) IL-17 and Th17 Cells. Annu Rev Immunol 27:485-517.

Kostic M, Zivkovic N, Stojanovic I (2013) Multiple sclerosis and glutamate excitotoxicity. Rev Neurosci 24:71-88.

Kotter M, Zhao C, Rooijen N, Franklin R (2005) Macrophage-depletion induced impairment of experimental CNS remyelination is associated with a reduced oligodendrocyte progenitor cell response and altered growth factor expression. neurobiology of Disease 18:166-175.

Kotter MR, Li WW, Zhao C, Franklin RJ (2006) Myelin impairs CNS remyelination by inhibiting oligodendrocyte precursor cell differentiation. J Neurosci 26:328-332.

Kramer MF, Coen DM (2001) Enzymatic amplification of DNA by PCR: standard procedures and optimization. Curr Protoc Immunol Chapter 10:Unit 10 20.

Kroemer G et al. (2009) Classification of cell death: recommendations of the Nomenclature Committee on Cell Death 2009. Cell Death Differ 16:3-11.

Kuhlmann T, Miron V, Cui Q, Wegner C, Antel J, Bruck W (2008) Differentiation block of oligodendroglial progenitor cells as a cause for remyelination failure in chronic multiple sclerosis. Brain 131:1749-1758.

Kuja-Panula J, Kiiltomäki M, Yamashiro T, Rouhiainen A, Rauvala H (2003) AMIGO, a transmembrane protein implicated in axon tract development, defines a novel protein family with leucine-rich repeats. JCB 160:963-973.

Kundi S, Bicknell R, Ahmed Z (2013) The role of angiogenic and wound-healing factors after spinal cord injury in mammals. Neurosci Res 76:1-9.

Kuo S, Tang G, Louis E, Ma K, Babij R, Balatbat M, Cortes E, Vonsattel J, Yamamoto A, Sulzer D, Faust P (2013) Lingo-1 expression is increased in essential cerebellum and is present in the basket cell pinceau. Acta Neuropathologica 126:879-889.

Kutzelnigg A, Lassmann H (2014) Pathology of multiple sclerosis and related inflammatory demyelinating diseases. Handb Clin Neurol 122:15-58.

Kwon H, Nakaya N, Abu-Asab M, Kim H, Tomarev S (2014) Myocilin is involved in NgR1/Lingo-1-mediated oligodendrocyte differentiation and myelination of the optic nerve. The Journal of Neuroscience 34:5539-5551.

Langrish CL, Chen Y, Blumenschein WM, Mattson J, Basham B, Sedgwick JD, McClanahan T, Kastelein RA, Cua DJ (2005) IL-23 drives a pathogenic T cell population that induces autoimmune inflammation. J Exp Med 201:233-240.

Lassmann H, Bradl M (2017) Multiple sclerosis: experimental models and reality. Acta Neuropathol 133:223-244.

Lassmann H, Bruck W, Lucchinetti CF (2007) The immunopathology of multiple sclerosis: an overview. Brain Pathol 17:210-218.

Lau LW, Keough MB, Haylock-Jacobs S, Cua R, Doring A, Sloka S, Stirling DP, Rivest S, Yong VW (2012) Chondroitin sulfate proteoglycans in demyelinated lesions impair remyelination. Ann Neurol 72:419-432.

Ledda F, Paratcha G (2016) Assembly of Neuronal Connectivity by Neurotrophic Factors and Leucine-Rich Repeat Proteins. Front Cell Neurosci 10:199.

Ledford H (2015) Drug that boosts nerve signals offers hope for multiple sclerosis. Nature 520:417.

Lee X, Shao Z, Sheng G, Pepinsky B, Mi S (2014) LINGO-1 regulates oligodendrocyte differentiation by inhibiting ErbB2 translocation and activation in lipid rafts. Mol Cell Neurosci 60:36-42.

Lee X, Yang Z, Shao Z, Rosenberg S, Levesque M, Pepinsky R, Qiu M, Miller R, Chan J, Mi S (2007) NGF regulates the expression of axonal LINGO-1 to inhibit oligodendrocyte differentiation and myelination. The Journal of Neuroscience 27:220-225.

Li X, Zhang Y, Yan Y, Ciric B, Ma CG, Chin J, Curtis M, Rostami A, Zhang GX (2017) LINGO-1-Fc-Transduced Neural Stem Cells Are Effective Therapy for Chronic Stage Experimental Autoimmune Encephalomyelitis. Mol Neurobiol 54:4365-4378.

Lin W, Kemper A, Dupree J, Harding H, Ron D, Popko B (2006) Interferon-γ inhibits central nervous system remyelination through a process modulated by endoplasmic reticulum stress. Brain 129:1306-1318.

Lindner M, Heine S, Haastert K, Garde N, Fokuhl J, Linsmeier F, Grothe C, Baumgartner W, Stangel M (2008) Sequential myelin protein expression during remyelination reveals fast and efficient repair after central nervous system demyelination. Neuropathol Appl Neurobiol 34:105-114.

Lindsay K, Bone I, Callander R (1997) Neurology and Neurosurgery Illustrated. Edinburgh: Churchill Livingstone.

Linker RA, Lee DH (2009) Models of autoimmune demyelination in the central nervous system: on the way to translational medicine. Exp Transl Stroke Med 1:5.

Littlewood-Evans A, Sarret S, Apfel V, Loesle P, Dawson J, Zhang J, Muller A, Tigani B, Kneuer R, Patel S, Valeaux S, Gommermann N, Rubic-Schneider T, Junt T, Carballido JM (2016) GPR91 senses extracellular succinate released from inflammatory macrophages and exacerbates rheumatoid arthritis. J Exp Med 213:1655-1662.

Liu J, Dietz K, DeLoyht JM, Pedre X, Kelkar D, Kaur J, Vialou V, Lobo MK, Dietz DM, Nestler EJ, Dupree J, Casaccia P (2012) Impaired adult myelination in the prefrontal cortex of socially isolated mice. Nat Neurosci 15:1621-1623.

Liu W, Shen Y, Plane J, Pleasure D, Deng W (2011) Neuroprotective potential of erythropoietin and its derivative carbamylated erythropoietin in periventricular leukomalacia. Experimental Neurology 230:227-239.

Llorens F, Gil V, Iraola S, Carim-Todd L, Martı´ E, Estivill X, Soriano E, del Rio J, Sumoy L (2008) Developmental analysis of Lingo-1/Lern1 protein expression inthe mouse brain: Interaction of its intracellular domain with Myt1l. Developmental Neurobiology 68:521-541.

Lock C, Hermans G, Pedotti R, Brendolan A, Schadt E, Garren H, Langer-Gould A, Strober S, Cannella B, Allard J, Klonowski P, Austin A, Lad N, Kaminski N, Galli SJ, Oksenberg JR, Raine CS, Heller R, Steinman L (2002) Gene-microarray analysis of multiple sclerosis lesions yields new targets validated in autoimmune encephalomyelitis. Nat Med 8:500-508.

Lodygensky GA, Marques JP, Maddage R, Perroud E, Sizonenko SV, Huppi PS, Gruetter R (2012) In vivo assessment of myelination by phase imaging at high magnetic field. Neuroimage 59:1979-1987.

Lopes Pinheiro MA, Kooij G, Mizee MR, Kamermans A, Enzmann G, Lyck R, Schwaninger M, Engelhardt B, de Vries HE (2016) Immune cell trafficking across the barriers of the central nervous system in multiple sclerosis and stroke. Biochim Biophys Acta 1862:461-471.

Lopez PH, Ahmad AS, Mehta NR, Toner M, Rowland EA, Zhang J, Dore S, Schnaar RL (2011) Myelin-associated glycoprotein protects neurons from excitotoxicity. J Neurochem 116:900-908.

Love S (2006) Demyelinating diseases. J Clin Pathol 59:1151-1159.

Lu C, Dong L, Zhou H, Li Q, Huang G, Bai SJ, Liao L (2018) G-Protein-Coupled Receptor Gpr17 Regulates Oligodendrocyte Differentiation in Response to Lysolecithin-Induced Demyelination. Sci Rep 8:4502.

Lublin FD (2014) New multiple sclerosis phenotypic classification. Eur Neurol 72 Suppl 1:1-5.

Lublin FD et al. (2014) Defining the clinical course of multiple sclerosis: the 2013 revisions. Neurology 83:278-286.

Lucas RM, Hughes AM, Lay ML, Ponsonby AL, Dwyer DE, Taylor BV, Pender MP (2011) Epstein-Barr virus and multiple sclerosis. J Neurol Neurosurg Psychiatry 82:1142-1148.

Mackenzie IS, Morant SV, Bloomfield GA, MacDonald TM, O'Riordan J (2014) Incidence and prevalence of multiple sclerosis in the UK 1990-2010: a descriptive study in the General Practice Research Database. J Neurol Neurosurg Psychiatry 85:76-84.

Maglione M, Tress O, Haas B, Karram K, Trotter J, Willecke K, Kettenmann H (2010) Oligodendrocytes in mouse corpus callosum are coupled via gap junction channels formed by connexin47 and connexin32. 58 9:1104-1117.

Mahmood T, Yang PC (2012) Western blot: technique, theory, and trouble shooting. N Am J Med Sci 4:429-434.

Marrie RA, Reider N, Cohen J, Stuve O, Sorensen PS, Cutter G, Reingold SC, Trojano M (2015) A systematic review of the incidence and prevalence of autoimmune disease in multiple sclerosis. Mult Scler 21:282-293.

Matsushima GK, Morell P (2001) The neurotoxicant, cuprizone, as a model to study demyelination and remyelination in the central nervous system. Brain Pathol 11:107-116.

Matsushima N, Tachi N, Kuroki Y, Enkhbayar P, Osaki M, Kamiya M, Kretsinger R (2005) Structural analysis of leucine-rich-repeat variants in proteins associated with human diseases. Cellular and Molecular Life Sciences 62:2771-2791.

Matveeva O, Bogie JFJ, Hendriks JJA, Linker RA, Haghikia A, Kleinewietfeld M (2018) Western lifestyle and immunopathology of multiple sclerosis. Ann N Y Acad Sci 1417:71-86.

McCarthy DP, Richards MH, Miller SD (2012) Mouse models of multiple sclerosis: experimental autoimmune encephalomyelitis and Theiler's virus-induced demyelinating disease. Methods Mol Biol 900:381-401.

McDonald JW, Althomsons SP, Hyrc KL, Choi DW, Goldberg MP (1998) Oligodendrocytes from forebrain are highly vulnerable to AMPA/kainate receptor-mediated excitotoxicity. Nat Med 4:291-297.

McGinley AM, Edwards SC, Raverdeau M, Mills KHG (2018) Th17cells, gammadelta T cells and their interplay in EAE and multiple sclerosis. J Autoimmun.

McLaurin J, Trudel GC, Shaw IT, Antel JP, Cashman NR (1995) A human glial hybrid cell line differentially expressing genes subserving oligodendrocyte and astrocyte phenotype. J Neurobiol 26:283-293.

McMahon EJ, Suzuki K, Matsushima GK (2002) Peripheral macrophage recruitment in cuprizone-induced CNS demyelination despite an intact blood-brain barrier. J Neuroimmunol 130:32-45.

Meabon JS, De Laat R, Ieguchi K, Wiley JC, Hudson MP, Bothwell M (2015) LINGO-1 protein interacts with the p75 neurotrophin receptor in intracellular membrane compartments. J Biol Chem 290:9511-9520.

Meabon JS, de Laat R, Ieguchi K, Serbzhinsky D, Hudson MP, Huber BR, Wiley JC, Bothwell M (2016) Intracellular LINGO-1 negatively regulates Trk neurotrophin receptor signaling. Mol Cell Neurosci 70:1-10.

266

Medina D, Shepherd F (1981) Selenium-mediated inhibition of 7,12-dimethylbenz[a]anthracene-induced mouse mammary tumorigenesis. Carciogenesis 2:451-455.

Mehta A, Prabhakar M, Kumar P, Deshmukh R, Sharma PL (2013) Excitotoxicity: bridge to various triggers in neurodegenerative disorders. Eur J Pharmacol 698:6-18.

Mei F, Chong S, Chan J (2013) Myelin- based inhibitors of oligodendrocyte myelination: clues from axonal growth and regeneration. Neurosci Bull 29:177-188.

Mei F, Guo S, He Y, Wang L, Wang H, Niu J, Kong J, Li X, Wu Y, Xiao L (2012) Quetiapine, an atypical antipsychotic, is protective against autoimmune-mediated demyelination by inhibiting effector T cell proliferation. PLoS One 7:e42746.

Menon B, Bedi SS, Rao GU (2014) Combined central and peripheral demyelination. J Neurosci Rural Pract 5:78-80.

Merrill J (2009) *In Vitro* and *In Vivo* Pharmacological Models to Assess Demyelination and Remyelination. Neuropsychopharmacology REVIEWS 34:55-73.

Mi S, Sandrock A, Miller R (2008) LINGO-1 and its role in CNS repair. The International Journal of Biochemistry & Cell Biology 40:1971-1978.

Mi S, Pepinsky R, Cadavid D (2013) Blocking LINGO-1 as a therapy to promote CNS repair: from concept to the clinic. CNS Drugs 27:493-503.

Mi S, Lee X, Shao Z, Thill G, Ji B, Relton J, Levesque M, Allaire N, Perrin S, Sands B, Crowell T, Cate R, McCoy J, Pepinsky R (2004) LINGO-1 is a component of the Nogo-66 receptor/p75 signaling complex. Nature Neuroscience 7:221-228.

Mi S, Miller R, Lee X, Scott M, Shulag-Morskaya S, Shao Z, Chang J, Thill G, Levesque M, Zhang M, Hession C, Sah D, Trapp B, He Z, Jung V, McCoy J, Pepinsky R (2005) LINGO-1 negatively regulates myelination by oligodendrocytes. Nature Neuroscience 8:745-751.

Mi S, Hu B, Hahm K, Luo Y, Hui E, Yuan Q, Wong W, Wang L, Su H, Chu T, Guo J, Zhang W, So K, Pepinsky R, Shao Z, Graff C, Garber E, Jung V, Wu E, Wu W (2007) LINGO-1 antagonist promotes spinal cord remyelination and axonal integrity in MOG-induced experimental autoimmune encephalomyelitis. Nature Medicine 13:1228-1233.

Mi S et al. (2009) Promotion of central nervous system remyelination by induced differentiation of oligodendrocyte precursor cells. Annals of Neurology 65:304-315.

Michailidou I, de Vries HE, Hol EM, van Strien ME (2014) Activation of endogenous neural stem cells for multiple sclerosis therapy. Front Neurosci 8:454.

Michalski JP, Kothary R (2015) Oligodendrocytes in a Nutshell. Front Cell Neurosci 9:340.

Miller RH (2002) Regulation of oligodendrocyte development in the vertebrate CNS. Prog Neurobiol 67:451-467.

Miller SD, Karpus WJ (2007) Experimental autoimmune encephalomyelitis in the mouse. Curr Protoc Immunol Chapter 15:Unit 15 11.

Mills E, O'Neill LA (2014) Succinate: a metabolic signal in inflammation. Trends Cell Biol 24:313-320.

Miron VE, Kuhlmann T, Antel JP (2011) Cells of the oligodendroglial lineage, myelination, and remyelination. Biochim Biophys Acta 1812:184-193.

Mitew S, Hay CM, Peckham H, Xiao J, Koenning M, Emery B (2014) Mechanisms regulating the development of oligodendrocytes and central nervous system myelin. Neuroscience 276:29-47.

Miyamoto N, Pham LD, Seo JH, Kim KW, Lo EH, Arai K (2014) Crosstalk between cerebral endothelium and oligodendrocyte. Cell Mol Life Sci 71:1055-1066.

Monk KR, Feltri ML, Taveggia C (2015) New insights on Schwann cell development. Glia 63:1376-1393.

Montani L, Gerrits B, Gehrig P, Kempf A, Dimou L, Wollscheid B, Schwab ME (2009) Neuronal Nogo-A modulates growth cone motility via Rho-GTP/LIMK1/cofilin in the unlesioned adult nervous system. J Biol Chem 284:10793-10807.

Morris G, Jiruska P, Jefferys JG, Powell AD (2016) A New Approach of Modified Submerged Patch Clamp Recording Reveals Interneuronal Dynamics during Epileptiform Oscillations. Front Neurosci 10:519.

Morrison BM, Lee Y, Rothstein JD (2013) Oligodendroglia: metabolic supporters of axons. Trends Cell Biol 23:644-651.

Mruk DD, Cheng CY (2011) Enhanced chemiluminescence (ECL) for routine immunoblotting: An inexpensive alternative to commercially available kits. Spermatogenesis 1:121-122.

MS-Society (2016) Anti-LINGO-1. In.

Multiple Sclerosis International Federation (2013) Atlas of MS 2013: Mapping Multiple Sclerosis Around the World (pdf). In.

Najm F et al. (2015) Drug-based modulation of endogenous stem cells promotes functional remyelination in vivo. Nature:Epub.

Nakahara J, Kanekura K, Nawa M, Aiso S, N S (2009) Abnormal expression of TIP30 and arrested nucleocytoplasmic transport within oligodendrocyte precursor cells in multiple sclerosis. The Journal of Clinical Investigation 119:169-181.

Narayanan SP, Flores AI, Wang F, Macklin WB (2009) Akt signals through the mammalian target of rapamycin pathway to regulate CNS myelination. J Neurosci 29:6860-6870.

Nathoo N, Yong VW, Dunn JF (2014) Understanding disease processes in multiple sclerosis through magnetic resonance imaging studies in animal models. Neuroimage Clin 4:743-756.

Nave KA (2010) Myelination and the trophic support of long axons. Nat Rev Neurosci 11:275-283.

Neishabouri A, Faisal AA (2014) Saltatory conduction in unmyelinated axons: clustering of Na(+) channels on lipid rafts enables micro-saltatory conduction in C-fibers. Front Neuroanat 8:109.

Nelson RE, Butler J, LaFleur J, Knippenberg K, AW CK, DuVall SL (2016) Determining Multiple Sclerosis Phenotype from Electronic Medical Records. J Manag Care Spec Pharm 22:1377-1382.

Neman J, de Vellis J (2008) Handbook of neurochemistry and molecular neurobiology, 3 Edition. U.S.A: Springer.

Nishiyama A, Komitova M, Suzuki R, Zhu X (2009) Polydendrocytes (NG2 cells): multifunctional cells with lineage plasticity. Nat Rev Neurosci 10:9-22.

O'Brien JS (1965) Stability of the Myelin Membrane. Science 147:1099-1107.

O'Gorman C, Lucas R, Taylor B (2012) Environmental risk factors for multiple sclerosis: a review with a focus on molecular mechanisms. Int J Mol Sci 13:11718-11752.

O'Meara R, Ryan S, Colognato H, Kothary R (2011) Derivation of Enriched Oligodendrocyte Cultures and Oligodendrocyte/Neuron Myelinating Co-cultures from Post-natal Murine Tissues. Journal of Visualized Experiments 54:3324.

Olek M (2018) Disease-modifying treatment of relapsing-remitting multiple sclerosis in adults. In: UpToDate.

Olesen J, Gustavsson A, Svensson M, Wittchen H, Jonsson B (2012) The economic cost of brain disorders in Europe. European Journal of Neurology 19:155-162.

Ou Z, Sun Y, Lin L, You N, Liu X, Li H, Ma Y, Cao L, Han Y, Liu M, Deng Y, Yao L, Lu QR, Chen Y (2016) Olig2-Targeted G-Protein-Coupled Receptor Gpr17 Regulates Oligodendrocyte Survival in Response to Lysolecithin-Induced Demyelination. J Neurosci 36:10560-10573.

Paez PM, Spreuer V, Handley V, Feng JM, Campagnoni C, Campagnoni AT (2007) Increased expression of golli myelin basic proteins enhances calcium influx into oligodendroglial cells. J Neurosci 27:12690-12699.

Paintlia AS, Paintlia MK, Singh AK, Singh I (2008) Inhibition of rho family functions by lovastatin promotes myelin repair in ameliorating experimental autoimmune encephalomyelitis. Mol Pharmacol 73:1381-1393.

Pal B (2018) Involvement of extrasynaptic glutamate in physiological and pathophysiological changes of neuronal excitability. Cell Mol Life Sci.

Pan H, Song Q, Huang Y, Wang J, Chai R, Yin S, Wang J (2017) Auditory Neuropathy after Damage to Cochlear Spiral Ganglion Neurons in Mice Resulting from Conditional Expression of Diphtheria Toxin Receptors. Sci Rep 7:6409.

Pang Y, Zheng B, Kimberly SL, Cai Z, Rhodes PG, Lin RC (2012) Neuron-oligodendrocyte myelination co-culture derived from embryonic rat spinal cord and cerebral cortex. Brain Behav 2:53-67.

Patani R, Balaratnam M, Vora A, Reynolds R (2007) Remyelination can be extensive in multiple sclerosis despite a long disease course. Neuropathology and Applied Neurobiology 33:277-287.

Patrikios P, Stadelmann C, Kutzelnigg A, Rauschka H, Schmidbauer M, Laursen H, Sorensen P, Brück W, Lucchinetti C, Lassmann H (2006) Remyelination is extensive in a subset of multiple sclerosis patients. Brain: a Journal of Neurology 129:3165-3172.

Pereira GB, Dobretsova A, Hamdan H, Wight PA (2011) Expression of myelin genes: comparative analysis of Oli-neu and N20.1 oligodendroglial cell lines. J Neurosci Res 89:1070-1078.

Peruzzotti-Jametti L, Bernstock JD, Vicario N, Costa A, Kwok C, Leonardi T, Booty L, Bicci I, Balzarotti B, Volpe G, Mallucci G, Manferrari G, Donega M, Iraci N, Braga A, Hallenbeck J, Murphy M, Edenhofer F, Frezza C, Pluchino S (2018) Macrophage-Derived Extracellular Succinate Licenses Neural Stem Cells to Suppress Chronic Neuroinflammation. Cell Stem Cell 22:1-14.

Pham LD, Hayakawa K, Seo JH, Nguyen MN, Som AT, Lee BJ, Guo S, Kim KW, Lo EH, Arai K (2012) Crosstalk between oligodendrocytes and cerebral endothelium contributes to vascular remodeling after white matter injury. Glia 60:875-881.

Plemel JR, Manesh SB, Sparling JS, Tetzlaff W (2013) Myelin inhibits oligodendroglial maturation and regulates oligodendrocytic transcription factor expression. Glia 61:1471-1487.

Podbielska M, Banik NL, Kurowska E, Hogan EL (2013) Myelin recovery in multiple sclerosis: the challenge of remyelination. Brain Sci 3:1282-1324.

Polak J, Noorden S (2003) Introduction to Immunocytochemistry: Oxford: Bios Scientific Publishers.

Polito A, Reynolds R (2005) NG2-expressing cells as oligodendrocyte progenitors in the normal and demyelinated adult central nervous system. J Anat 207:707-716.

Ponzio M, Gerzeli S, Brichetto G, Bezzini D, Mancardi G, Zaratin P, Battaglia M (2015) Economic impact of multiple sclerosis in Italy: focus on rehabilitation costs. Neurological Sciences 36:227-234.

Praet J, Guglielmetti C, Berneman Z, Van der Linden A, Ponsaerts P (2014) Cellular and molecular neuropathology of the cuprizone mouse model: clinical relevance for multiple sclerosis. Neurosci Biobehav Rev 47:485-505.

Priest CA, Manley NC, Denham J, Wirth ED, 3rd, Lebkowski JS (2015) Preclinical safety of human embryonic stem cell-derived oligodendrocyte progenitors supporting clinical trials in spinal cord injury. Regen Med 10:939-958.

Pugliatti M, Rosati G, Carton H, Riise T, Drulovic J, Vecsei L, Milanov I (2006) The epidemiology of multiple sclerosis in Europe. European Journal of Neurology 13:700-722.

Purger D, Gibson EM, Monje M (2016) Myelin plasticity in the central nervous system. Neuropharmacology 110:563-573.

Quarles R, Macklin W, Morell P (2006) basic neurochemistry: molecular, cellular and medical aspects: Elsevier Inc.

Rangachari M, Kuchroo VK (2013) Using EAE to better understand principles of immune function and autoimmune pathology. J Autoimmun 45:31-39.

Robinson AP, Rodgers JM, Goings GE, Miller SD (2014a) Characterization of oligodendroglial populations in mouse demyelinating disease using flow cytometry: clues for MS pathogenesis. PLoS One 9:e107649.

Robinson AP, Harp CT, Noronha A, Miller SD (2014b) The experimental autoimmune encephalomyelitis (EAE) model of MS: utility for understanding disease pathophysiology and treatment. Handb Clin Neurol 122:173-189.

Rodriguez D (2013) Leukodystrophies with astrocytic dysfunction. Handb Clin Neurol 113:1619-1628.

Saab AS, Nave KA (2017) Myelin dynamics: protecting and shaping neuronal functions. Curr Opin Neurobiol 47:104-112.

Saha N, Kolev M, Nikolov DB (2014a) Structural features of the Nogo receptor signaling complexes at the neuron/myelin interface. Neurosci Res 87:1-7.

Saha N, Kolev M, Nikolov D (2014b) Structural features of the Nogo receptor signaling complexes at the neuron/myelin interface. Neuroscience Research 87:1-7.

Sakry D, Yigit H, Dimou L, Trotter J (2015) Oligodendrocyte precursor cells synthesize neuromodulatory factors. PLoS One 10:e0127222.

Salzer JL (2015) Schwann cell myelination. Cold Spring Harb Perspect Biol 7:a020529.

Sanchez-Gomez MV, Alberdi E, Perez-Navarro E, Alberch J, Matute C (2011) Bax and calpain mediate excitotoxic oligodendrocyte death induced by activation of both AMPA and kainate receptors. J Neurosci 31:2996-3006.

Sandvig A, Berry M, Barrett L, Butt A, Logan A (2004) Myelin-, reactive glia-, and scar-derived CNS axon growth inhibitors: expression, receptor signaling, and correlation with axon regeneration. Glia 46:225-251.

Sarbu N, Shih RY, Jones RV, Horkayne-Szakaly I, Oleaga L, Smirniotopoulos JG (2016) White Matter Diseases with Radiologic-Pathologic Correlation. Radiographics 36:1426-1447.

Satoh J, Onoue H, Arima K, Yamamura T (2005) Nogo-A and nogo receptor expression in demyelinating lesions of multiple sclerosis. Journal of Neuropathology and Experimental Neurology 64:129-138.

Satoh J, Tabunoki H, Yamamura T, Arima K, Konno H (2007) TROY and LINGO-1 expression in astrocytes and macrophages/microglia in multiple sclerosis lesions. Neuropathology and Applied Neurobiology 33:99-107.

Seidl AH (2014) Regulation of conduction time along axons. Neuroscience 276:126-134.

Seyedsadr MS, Ineichen BV (2017) Gpr17, a Player in Lysolecithin-Induced Demyelination, Oligodendrocyte Survival, and Differentiation. J Neurosci 37:2273-2275.

Shao Z, Lee X, Huang G, Sheng G, Henderson CE, Louvard D, Sohn J, Pepinsky B, Mi S (2017) LINGO-1 Regulates Oligodendrocyte Differentiation through the Cytoplasmic Gelsolin Signaling Pathway. J Neurosci 37:3127-3137.

Shen S, Li J, Casaccia-Bonnefil P (2005) Histone modifications affect timing of oligodendrocyte progenitor differentiation in the developing rat brain. J Cell Biol 169:577-589.

Shen S, Liu A, Li J, Wolubah C, Casaccia-Bonnefil P (2008) Epigenetic memory loss in aging oligodendrocytes in the corpus callosum. Neurobiology of Aging 29:452-463.

Simpson S, Jr., Blizzard L, Otahal P, Van der Mei I, Taylor B (2011) Latitude is significantly associated with the prevalence of multiple sclerosis: a meta-analysis. J Neurol Neurosurg Psychiatry 82:1132-1141.

Slierendregt BL, Hall M, t Hart B, Otting N, Anholts J, Verduin W, Claas F, Jonker M, Lanchbury JS, Bontrop RE (1995) Identification of an Mhc-DPB1 allele involved in susceptibility to experimental autoimmune encephalomyelitis in rhesus macaques. Int Immunol 7:1671-1679.

Sloane JA, Batt C, Ma Y, Harris ZM, Trapp B, Vartanian T (2010) Hyaluronan blocks oligodendrocyte progenitor maturation and remyelination through TLR2. Proc Natl Acad Sci U S A 107:11555-11560.

Snaidero N, Mobius W, Czopka T, Hekking LH, Mathisen C, Verkleij D, Goebbels S, Edgar J, Merkler D, Lyons DA, Nave KA, Simons M (2014) Myelin membrane wrapping of CNS axons by PI(3,4,5)P3-dependent polarized growth at the inner tongue. Cell 156:277-290.

Söllner C, Wright G (2009) A cell surface interaction network of neural leucine-rich repeat receptors. Genome Biology 10:R99.

Sommer I, Schachner M (1981) Monoclonal antibodies (O1 to O4) to oligodendrocyte cell surfaces: an immunocytological study in the central nervous system. Dev Biol 83:311-327.

Sow A, Lamant M, Bonny J, Larvaron P, Piaud O, Lécureuil C, Fontaine I, Saleh M, Otin A, Renou J, Baron B, Zakin M, Guillou F (2006) Oligodendrocyte differentiation is increased in transferrin transgenic mice. Journal of Neuroscience Research 83:403-414.

Squire L (2009) Encyclopedia of neuroscience. U.S.A.: Academic Press.

Sriram S, Steiner I (2005) Experimental allergic encephalomyelitis: a misleading model of multiple sclerosis. Ann Neurol 58:939-945.

Steckner C, Weber A, Mausberg AK, Heininger M, Opdenhovel F, Kieseier BC, Hartung HP, Hofstetter HH (2016) Alteration of the cytokine signature by various TLR ligands in different T cell populations in MOG37-50 and MOG35-55-induced EAE in C57BL/6 mice. Clin Immunol 170:22-30.

Stone S, Jamison S, Yue Y, Durose W, Schmidt-Ullrich R, Lin W (2017) NF-kappaB Activation Protects Oligodendrocytes against Inflammation. J Neurosci 37:9332-9344.

Strachan LR, Stevenson TJ, Freshner B, Keefe MD, Miranda Bowles D, Bonkowsky JL (2017) A zebrafish model of X-linked adrenoleukodystrophy recapitulates key disease features and demonstrates a developmental requirement for abcd1 in oligodendrocyte patterning and myelination. Hum Mol Genet 26:3600-3614.

Sturrock R (1980) Myelination of the mouse corpus callosum. Neuropathology and Applied Neurobiology 6:415-420.

Stys PK, Zamponi GW, van Minnen J, Geurts JJ (2012) Will the real multiple sclerosis please stand up? Nat Rev Neurosci 13:507-514.

Sullivan GM, Mierzwa AJ, Kijpaisalratana N, Tang H, Wang Y, Song SK, Selwyn R, Armstrong RC (2013) Oligodendrocyte lineage and subventricular zone response to traumatic axonal injury in the corpus callosum. J Neuropathol Exp Neurol 72:1106-1125.

Sun J, Ren Q, Xu L, Zhang Z (2015) LINGO-1 antibody ameliorates myelin impairment and spatial memory deficits in experimental autoimmune encephalomyelitis mice. Scientific Reports 5:14235.

Sypecka J, Gajkowska B, Domanska-Janik K (1995) Oligodendrocyte development in PLP "pt" mutant rabbits: glycolipid antigens and PLP gene expression. Metab Brain Dis 10:321-333.

Tajadini M, Panjehpour M, Javanmard SH (2014) Comparison of SYBR Green and TaqMan methods in quantitative real-time polymerase chain reaction analysis of four adenosine receptor subtypes. Adv Biomed Res 3:85.

Takahashi H, Katayama K, Sohya K, Miyamoto H, Prasad T, Matsumoto Y, Ota M, Yasuda H, Tsumoto T, Aruga J, Craig AM (2012) Selective control of inhibitory synapse development by Slitrk3-PTPdelta trans-synaptic interaction. Nat Neurosci 15:389-398, S381-382.

Takebayashi H, Ikenaka K (2015) Oligodendrocyte generation during mouse development. Glia 63:1350-1356.

Targett MP, Sussman J, Scolding N, O'Leary MT, Compston DA, Blakemore WF (1996) Failure to achieve remyelination of demyelinated rat axons following transplantation of glial cells obtained from the adult human brain. Neuropathol Appl Neurobiol 22:199-206.

The Jackson Laboratory (2007) Breeding strategies for maintaining colonies of laboratory mice. In.

Theotokis P, Touloumi O, Lagoudaki R, Nousiopoulou E, Kesidou E, Siafis S, Tselios T, Lourbopoulos A, Karacostas D, Grigoriadis N, Simeonidou C (2016) Nogo receptor complex expression dynamics in the inflammatory foci of central nervous system experimental autoimmune demyelination. J Neuroinflammation 13:265.

Tickle J (2013) The role of amphoterin-induced gene and open reading frame (AMIGO) family in myelination and neurodegeneration. In: School of Clinical and Experimental Medicine: University of Birmingham.

Torii T, Miyamoto Y, Yamauchi J, Tanoue A (2014) Pelizaeus-Merzbacher disease: cellular pathogenesis and pharmacologic therapy. Pediatr Int 56:659-666.

Torkildsen O, Brunborg LA, Myhr KM, Bo L (2008) The cuprizone model for demyelination. Acta Neurol Scand Suppl 188:72-76.

Totoiu MO, Keirstead HS (2005) Spinal cord injury is accompanied by chronic progressive demyelination. J Comp Neurol 486:373-383.

Trapp BD, Nave KA (2008) Multiple sclerosis: an immune or neurodegenerative disorder? Annu Rev Neurosci 31:247-269.

Tullman MJ (2013) Overview of the epidemiology, diagnosis, and disease progression associated with multiple sclerosis. Am J Manag Care 19:S15-20.

van der Hiele K, van Gorp DA, Heerings MA, van Lieshout I, Jongen PJ, Reneman MF, van der Klink JJ, Vosman F, Middelkoop HA, Visser LH, Group MSWS (2015) The MS@Work study: a 3-year prospective observational study on factors involved with work participation in patients with relapsing-remitting Multiple Sclerosis. BMC Neurol 15:134.

van der Star BJ, Vogel DY, Kipp M, Puentes F, Baker D, Amor S (2012) In vitro and in vivo models of multiple sclerosis. CNS Neurol Disord Drug Targets 11:570-588.

van Tilborg E, de Theije CGM, van Hal M, Wagenaar N, de Vries LS, Benders MJ, Rowitch DH, Nijboer CH (2018) Origin and dynamics of oligodendrocytes in the developing brain: Implications for perinatal white matter injury. Glia 66:221-238.

Vanderver A, Prust M, Tonduti D, Mochel F, Hussey HM, Helman G, Garbern J, Eichler F, Labauge P, Aubourg P, Rodriguez D, Patterson MC, Van Hove JL, Schmidt J, Wolf NI, Boespflug-Tanguy O, Schiffmann R, van der Knaap MS, Consortium G (2015) Case definition and classification of leukodystrophies and leukoencephalopathies. Mol Genet Metab 114:494-500.

Veldhoen M, Hocking RJ, Flavell RA, Stockinger B (2006) Signals mediated by transforming growth factor-beta initiate autoimmune encephalomyelitis, but chronic inflammation is needed to sustain disease. Nat Immunol 7:1151-1156.

Vereyken EJ, Fluitsma DM, Bolijn MJ, Dijkstra CD, Teunissen CE (2009) An in vitro model for de- and remyelination using lysophosphatidyl choline in rodent whole brain spheroid cultures. Glia 57:1326-1340.

Villoslada P (2016) Neuroprotective therapies for multiple sclerosis and other demyelinating diseases. Multiple Sclerosis and Demyelinating Disorders 1:1.

Wallin MT, Culpepper WJ, Coffman P, Pulaski S, Maloni H, Mahan CM, Haselkorn JK, Kurtzke JF, Veterans Affairs Multiple Sclerosis Centres of Excellence Epidemiology G (2012) The

Gulf War era multiple sclerosis cohort: age and incidence rates by race, sex and service. Brain 135:1778-1785.

Wang C, Qu C, Zhang J, Fu P, Guo S, Tang R (2014) Lingo-1 Inhibited by RNA Interference Promotes Functional Recovery of Experimental Autoimmune Encephalomyelitis. The Anatomical Record 297:2356-2363.

Wang Y, Zhang J, Mori S, Nathans J (2006) Axonal growth and guidance defects in frizzled3 knock-out mice: a comparison of diffusion tensor magnetic resonance imaging, neurofilament staining, and genetically directed cell labeling. The journal of Neuroscience 26:355-364.

Waschbisch A, Sanderson N, Krumbholz M, Vlad G, Theil D, Schwab S, Maurer M, Derfuss T (2014) Interferon beta and vitamin D synergize to induce immunoregulatory receptors on peripheral blood monocytes of multiple sclerosis patients. PLoS One 9:e115488.

Waxman S (1982) Membranes, myelin, and the pathophysiology of multiple sclerosis. The New England Journal of Medicine 306:1529-1533.

Waxman SG (1997) Axon-glia interactions: building a smart nerve fiber. Curr Biol 7:R406-410.

Waxman SG, Pappas GD, Bennett MV (1972) Morphological correlates of functional differentiation of nodes of Ranvier along single fibers in the neurogenic electric organ of the knife fish Stern archus. J Cell Biol 53:210-224.

Wergeland S, Torkildsen O, Myhr KM, Mork SJ, Bo L (2012) The cuprizone model: regional heterogeneity of pathology. APMIS 120:648-657.

Werner P, Pitt D, Raine CS (2000) Glutamate excitotoxicity--a mechanism for axonal damage and oligodendrocyte death in Multiple Sclerosis? J Neural Transm Suppl:375-385.

Whittemore E, Loo D, Watt J, Cotman C (1995) A detailed analysis of hydrogen peroxide-induced cell death in primary neuronal culture. Neuroscience 67:921-932.

Wilkins A, Majed H, Layfield R, Compston A, Chandran S (2003) Oligodendrocytes promote neuronal survival and axonal length by distinct intracellular mechanisms: a novel role for oligodendrocyte-derived glial cell line-derived neurotrophic factor. J Neurosci 23:4967-4974.

Wong A, Xiao J, Kemper D, Kilpatrick T, Murray S (2013) Oligodendroglial expression of TrkB independently regulates myelination and progenitor cell proliferation. The Journal of Neuroscience 33:4947-4957.

Wu B, Sun L, Li P, Tian M, Luo Y, Ren X (2011) Transplantation of oligodendrocyte precursor cells improves myelination and promotes functional recovery after spinal cord injury. Injury 43:794-801.

Wu G, Alvarez E (2011) The immuno-pathophysiology of multiple sclerosis. Neurologic Clinics 29:257-278.

Yim YS, Kwon Y, Nam J, Yoon HI, Lee K, Kim DG, Kim E, Kim CH, Ko J (2013) Slitrks control excitatory and inhibitory synapse formation with LAR receptor protein tyrosine phosphatases. Proc Natl Acad Sci U S A 110:4057-4062.

Yin W, Hu B (2014) Knockdown of Lingo1b protein promotes myelination and oligodendrocyte differentiation in zebrafish. Experimental Neurology 251:72-83.

Yin X, Baek RC, Kirschner DA, Peterson A, Fujii Y, Nave KA, Macklin WB, Trapp BD (2006) Evolution of a neuroprotective function of central nervous system myelin. J Cell Biol 172:469-478.

Yiu G, He Z (2006) Glial inhibition of CNS axon regeneration. Nature Reviews Neuroscience 7:617-627.

You Y, Gupta V (2018) The Extracellular Matrix and Remyelination Strategies in Multiple Sclerosis. eNeuro 5.

Yu J, Bao S, Yu S, Zhang D, Loo W, Chow L, Su L, Cui Z, Chen K, Ma L, Zhang N, Yu H, Yang Y, Dong Y, Yip A, Ng E (2012) Mouse model of plasma cell mastitis. Journal of Translational Medicine 10.

Yuen T, Silbereis J, Griveau A, Chang S, Daneman R, Fancy S, Zahed H, Maltepe E, Rowitch D (2014) Oligodendrocyte-encoded HIF function couples postnatal myelination and white matter angiogenesis. Cell 158:383-396.

Zabala A, Vazquez-Villoldo N, Rissiek B, Gejo J, Martin A, Palomino A, Perez-Samartin A, Pulagam KR, Lukowiak M, Capetillo-Zarate E, Llop J, Magnus T, Koch-Nolte F, Rassendren F, Matute C, Domercq M (2018) P2X4 receptor controls microglia activation and favors remyelination in autoimmune encephalitis. EMBO Mol Med 10.

Zeinali H, Baluchnejadmojarad T, Fallah S, Sedighi M, Moradi N, Roghani M (2018) S-allyl cysteine improves clinical and neuropathological features of experimental autoimmune encephalomyelitis in C57BL/6 mice. Biomed Pharmacother 97:557-563.

Zephir H, Stojkovic T, Latour P, Lacour A, de Seze J, Outteryck O, Maurage CA, Monpeurt C, Chatelet P, Ovelacq E, Vermersch P (2008) Relapsing demyelinating disease affecting both the central and peripheral nervous systems. J Neurol Neurosurg Psychiatry 79:1032-1039.

Zhang H, Jarjour AA, Boyd A, Williams A (2011) Central nervous system remyelination in culture--a tool for multiple sclerosis research. Exp Neurol 230:138-148.

Zhang K, Sejnowski TJ (2000) A universal scaling law between gray matter and white matter of cerebral cortex. Proc Natl Acad Sci U S A 97:5621-5626.

Zhang Y, Zhang YP, Pepinsky B, Huang G, Shields LB, Shields CB, Mi S (2015a) Inhibition of LINGO-1 promotes functional recovery after experimental spinal cord demyelination. Exp Neurol 266:68-73.

Zhang Z, Xu X, Zhang Y, Zhou J, Yu Z, He C (2009) LINGO-1 interacts with WNK1 to regulate nogo-induced inhibition of neurite extension. J Biol Chem 284:15717-15728.

276

Zhang ZH, Li JJ, Wang QJ, Zhao WQ, Hong J, Lou SJ, Xu XH (2015b) WNK1 is involved in Nogo66 inhibition of OPC differentiation. Mol Cell Neurosci 65:135-142.

Zhao C, Li WW, Franklin RJ (2006) Differences in the early inflammatory responses to toxin-induced demyelination are associated with the age-related decline in CNS remyelination. Neurobiol Aging 27:1298-1307.

Zhao X, Kuja-Panula J, Sundvik M, Chen YC, Aho V, Peltola MA, Porkka-Heiskanen T, Panula P, Rauvala H (2014) Amigo adhesion protein regulates development of neural circuits in zebrafish brain. J Biol Chem 289:19958-19975.

Zhou Z, Sathiyamoorthy S, Tan E (2012) LINGO-1 and neurodegeneration: pathophysiologic clues for essential tremor? Tremor and Other Hyperkinetic Movements 2:tre-02-51-249-241.